Table of Contents

11.0 ACCIDENT ANALYSES 11-1
11.1 Off-Normal Events 11.1.1-1
11.1.1 Severe Ambient Temperature Conditions (106°F and -40°F) 11.1.1-1
11.1.1.1 Cause of Severe Ambient Temperature Event 11.1.1-1
11.1.1.2 Detection of Severe Ambient Temperature Event 11.1.1-1
11.1.1.3 Analysis of Severe Ambient Temperature Event 11.1.1-1
11.1.1.4 Corrective Actions 11.1.1-2
11.1.1.5 Radiological Impact 11.1.1-2
11.1.2 Blockage of Half of the Air Inlets 11.1.2-1
11.1.2.1 Cause of the Blockage Event 11.1.2-1
11.1.2.2 Detection of the Blockage Event 11.1.2-1
11.1.2.3 Analysis of the Blockage Event 11.1.2-1
11.1.2.4 Corrective Actions 11.1.2-2
11.1.2.5 Radiological Impact 11.1.2-2
11.1.3 Off-Normal Canister Handling Load 11.1.3-1
11.1.3.1 Cause of Off-Normal Canister Handling Load Event 11.1.3-1
11.1.3.2 Detection of Off-Normal Canister Handling Load Event 11.1.3-1
11.1.3.3 Analysis of Off-Normal Canister Handling Load Event 11.1.3-1
11.1.3.4 Corrective Actions 11.1.3-3
11.1.3.5 Radiological Impact 11.1.3-3
11.1.4 Failure of Instrumentation 11.1.4-1
11.1.4.1 Cause of Instrumentation Failure Event 11.1.4-1
11.1.4.2 Detection of Instrumentation Failure Event 11.1.4-1
11.1.4.3 Analysis of Instrumentation Failure Event 11.1.4-1
11.1.4.4 Corrective Actions 11.1.4-2
11.1.4.5 Radiological Impact 11.1.4-2
11.1.5 Small Release of Radioactive Particulate From the Canister Exterior 11.1.5-1
11.1.5.1 Cause of Radioactive Particulate Release Event 11.1.5-1
11.1.5.2 Detection of Radioactive Particulate Release Event 11.1.5-1
11.1.5.3 Analysis of Radioactive Particulate Release Event 11.1.5-1
11.1.5.4 Corrective Actions 11.1.5-2
11.1.5.5 Radiological Impact 11.1.5-2

Table of Contents (Continued)

11.1.6 Off-Normal Events Evaluation for Site Specific Spent Fuel 11.1.6-1
11.1.6.1 Off-Normal Events Evaluation for Maine Yankee Site Specific Spent Fuel 11.1.6-1

11.2 Accidents and Natural Phenomena 11.2-1
11.2.1 Accident Pressurization 11.2.1-1
11.2.1.1 Cause of Pressurization 11.2.1-1
11.2.1.2 Detection of Accident Pressurization 11.2.1-1
11.2.1.3 Analysis of Accident Pressurization 11.2.1-1
11.2.1.4 Corrective Actions 11.2.1-4
11.2.1.5 Radiological Impact 11.2.1-4
11.2.2 Failure of All Fuel Rods With a Ground Level Breach of the Canister 11.2.2-1
11.2.3 Fresh Fuel Loading in the Canister 11.2.3-1
11.2.3.1 Cause of Fresh Fuel Loading 11.2.3-1
11.2.3.2 Detection of Fresh Fuel Loading 11.2.3-1
11.2.3.3 Analysis of Fresh Fuel Loading 11.2.3-1
11.2.3.4 Corrective Actions 11.2.3-2
11.2.3.5 Radiological Impact 11.2.3-2
11.2.4 24-Inch Drop of Vertical Concrete Cask 11.2.4-1
11.2.4.1 Cause of 24-Inch Cask Drop 11.2.4-1
11.2.4.2 Detection of 24-Inch Cask Drop 11.2.4-1
11.2.4.3 Analysis of 24-Inch Cask Drop 11.2.4-2
11.2.4.4 Corrective Actions 11.2.4-12
11.2.4.5 Radiological Impact 11.2.4-12
11.2.5 Explosion 11.2.5-1
11.2.5.1 Cause of Explosion 11.2.5-1
11.2.5.2 Analysis of Explosion 11.2.5-1
11.2.5.3 Corrective Actions 11.2.5-1
11.2.5.4 Radiological Impact 11.2.5-1
11.2.6 Fire Accident 11.2.6-1
11.2.6.1 Cause of Fire 11.2.6-1
11.2.6.2 Detection of Fire 11.2.6-1
11.2.6.3 Analysis of Fire 11.2.6-1

Table of Contents (Continued)

11.2.6.4 Corrective Actions 11.2.6-3
11.2.6.5 Radiological Impact 11.2.6-3
11.2.7 Maximum Anticipated Heat Load (133°F Ambient Temperature) 11.2.7-1
1.2.7.1 Cause of Maximum Anticipated Heat Load 11.2.7-1
11.2.7.2 Detection of Maximum Anticipated Heat Load 11.2.7-1
11.2.7.3 Analysis of Maximum Anticipated Heat Load 11.2.7-1
11.2.7.4 Corrective Actions 11.2.7-2
11.2.7.5 Radiological Impact 11.2.7-2
11.2.8 Earthquake Event 11.2.8-1
11.2.8.1 Cause of the Earthquake Event 11.2.8-1
11.2.8.2 Earthquake Event Analysis 11.2.8-1
11.2.8.3 Corrective Actions 11.2.8-8
11.2.8.4 Radiological Impact 11.2.8-8
11.2.9 Flood 11.2.9-1
11.2.9.1 Cause of Flood 11.2.9-1
11.2.9.2 Analysis of Flood 11.2.9-1
11.2.9.3 Corrective Actions 11.2.9-5
11.2.9.4 Radiological Impact 11.2.9-5
11.2.10 Lightning Strike 11.2.10-1
11.2.10.1 Cause of Lightning Strike 11.2.10-1
11.2.10.2 Detection of Lightning Strike 11.2.10-1
11.2.10.3 Analysis of the Lightning Strike Event 11.2.10-1
11.2.10.4 Corrective Actions 11.2.10-4
11.2.10.5 Radiological Impact 11.2.10-4
11.2.11 Tornado and Tornado Driven Missiles 11.2.11-1
11.2.11.1 Cause of Tornado and Tornado Driven Missiles 11.2.11-1
11.2.11.2 Detection of Tornado and Tornado Driven Missiles 11.2.11-1
11.2.11.3 Analysis of Tornado and Tornado Driven Missiles 11.2.11-1
11.2.11.4 Corrective Actions 11.2.11-13
11.2.11.5 Radiological Impact 11.2.11-13
11.2.12 Tip-Over of Vertical Concrete Cask 11.2.12-1
11.2.12.1 Cause of Cask Tip-Over 11.2.12-1
11.2.12.2 Detection of Cask Tip-Over 11.2.12-1
11.2.12.3 Analysis of Cask Tip-Over 11.2.12-1
11.2.12.4 Analysis of Canister and Basket for Cask Tip-Over Event 11.2.12-11

Table of Contents (Continued)

11.2.12.5 Corrective Actions 11.2.12-69
11.2.12.6 Radiological Impact 11.2.12-69
11.2.13 Full Blockage of Vertical Concrete Cask Air Inlets and Outlets 11.2.13-1
11.2.13.1 Cause of Full Blockage 11.2.13-1
11.2.13.2 Detection of Full Blockage 11.2.13-1
11.2.13.3 Analysis of Full Blockage 11.2.13-1
11.2.13.4 Corrective Actions 11.2.13-2
11.2.13.5 Radiological Impact 11.2.13-2
11.2.14 Canister Closure Weld Evaluation 11.2.14-1
11.2.15 Accident and Natural Phenomena Events Evaluation for Site Specific Spent Fuel 11.2.15-1
11.2.15.1 Accident and Natural Phenomena Events Evaluation for Maine Yankee Site Specific Spent Fuel 11.2.15-1
11.2.16 Damaged Fuel Assembly Hardware Evaluation 11.2.16-1

11.3 References 11.3-1

List of Figures

Figure 11.1.1-1 Concrete Temperature (°F) for Off-Normal Storage Condition 106°F Ambient Temperature (PWR Fuel) 11.1.1-3
Figure 11.1.1-2 Vertical Concrete Cask Air Temperature (°F) Profile for Off-Normal Storage Condition 106°F Ambient Temperature (PWR) Fuel) 11.1.1-4
Figure 11.1.1-3 Concrete Temperature (°F) for Off-Normal Storage Condition -40°F Ambient Temperature (PWR Fuel) 11.1.1-5
Figure 11.1.1-4 Vertical Concrete Cask Air Temperature (°F) Profile for Off-Normal Storage Condition -40°F Ambient Temperature (PWR Fuel) 11.1.1-6
Figure 11.1.3.1-1 Canister Finite Element Model 11.1.3-4
Figure 11.2.4-1 Concrete Cask Base Weldment 11.2.4-13
Figure 11.2.4-2 Concrete Cask Base Weldment Finite Element Model 11.2.4-14
Figure 11.2.4-3 Strain Rate Dependent Stress-Strain Curves for Concrete Cask Base Weldment Structural Steel 11.2.4-15
Figure 11.2.4-4 Acceleration Time-History of the Canister Bottom During the Concrete Cask 24-Inch Drop Accident With Static Strain Properties 11.2.4-16
Figure 11.2.4-5 Acceleration Time-History of the Canister Bottom During the Concrete Cask 24-Inch Drop Accident With Strain Rate Dependent Properties 11.2.4-17
Figure 11.2.4-6 Quarter Model of the PWR Basket Support Disk 11.2.4-18
Figure 11.2.4-7 Quarter Model of the BWR Basket Support Disk 11.2.4-19
Figure 11.2.4-8 Canister Finite Element Model for 60g Bottom End Impact 11.2.4-20
Figure 11.2.4-9 Identification of the Canister Section for the Evaluation of Canister Stresses due to a 60g Bottom End Impact 11.2.4-21
Figure 11.2.6-1 Temperature Boundary Condition Applied to the Nodes of the Inlet for the Fire Accident Condition 11.2.6-4
Figure 11.2.11-1 Principal Dimensions and Moment Arms Used in Tornado Evaluation 11.2.11-14
Figure 11.2.12.4.1-1 Basket Drop Orientations Analyzed for Tip-Over Conditions – PWR 11.2.12-26
Figure 11.2.12.4.1-2 Fuel Basket/Canister Finite Element Model – PWR 11.2.12-27
Figure 11.2.12.4.1-3 Fuel Basket/Canister Finite Element Model – Canister 11.2.12-28
Figure 11.2.12.4.1-4 Fuel Basket/Canister Finite Element Model – Support Disk – PWR 11.2.12-29

List of Figures (Continued)

Figure 11.2.12.4.1-5 Fuel Basket/Canister Finite Element Model – Support Disk Loading – PWR 11.2.12-30
Figure 11.2.12.4.1-6 Canister Section Stress Locations 11.2.12-31
Figure 11.2.12.4.1-7 Support Disk Section Stress Locations – PWR – Full Model 11.2.12-32
Figure 11.2.12.4.1-8 PWR – 109.7 Hz Mode Shape 11.2.12-33
Figure 11.2.12.4.1-9 PWR – 370.1 Hz Mode Shape 11.2.12-34
Figure 11.2.12.4.1-10 PWR – 371.1 Hz Mode Shape 11.2.12-35
Figure 11.2.12.4.2-1 Fuel Basket Drop Orientations Analyzed for Tip-Over Condition – BWR 11.2.12-52
Figure 11.2.12.4.2-2 Fuel Basket/Canister Finite Element Model – BWR 11.2.12-53
Figure 11.2.12.4.2-3 Fuel Basket/Canister Finite Element Model – Support Disk – BWR 11.2.12-54
Figure 11.2.12.4.2-4 Support Disk Section Stress Locations – BWR – Full Model 11.2.12-55
Figure 11.2.12.4.2-5 BWR – 79.3 Hz Mode Shape 11.2.12-56
Figure 11.2.12.4.2-6 BWR – 80.2 Hz Mode Shape 11.2.12-57
Figure 11.2.12.4.2-7 BWR – 210.9 Hz Mode Shape 11.2.12-58
Figure 11.2.13-1 PWR Configuration Temperature History—All Vents Blocked 11.2.13-3
Figure 11.2.13-2 BWR Configuration Temperature History—All Vents Blocked 11.2.13-3
Figure 11.2.15.1.2-1 Two-Dimensional Support Disk Model 11.2.15-9
Figure 11.2.15.1.2-2 PWR Basket Impact Orientations and Case Study Loading Positions for Maine Yankee Consolidated Fuel 11.2.15-10
Figure 11.2.15.1.5-1 Two-Dimensional Beam Finite Element Model for Maine Yankee Fuel Rod 11.2.15-27
Figure 11.2.15.1.5-2 Mode Shape and First Buckling Shape for the Maine Yankee Fuel Rod 11.2.15-28
Figure 11.2.16-1 Two-Dimensional Beam FEM for Fuel Rod with Missing Grid 11.2.16-2
Figure 11.2.16-2 Modal Shape and First Buckling Mode Shape for a Fuel Rod with a Missing Grid 11.2.16-3

List of Tables

Table 11.1.2-1 Component Temperatures (°F) for Half of Inlets Blocked Off-Normal Event 11.1.2-3
Table 11.1.3-1 Canister Off-Normal Handling (No Internal Pressure) Primary Membrane (P_m) Stresses (ksi) 11.1.3-5
Table 11.1.3-2 Canister Off-Normal Handling (No Internal Pressure) Primary Membrane plus Bending ($P_m + P_b$) Stresses (ksi) 11.1.3-6
Table 11.1.3-3 Canister Off-Normal Handling plus Normal/Off-Normal Internal Pressure (15 psig) Primary Membrane (P_m) Stresses (ksi) 11.1.3-7
Table 11.1.3-4 Canister Off-Normal Handling plus Normal/Off-Normal Internal Pressure (15 psig) Primary Membrane plus Bending ($P_m + P_b$) Stresses (ksi) 11.1.3-8
Table 11.1.3-5 Canister Off-Normal Handling plus Normal/Off-Normal Internal Pressure (15 psig) Primary plus Secondary (P + Q) Stresses (ksi) 11.1.3-9
Table 11.1.3-6 P_m Stresses for PWR Support Disk Off-Normal Conditions (ksi) 11.1.3-10
Table 11.1.3-7 $P_m + P_b$ Stresses for PWR Support Disk Off-Normal Conditions (ksi) 11.1.3-11
Table 11.1.3-8 $P_m + P_b + Q$ Stresses for PWR Support Disk Off-Normal Conditions (ksi) 11.1.3-12
Table 11.1.3-9 P_m Stresses for BWR Support Disk Off-Normal Conditions (ksi) 11.1.3-13
Table 11.1.3-10 $P_m + P_b$ Stresses for BWR Support Disk Off-Normal Conditions (ksi) 11.1.3-14
Table 11.1.3-11 $P_m + P_b + Q$ Stresses for BWR Support Disk Off-Normal Conditions (ksi) 11.1.3-15
Table 11.1.3-12 Summary of Maximum Stresses for PWR and BWR Fuel Basket Weldments - Off-Normal Condition (ksi) 11.1.3-16
Table 11.2.1-1 Canister Accident Internal Pressure (65 psig) Only Primary Membrane (P_m) Stresses (ksi). 11.2.1-5
Table 11.2.1-2 Canister Accident Internal Pressure (65 psig) Only Primary Membrane plus Bending ($P_m + P_b$) Stresses (ksi) 11.2.1-6
Table 11.2.1-3 Canister Normal Handling plus Accident Internal Pressure (65 psig) Primary Membrane (P_m) Stresses (ksi). 11.2.1-7

List of Tables (Continued)

Table 11.2.1-4 Canister Normal Handling plus Accident Internal Pressure (65 psig) Primary Membrane plus Bending ($P_m + P_b$) Stresses (ksi). 11.2.1-8
Table 11.2.4-1 PWR Canister P_m Stresses During a 60g Bottom Impact (25 psig Internal Pressure) 11.2.4-22
Table 11.2.4-2 PWR Canister $P_m + P_b$ Stresses During a 60g Bottom Impact (25 psig Internal Pressure) 11.2.4-23
Table 11.2.4-3 BWR Canister P_m Stresses During a 60g Bottom Impact (25 psig Internal Pressure) 11.2.4-24
Table 11.2.4-4 BWR Canister $P_m + P_b$ Stresses During a 60g Bottom Impact (25 psig Internal Pressure) 11.2.4-25
Table 11.2.4-5 Summary of Maximum Stresses for PWR and BWR Basket Weldments During a 60g Bottom Impact 11.2.4-26
Table 11.2.4-6 PWR Canister P_m Stresses During a 60g Bottom Impact (No Internal Pressure) 11.2.4-26
Table 11.2.4-7 BWR Canister P_m Stresses During a 60g Bottom Impact (No Internal Pressure) 11.2.4-27
Table 11.2.4-8 Canister Buckling Evaluation Results for 60g Bottom End Impact 11.2.4-28
Table 11.2.4-9 $P_m + P_b$ Stresses for PWR Support Disk - 60g Concrete Cask Bottom End Impact (ksi) 11.2.4-29
Table 11.2.4-10 $P_m + P_b$ Stresses for BWR Support Disk - 60g Concrete Cask Bottom End Impact (ksi) 11.2.4-30
Table 11.2.6-1 Maximum Component Temperatures (°F) During and After the Fire Accident 11.2.6-5
Table 11.2.9-1 Canister Increased External Pressure (22 psi) with No Internal Pressure (0 psi) Primary Membrane (P_m) Stresses (ksi). 11.2.9-6
Table 11.2.9-2 Canister Increased External Pressure (22 psi) with No Internal Pressure (0 psi) Primary Membrane plus Bending ($P_m + P_b$) Stresses (ksi). 11.2.9-7
Table 11.2.12.4.1-1 Canister Primary Membrane (P_m) Stresses for Tip-Over Conditions – PWR - 45° Basket Drop Orientation (ksi) 11.2.12-36

List of Tables (Continued)

Table 11.2.12.4.1-2 Canister Primary Membrane + Primary Bending ($P_m + P_b$) Stresses for Tip-Over Conditions – PWR - 45° Basket Drop Orientation (ksi) 11.2.12-37

Table 11.2.12.4.1-3 Support Disk Section Location for Stress Evaluation – PWR – Full Model 11.2.12-38

Table 11.2.12.4.1-4 Summary of Maximum Stresses for PWR Support Disk for Tip-Over Condition 11.2.12-39

Table 11.2.12.4.1-5 Summary of Buckling Evaluation of PWR Support Disk for Tip-Over Condition 11.2.12-39

Table 11.2.12.4.1-6 Support Disk Primary Membrane (P_m) Stresses for Tip-Over Condition – PWR Disk No. 5 – 26.28° Drop Orientation (ksi) 11.2.12-40

Table 11.2.12.4.1-7 Support Disk Primary Membrane + Primary Bending ($P_m + P_b$) Stresses for Tip-Over Condition – PWR Disk No. 5 – 26.28° Drop Orientation (ksi) 11.2.12-41

Table 11.2.12.4.1-8 Summary of Support Disk Buckling Evaluation for Tip-Over Condition – PWR Disk No.5 – 26.28° Drop Orientation 11.2.12-42

Table 11.2.12.4.2-1 Canister Primary Membrane (P_m) Stresses for Tip-Over Conditions – BWR - 49.46° Basket Drop Orientation (ksi) 11.2.12-59

Table 11.2.12.4.2-2 Canister Primary Membrane + Primary Bending ($P_m + P_b$) Stresses for Tip-Over Conditions – BWR – 49.46° Basket Drop Orientation (ksi) 11.2.12-60

Table 11.2.12.4.2-3 Support Disk Section Locations for Stress Evaluation – BWR – Full Model 11.2.12-61

Table 11.2.12.4.2-4 Summary of Maximum Stresses for BWR Support Disk for Tip-Over Condition 11.2.12-65

Table 11.2.12.4.2-5 Summary of Buckling Evaluation of BWR Support Disk for Tip-Over Condition 11.2.12-65

Table 11.2.12.4.2-6 Support Disk Primary Membrane (P_m) Stresses for Tip-Over Condition – BWR Disk No.5 – 77.92° Drop Orientation (ksi) 11.2.12-66

Table 11.2.12.4.2-7 Support Disk Primary Membrane + Primary Bending (P_m+P_b) Stresses for Tip-Over Condition – BWR Disk No.5 – 77.92° Drop Orientation (ksi) 11.2.12-67

List of Tables (Continued)

Table 11.2.12.4.2-8 Summary of Support Disk Buckling Evaluation for Tip-Over Condition – BWR Disk No.5 – 77.92° Drop Orientation 11.2.12-68

Table 11.2.15.1.2-1 Normalized Stress Ratios – PWR Basket Support Disk Maximum Stresses 11.2.15-11

Table 11.2.15.1.2-2 Support Disk Primary Membrane (P_m) Stresses for Case 4, 26.28° Drop Orientation (ksi) 11.2.15-12

Table 11.2.15.1.2-3 Support Disk Primary Membrane + Primary Bending ($P_m + P_b$) Stresses for Case 4, 26.28° Drop Orientation (ksi)..... 11.2.15-13

11.0 ACCIDENT ANALYSES

The analyses of the off-normal and accident design events, including those identified by ANSI/ANS 57.9-1992 [1], are presented in this chapter. Section 11.1 describes the off-normal events that could occur during the use of the Universal Storage System, possibly as often as once per calendar year. Section 11.2 addresses very low probability events that might occur once during the lifetime of the ISFSI or hypothetical events that are postulated because their consequences may result in the maximum potential impact on the surrounding environment.

The Universal Storage System includes Transportable Storage Canisters and Vertical Concrete Casks of five different lengths to accommodate three classes of PWR fuel or two classes of BWR fuel. In the analyses of this chapter, the bounding concrete cask parameters (such as weight and center of gravity) are conservatively used, as appropriate, to determine the cask's capability to withstand the effects of the analyzed events.

The load conditions imposed on the canisters and the baskets by the design basis normal, off-normal, and accident conditions of storage are less rigorous than those imposed by the transport conditions–including the 30-foot drop impacts and the fire accident (10 CFR 71) [2]. Consequently, the evaluation of the canisters and the baskets for transport conditions bounds those for storage conditions evaluated in this chapter. A complete evaluation of the normal and accident transport condition loading on the PWR and BWR canisters and the baskets is presented in the Safety Analysis Report for the Universal Transport Cask. [3]

This chapter demonstrates that the Universal Storage System satisfies the requirements of 10 CFR 72.24 and 10 CFR 72.122 [4] for off-normal and accident conditions. These analyses are based on conservative assumptions to ensure that the consequences of off-normal conditions and accident events are bounded by the reported results. If required for a site specific application, a more detailed evaluation could be used to extend the limits defined by the events evaluated in this chapter.

THIS PAGE INTENTIONALLY LEFT BLANK

11.1 Off-Normal Events

This section evaluates postulated events that might occur once during any calendar year of operations. The actual occurrence of any of these events is, therefore, infrequent.

11.1.1 Severe Ambient Temperature Conditions (106°F and -40°F)

This section evaluates the Universal Storage System for the steady state effects of severe ambient temperature conditions (106°F and -40°F).

11.1.1.1 Cause of Severe Ambient Temperature Event

Large geographical areas of the United States are subjected to sustained summer temperatures in the 90°F to 100°F range and winter temperatures that are significantly below zero. To bound the expected steady state temperatures of the canister and storage cask during these severe ambient conditions, analyses are performed to calculate the steady state storage cask, canister, and fuel cladding temperatures for a 106°F ambient temperature and solar loads (see Table 4.1-1). Similarly, winter weather analyses are performed for a -40°F ambient temperature with no solar load. Neither ambient temperature condition is expected to last more than several days.

11.1.1.2 Detection of Severe Ambient Temperature Event

Detection of off-normal ambient temperatures would occur during the daily measurement of ambient temperature and storage cask outlet air temperature.

11.1.1.3 Analysis of Severe Ambient Temperature Event

Off-normal temperature conditions are evaluated by using the thermal models described in Section 4.4.1. The design basis heat load of 23.0 kW is used in the evaluation of PWR and BWR fuels. The concrete temperatures are determined using the two-dimensional axisymmetric air flow and concrete cask models (Section 4.4.1.1) and the canister, basket and fuel cladding temperatures are determined using the three-dimensional canister models (Section 4.4.1.2). A steady state condition is considered in all analyses. The temperature profiles for the concrete cask and for the air flow associated with a 106°F ambient condition are shown in Figure 11.1.1-1 and Figure 11.1.1-2, respectively. Temperature profiles for the -40°F ambient temperature condition for the PWR fuel

are shown in Figure 11.1.1-3 and Figure 11.1.1-4. Temperature profiles for the BWR cask are similar.

The principal component temperatures for each of the ambient temperature conditions discussed above are summarized in the following table along with the allowable temperatures. As the table shows, the component temperatures are within the allowable values for the off-normal ambient conditions.

Component	106°F Ambient Max Temp. (°F)		-40°F Ambient Max Temp. (°F)		Allowable Temp. (°F)	
	PWR	BWR	PWR	BWR	PWR	BWR
Fuel Cladding	694	677	584	548	1058	1058
Support Disks	642	651	521	515	800	700
Heat Transfer Disks	638	648	516	513	700	700
Canister Shell	381	405	226	252	800	800
Concrete	228	231	17	20	350	350

The thermal stress evaluations for the concrete cask for these off-normal conditions are bounded by those for the accident condition of "Maximum Anticipated Heat Load (133°F ambient temperature)" as presented in Section 11.2.7. Thermal stress analyses for the canister and basket components are performed using the ANSYS finite element models as described in Section 3.4.4. Evaluations of the thermal stresses combined with the stresses due to other off-normal loads (e.g., canister internal pressure and handling) are shown in Section 11.1.3.

There are no adverse consequences for these off-normal conditions. The maximum component temperatures are within the allowable temperature values.

11.1.1.4 Corrective Actions

No corrective actions are required for this off-normal condition.

11.1.1.5 Radiological Impact

There is no radiological impact due to this off-normal event.

Figure 11.1.1-1 Concrete Temperature (°F) for Off-Normal Storage Condition 106°F Ambient Temperature (PWR Fuel)

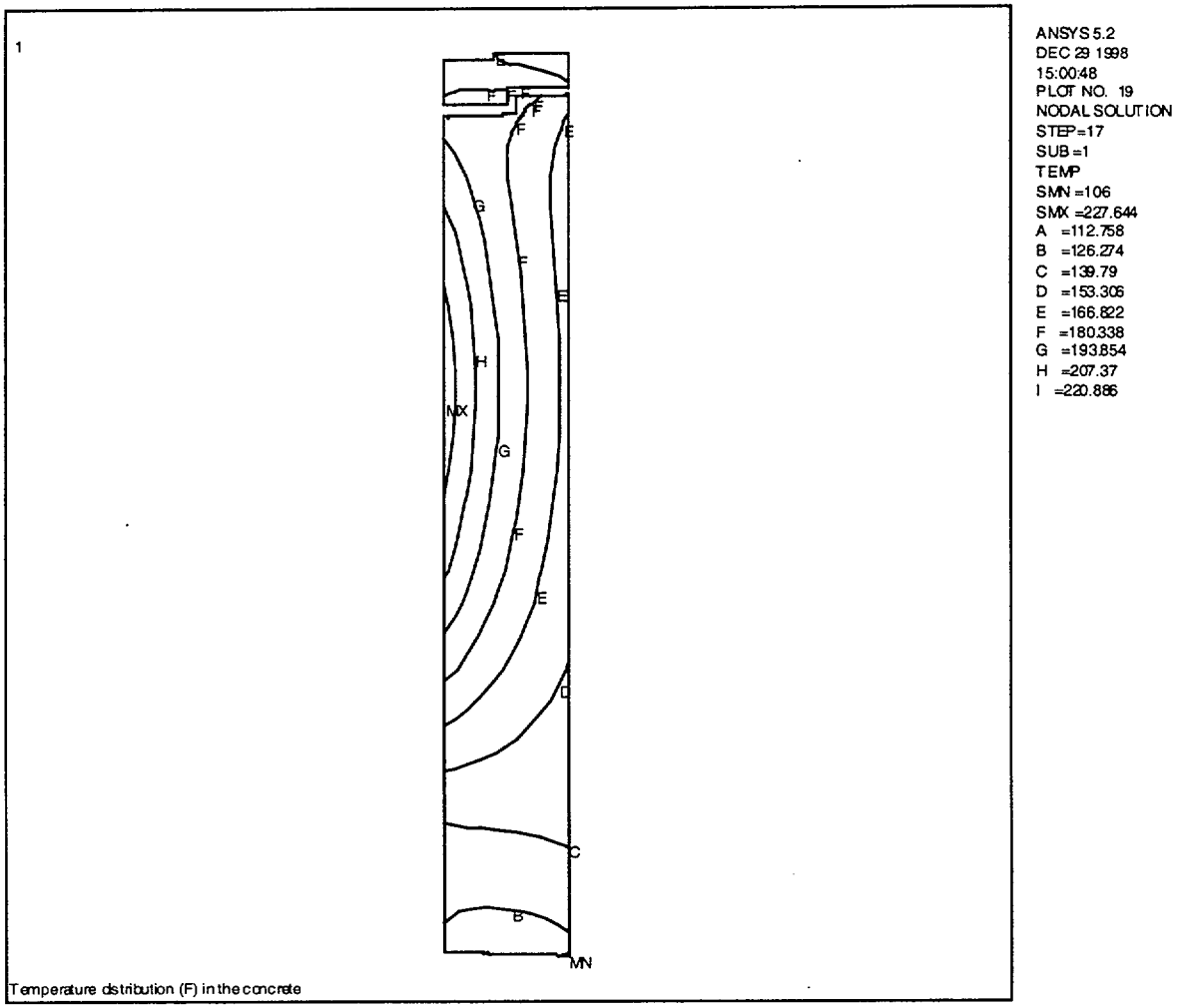

Figure 11.1.1-2 Vertical Concrete Cask Air Temperature (°F) Profile for Off-Normal Storage Condition 106°F Ambient Temperature (PWR Fuel)

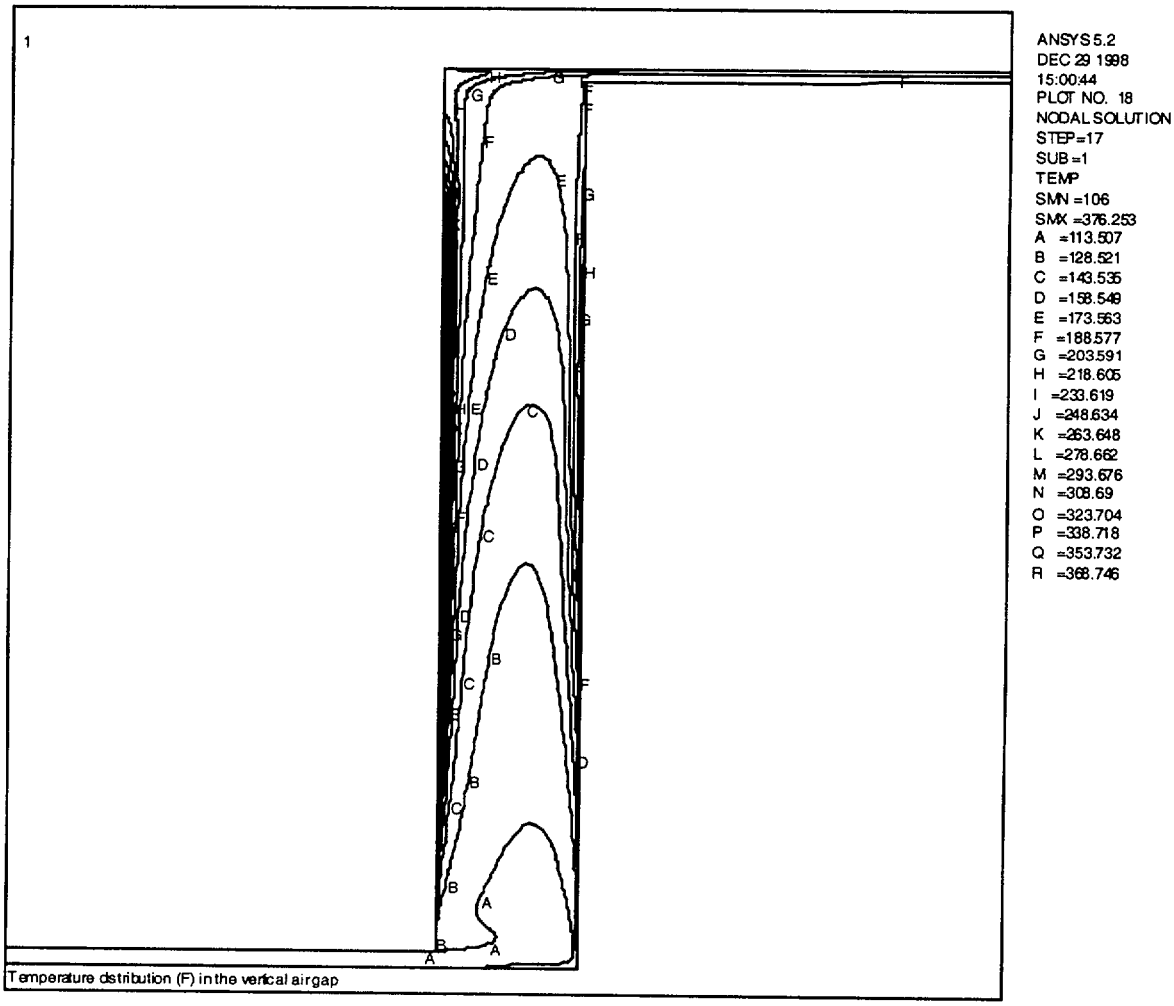

Figure 11.1.1-3 Concrete Temperature (°F) for Off-Normal Storage Condition -40°F Ambient Temperature (PWR Fuel)

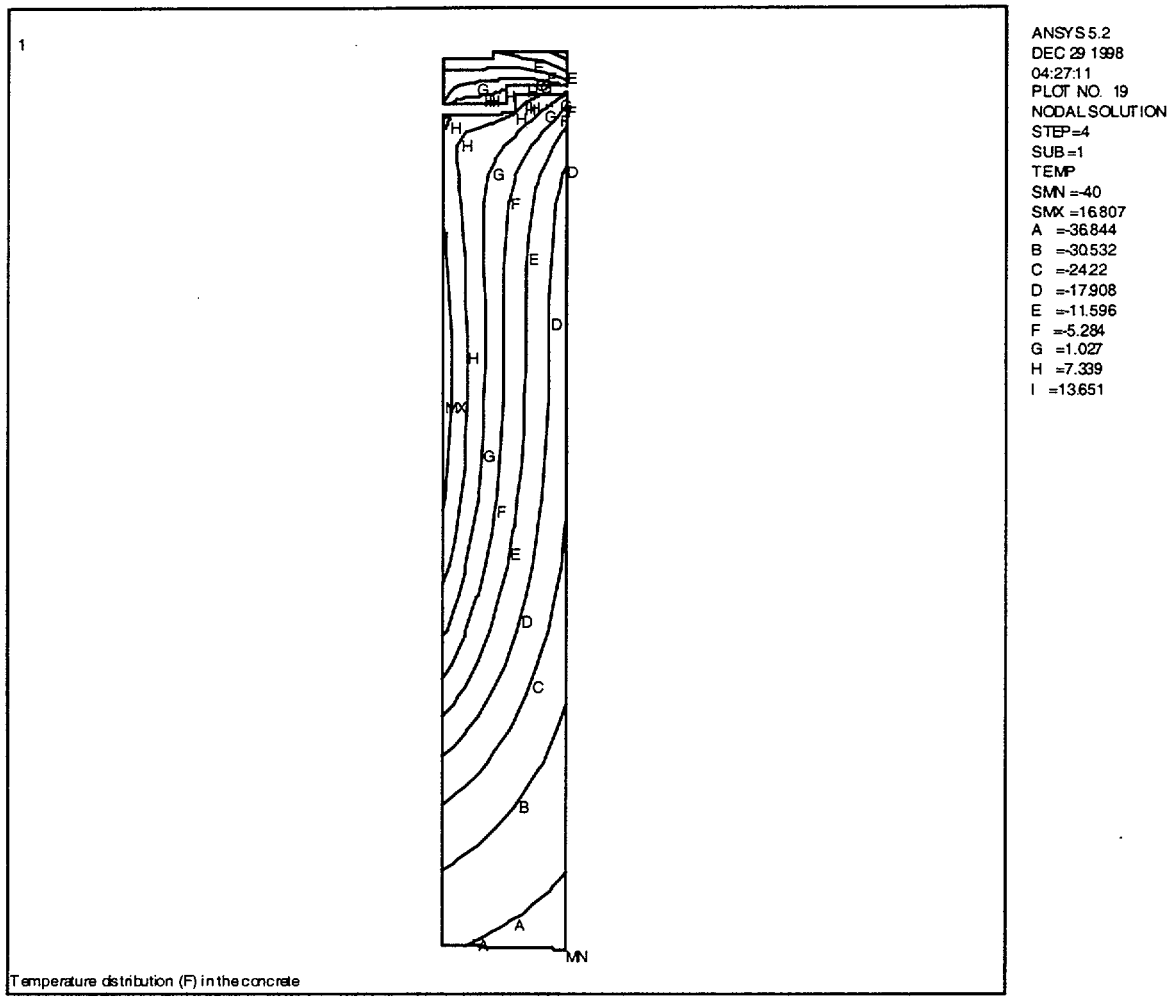

Figure 11.1.1-4 Vertical Concrete Cask Air Temperature (°F) Profile for Off-Normal Storage Condition -40°F Ambient Temperature (PWR Fuel)

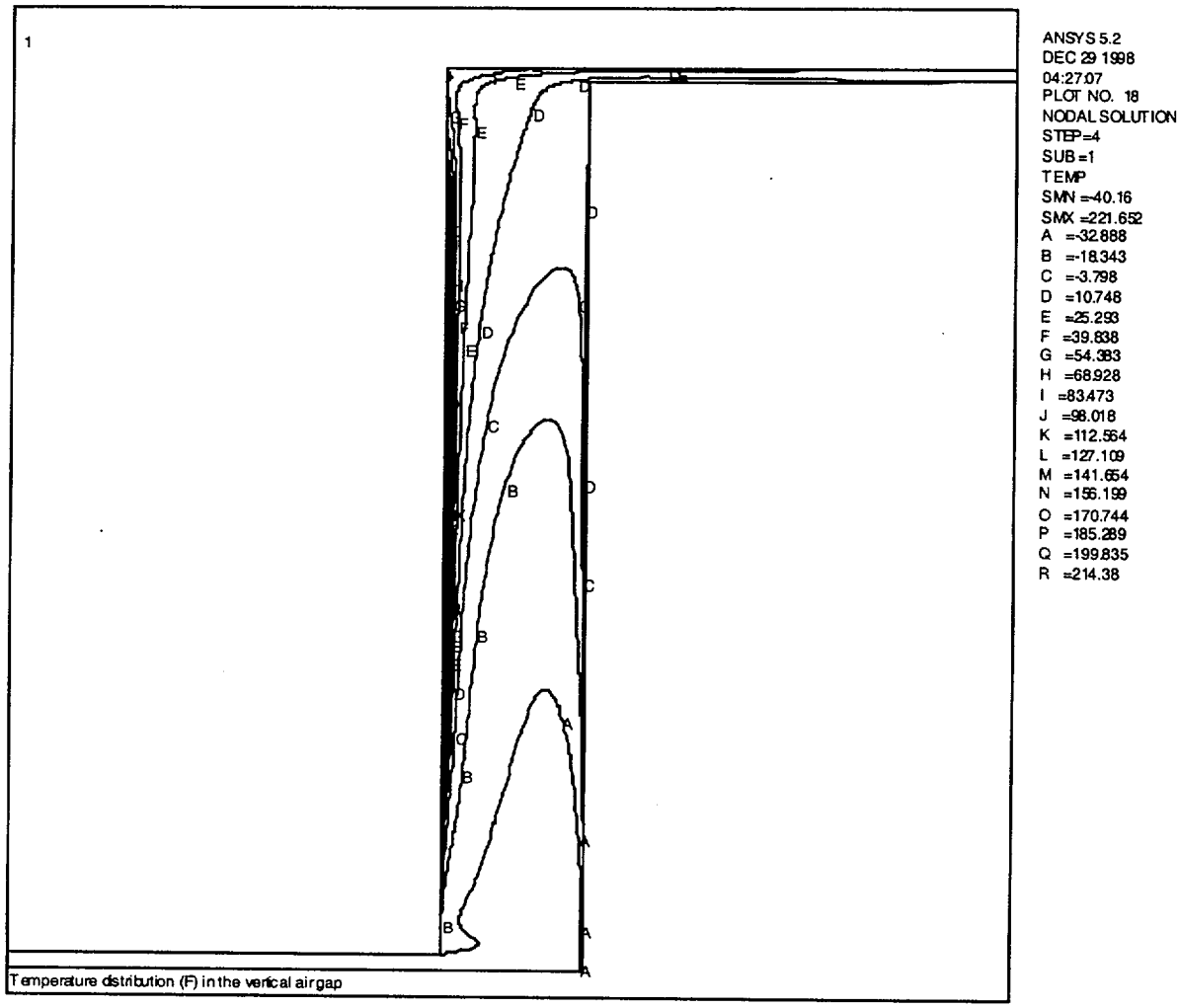

11.1.2 Blockage of Half of the Air Inlets

This section evaluates the Universal Storage System for the steady state effects of a blockage of one-half of the air inlets at the normal ambient temperature (76°F).

11.1.2.1 Cause of the Blockage Event

Although unlikely, blockage of half of the air inlets may occur due to blowing debris, snow, intrusion of a burrowing animal, etc. The screens over the inlets are expected to minimize any blockage of the inlet channels.

11.1.2.2 Detection of the Blockage Event

This event would be detected visually by the persons inspecting the air inlets and gathering outlet air temperature data on a daily basis. It could also be detected by security forces, or other operations personnel, engaged in other routine activities such as fence inspection, or grounds maintenance.

11.1.2.3 Analysis of the Blockage Event

Using the same methods and the same thermal models described in Section 11.1.1 for the off-normal conditions of severe ambient temperatures, thermal evaluations are performed for the concrete cask and the canister and its contents for this off-normal condition. The boundary condition of the two-dimensional axisymmetric air flow and concrete cask model is modified to allow only half of the air flow into the air inlet to simulate the half inlets blocked condition. The calculated maximum component temperatures due to this off-normal condition are compared to the allowable component temperatures. Table 11.1.2-1 summarizes the component temperatures for off-normal conditions. As the table demonstrates, the calculated temperatures are shown to be below the component allowable temperatures.

The thermal stress evaluations for the concrete cask for this off-normal condition are bounded by those for the accident condition of "Maximum Anticipated Heat Load (133°F ambient temperature)" as presented in Section 11.2.7. Thermal stress analyses for the canister and basket components are performed using the ANSYS finite element models described in Section 3.4.4. Evaluations of the thermal stresses combined with stresses due to other off-normal loads (e.g., canister internal pressure and handling) are shown in Section 11.1.3.

11.1.2.4 Corrective Actions

The debris blocking the affected air inlets must be manually removed. The nature of the debris may indicate that other actions are required to prevent recurrence of the blockage.

11.1.2.5 Radiological Impact

There are no significant radiological consequences for this event. Personnel will be subject to an estimated maximum contact dose rate of 66 mrem/hr when clearing the PWR cask inlets. If it is assumed that a worker kneeling with his hands on the inlets would require 15 minutes to clear the inlets, the estimated maximum extremity dose is 17 mrem. For clearing the BWR cask inlets, the maximum contact dose rate and the maximum extremity dose are estimated to be 51 mrem/hr and 13 mrem, respectively. The whole body dose in both PWR and BWR cases will be significantly less.

Table 11.1.2-1 Component Temperatures (°F) for Half of Inlets Blocked Off-Normal Event

Component	Half of Inlets Blocked Max Temperature (°F)		Allowable Temperature (°F)	
	PWR	BWR	PWR	BWR
Fuel Cladding	671	652	1058	1058
Support Disks	617	625	800	700
Heat Transfer Disks	613	622	700	700
Canister Shell	350	374	800	800
Concrete	191	195	350	350

THIS PAGE INTENTIONALLY LEFT BLANK

11.1.3 Off-Normal Canister Handling Load

This section evaluates the consequence of loads on the Transportable Storage Canister during the installation of the canister in the Vertical Concrete Cask, or removal of the canister from the concrete cask or from the transfer cask.

11.1.3.1 Cause of Off-Normal Canister Handling Load Event

Unintended loads could be applied to the canister due to misalignment or faulty crane operation, or inattention of the operators.

11.1.3.2 Detection of Off-Normal Canister Handling Load Event

The event can be detected visually during the handling of the canister, or banging or scraping noise associated with the canister movement. The event is expected to be obvious to the operators at the time of occurrence.

11.1.3.3 Analysis of Off-Normal Canister Handling Load Event

The canister structural analysis, including lifting loads, is performed by using an ANSYS finite element model as shown in Figure 11.1.3.1-1. The model is based on the canister model presented in Section 3.4.4.1 with the elements fuel basket (support disks and top and bottom weldment disks) added. The disks are modeled with SHELL63 elements. These elements are included to transfer loads from the basket to the canister shell for horizontal loading conditions. The interface between the disks and the canister shell is simulated by CONTAC52 elements. For the horizontal loading conditions, uniform pressure loads representing the weight (including appropriate g-loading) of the fuel assemblies, fuel tubes, heat transfer disks, tie-rods, spacers, washers, and nuts are applied to the slots of the support/weldment disks. Interaction between the fuel basket and the canister during vertical load conditions is modeled by applying a uniform pressure representing the weight of the fuel assemblies and basket (including appropriate g-loading) to the canister bottom plate. The model is used to evaluate the canisters for both PWR and BWR fuel types by modeling the shortest canister (Class 1 PWR) with the heaviest fuel/fuel basket weight (Class 5 BWR).

The off-normal canister handling loads are defined as 0.5g applied in all directions (i.e., in the global x, y, and z directions) in addition to a 1g lifting load applied in the finite element model. The resulting off-normal handling accelerations are 0.7071g in the lateral direction and 1.5g(0.5g + 1g) in the vertical direction.

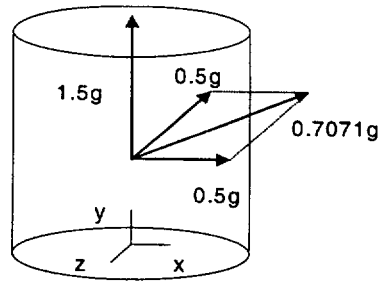

The boundary conditions (restraints) for the canister model are the same as those described in Section 3.4.4.1.4 for the normal handling condition. In addition, for the lateral loading, the canister is assumed to be handled inside the vertical concrete cask. The interface between the canister shell and the concrete cask inner surface is represented using CONTAC52 elements.

The resulting maximum canister stresses for off-normal handling loads are summarized in Tables 11.1.3-1 and 11.1.3-2 for primary membrane and primary membrane plus bending stresses, respectively.

The resulting maximum canister stresses for combined off-normal handling, maximum off-normal internal pressure (15 psig), and thermal stress loads are summarized in Tables 11.1.3-3, 11.1.3-4, and 11.1.3-5 for primary membrane, primary membrane plus bending, and primary plus secondary stresses, respectively.

The sectional stresses shown in Tables 11.1.3-1 through 11.1.3-5 at 16 axial locations are obtained for each angular division of the model (a total of 19 angular locations for each axial location). The locations of the stress sections are shown in Figure 3.4.4.1-4.

To determine the structural adequacy of the PWR and BWR fuel basket support disks and weldments for off-normal conditions, a structural analysis is performed by using ANSYS to evaluate off-normal handling loads (See Section 3.4.4.1.8.). To simulate off-normal loading conditions, an inertial load of 1.5g is applied to the support disk and the weldments in the axial (out of plane) direction and 0.5g in two orthogonal horizontal directions (0.7071g resultant).

Stresses in the support disks and weldments are calculated by applying the off-normal loads to the ANSYS models described in Sections 3.4.4.1.8 and 3.4.4.1.9. An additional in-plane displacement constraint is applied to each model at one node (conservative) at the periphery of the disk or the weldment plate to simulate the side restraint of the canister shell for the lateral load (0.7071g). To

evaluate the most critical regions of the support disks, a series of cross sections is considered. The locations of these sections on the PWR and BWR support disks are shown in Figures 3.4.4.1-7, 3.4.4.1-8, and Figures 3.4.4.1-13 through 3.4.4.1-16. The stress evaluation for the support disk and weldment is performed according to ASME Code, Section III, Subsection NG. For off-normal conditions, Level C allowable stresses are used: the allowable stress is 1.2 S_m or S_y, 1.8 S_m or 1.5S_y, and 3.0 S_m for the P_m, P_m+P_b, and P_m+P_b+Q stress categories, respectively. The stress evaluation results are presented in Tables 11.1.3-6 through 11.1.3-8 for the PWR support disks and in Tables 11.1.3-9 through 11.1.3-11 for the BWR support disks. The tables list the 40 sections with the highest P_m, P_m+P_b, and P_m+P_b+Q stress intensities. All of the support disk sections have large margins of safety. The stress results for the PWR and BWR weldments are shown in Table 11.1.3-12.

The canisters and fuel baskets maintain positive margins of safety for the off-normal handling condition. There is no deterioration of canister or fuel basket performance. The Universal Storage System is in compliance with all applicable regulatory criteria.

11.1.3.4 Corrective Actions

Operations should be halted until the cause of the misalignment, interference or faulty operation is identified and corrected. Since the radiation level of the canister sides and bottom is high, extreme caution should be exercised if inspection of these surfaces is required.

11.1.3.5 Radiological Impact

There are no radiological consequences associated with this off-normal event.

Figure 11.1.3.1-1 Canister Finite Element Model

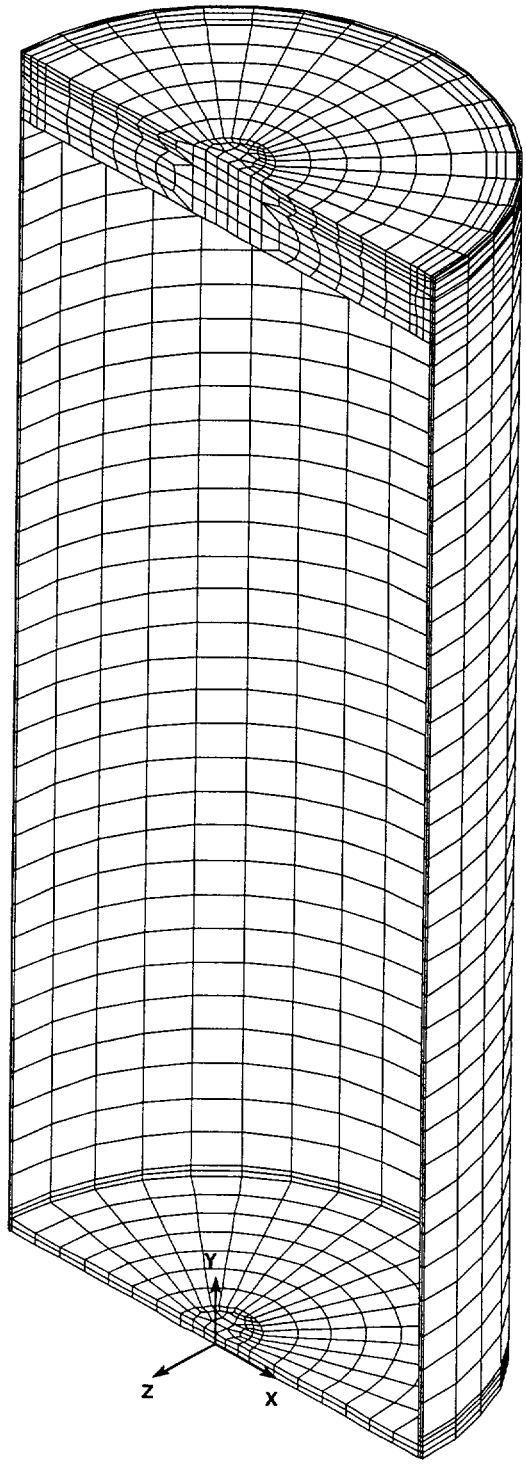

Table 11.1.3-1 Canister Off-Normal Handling (No Internal Pressure) Primary Membrane (P_m) Stresses (ksi)

Section No.[1]	Angle (degrees)	SX	SY	SZ	SXY	SYZ	SXZ	Stress Intensity
1	0	-0.7	3.7	0.7	0.2	0	-0.1	4.47
2	0	3.2	-1.7	-2.3	0.1	-0.1	-0.5	5.59
3	0	-0.3	1.7	-3.5	1.3	0.1	-0.1	5.85
4	0	-0.1	0.8	0	0.1	0	0	0.91
5	0	-0.1	0.8	0	0	0	0	0.85
6	0	-0.1	0.8	0	0	0	0	0.91
7	0	-0.1	0.9	0	0	0	0	1.08
8	0	0	1.9	0	0	0.2	0	1.95
9	0	0.4	2.8	0.7	0.2	0.3	0	2.46
10	0	-0.6	3.4	0.4	0.3	0.4	0.1	4.11
11	0	-0.6	2.5	1.1	-0.7	0.4	0	3.45
12	0	0	4	0.9	0.4	0.2	0.1	4.03
13	0	-2.3	-0.2	1.2	-1.6	0.1	0.1	4.44
14	80	0.2	0	0.3	0.3	-0.2	0	0.86
15	160	0	0	0	0	0	0	0.01
16	180	0	0	0	0	0	0	0.09

[1] See Figure 3.4.4.1-4 for definition of locations and angles of stress sections.

Table 11.1.3-2 Canister Off-Normal Handling (No Internal Pressure) Primary Membrane plus Bending ($P_m + P_b$) Stresses (ksi)

Section No.[1]	Angle (degrees)	SX	SY	SZ	SXY	SYZ	SXZ	Stress Intensity
1	0	5.6	9.7	1.6	0.8	0.2	-0.1	8.30
2	0	1.1	-16.2	-6.9	-0.9	-0.4	-0.8	17.53
3	0	-1.6	20.9	1.3	1.5	0.8	0.4	22.77
4	0	-0.2	0.9	0.2	0.1	0	0	1.02
5	20	0.0	0.7	-0.1	0	0	0	0.86
6	120	-0.2	0.7	-0.1	0	0	0.1	0.95
7	0	-0.2	1.0	0.1	0	0	0	1.14
8	0	0	1.8	-0.1	0	0.2	0	1.99
9	0	-0.3	2.7	0.4	0.2	0.5	-0.1	3.08
10	0	-0.9	5.8	1.0	0.5	0.2	0.2	6.78
11	0	-1.0	1.9	1.2	-1.6	0.3	0	4.36
12	0	-1.0	5.3	0.9	0.4	0.2	0.2	6.35
13	0	-5.4	-1.8	0.9	-1.5	0	0.2	6.81
14	180	8.4	0.1	8.5	0.3	-0.3	0	8.43
15	30	-0.1	0	-0.1	0	0	0	0.13
16	0	1.0	0	1.1	0	0	0	1.09

[1] See Figure 3.4.4.1-4 for definition of locations and angles of stress sections.

Table 11.1.3-3 Canister Off-Normal Handling plus Normal/Off-Normal Internal Pressure (15 psig) Primary Membrane (P_m) Stresses (ksi)

Section No.[1]	Angle (degrees)	SX	SY	SZ	SXY	SYZ	SXZ	Stress Intensity	Stress Allowable[2]	Margin of Safety
1	0	-0.6	4.2	1.2	-0.2	0	0	4.83	21.93	3.54
2	0	3	-2.3	-3.6	-0.4	-0.1	-0.5	6.76	21.91	2.24
3	0	-0.5	1.6	-5.5	1.3	-0.1	-0.4	7.76	21.83	1.81
4	0	0	1.3	0.8	0	0	0.1	1.30	19.88	14.23
5	0	-0.1	1.2	0.8	0	0	0.1	1.27	18.49	13.51
6	0	-0.1	1.2	0.8	0	0	0.1	1.33	18.26	12.72
7	0	-0.2	1.3	0.7	0	0	0.1	1.50	19.28	11.85
8	0	0.1	2.4	0.5	-0.1	0.2	0.2	2.38	20.32	7.55
9	0	0.1	3.1	0.8	0.1	0.3	0.1	3.06	20.58	5.72
10	0	-0.5	3.8	0.7	0.1	0.4	0.1	4.32	20.59	3.77
11	0	-0.4	2.4	1.2	-0.7	0.3	0.1	3.17	20.67	5.53
12	0	-0.2	3.3	0.8	0.2	0.2	0.1	3.59	20.58	4.73
13	0	-1.7	-0.1	1.5	-1.5	0.1	0.2	4.12	20.67	4.02
14	80	0.4	0	0.5	0.5	-0.4	0	1.36	21.09	14.52
15	0	0	0	0	0	0	0	0.02	20.6	944.24
16	180	0	0	0.1	0	0	0	0.09	20.69	224.80

[1] See Figure 3.4.4.1-4 for definition of locations and angles of stress sections.

[2] ASME Service Level C is used for material allowable stress.

Table 11.1.3-4 Canister Off-Normal Handling plus Normal/Off-Normal Internal Pressure (15 psig) Primary Membrane plus Bending ($P_m + P_b$) Stresses (ksi)

Section No.[1]	Angle (degrees)	SX	SY	SZ	SXY	SYZ	SXZ	Stress Intensity	Stress Allowable[2]	Margin of Safety
1	0	4.9	10.6	0.7	0.3	0.0	-0.2	9.96	32.89	2.30
2	0	1.2	-18.9	-9.0	-1.3	-0.2	-0.9	20.32	32.86	0.62
3	0	-2.1	26.6	1.3	1.6	0.1	0.2	28.83	32.74	0.14
4	0	0.0	1.4	1.1	0.0	0	0.1	1.39	28.42	19.52
5	0	-0.1	1.2	0.8	0	0	0.1	1.28	25.60	18.99
6	0	-0.1	1.2	0.9	0	0	0.1	1.38	25.29	17.33
7	0	-0.2	1.4	1.0	0	0	0.1	1.59	27.00	16.00
8	0	0.2	2.8	0.7	-0.1	0.2	0.2	2.68	29.49	10.01
9	0	-0.1	3.8	0.8	0.1	0.4	0.0	3.94	30.10	6.65
10	0	-0.7	4.7	1.0	0.3	0.3	0.2	5.49	30.13	4.49
11	0	-0.7	2.3	1.4	-1.6	0.3	0	4.47	30.33	5.78
12	0	-0.8	4.3	0.9	0.2	0.3	0.2	5.14	30.11	4.86
13	0	-4.3	-1.6	1.2	-1.3	0	0.3	6.09	30.34	3.98
14	180	13.3	0.1	13.4	0.5	-0.4	0	13.32	31.34	1.35
15	0	-0.3	0	-0.3	0	0	0	0.28	30.15	107.19
16	0	1.0	0	1.1	0	0	0	1.12	30.37	26.02

(1) See Figure 3.4.4.1-4 for definition of locations and angles of stress sections.

(2) ASME Service Level C is used for material allowable stress.

Table 11.1.3-5 Canister Off-Normal Handling plus Normal/Off-Normal Internal Pressure (15 psig) Primary plus Secondary (P + Q) Stresses (ksi)

Section No.[1]	Angle (degrees)	SX	SY	SZ	SXY	SYZ	SXZ	Stress Intensity	Stress Allowable[2]	Margin of Safety
1	60	2.1	13.9	4.1	0.0	-0.3	-1.4	12.56	50.10	2.99
2	60	-7.5	-22.8	-1.4	-0.9	1.2	-5.2	24.47	50.10	1.05
3	60	0.7	30.5	-1.3	0.5	-1.5	1.7	32.92	50.10	0.52
4	0	-0.3	1.1	3.0	-0.1	-0.3	0.2	3.35	49.70	13.84
5	0	-1.2	0.3	7.8	-0.1	-0.6	0.8	9.20	46.23	4.03
6	0	-1.3	0.5	8.2	0.1	0.6	0.8	9.65	45.65	3.73
7	0	-0.5	1.9	3.6	0	0.4	0.3	4.20	48.19	10.48
8	0	0	7.4	3.7	0.6	0.2	0.6	7.58	50.10	5.61
9	10	0.9	4.8	1.3	1.0	0.2	0.2	4.44	50.10	10.27
10	0	-5.3	3.2	-1.3	-0.4	0.1	0.3	8.59	50.10	4.83
11	20	1.6	-8.6	-1.4	0.5	-0.6	-1.3	10.81	50.10	3.63
12	0	-5.3	3.2	-1.3	-0.4	0.1	0.3	8.59	50.10	4.83
13	0	1.5	5.5	2.9	-1.4	0.2	0.2	5.02	50.10	8.99
14	0	24.3	7.4	24.0	0.4	0.5	-0.1	16.98	50.10	1.95
15	0	-3.0	-2.3	-2.6	0	-0.2	0	0.77	50.10	64.01
16	110	-0.1	-0.9	-0.2	0	0.1	0	0.79	50.10	62.12

[1] See Figure 3.4.4.1-4 for definition of locations and angles of stress sections.

[2] ASME Service Level C is used for material allowable stress.

Table 11.1.3-6 P_m Stresses for PWR Support Disk Off-Normal Conditions (ksi)

Section[1]	S_x	S_y	S_{xy}	Stress Intensity	Allowable Stress	Margin of Safety
120	0.8	-0.8	0.1	1.6	89	54
114	-0.5	1	-0.1	1.5	89	58
37	-1.1	-0.3	0.1	1.1	86.5	78
35	1	0	0.2	1.1	86.5	80
21	-0.3	-1	0.1	1	86.5	82
23	0	1	0.2	1	86.5	83
98	-0.5	-0.8	-0.3	1	89	92
28	-0.8	0.1	0.1	0.9	88.3	98
112	0.5	-0.3	0.2	0.9	87.9	98
40	0.1	-0.8	0.1	0.9	88.3	99
72	-0.9	-0.8	0	0.9	89	100
111	-0.3	0.4	0.2	0.8	87.9	105
7	0.1	0.8	0.1	0.8	86.5	107
51	0.8	0.1	0.1	0.8	86.5	108
110	-0.8	0	0.1	0.8	88.7	109
119	0	-0.8	0.1	0.8	88.7	109
42	-0.4	-0.8	0.1	0.8	88.3	110
26	-0.8	-0.4	0.1	0.8	88.3	110
123	-0.5	0.3	-0.1	0.8	89.5	111
64	-0.8	0	0.1	0.8	87.9	111
49	-0.7	0	0.1	0.8	86.5	112
9	0	-0.7	0.1	0.8	86.5	113
95	0	-0.7	0.1	0.8	87.9	114
71	0	-0.8	0.1	0.8	88.7	115
94	-0.8	0	0.1	0.8	88.7	115
91	-0.4	0.2	-0.2	0.7	89.5	130
63	0.1	-0.4	0.2	0.7	87.9	131
99	-0.5	0.1	-0.1	0.7	89	132
74	0.1	-0.5	-0.1	0.7	89	132
96	-0.4	0.1	0.2	0.7	87.9	131
92	0.2	-0.4	-0.2	0.7	89.5	135
104	-0.5	0	-0.2	0.6	89	142
113	0.3	-0.4	0	0.6	88.1	144
117	-0.3	0.3	0	0.6	88.1	146
67	-0.5	0.1	-0.1	0.6	89	147
106	0.1	-0.4	-0.1	0.6	89	151
66	0.1	-0.4	0.1	0.6	89	158
76	-0.1	0.3	-0.2	0.6	89.5	158
25	-0.5	0	0.1	0.6	88.3	159
88	0.5	0.2	-0.1	0.5	89	164

1. Section locations are shown in Figures 3.4.4.1-7 and 3.4.4.1-8.

Table 11.1.3-7 $P_m + P_b$ Stresses for PWR Support Disk Off -Normal Conditions (ksi)

Section[1]	S_x	S_y	S_{xy}	Stress Intensity	Allowable Stress	Margin of Safety
21	-5.1	-2.5	0.6	5.2	76.8	14
37	-2.5	-5	0.6	5.2	76.8	14
120	-0.3	-5	0.4	5	78.5	15
35	2.4	4.5	0.6	4.7	76.8	15
23	4.5	2.4	0.6	4.6	76.8	16
1	4.3	3	0.4	4.5	74.6	16
4	3	4.3	0.4	4.4	74.6	16
111	-4.5	-1.4	0	4.5	77.7	16
112	-1.4	-4.5	0	4.5	77.7	16
7	4.3	2	0.5	4.4	76.8	16
51	2	4.2	0.5	4.3	76.8	17
66	4.1	0.8	0.4	4.2	78.5	18
2	-2.8	-3.7	0.5	3.9	74.6	18
9	-3.9	-1.9	0.5	4	76.8	18
49	-1.9	-3.9	0.5	4	76.8	18
3	-3.7	-2.8	0.5	3.9	74.6	18
26	-4	-0.9	0.2	4	78	18
34	-3.7	-2.9	0.4	3.9	76.8	18
63	4	0.9	0	4	77.7	19
20	-2.9	-3.7	0.4	3.9	76.8	19
42	-0.9	-3.9	0.2	3.9	78	19
96	0.9	3.9	0	3.9	77.7	19
28	-3.7	-0.4	0.1	3.7	78	20
40	-0.4	-3.6	0.1	3.6	78	20
64	-2.1	-3.3	0.5	3.5	77.7	21
95	-3.3	-2	0.5	3.4	77.7	22
6	2.4	3.1	0.3	3.2	76.8	23
48	3	2.4	0.3	3.2	76.8	23
14	3.1	0.7	0.2	3.2	78	24
54	0.7	3.1	0.1	3.1	78	24
12	3.1	0.4	0	3.1	78	24
56	0.4	3	0	3	78	25
79	2.9	1.8	0.4	3	77.7	25
80	1.8	2.8	0.4	2.9	77.7	25
115	-0.4	-2.9	0.4	2.9	78.5	26
122	-2.8	-0.4	0.4	2.9	78.5	26
72	-1.5	-2.6	0.3	2.7	78.5	28
82	-2.4	-0.4	0.3	2.4	78.5	31
123	-1.9	0.2	-0.5	2.3	78.8	33
16	0.8	2.3	0.2	2.3	78.8	34

1. Section locations are shown in Figures 3.4.4.1-7 and 3.4.4.1-8.

Table 11.1.3-8 $P_m + P_b + Q$ Stresses for PWR Support Disk Off-Normal Conditions (ksi)

Section[1]	S_x	S_y	S_{xy}	Stress Intensity	Allowable Stress	Margin of Safety
21	-18.9	-6.9	2.1	19.3	128	6
37	-7.2	-18.8	2.2	19.2	128	6
9	-18	-6.7	2	18.4	128	6
49	-6.6	-17.9	2	18.3	128	6
111	-17.3	-7.3	1.5	17.5	129.5	6
112	-6.9	-16.9	1.4	17	129.5	7
92	1.9	15.1	4.1	16.2	131.4	7
79	-15.6	-6.5	1.4	15.8	129.5	7
80	-6.4	-15.5	1.4	15.7	129.5	7
91	15.1	1.4	3.5	15.9	131.4	7
31	15.1	-0.2	0.8	15.5	131.3	8
32	14.7	-0.2	-0.9	15	131.3	8
46	-0.8	13	2.8	14.9	131.3	8
18	14.8	0	0.9	14.9	131.3	8
45	-0.4	14.3	-0.9	14.8	131.3	8
59	-0.2	14.5	1	14.8	131.3	8
34	-11	-10.2	3.6	14.2	128	8
60	0	14.4	-0.8	14.5	131.3	8
20	-10.2	-10.5	3.6	13.9	128	8
17	13.8	0	-0.8	14	131.3	8
6	-9.7	-10.2	3.4	13.4	128	9
48	-10.1	-9.7	3.5	13.4	128	9
26	-13.4	-4.7	1.1	13.6	130	9
76	1.5	12.8	-3.2	13.6	131.4	9
108	1.3	12.6	-3.1	13.4	131.4	9
30	-8.5	-10.7	3.5	13.3	131.3	9
124	3.2	11.6	4	13.2	131.4	9
120	-3.1	-13	1	13.1	130.9	9
107	12.2	1.7	-3.3	13.1	131.4	9
44	-10.4	-8.2	3.5	13	131.3	9
123	12.1	1.3	3.3	13	131.4	9
75	12.2	1.2	-3.1	13	131.4	9
42	-4.6	-12.6	1.1	12.7	130	9
16	-7	-10.2	3	12	131.3	10
58	-9.7	-7.4	3	11.8	131.3	10
14	-11.5	-4	0.9	11.6	130	10
54	-4	-11.4	0.9	11.5	130	10
51	-3.1	-11	-1.3	11.2	128	10
64	-4.7	-10.5	-1.7	10.9	129.5	11
95	-10.4	-4.6	-1.6	10.8	129.5	11

1. Section locations are shown in Figures 3.4.4.1-7 and 3.4.4.1-8.

Table 11.1.3-9 P_m Stresses for BWR Support Disk Off-Normal Conditions (ksi)

Section[1]	S_x	S_y	S_{xy}	Stress Intensity	Allowable Stress	Margin of Safety
277	0.8	-0.8	0.1	1.7	63.1	37
265	-0.9	0.6	0.1	1.6	63.2	40
262	-0.8	0.6	0.1	1.5	63	41
259	-0.7	0.6	0.1	1.3	63	46
77	0.5	-0.7	0	1.3	63.1	48
194	-0.6	0.5	0.1	1.2	63	52
229	-0.9	0.2	0.1	1.1	63.2	57
197	-0.6	0.5	0.1	1.1	63.1	57
263	-0.9	-0.9	0.1	1	63.1	60
10	0.2	-0.5	-0.4	1	63.2	62
276	0.6	-0.4	0.1	1	62.9	63
264	-0.9	0	0.1	1	63.1	64
286	0.5	-0.5	0.1	1	63	65
76	0.6	-0.3	0.1	1	62.8	65
16	-0.4	0.4	-0.3	1	63.2	65
260	-0.8	-0.8	0.1	0.9	63	69
261	-0.8	0	0.1	0.9	63	73
289	-0.8	-0.6	0.1	0.8	63	74
269	-0.7	-0.8	0	0.8	63.1	74
88	0.6	-0.2	0.1	0.8	62.9	75
273	0	-0.8	0	0.8	63.1	75
193	-0.7	-0.7	0.1	0.8	63	77
11	0	-0.1	-0.4	0.8	63.2	77
9	0	-0.1	-0.4	0.8	63.2	79
85	-0.8	-0.7	0	0.8	63.1	80
103	-0.8	-0.1	0.1	0.8	63.2	80
97	0.6	-0.1	0.1	0.8	63	82
268	-0.7	-0.4	0.1	0.8	62.8	82
258	-0.7	0	0.1	0.8	63	82
14	-0.3	-0.2	-0.4	0.8	63.2	83
13	0.2	-0.3	-0.3	0.8	63.2	83
294	-0.7	-0.1	0.2	0.7	63	84
81	0	-0.7	0	0.7	63.1	85
280	-0.7	-0.5	0.1	0.7	62.9	86
196	-0.6	-0.6	0.1	0.7	63	87
166	0.7	0.1	0.1	0.7	63.2	87
84	-0.7	-0.3	0.1	0.7	62.9	89
73	0.2	-0.5	0.1	0.7	63.2	89
211	-0.4	0.3	0.1	0.7	63.1	92
295	0	-0.6	0.1	0.7	63.2	92

1. Section locations are shown in Figures 3.4.4.1-13 through 3.4.4.1-16.

Table 11.1.3-10 $P_m + P_b$ Stresses for BWR Support Disk Off-Normal Conditions (ksi)

Section[1]	S_x	S_y	S_{xy}	Stress Intensity	Allowable Stress	Margin of Safety
295	-1.4	-5	0.5	5	54	10
294	-2.2	-4.9	0.5	5	54	10
254	-4.8	-2.2	0.5	4.9	54	10
265	-4.7	-0.7	0.4	4.7	54	11
289	-2.3	-4.3	0.6	4.4	54	11
293	-1.9	-4.3	0.4	4.4	54	11
24	-4.3	-1.4	0.1	4.3	54	11
257	-4.2	-1.5	0.5	4.3	54	11
243	-4.3	-1.5	0.2	4.3	54	11
275	1.7	4.3	0.3	4.3	54	11
263	-4	-2.4	0.7	4.3	54	12
252	4.2	1.7	0.3	4.2	54	12
274	1.7	4.1	0.3	4.2	54	12
267	-1.6	-4.1	0.2	4.2	54	12
241	4.1	1.4	0.2	4.1	54	12
22	-4.1	-1.7	0.3	4.1	54	12
75	-1.7	-4.1	0.3	4.1	54	12
288	1.8	4	0.4	4.1	54	12
227	0.9	4.1	0.2	4.1	54	12
246	-4	-1.6	0.5	4.1	54	12
208	-1.5	-4	0.3	4	54	12
237	4	1.8	0.3	4	54	12
51	4	1	0.1	4	54	12
83	-1.6	-4	0.3	4	54	12
32	3.9	1.6	0.3	4	54	13
240	3.9	1.8	0.3	4	54	13
21	3.9	1.7	0.3	4	54	13
62	3.9	1.3	0.4	3.9	54	13
174	3.9	1.7	0.3	3.9	54	13
238	3.9	1.4	0.2	3.9	54	13
19	3.9	1.6	0.3	3.9	54	13
209	-1.5	-3.9	0.3	3.9	54	13
74	1.6	3.8	0.3	3.9	54	13
228	0.8	3.9	0.3	3.9	54	13
49	-3.8	-1.5	0.2	3.9	54	13
18	3.8	1.6	0.3	3.9	54	13
184	-3.8	-1.6	0.3	3.8	54	13
249	-3.8	-1.4	0.1	3.8	54	13
266	1.6	3.8	0.3	3.8	54	13
287	1.5	3.8	0.3	3.8	54	13

1. Section locations are shown in Figures 3.4.4.1-13 through 3.4.4.1-16.

Table 11.1.3-11 $P_m + P_b + Q$ Stresses for BWR Support Disk Off-Normal Conditions (ksi)

Section[1]	S_x	S_y	S_{xy}	Stress Intensity	Allowable Stress	Margin of Safety
295	-2.1	-16.4	1	16.5	90	4
268	-7.5	-15.4	1.8	15.8	90	5
289	-5.5	-15.3	1.4	15.5	90	5
16	11.5	5.3	5.4	14.6	90	5
265	-14.3	-4.9	1.3	14.4	90	5
139	-6.9	-14.1	1.6	14.4	90	5
276	-4.8	-14.2	0.9	14.3	90	5
24	-13	-8.3	2.3	13.9	90	5
266	-7.7	-13.3	1.7	13.8	90	6
137	-7.6	-13.2	1.7	13.7	90	6
1	-0.4	13.3	-0.1	13.7	90	6
2	-0.4	13.3	-0.1	13.7	90	6
18	-13	-7	2.1	13.6	90	6
21	-13.1	-6.3	1.9	13.6	90	6
263	-13.3	-5.5	1.3	13.5	90	6
31	-12.8	-6.9	2	13.5	90	6
166	-1.1	-13.3	0.8	13.4	90	6
4	-0.1	13.2	-0.2	13.3	90	6
3	-0.1	13.2	-0.2	13.3	90	6
274	-6.3	-13	1.5	13.3	90	6
34	-12.7	-6.1	1.9	13.2	90	6
246	-12.9	-4.2	1.3	13.1	90	6
160	-4.4	-12.9	1.2	13	90	6
269	-6.1	-12.6	1.5	13	90	6
241	-12.8	-5.6	1.1	12.9	90	6
238	-12.6	-6.8	1.4	12.9	90	6
243	-12.7	-5.5	1	12.9	90	6
147	-4.7	-12.7	0.9	12.8	90	6
145	-6.2	-12.5	1.4	12.8	90	6
267	-7.4	-12.3	1.5	12.7	90	6
37	-11.8	-7.6	2.1	12.6	90	6
111	-12.3	-6.6	1.4	12.6	90	6
15	10.8	3.1	-3.8	12.3	90	6
138	-7.3	-11.7	1.5	12.2	90	6
14	11	1.6	3.5	12.1	90	6
19	-11.9	-3.1	0.9	12	90	7
119	-11.8	-2.9	1	11.9	90	7
32	-11.8	-3	0.9	11.9	90	7
275	-6.1	-11.7	1	11.9	90	7
277	-2.8	-11.8	1.1	11.9	90	7

1. Section locations are shown in Figures 3.4.4.1-13 through 3.4.4.1-16.

Table 11.1.3-12 Summary of Maximum Stresses for PWR and BWR Fuel Basket Weldments – Off-Normal Condition (ksi)

Case	Loading	Maximum Stress Intensity[1]	Stress Allowable[2]	Margin of Safety
PWR Top Weldment	$P_m + P_b$	0.7	21.0[3]	+Large
	$P_m + P_b + Q$	35.5	52.5	0.48
PWR Bottom Weldment	$P_m + P_b$	0.5	24.0[3]	+Large
	$P_m + P_b + Q$	11.0	60.0	+Large
BWR Top Weldment	$P_m + P_b$	0.9	21.7[3]	+Large
	$P_m + P_b + Q$	10.2	54.3	+Large
BWR Bottom Weldment	$P_m + P_b$	1.5	23.2[3]	+Large
	$P_m + P_b + Q$	34.0	58.1	0.71

1. Nodal stresses are from the finite element analysis.
2. Allowable stresses are conservatively determined at the maximum temperature of the weldments.
3. Allowable stresses for primary membrane stresses are conservatively used.

11.1.4 Failure of Instrumentation

The Universal Storage System uses an electronic temperature sensing system to read and record the outlet air temperature at each of the four air outlets on each Vertical Concrete Cask. The temperatures are read and recorded daily.

11.1.4.1 Cause of Instrumentation Failure Event

Failure of the temperature measuring instrumentation could occur as a result of component failure, or as a result of another accident condition that interrupted power or damaged the sensing or reader terminals.

11.1.4.2 Detection of Instrumentation Failure Event

The failure is identified by the lack of a reading at the temperature reader terminal. The failure could also be identified by disparities between outlet temperatures in a cask or between similar casks.

11.1.4.3 Analysis of Instrumentation Failure Event

Since the temperature of each outlet of each concrete cask is recorded daily, the maximum time period during which the instrumentation failure may go undetected is 24 hours. Therefore, the maximum time period, during which an increase in the outlet air temperatures may go undetected, is 24 hours. The principal condition that could cause an increase in temperature is the blockage of the cooling air inlets or outlets. Section 11.2.13 shows that even if all of the inlets and outlets of a single cask are blocked immediately after a temperature measurement, it would take longer than 24 hours before any component approaches its allowable temperature limit. Therefore, the opportunity exists to identify and correct a defect prior to reaching the temperature limits. During the period of loss of instrumentation, no significant change in canister temperature will occur under normal conditions.

The purpose of the daily temperature monitoring is to ensure that the passive cooling system is continuing to operate normally. Instrument failure would be of no consequence, if the affected storage cask continued to operate in normal storage conditions.

Because the canister and the concrete cask are a large heat sink, and because there are few conditions that could result in a cooling air temperature increase, the temporary loss of remote sensing and monitoring of the outlet air temperature is not a major concern. No applicable regulatory criteria are violated by the failure of the temperature instrumentation system.

11.1.4.4 Corrective Actions

This event requires that the temperature reporting equipment be either replaced or repaired and calibrated. Prior to repair or replacement, the temperature shall be recorded manually.

11.1.4.5 Radiological Impact

There are no radiological consequences for this event.

11.1.5 Small Release of Radioactive Particulate From the Canister Exterior

The procedures for loading the canister provide for steps to minimize exterior surface contact with contaminated spent fuel pool water, and the exterior surface of the canister is surveyed by smear at the top end to verify canister surface conditions. Design features are also employed to ensure that the canister surface is generally free of surface contamination prior to its installation in the concrete cask. The surface of the canister is free of traps that could hold contamination. The presence of contamination on the external surface of the canister is unlikely, and, therefore, no particulate release from the canister exterior surface is expected to occur in normal use.

11.1.5.1 Cause of Radioactive Particulate Release Event

In spite of precautions taken to preclude contamination of the external surface of the canister, it is possible that a portion of the canister surface may become slightly contaminated during fuel loading by the spent fuel pool water and that the contamination may go undetected. Surface contamination could become airborne and be released as a result of the air flow over the canister surface.

11.1.5.2 Detection of Radioactive Particulate Release Event

The release of small amounts of radioactive particles over time is difficult to detect. Any release is likely to be too low to be detected by any of the normally employed long-term radiation dose monitoring methods (such as TLDs). It is possible that a suspected release could be verified by a smear survey of the air outlets.

11.1.5.3 Analysis of Radioactive Particulate Release Event

A calculation is made to determine the level of surface contamination that if released would result in a dose of one tenth of one (0.1) mrem at a minimum distance of 100 meters from a design basis storage cask. ISFSI-specific allowable dose rates and surface contamination limits will be calculated on a site specific basis to conform to 10 CFR 72. The method for determining the residual contamination limit is based on the plume dispersion calculations presented in U.S. NRC Regulatory Guides 1.109 [9] and 1.145 [13] and is highly conservative. The calculation shows that a residual contamination of approximately 1.57×10^5 dpm/100 cm^2 β-γ and 5.24×10^2 dpm/100 cm^2 α activity, on the surface of the design basis canister, is required to yield a dose of one tenth of one (0.1) mrem at the minimum distance of 100 meters. The canister surface area is inversely

proportional to the allowable surface contamination. The design basis cask is, therefore, the Class 3 PWR cask, which has the largest canister surface area at 3.06×10^5 cm^2.

The above analysis demonstrates that the off-site radiological consequences from the release of canister surface contamination is negligible, and all applicable regulatory criteria can be met for an ISFSI array.

11.1.5.4 Corrective Actions

No corrective action is required since the radiological consequence is negligible.

11.1.5.5 Radiological Impact

As shown above, the potential off-site radiological impact due to the release of canister surface contamination is negligible.

11.1.6 Off-Normal Events Evaluation for Site Specific Spent Fuel

This section presents the off-normal events evaluation of spent fuel assemblies or configurations, which are unique to specific reactor sites. These site specific fuel configurations result from conditions that occurred during reactor operations, participation in research and development programs, and from testing programs intended to improve reactor operations. Site specific fuel includes fuel assemblies that are uniquely designed to accommodate reactor physics, such as axial fuel blankets and variable enrichment assemblies, fuel with burnup that exceeds the design basis, and fuel that is classified as damaged.

Site specific fuel assembly configurations are either shown to be bounded by the analysis of the standard design basis fuel assembly of the same type (PWR or BWR), or are shown to be acceptable contents, by specific evaluation of the configuration.

11.1.6.1 Off-Normal Events Evaluation for Maine Yankee Site Specific Spent Fuel

Maine Yankee site specific fuels are described in Section 1.3.2.1. A thermal evaluation has been performed for Maine Yankee site specific fuels that exceed the design basis burnup as shown in Section 4.5.1.2. As shown in that section, loading of fuel with a burnup between 45,000 and 50,000 MWD/MTU is subject to preferential loading in designated basket positions in the Transportable Storage Canister.

With preferential loading, the design basis total heat load of the canister is not changed. Consequently, the thermal performance for the Maine Yankee site specific fuels is bounded by the design basis PWR fuels. Therefore, no further evaluation is required for the off-normal thermal events (severe ambient temperature conditions and blockage of half of the air inlets) as shown in Sections 11.1.1 and 11.1.2. In Section 3.6.1.1, the total weight of the canister contents for Maine Yankee site specific fuels is shown to be bounded by the PWR design basis fuels. Therefore, the evaluation for the off-normal canister handling load in Section 11.1.3 bounds the canister configuration loaded with Maine Yankee fuels.

THIS PAGE INTENTIONALLY LEFT BLANK

11.2 Accidents and Natural Phenomena

This section presents the results of analyses of the design basis and hypothetical accident conditions evaluated for the Universal Storage System. In addition to design basis accidents, this section addresses very low probability events, including natural phenomena, that might occur over the lifetime of the ISFSI, or hypothetical events that are postulated to occur because their consequences may result in the maximum potential impact on the immediate environment.

The Universal Storage System includes Transportable Storage Canisters and Vertical Concrete Casks of five different lengths to accommodate three classes of PWR fuel or two classes of BWR fuel. In the accident analyses of this section, the bounding cask parameters (such as weight and center of gravity) are conservatively used, as appropriate, to determine the cask's capability to withstand the effects of the accidents.

The results of analyses show that no credible potential accident exists that will result in a dose of ≥ 5 rem beyond the postulated controlled area. The Universal Storage System is demonstrated to have a substantial design margin of safety and to provide protection to the public and to occupational personnel during storage of spent nuclear fuel.

THIS PAGE INTENTIONALLY LEFT BLANK

11.2.1 Accident Pressurization

Accident pressurization is a hypothetical event that assumes the failure of all of the fuel rods contained within the Transportable Storage Canister (canister). No storage conditions are expected to lead to the rupture of all of the fuel rods.

Results of analysis of this event demonstrate that the canister is not significantly affected by the increase in internal pressure that results from the hypothetical rupture of all PWR or BWR fuel rods contained within the canister. Positive margins of safety exist throughout the canister.

11.2.1.1 Cause of Pressurization

The hypothetical failure of all of the fuel rods in a canister would release the fission and fill gases to the interior of the canister, resulting in the pressurization of the canister.

11.2.1.2 Detection of Accident Pressurization

The rupture of fuel rods within the canister is unlikely to be detected by any measurements or inspections that could be undertaken from the exterior of the canister or the concrete cask.

11.2.1.3 Analysis of Accident Pressurization

Analysis of this accident involves evaluation of the maximum canister internal pressure and the canister stress due to the maximum internal pressure. These evaluations are provided below.

Maximum Canister Accident Condition Internal Pressure

The analysis requires the calculation of the free volume of the canister, calculation of the quantity of fill and fission gas in the fuel assemblies, and the subsequent calculation of the pressure in the canister if these gases are added to the helium pressure (initially at 1 atm) already present in the canister (Section 4.4.5). The quantity of fission gases is conservatively estimated assuming that 30% of the total gases present are released from the fuel. All fuel rod backfill gas is conservatively assumed to be released.

The internal pressure is a function of rod-fill, fission, and canister backfill gases. All of the gases except the fission gases are assumed to be helium. The total pressure for each volume is found by calculating the molar quantity of each gas and summing those quantities directly.

Maximum Accident Condition Internal Pressure for PWR Canister

The design basis PWR fuel assembly for the internal pressure calculation is the Westinghouse 17 x 17 fuel assembly, which has the highest fuel rod back-fill pressure (500 psig). A burnup of 55,000 MWD/MTU is conservatively assumed. The PWR internal pressure calculations are performed on a Class 1 PWR system. This is conservative because the highest quantity of fission gas is coupled with the smallest free gas volume, thus representing the bounding analysis with respect to internal pressure. The bulk temperature of the helium is conservatively taken to be 580°F. This temperature bounds the calculated bulk temperature of helium for any of the evaluated normal, off-normal or accident conditions. This accident condition considers the maximum temperature and the rupture of 100% of the fuel rods.

The number of moles of the backfill gases is calculated using the Ideal Gas Law, PV = NRT. Backfill gases for the canister and cavity are assumed to be initially at 1 atmosphere. The quantity of fission gas is derived using 0.3125 atoms of gas/fission, based on the results of the SAS2H analysis.

Assuming that 100% of the fuel rods fail, releasing 30% of their total fission gas and all of their rod backfill gas, the number of moles of gas in the canister is:

$$N = N_{TSC\ backfill} + N_{rod\ backfill} + 0.3\left(N_{fission\ gas}\right)$$

The number of moles of helium contained in the canister as backfill and the number of moles of gas in the fuel rods (as helium backfill and fission products) are calculated in Section 4.4.5.

The number of moles of gas, N, due to the hypothetical failure of 100% of the fuel rods is:

$$N = N_{TSC\ backfill} + N_{rod\ backfill} + 0.3\left(N_{fission\ gas}\right)$$

$$= 185.96\frac{\text{Moles}}{\text{canister}} + 153.31\frac{\text{Moles}}{\text{canister}} + 0.3\left(888.22\frac{\text{Moles}}{\text{canister}}\right)$$

$$= 606 \frac{\text{Moles}}{\text{canister}}$$

Thus, using the ideal gas law, the internal pressure in the PWR fuel canister with 100% failed fuel rods is:

$$P = \frac{\left(606 \frac{\text{Moles}}{\text{canister}}\right) \times \left(0.0821 \frac{\text{atm}\,\ell}{\text{mole K}}\right) \times 577.79\text{ K}}{\left(5{,}968 \frac{\ell}{\text{canister}}\right)} = 4.82\text{ atm} \approx 56.1\text{ psig}$$

Maximum Accident Condition Internal Pressure for BWR Canister

The Exxon-ANF 9×9 fuel assembly is used as the design basis BWR fuel assembly for the internal pressure calculation. This assembly has the highest fuel rod back-fill pressure (60 psig). The BWR internal pressure calculations are performed on a Class 4 BWR system. It should be noted that the design basis BWR fuel assembly for the internal pressure calculations represents an impossible configuration since the Exxon-ANF 9 × 9 fuel assembly will not fit in the Class 4 BWR canister; however, this configuration represents the case that would maximize the internal pressures, thus bounding all other BWR configurations.

Using the same method as for the PWR canister and conservatively taking the bulk temperature of the helium to be 600°F, the maximum calculated BWR canister internal accident condition pressure is 35.3 psig.

Maximum Canister Stress Due to Internal Pressure

The stresses that result in the canister due to the internal pressure are evaluated using the ANSYS finite element model that envelopes both PWR and BWR configurations as described in Section 3.4.4. The pressure used for the model is 65 psig, which bounds the results of 56.1 and 35.3 psig for the PWR and BWR, respectively.

The resulting maximum canister stresses for accident pressure loads are summarized in Tables 11.2.1-1 and 11.2.1-2 for primary membrane and primary membrane plus bending stresses, respectively.

The resulting maximum canister stresses and margins of safety for combined normal handling (Tables 3.4.4.1-4 and 3.4.4.1-5) and maximum accident internal pressure (65 psig) are summarized in Tables 11.2.1-3 and 11.2.1-4 for primary membrane and primary membrane plus bending stresses, respectively.

The sectional stresses shown in Tables 11.2.1-1 through 11.2.1-4 at 16 axial locations are obtained for each angular division of the model (a total of 19 angular locations for each axial location). The locations of the stress sections are shown in Figure 3.4.4.1-4.

All margins of safety are positive. Consequently, there is no adverse consequence to the canister as a result of the combined normal handling and maximum accident internal pressure (65 psig).

11.2.1.4 Corrective Actions

No recovery or corrective actions are required for this hypothetical accident.

11.2.1.5 Radiological Impact

There are no dose consequences due to this accident.

Table 11.2.1-1 Canister Accident Internal Pressure (65 psig) Only Primary Membrane (P_m) Stresses (ksi)

Section No.[1]	Angle (degrees)	SX	SY	SZ	SXY	SYZ	SXZ	Stress Intensity
1	0	0.4	6.3	2.5	-0.9	0.1	0.2	6.18
2	0	4.2	-4.1	-5.3	-0.9	0.1	-0.7	9.69
3	0	-0.8	1.8	-8.1	1.8	-0.2	-0.7	10.89
4	0	0	1.7	3.4	0	0	0.3	3.49
5	0	0	1.7	3.4	0	0	0.3	3.45
6	0	0	1.7	3.4	0	0	0.3	3.45
7	0	0	1.7	3.4	0	0	0.3	3.46
8	0	0	1.7	1.7	-0.1	0	0.2	1.76
9	0	0.2	1.2	0.9	0.1	0	0.1	1.11
10	0	-0.6	0.8	0.6	-0.2	0	0.1	1.45
11	60	0.5	-0.2	0.6	0	0	-0.2	0.90
12	80	0.1	-0.8	-0.3	0	0.3	0.1	1.08
13	0	-0.1	0.8	0.5	0.1	0	0.1	0.93
14	80	0.8	-0.1	0.8	0.8	-0.6	0	2.16
15	70	-0.1	0	-0.1	0	0	0	0.05
16	70	0.1	0	0.1	0	0	0	0.12

[1] See Figure 3.4.4.1-4 for definition of locations and angles of stress sections.

Table 11.2.1-2 Canister Accident Internal Pressure (65 psig) Only Primary Membrane plus Bending ($P_m + P_b$) Stresses (ksi)

Section No. [1]	Angle (degrees)	SX	SY	SZ	SXY	SYZ	SXZ	Stress Intensity
1	0	4.8	15.3	0.5	-0.1	0.1	-0.2	14.76
2	0	2.0	-29.4	-13.3	-2.1	0.1	-1.3	31.86
3	0	-3.1	41.2	2.9	2.3	-0.2	0.4	44.49
4	0	0.0	1.6	3.4	0.0	0	0.3	3.52
5	0	0.0	1.7	3.4	0	0	0.3	3.51
6	0	0.0	1.7	3.4	0	0	0.3	3.51
7	0	0.0	1.7	3.4	0	0	0.3	3.51
8	0	0	1.9	1.8	-0.1	0.0	0.2	1.92
9	0	0.2	2.6	1.3	0.4	0.0	0.1	2.50
10	0	-0.4	3.2	1.3	0.1	0.0	0.1	3.66
11	80	-0.2	-2.0	0.6	0.0	-0.1	-0.1	2.58
12	80	-0.2	-1.5	-0.8	-0.1	0.4	0.1	1.55
13	0	-1.0	0.3	0.1	0.1	0	0.1	1.32
14	180	20.9	0.1	21.1	0.7	-0.7	0.1	21.01
15	0	-1.5	-0.1	-1.5	0	0	0	1.49
16	0	0.8	0	0.8	0	0	0	0.76

[1] See Figure 3.4.4.1-4 for definition of locations and angles of stress sections.

Table 11.2.1-3 Canister Normal Handling plus Accident Internal Pressure (65 psig) Primary Membrane (P_m) Stresses (ksi)

Section No.[1]	Angle (degrees)	SX	SY	SZ	SXY	SYZ	SXZ	Stress Intensity	Stress Allowable[2]	Margin of Safety
1	0	0.6	8.1	3.2	-1.2	0.1	0.2	7.94	40.08	4.05
2	0	5.4	-5.3	-6.9	-1.2	0.1	-0.9	12.61	40.08	2.18
3	0	-1	2.4	-10.7	2.3	-0.2	-0.9	14.31	40.08	1.80
4	180	0	2.2	3.4	0	0	-0.3	3.50	39.76	10.36
5	180	0	2.2	3.4	0	0	-0.3	3.46	36.98	9.68
6	180	0	2.1	3.4	0	0	-0.3	3.46	36.52	9.54
7	180	0	2	3.4	0	0	-0.3	3.46	38.55	10.14
8	0	0	2.8	1.7	-0.1	0.1	0.2	2.83	40.08	13.16
9	0	0.2	2.7	1.2	0.2	0.1	0.1	2.54	40.08	14.80
10	0	-0.8	2.6	0.9	-0.1	0.2	0.1	3.46	40.08	10.58
11	150	0.9	-0.3	0.4	0	-0.2	0.2	1.30	40.08	29.76
12	90	0	-1.4	-0.3	-0.2	0.4	0.1	1.56	40.08	24.73
13	0	0.2	0.6	1.4	-0.5	0	0.2	1.66	40.08	23.19
14	80	1	-0.1	1	1	-0.8	0	2.81	40.08	13.28
15	170	-0.1	0	-0.1	0	0	0	0.08	40.08	471.31
16	70	0.1	0	0.1	0	0	0	0.14	40.08	292.20

[1] See Figure 3.4.4.1-4 for definition of locations and angles of stress sections.

[2] ASME Service Level D is used for material allowable stress.

Table 11.2.1-4 Canister Normal Handling plus Accident Internal Pressure (65 psig) Primary Membrane plus Bending ($P_m + P_b$) Stresses (ksi)

Section No.[1]	Angle (degrees)	SX	SY	SZ	SXY	SYZ	SXZ	Stress Intensity	Stress Allowable[2]	Margin of Safety
1	0	6.2	19.7	0.5	-0.1	0.1	-0.3	19.19	60.12	2.13
2	0	2.6	-37.8	-17.3	-2.7	0.2	-1.7	40.91	60.12	0.47
3	0	-3.9	53.1	3.4	2.9	-0.2	0.5	57.32	60.12	0.05
4	180	0.0	2.1	3.5	0.0	0	-0.3	3.60	59.64	15.57
5	180	0.0	2.2	3.6	0	0	-0.3	3.65	55.47	14.19
6	180	0.0	2.2	3.6	0	0	-0.3	3.70	54.79	13.80
7	180	0.0	2.1	3.6	0	0	-0.3	3.67	57.83	14.75
8	0	0	3.0	1.7	-0.1	0.1	0.1	3.00	60.12	19.02
9	0	0.1	4.2	1.6	0.4	0.2	0.1	4.13	60.12	13.55
10	0	-0.6	4.2	1.4	0.1	0.3	0.1	4.85	60.12	11.39
11	150	0.5	-2.5	-0.2	0.0	-0.2	0.5	3.32	60.12	17.10
12	90	-0.3	-2.2	-0.7	-0.2	0.6	0.1	2.16	60.12	26.83
13	0	0.2	1.5	1.3	-0.9	0.1	0.1	2.26	60.12	25.59
14	180	27.3	0.2	27.4	1.0	-0.9	0.1	27.33	60.12	1.20
15	0	-1.7	0	-1.7	0	0	0	1.66	60.12	35.17
16	70	0.3	0	0.3	-0.1	0	0	0.31	60.12	194.89

[1] See Figure 3.4.4.1-4 for definition of locations and angles of stress sections.

[2] ASME Service Level D is used for material allowable stress.

11.2.2 Failure of All Fuel Rods With a Ground Level Breach of the Canister

Since no mechanistic failure of the canister occurs and since the canister is leaktight, this potential accident condition is not evaluated.

THIS PAGE INTENTIONALLY LEFT BLANK

11.2.3 Fresh Fuel Loading in the Canister

This section evaluates the effects of an inadvertent loading of up to 24 fresh, unburned PWR fuel assemblies or up to 56 fresh, unburned BWR fuel assemblies in a canister. There are no adverse effects on the canister due to this event since the criticality control features of the Universal Storage System ensure that the k_{eff} of the fuel is less than 0.95 for all loading conditions of fresh fuel.

11.2.3.1 Cause of Fresh Fuel Loading

The cause of this event is operator and/or procedural error. In-plant operational procedures and engineering and quality control programs are expected to preclude occurrence of this event. Nonetheless, it is evaluated here to demonstrate the adequacy of the canister design for accommodating fresh fuel without a resulting criticality event.

11.2.3.2 Detection of Fresh Fuel Loading

This accident is expected to be identified immediately by observation of the condition of the fuel installed in the canister or by a review of the fuel handling records.

11.2.3.3 Analysis of Fresh Fuel Loading

The criticality analysis presented in Chapter 6.0 assumes the loading of up to 24 design basis PWR or up to 56 design basis BWR fuel assemblies having no burn up. This analysis shows that for the PWR canister, the maximum k_{eff} for the dry normal condition is 0.3833. The maximum k_{eff} for the accident conditions is calculated to be 0.9470. The accident condition assumes the most reactive configuration of the fuel and full moderator intrusion.

For the BWR canister, the values of maximum k_{eff} for the dry normal condition and the accident conditions are calculated to be 0.3817 and 0.9233, respectively.

The criticality control features of the Transportable Storage Canister and the basket ensure that the k_{eff} of the fuel is less than 0.95 for all loading conditions of fresh fuel. Therefore, there is no adverse impact on the Universal Storage System due to this event.

11.2.3.4 Corrective Actions

This event requires that the canister be unloaded when the incorrect fuel loading is identified. The cause for the error should be identified and procedural actions implemented to preclude recurrence.

11.2.3.5 Radiological Impact

There are no dose implications due to this event.

11.2.4 24-Inch Drop of Vertical Concrete Cask

This analysis evaluates a loaded Vertical Concrete Cask for a 24-inch drop onto a concrete storage pad. The cask containing the Transportable Storage Canister loaded with Class 5 BWR fuel is identified as the heaviest cask, and is conservatively used in the analysis as the bounding case. The results of the evaluation show that neither the concrete cask nor the Transportable Storage Canister experience significant adverse effects due to the 24-inch drop accident.

11.2.4.1 Cause of 24-Inch Cask Drop

The Vertical Concrete Cask may be lifted and moved using either an air pad system, which lifts the concrete cask from the bottom, or a mobile lifting frame, which lifts the concrete casks using lifting lugs in the top of the cask.

Using the air pad system, the concrete cask, containing a loaded canister, must be raised approximately 3 inches to enable installation of the inflatable air-pads beneath it. The air pads use pressurized air to allow the cask to be moved across the surfaces of the transporter and the ISFSI pad to the designated position. The cask is raised using hydraulic jacks installed at jack-points in the cask's air inlets. The failure of one or more of the jacks or of the air pad system could result in a drop of the cask.

The concrete cask may be lifted and moved by a mobile lifting frame, which may be self-propelled or towed. The lifting frame uses hydraulic power to raise the cask approximately 20 inches using a lifting attachment that connects to the four cask lifting lugs. The failure of one or more of the lifting lugs, or the failure of the hydraulic pistons, could result in a drop of the cask.

Although a lift of only about 3 inches is required to install and remove the air pads, the mobile lifting frame will lift the cask approximately 20 inches, so this analysis conservatively evaluates the consequences of a 24-inch drop.

11.2.4.2 Detection of 24-Inch Cask Drop

This event will be detected by the operators as it occurs.

11.2.4.3 Analysis of 24-Inch Cask Drop

A bottom end impact is assumed to occur normal to the concrete cask bottom surface, transmitting the maximum load to the concrete cask and the canister. The energy absorption is computed as the product of the compressive force acting on the concrete cask and its displacement. Conservatively assuming that the storage surface impacted is an infinitely rigid surface, the concrete cask body will crush until the impact energy is absorbed.

A compressive strength of 4,000 psi is used for the cask concrete. The evaluation conservatively ignores any energy absorption by the internal friction of the aggregate as crushing occurs.

The canister rests upon a base weldment designed to allow cooling of the canister. Following the initial impact, the inlet system will partially collapse, providing an energy absorption mechanism that somewhat reduces the deceleration force on the canister.

Evaluation of the Concrete Cask

In the 24-inch bottom drop of the concrete cask, the cylindrical portion of the concrete is in contact with the steel bottom plate that is a part of the base weldment. The plate is assumed to be part of an infinitely rigid storage pad. No credit is taken for the crush properties of the storage pad or the underlying soil layer. Therefore, energy absorbed by the crushing of the cylindrical concrete region of the concrete cask equals the product of the compressive strength of the concrete, the crush depth of the concrete, and the projected area of the concrete cylinder. Crushing of the concrete continues until the energy absorbed equals the potential energy of the cask at the initial drop height. The canister is not rigidly attached to the concrete cask, so it is not considered to contribute to the concrete crushing. The energy balance equation is:

$$w(h+\delta) = P_o A\delta,$$

where:

h = 24 in., the drop height,
δ = the crush depth of the concrete cask,
P_o = 4000 psi, the compressive strength of the concrete,
A = $\pi(R_1^2 - R_2^2)$ = 7,904 in^2, the projected area of the concrete shield wall,
w = 176,010 lbs (concrete ≅ 170,000 lbs plus reinforcing steel ≅ 6,010 lbs)

It is assumed that the maximum force that can be exerted on the concrete cask is the compressive strength of the concrete multiplied by the area of the concrete being crushed. The concrete cask's steel shell will not experience any significant damage during a 24-inch drop. Therefore, its functionality will not be impaired due to the drop.

The crush distance computed from the energy balance equation is:

$$\delta = \frac{hw}{P_o A - w} = \frac{(24)(176{,}010)}{(4000)(7{,}904) - (176{,}010)} = 0.134 \text{ inch}$$

where, w = 176,010 lbs (the highest weight is used to obtain the maximum deformation)

The resultant inlet deformation is 0.134 inch.

Evaluation of the Canister for a 24-inch Bottom End Drop

Upon a bottom end impact of the concrete cask, the canister produces a force on the base weldment located near the bottom of the cask (see Figure 11.2.4-1). The ring above the air inlets is expected to yield. To determine the resulting acceleration of the canister and deformation of the pedestal, a LS-DYNA analysis is used.

A half-symmetry model of the base weldment is built using the ANSYS preprocessor (see Figure 11.2.4-2). The model is constructed of 8-node brick and 4-node shell elements. Symmetry conditions are applied along the plane of symmetry (X-Z plane). Lumped mass elements located in the canister bottom plate represent the loaded canister. The impact plane is represented as a rigid plane, which is considered conservative, since the energy absorption due to the impact plane is neglected (infinitely rigid). To determine the maximum acceleration and deformations, impact analyses are solved using LS-DYNA program.

The weldment ring, weldment plate, and the inner cone (see Figure 11.2.4-1) materials are modeled using LS-DYNA's piece wise linear plasticity model. This material model accepts stress–strain curves for different strain rates. These stress strain curves were obtained from the Atlas of Stress-Strain Curves [44] and are shown in Figure 11.2.4-3. To ensure that maximum deformations and accelerations are determined, two analyses are performed. One analysis, which uses the static stress strain curve, envelopes the maximum deformation of the pedestal. The second analysis employs the multiple stress-strain curves to account for different strain rates.

The maximum accelerations of the canister during the 24-inch bottom end impact is 45.0g and 44.5g for the variable strain rate material model and the static stress-strain curve, respectively. The resulting acceleration time histories of the bottom canister plate, which correspond to a filter frequency of 200 Hz, are shown in Figure 11.2.4-4 for the analysis using the static stress-strain curve and Figure 11.2.4-5 for the analysis corresponding to the series of stress-strain curves at different strain rates. These time histories indicate that the maximum accelerations do not occur at the beginning where the strain rate is maximum, but rather, at a time where the strain rate has a marginal effect on the accelerations. Therefore, the use of the multiple strain rate material model is consider to bound the accelerations imposed on the canister, since it considers the effect of strain rate on the stress-strain curves.

The filter frequency used in the LS-DYNA evaluation is determined by performing two modal analyses of a quarter symmetry model of the base weldment. Symmetry boundary conditions are applied of the planes of symmetry of the model for both analyses. The second analysis considers a boundary condition that is the center node of the base weldment bottom plate, restrained in the vertical direction. These analyses result in a modal frequency of 173 Hz and 188 Hz, respectively. Therefore, a filter frequency of 200 Hz is selected.

Results of the LS-DYNA analysis show that the maximum deformation of the base weldment is about 1 inch. This deformation is small when compared to the 12-inch height of the air inlet. Therefore, a 24-inch drop of the concrete cask does not result in a blockage of the air inlets.

The dynamic response of the canister and basket on impact is amplified by the most flexible components of the system. In the case of the canister and basket, the basket support disk bounds this response. To account for the transient response of the support disk, a dynamic load factor (DLF) for the support disk is computed for the inertia loading developed during the deceleration of the canister bottom plate. The DLF is determined using quarter symmetry models of the PWR and BWR disks as shown in Figures 11.2.4-6 and 11.2.4-7, respectively. These models are generated using ANSYS, Revision 5.5.

To support the disks in the models, restraints are applied at the basket tie-rod locations. For each tie-rod locations, a single node is restrained in the vertical direction allowing the support disks to vibrate freely when the accelerations are applied at the tie rod locations. A transient analysis using ANSYS, Revision 5.5 is performed which uses the acceleration time histories computed from the LS-DYNA analyses. The time history corresponding to the stress–strain curves at different strain

rates is used. This case is considered bounding since the maximum acceleration occurs when the rate dependent stress-strain curves are used.

The DLF is determined to be the maximum deflection of the disk (which occurs at the center of the disk) divided by the static displacement (The static analysis used the maximum acceleration determined from the LS-DYNA analysis). The DLF for the PWR and the BWR are determined to be 1.01 and 1.29, respectively.

Therefore, multiplying the calculated accelerations by the DLF's results in effective accelerations of 45.5g and 58.1g for the PWR and BWR canisters, respectively. These values are enveloped by the 60g acceleration employed in the stress evaluation of the end impact of the canister and support disks. These accelerations are considered to be bounding since they incorporate the effect of the strain rate on the plastic behavior of the pedestal and ignores any energy absorption by the impact plane.

Canister Stress Evaluation

The Transportable Storage Canister stress evaluation for the concrete cask 24-inch bottom end drop accident is performed using a load of 60g. This evaluation bounds the 57.4g load that is calculated for the 24-inch bottom end drop event determined above. This canister evaluation is performed using the ANSYS finite element program. The canister finite element model is shown in Figure 11.2.4-8. The construction and details of the finite element model are described in Section 3.4.4.1.1. Stress evaluations are performed with and without an internal pressure of 25 psig.

The principal components of the canister are the canister shell, including the bottom plate, the fuel basket, the shield lid, and the structural lid. The geometry and materials of construction of the canister, baskets, and lids are described in Section 1.2. The structural design criteria for the canister are contained in the ASME Code, Section III, Subsection NB. This analysis shows that the structural components of the canister (shell, bottom plate, and structural lid) satisfy the allowable stress intensity limits.

The results of the analysis of the PWR and BWR canisters for the 60g bottom end impact loading are presented in Tables 11.2.4-1 through 11.2.4-4. These results are for the load case that includes a canister internal pressure of 25 psig, since that case results in the minimum margin of safety.

The minimum margin of safety at each section of the canister is presented by denoting the circumferential angle at which the minimum margin of safety occurs. A cross-section of the

canister showing the section locations is presented in Figure 11.2.4-9. Stresses are evaluated at 9° increments around the circumference of the canister for each of the locations shown. The minimum margin of safety is denoted by an angular location at each section.

For the canister to structural lid weld (Section 13, Figure 11.2.4-9), base metal properties are used to define the allowable stress limits since the tensile properties of the weld filler metal are greater than those of the base metal. The allowable stress at Section 13 is multiplied by a stress reduction factor of 0.8 in accordance with NRC Interim Staff Guidance (ISG) No. 4, Revision 1.

The allowable stresses presented in Tables 11.2.4-1 through 11.2.4-4, and in Tables 11.2.4-6 and 11.2.4-7, are for Type 304L stainless steel. Because the shield lid is constructed of Type 304 stainless steel, which possesses higher allowable stresses, a conservative evaluation results. The allowable stresses are evaluated at 380°F. A review of the thermal analyses shows that the maximum temperature of the canister is 351°F (Table 4.1-4) for PWR fuel and 376°F (Table 4.1-5) for BWR fuel, which occurs in the center portion of the canister wall (Sections 5 and 6).

Canister Buckling Evaluation

Code Case N-284-1 of the ASME Boiler and Pressure Vessel Code is used to analyze the canister for the 60g bottom end impact. The evaluation requirements of Regulatory Guide 7.6, Paragraph C.5, are shown to be satisfied by the results of the buckling interaction equation calculations.

The internal stress field that controls the buckling of a cylindrical shell consists of the longitudinal (axial) membrane, circumferential (hoop) membrane, and in-plane shear stresses. These stresses may exist singly or in combination, depending on the applied loading. The buckling evaluation is performed without the internal 25 psig pressure, since this results in the minimum margin of safety.

The primary membrane stress results for the 60g bottom impact with no internal pressure are presented in Table 11.2.4-6 for the PWR canister, and in Table 11.2.4-7 for the BWR canister.

The stress results from the ANSYS analyses are screened for the maximum values of the longitudinal compression, circumferential compression, and in-plane shear stresses for the 60g bottom end impact. For each loading case, the largest of each of the three stress components, regardless of location within the canister shell are combined.
The maximum stress components used in the evaluation and the resulting buckling interaction equation ratios are provided in Table 11.2.4-8. The results show that all interaction equation

ratios are less than 1.0. Therefore, the buckling criteria of Code Case N-284-1 are satisfied, demonstrating that buckling of the canister does not occur.

Basket Stress Evaluation

Stresses in the support disks and weldments are calculated by applying the accident loads to the ANSYS models described in Sections 3.4.4.1.8 and 3.4.4.1.9. An inertial load of 60g is conservatively applied to the support disks and weldments in the axial (out of plane) direction. To evaluate the most critical regions of the support disks, a series of cross sections are considered. The locations of these sections on the PWR and BWR support disks are shown in Figures 3.4.4.1-7, 3.4.4.1-8 and Figures 3.4.4.1-13 through 3.4.4.1-16. The stress evaluations for the support disk and weldments are performed according to ASME Code, Section III, Subsection NG. For accident conditions, Level D allowable stresses are used: the allowable stress is $0.7S_u$ and S_u for P_m and P_m+P_b stress categories, respectively. The stress evaluation results are presented in Tables 11.2.4-9 and 11.2.4-10 for the PWR and BWR support disks, respectively. The tables list the 40 highest P_m+P_b stress intensities. The minimum margins of safety are +1.86 and +0.56 for PWR and BWR disks, respectively. The stress results for the PWR and BWR weldments are shown in Table 11.2.4-5. The minimum margin of safety is +1.31 and +0.26 for the PWR and BWR weldments, respectively. Note that the P_m stresses for the disks and weldments are essentially zero, since there are no loads in the plane of the support disk or weldment for a bottom end impact.

Fuel Basket Tie Rod Evaluation

The tie rods serve basket assembly purposes and are not part of the load path for the conditions evaluated. The tie rods are loaded during basket assembly by a 50 ± 10 ft-lbs torque applied to the tie rod end nut. The tensile pre-load on the tie rod, P_B, is [41]:

$$T = P_B\,(0.159\,L + 1.156\,\mu\,d)$$

where:

$T = 60$ ft-lb
$L = 1/8$
$\mu = 0.15$
$d = 1.625$ in.

Solving for P_B:

$P_B = 2{,}387$ lbs. per rod

The maximum tensile stress in the tie rod occurs while the basket is being lifted for installation in the canister. The BWR basket configuration is limiting because it has six tie rods, compared to eight tie rods in the PWR basket, and weighs more than the PWR basket. The load on each BWR basket tie rod is:

$$P = 2{,}387 + \frac{1.1 \times 18{,}199}{6} = 5{,}723 \text{ lbs.}$$

where the weight of the BWR basket is 18,199 pounds.

The maximum tensile stress, S, at room temperature (70°F) is:

$$S = \frac{5{,}723}{\pi \times 0.25 \times 1.625^2} = 2{,}760 \text{ psi}$$

Therefore, the margin of safety is:

$$MS = \frac{20{,}000}{2{,}760} - 1 = +\text{Large}$$

This result bounds that for the PWR basket configuration. The tie rod is not loaded in drop events; therefore, no additional analysis of the tie rod is required.

PWR and BWR Tie Rod Spacer Analysis

The PWR and BWR basket support disks and heat transfer disks are connected by tie rods (8 for PWR and 6 for BWR) and located by spacers to maintain the disk spacing. The PWR and BWR spacers are constructed from ASME SA479 Type 304 stainless steel or ASME SA312 Type 304 stainless steel. The difference in using the two materials is the cross-sectional area of the spacers.

The geometry of the spacers is:

For SA479 stainless steel:

Spacer:	Outside Diameter	= 3.00 in.
	Inside Diameter	= 1.75 in.
Split Spacer:	Outside Diameter	= 2.50 in. (Machined down section)
	Inside Diameter	= 1.75 in.
	Outside Diameter	= 3.00 in.

For the full spacer, the cross-section area is 4.66 inches^2, and for the split spacer, the cross-section area is 2.5 inches^2.

For SA312 stainless steel:

Spacer:	Outside Diameter	= 2.875 in.
	Inside Diameter	= 1.771 in.
Split Spacer:	Outside Diameter	= 2.50 in. (Machined down section)
	Inside Diameter	= 1.771 in.
	Outside Diameter	= 2.875 in.

For the full spacer, the cross-section area is 4.03 inches^2, and for the split spacer, the cross-section area is 2.45 inches^2.

During a 24-inch drop, the weight of the support disks, top weldment, heat transfer disks, spacers, and end nuts are supported by the spacers on the tie rods. A conservative deceleration of 60g is applied to the spacers. The bounding spacer load occurs at the bottom weldment of the BWR basket. The bounding split-spacer load occurs at the 10th support disk (from bottom of the basket) of the BWR basket.

The applied load on the BWR bottom spacer is 131,507 lbs.

$$P = 60(P_S) + P_T = 131{,}507 \text{ lbs.}$$

where:

$P_T = 2387$ lbs	torque pre-load
$P_s = 2152$ lbs	load on the spacer due to basket structure above the spacer location

$$P_s = \frac{18{,}199 - 623 - 4665}{6} = 2{,}152 \text{ lbs}$$

where:

18,199 lb.	BWR basket weight
623 lb.	BWR bottom weldment weight
4,665 lb.	BWR fuel tube weight

The applied load on the BWR split spacer is 108,227 lbs.

$$P = 60(P_S) + P_T = 108{,}227 \text{ lbs}$$

where:

P_T = 2387 lbs torque pre-load

P_s = 1764 lbs load on the spacer due to basket structure above the spacer location

$$P_s = \frac{18199 - 623 - 4665 - 10 \times 203 - 60 \times 5}{6} = 1{,}764 \text{ lbs}$$

18,199 lbs	BWR basket weight
623 lbs	BWR bottom weldment weight
4,665 lbs	BWR fuel tube weight
203 lbs	BWR support disk weight (Qty = 10)
5 lbs	BWR full spacer weight (Qty = 60)

The margins of safety for the spacers are:

	Applied Load (lbs)	Cross-sectional area (in^2)	Stress (psi)	Temperature (°F)	Allowable Stress (psi)	Margin of Safety
Spacer						
SA479	131507	4.66	28,220	250	47,950	0.70
SA312	131507	4.03	32,632	250	47,950	0.46
Split Spacer						
SA479	108227	2.50	43,291	350	45,640	0.05
SA312	108227	2.45	44174	350	45,640	0.03

The temperatures used bound the analysis locations for all storage conditions. The actual temperatures at these locations for storage for the BWR spacer at the bottom weldment is 118°F (minimum bottom weldment temperature), and 329°F (minimum temperature of 10th support disk) for the split spacer. The 10th support disk is counted from bottom weldment.

Fuel Tube Analysis

During the postulated 24-inch end drop of the concrete cask, fuel assemblies are supported by the canister bottom plate. The fuel assembly weight is not carried by the fuel tubes in the end drop. Therefore, evaluation of the fuel tube is performed considering the weight of the fuel tube, the canister deceleration and the minimum fuel tube cross-section. The minimum cross-section is located at the contact point of the fuel tube with the basket bottom weldment. The PWR fuel tube analysis is bounding because its weight (153 pounds/tube) is approximately twice that of the BWR fuel tube (83 pounds/tube). The minimum cross-section area of the PWR fuel tube is:

$$A = (\text{thickness})(\text{mean perimeter})$$

$$A = (0.048 \text{ in.})(8.80 \text{ in.} + 0.048 \text{ in.})(4) = 1.69 \text{ in}^2$$

The maximum compressive and bearing stress in the fuel tube is:

$$S_b = \frac{(60g)(153 \text{ lbs})}{1.69 \text{ in}^2} = 5{,}432 \text{ psi}$$

The Type 304 stainless steel yield strength is 17,300 psi at a conservatively high temperature of 750°F. The margin of safety is:

$$MS = \frac{S_y}{S_b} - 1 = \frac{17{,}300 \text{ psi}}{5{,}432 \text{ psi}} - 1 = +2.18 \text{ at } 750°F$$

Summary of Results

Evaluation of the UMS cask and canister during a 24-inch drop accident shows that the resulting maximum acceleration of the canister is 57.4g. The acceleration determined for the canister during the 24-inch drop is less than its design allowable g-load and, therefore, is considered bounded. This accident condition does not lead to a reduction in the cask's shielding effectiveness. The base weldment, which includes the air inlets, is crushed approximately 1-inch as the result of the 24-inch drop. The effect of the reduction of the inlet area by the drop is to reduce cooling airflow. This

condition is bounded by the consequences of the loss of one-half of the air inlets evaluated in Section 11.1.2.

11.2.4.4 Corrective Actions

Although the concrete cask remains functional following this event and no immediate recovery actions are required, the canister should be moved to a new concrete cask as soon as one is available. The damaged cask should be inspected for stability, and repaired as required prior to continued use.

11.2.4.5 Radiological Impact

There are no radiological consequences for this accident.

Figure 11.2.4-1 Concrete Cask Base Weldment

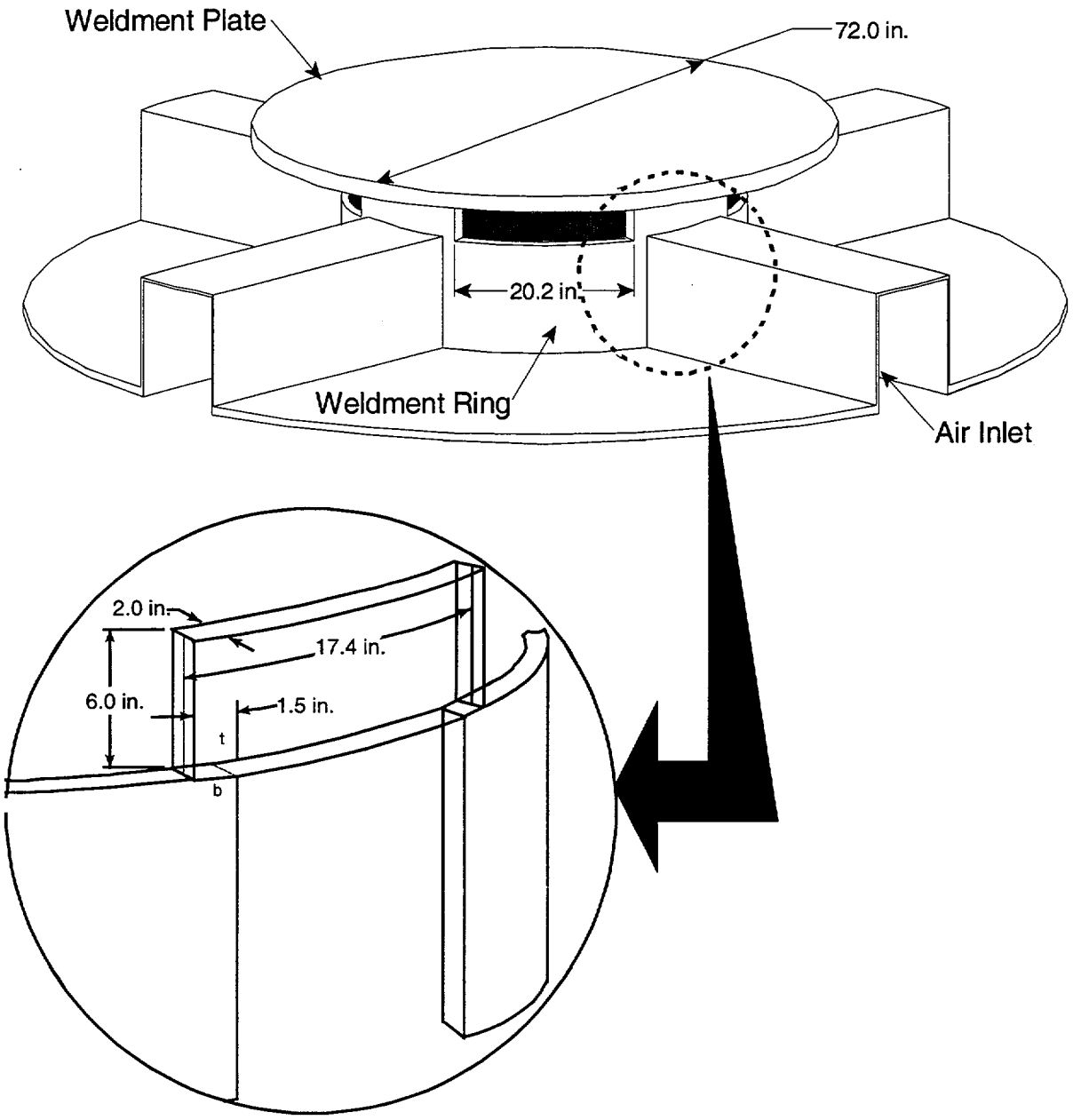

Figure 11.2.4-2 Concrete Cask Base Weldment Finite Element Model

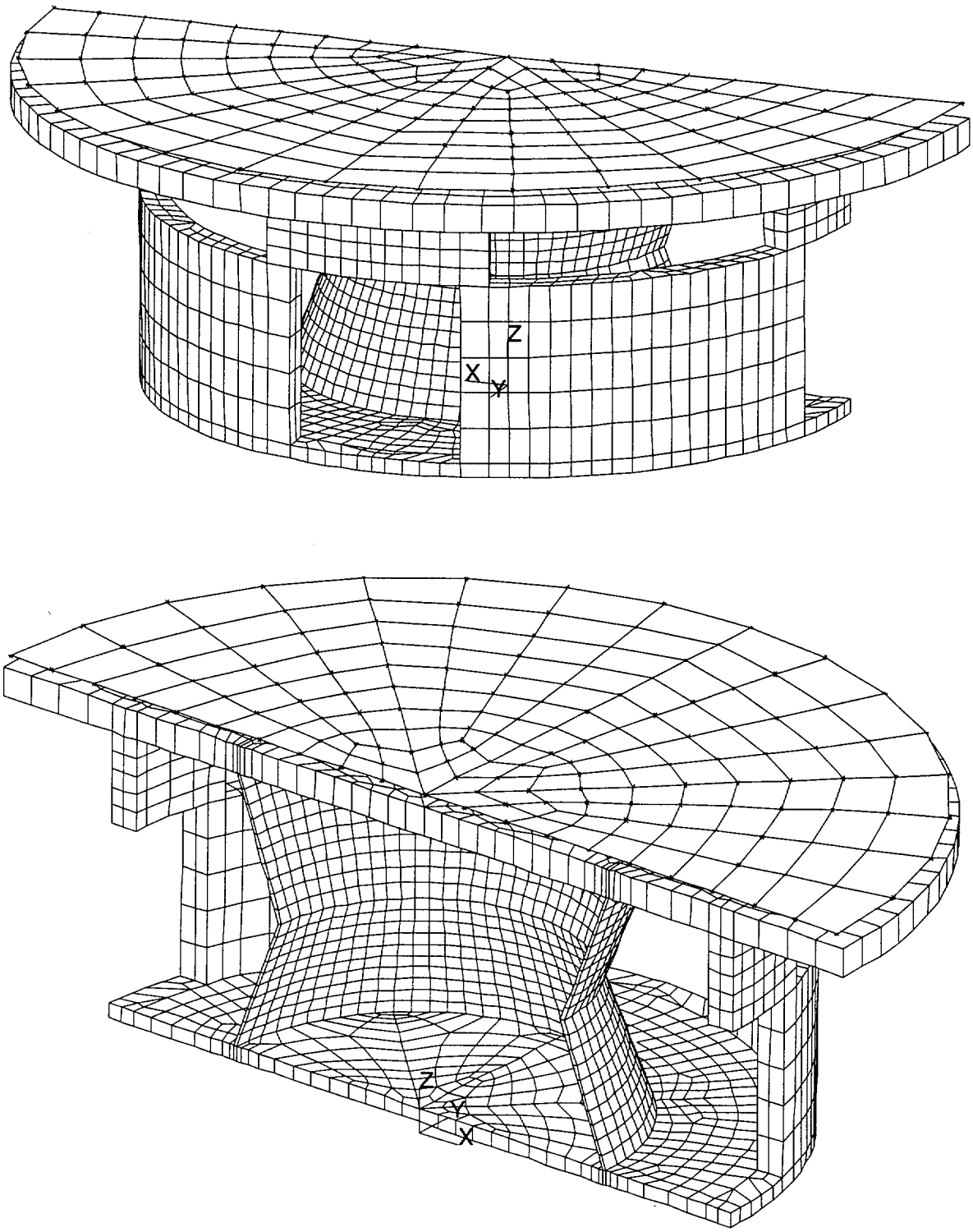

Figure 11.2.4-3 Strain Rate Dependent Stress-Strain Curves for Concrete Cask Base Weldment Structural Steel

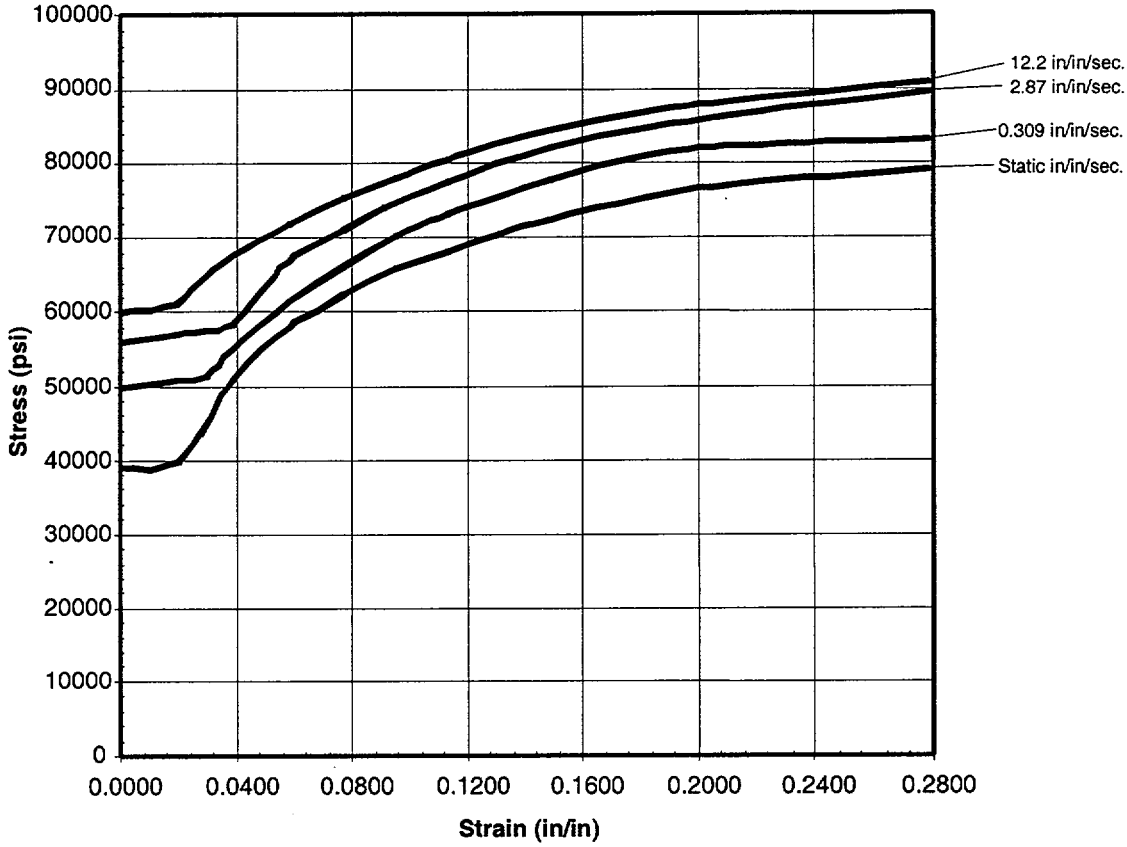

Figure 11.2.4-4 Acceleration Time-History of the Canister Bottom During the Concrete Cask 24-Inch Drop Accident With Static Strain Properties

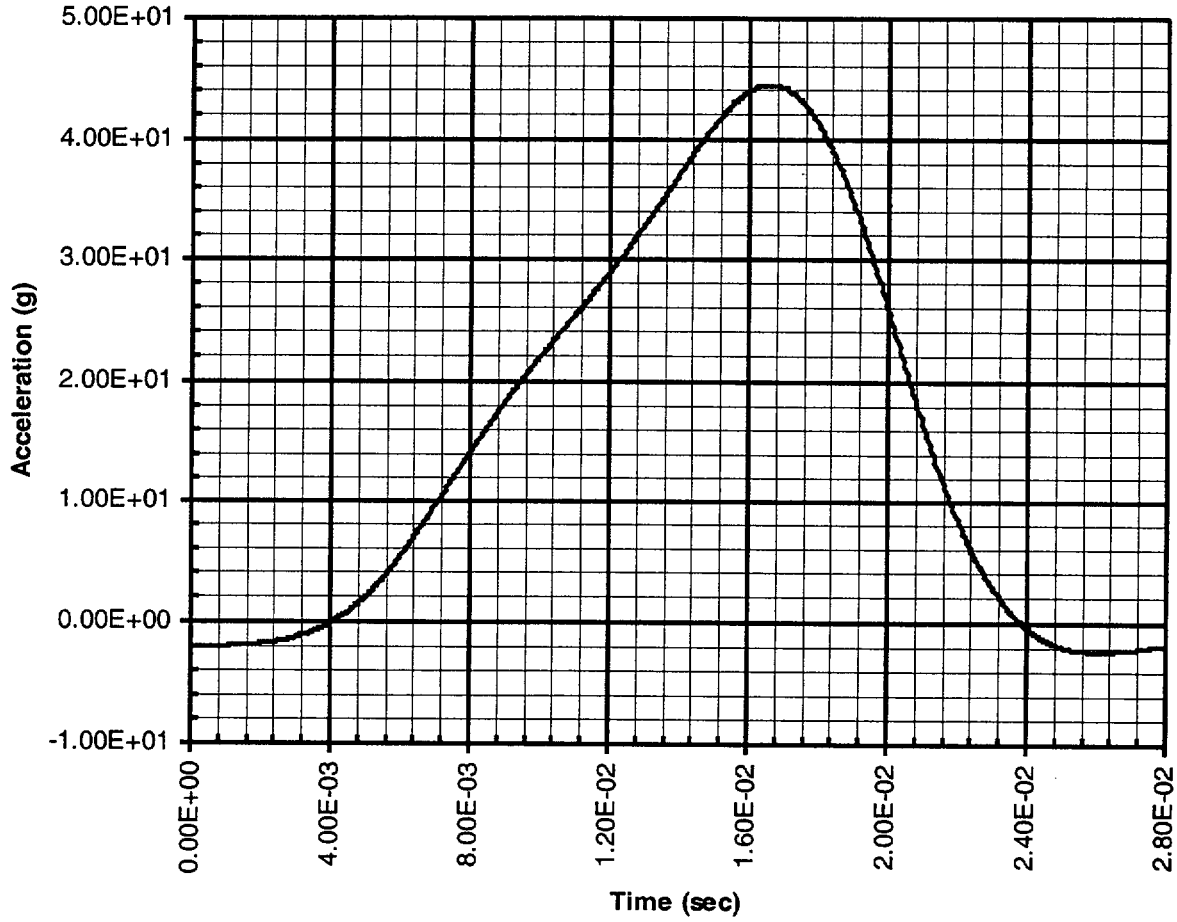

Figure 11.2.4-5 Acceleration Time-History of the Canister Bottom During the Concrete Cask 24-Inch Drop Accident With Strain Rate Dependent Properties

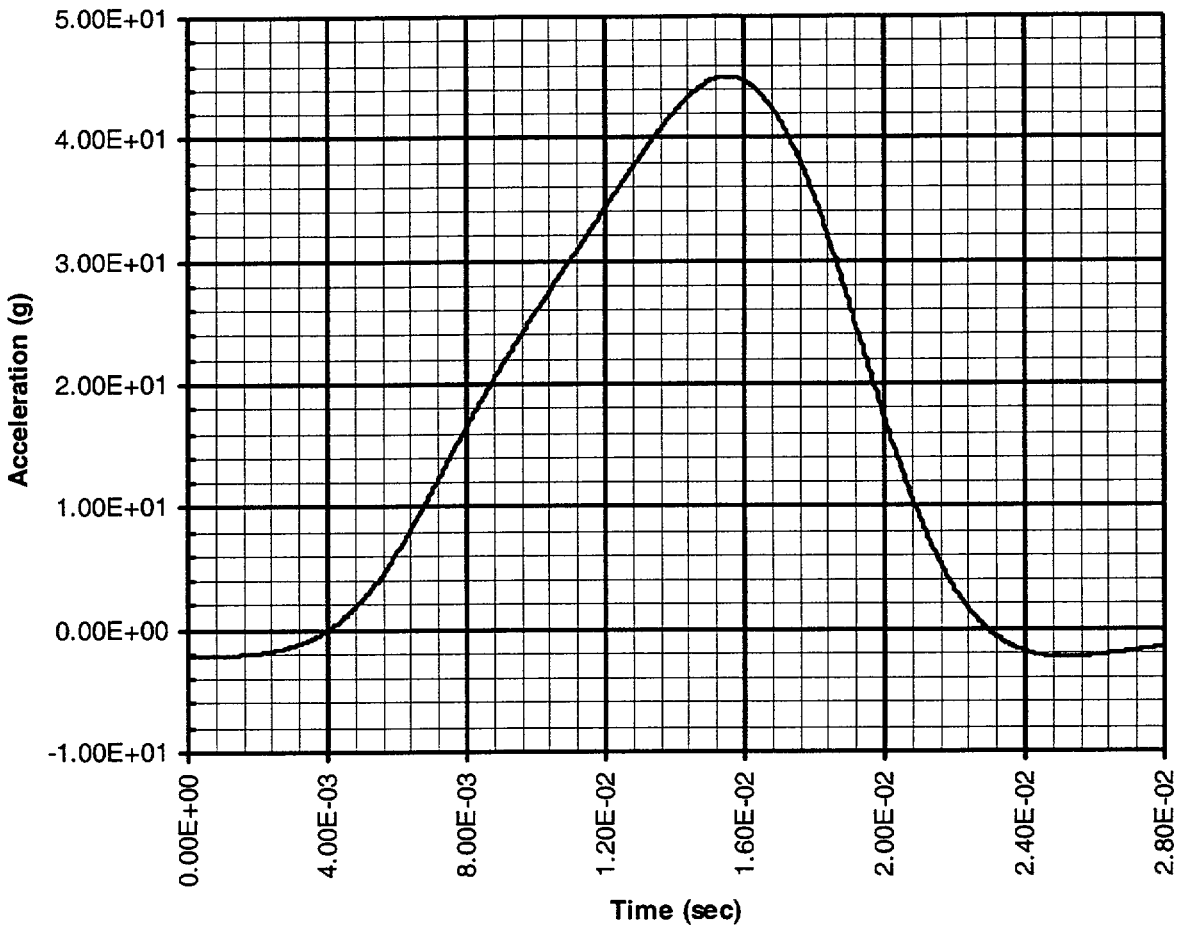

Figure 11.2.4-6 Quarter Model of the PWR Basket Support Disk

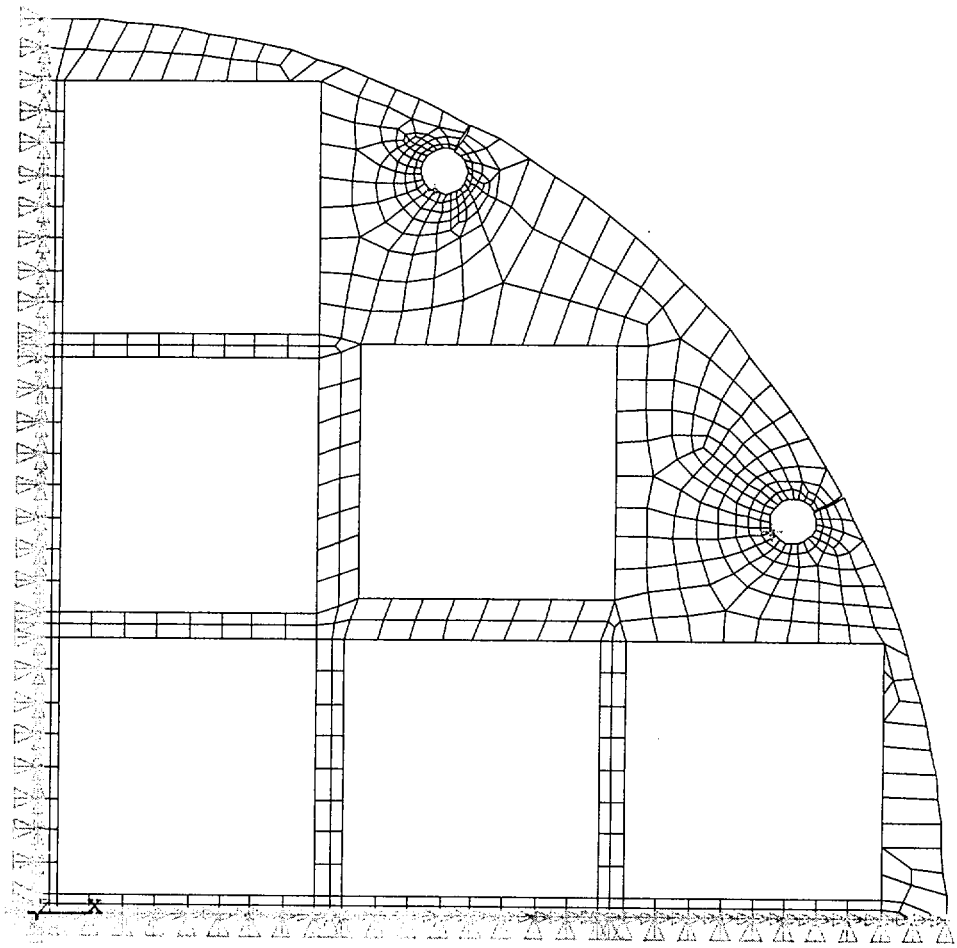

Figure 11.2.4-7 Quarter Model of the BWR Basket Support Disk

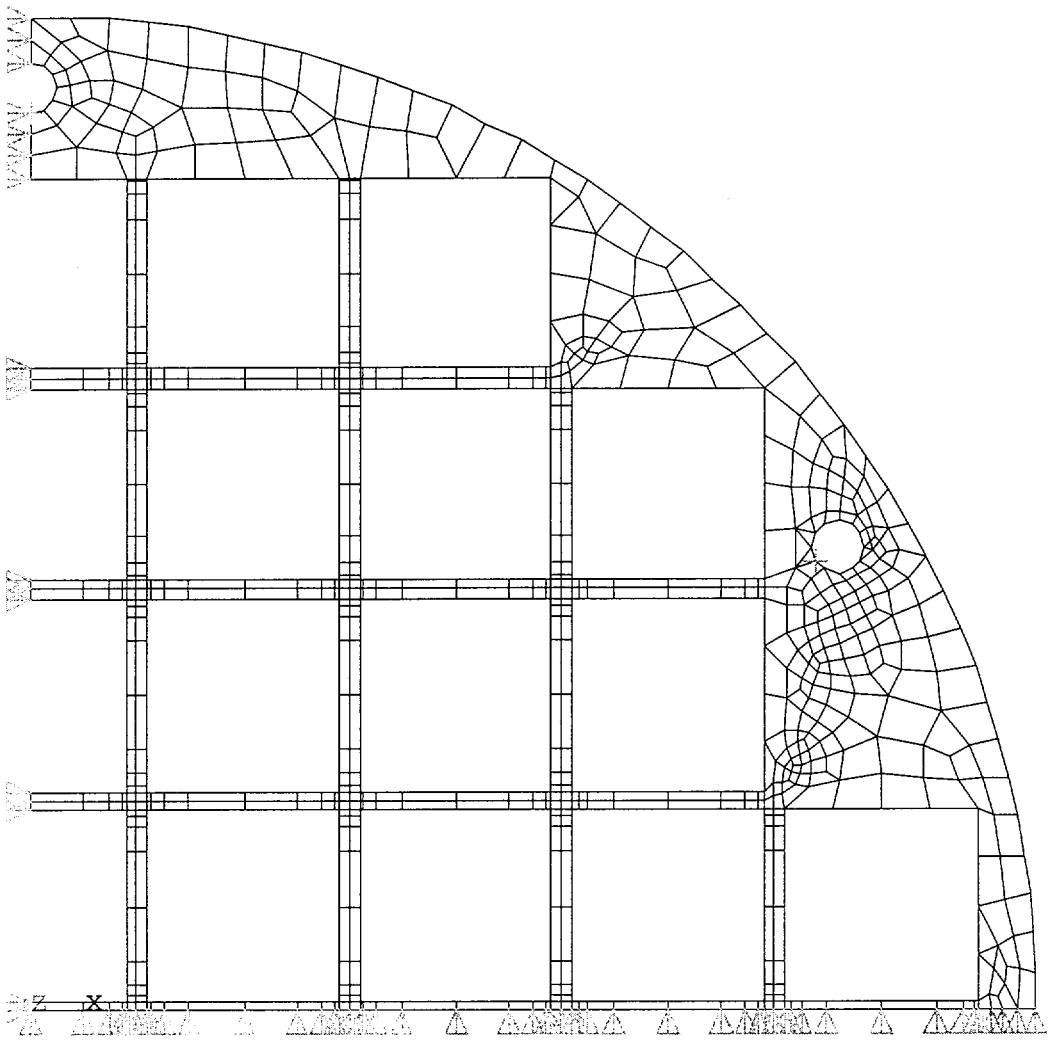

Figure 11.2.4-8 Canister Finite Element Model for 60g Bottom End Impact

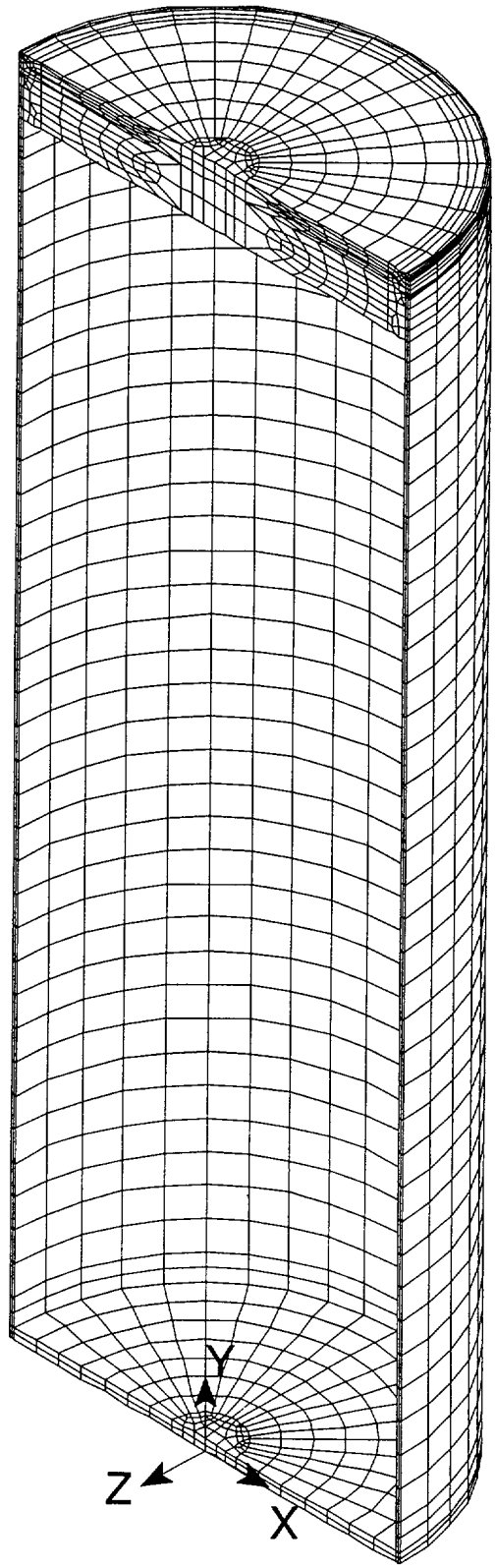

Figure 11.2.4-9 Identification of the Canister Sections for the Evaluation of Canister Stresses due to a 60g Bottom End Impact

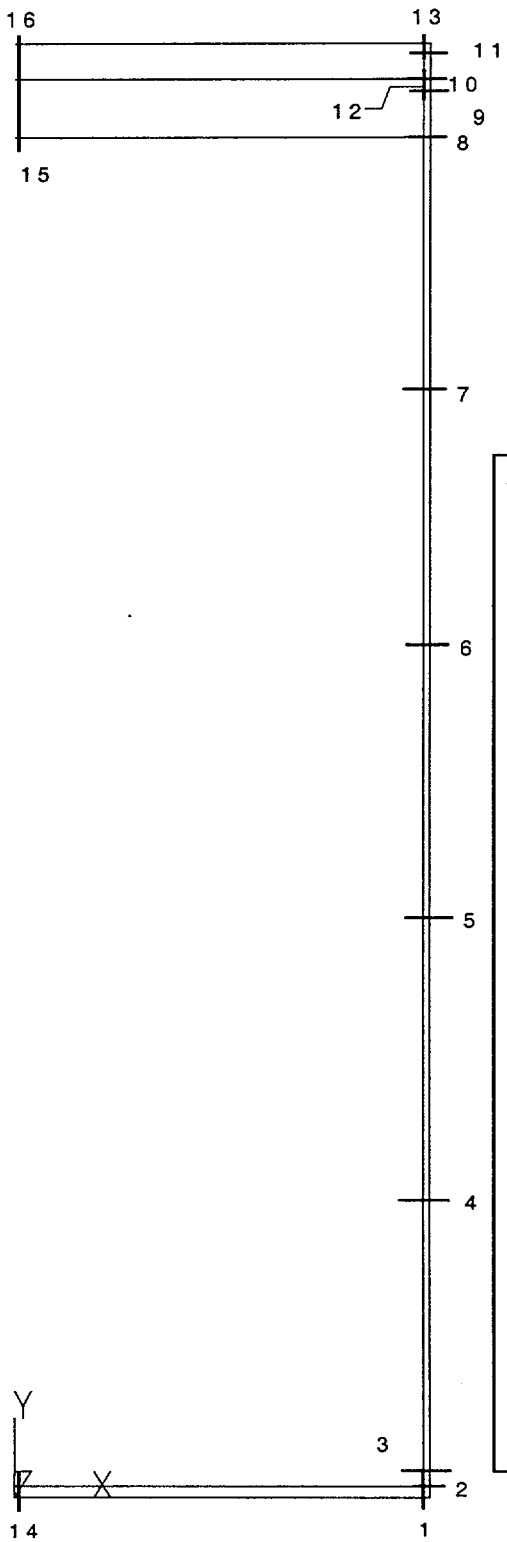

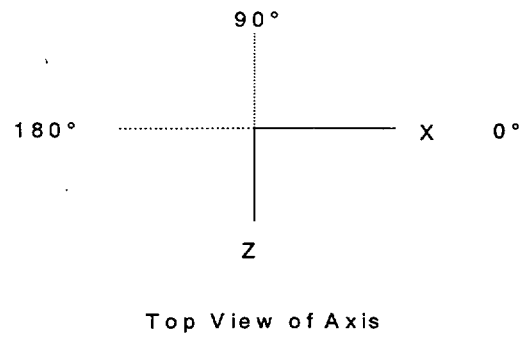

PWR Section Coordinates at Z = 0

Axial Section	Node 1		Node 2	
	x	y	x	y
1	32.905	0.0	32.905	1.75
2	32.905	1.75	33.53	1.75
3	32.905	2.25	33.53	2.25
4	32.905	34.15	33.53	34.15
5	32.905	66.55	33.53	66.55
6	32.905	98.95	33.53	98.95
7	32.905	131.35	33.53	131.35
8	32.905	163.75	33.53	163.75
9	32.905	170.25	33.53	170.25
10	32.905	170.75	33.53	170.75
11	32.905	172.87	33.53	172.87
12	32.905	170.25	32.905	170.75
13	32.905	172.87	32.905	173.75
14	0.1	0.0	0.1	1.75
15	0.1	163.75	0.1	170.73
16	0.1	170.75	0.1	173.75

BWR Section Coordinates at Z = 0

Axial Section	Node 1		Node 2	
	x	y	x	y
1	32.905	0.0	32.905	1.75
2	32.905	1.75	33.53	1.75
3	32.905	2.25	33.53	2.25
4	32.905	37.79	33.53	37.79
5	32.905	73.83	33.53	73.83
6	32.905	109.87	33.53	109.87
7	32.905	145.91	33.53	145.91
8	32.905	181.95	33.53	181.95
9	32.905	188.45	33.53	188.45
10	32.905	188.95	33.53	188.95
11	32.905	191.07	33.53	191.07
12	32.905	188.45	32.905	188.95
13	32.905	191.07	32.905	191.95
14	0.1	0.0	0.1	1.75
15	0.1	181.95	0.1	188.73
16	0.1	188.97	0.1	191.95

Table 11.2.4-1 PWR Canister P_m Stresses During a 60g Bottom Impact (25 psig Internal Pressure)

Section Location	P_m Stress (ksi)						SI (ksi)	Allowable Stress (ksi)	Margin of Safety
	Sx	Sy	Sz	Sxy	Syz	Sxz			
1	0	-2.6	-0.4	0.2	0.1	0	2.6	38.4	13.85
2	0.7	-6.3	-1.1	0.3	0.1	0.1	7.1	38.4	4.43
3	0.1	-6.9	-1.2	0	0.1	0.1	7	38.4	4.49
4	0	-6.3	1.3	0	0	-0.1	7.7	38.4	4.01
5	0	-5.8	1.3	0	0	-0.1	7.1	38.4	4.41
6	0	-5.2	1.3	0	0	-0.1	6.5	38.4	4.88
7	0	-4.6	1.3	0	0	-0.1	6	38.4	5.44
8	0.7	-3.1	0.1	0	-0.1	0.1	3.8	38.4	9.03
9	-1.7	-1.9	-0.7	-0.1	0.4	-0.4	1.6	38.4	22.94
10	1.7	-1.3	-1	-0.3	0	0.2	3.1	38.4	11.5
11	-2	0.5	-0.9	0	0	0.1	2.5	38.4	14.17
12	0.7	1.8	-0.4	0.2	0.1	-0.1	2.2	38.4	16.18
13	0	-2	-1.2	0	0	0.1	2	30.72*	14.36
14	0.1	-1.1	0.1	0	0	0	1.2	38.4	30.57
15	0.2	-0.1	0.2	0	0	0	0.2	38.4	186.72
16	-0.2	0	-0.2	0	0	0	0.2	38.4	223.94

* Allowable stress includes a stress reduction factor for the weld: 0.8 x allowable stress.

Table 11.2.4-2 PWR Canister $P_m + P_b$ Stresses During a 60g Bottom Impact (25 psig Internal Pressure)

Section Location	$P_m + P_b$ Stress (ksi)						SI (ksi)	Allowable Stress (ksi)	Margin of Safety
	Sx	Sy	Sz	Sxy	Syz	Sxz			
1	0.4	-2.9	-0.2	0.3	0.1	0	3.4	57.5	16.11
2	0.4	-9.5	-2.1	0.1	0.1	0.2	9.9	57.5	4.84
3	0.1	-8.9	-1.8	-0.1	0.1	0.1	9	57.5	5.39
4	0	-6.3	1.3	0	0	-0.1	7.7	57.5	6.49
5	0	-5.8	1.3	0	0	0.1	7.1	57.5	7.1
6	0	-5.2	1.3	0	0	-0.1	6.5	57.5	7.8
7	0	-4.6	1.3	0	0	-0.1	6	57.5	8.64
8	0.6	-3.4	0.3	0	-0.2	0	4.1	57.5	13.03
9	-2.4	-3.9	-0.4	0	0.7	0	3.7	57.5	14.53
10	-2.9	-6.6	0.6	0	0.2	0	7.3	57.5	6.91
11	-1.1	5.6	0.9	-0.4	0	0.1	6.8	57.5	7.52
12	2.6	3.6	0.7	0.7	0	-0.1	3.3	57.5	16.27
13	2.3	0.1	0.1	0.4	0.1	0.2	2.4	46.0*	18.17
14	0.1	-1.2	0.1	0	0	0	1.3	57.5	43.49
15	3.6	0	3.6	0	0	0	3.6	57.5	14.82
16	-1.8	0	-1.8	0	0	0	1.8	57.5	31.14

* Allowable stress includes a stress reduction factor for the weld: 0.8 x allowable stress.

Table 11.2.4-3 BWR Canister P_m Stresses During a 60g Bottom Impact (25 psig Internal Pressure)

Section Location	P_m Stress (ksi)						SI (ksi)	Allowable Stress (ksi)	Margin of Safety
	Sx	Sy	Sz	Sxy	Syz	Sxz			
1*	-0.1	-2.8	-0.4	0.2	0.1	0	2.8	38.4	12.57
2	0.6	-6.5	-1.2	0.3	0.1	0.1	7.1	38.4	4.39
3	0.4	-6.7	-1.1	0.2	0.1	0.1	7.1	38.4	4.37
4	0	-6.6	1.3	0	0	-0.1	7.9	38.4	3.85
5	0	-6	1.3	0	0	-0.1	7.3	38.4	4.27
6	0	-5.3	1.3	0	0	-0.1	6.6	38.4	4.77
7	0	-4.7	1.3	0	0	-0.1	6	38.4	5.37
8	0.5	-3.1	0.3	0	0	0.3	3.8	38.4	9.03
9	-1.7	-1.9	-0.7	-0.1	0.4	-0.4	1.6	38.4	22.94
10	1.7	-1.3	-1	-0.3	0	0.2	3.1	38.4	11.5
11	-2	0.5	-0.9	0	0	0.1	2.5	38.4	14.17
12	0.7	1.8	-0.4	0.2	0.1	-0.1	2.2	38.4	16.18
13	0	-2	-1.2	0	0	0.1	2	30.72**	14.36
14*	0.1	-1.1	0.1	0	0	0	1.3	38.4	29.44
15	0.2	-0.1	0.2	0	0	0	0.2	38.4	186.72
16	-0.2	0	-0.2	0	0	0	0.2	38.4	223.54

* Stresses at these locations are increased by 5% to account for the heavier BWR fuel basket/fuel assemblies.

** Allowable stress includes stress reduction factor for weld: 0.8 x stress allowable.

Table 11.2.4-4 BWR Canister $P_m + P_b$ Stresses During a 60g Bottom Impact (25 psig Internal Pressure)

Section Location	$P_m + P_b$ Stress (ksi)						SI (ksi)	Allowable Stress (ksi)	Margin of Safety
	Sx	Sy	Sz	Sxy	Syz	Sxz			
1*	0.3	-3.2	-0.3	0.3	0.1	0	3.7	57.5	14.54
2	0.3	-9.4	-2.1	0.2	0.1	0.2	9.7	57.5	4.95
3	0.2	-9	-1.8	0.1	0.1	0.1	9.2	57.5	5.28
4	0	-6.6	1.3	0	0	-0.1	7.9	57.5	6.25
5	0	-6	1.3	0	0	0.1	7.3	57.5	6.89
6	0	-5.3	1.3	0	0	-0.1	6.7	57.5	7.64
7	0	-4.7	1.3	0	0	-0.1	6	57.5	8.54
8	0.5	-3.4	0.5	0.1	-0.1	0.2	4.1	57.5	13.03
9	-2.4	-3.9	-0.4	0	0.7	0	3.7	57.5	14.53
10	-2.9	-6.6	0.6	0	0.2	0	7.3	57.5	6.91
11	-1.1	5.6	0.9	-0.4	0	0.1	6.8	57.5	7.52
12	2.6	3.6	0.7	0.7	0	-0.1	3.3	57.5	16.27
13	2.3	0.1	0.1	0.4	0.1	0.2	2.4	46.0**	18.17
14*	0.1	-1.1	0.1	0	0	0	1.4	57.5	37.33
15	3.6	0	3.6	0	0	0	3.6	57.5	14.82
16	-1.8	0	-1.8	0	0	0	1.8	57.5	31.14

* Stresses at these locations are increased by 5% to account for the heavier BWR fuel basket/fuel assemblies.

** Allowable stress includes stress reduction factor for weld: 0.8 x stress allowable.

Table 11.2.4-5 Summary of Maximum Stresses for PWR and BWR Basket Weldments During a 60g Bottom Impact

Case	Stress Category	Maximum Stress Intensity[1] (ksi)	Allowable Stress[2] (ksi)	Margin of Safety
PWR Top Weldment	$P_m + P_b$	27.5	63.5	1.31
PWR Bottom Weldment	$P_m + P_b$	12.0	68.5	+Large
BWR Top Weldment	$P_m + P_b$	34.1	64.0	0.88
BWR Bottom Weldment	$P_m + P_b$	51.9	65.2	0.26

1. Nodal stresses from the finite element analysis results are used.
2. Allowable stresses are conservatively determined at the maximum temperatures of the weldments.

Table 11.2.4-6 PWR Canister P_m Stresses During a 60g Bottom Impact (No Internal Pressure)

Section Location	P_m Stress (ksi)						SI (ksi)	Allowable Stress (ksi)	Margin of Safety
	Sx	Sy	Sz	Sxy	Syz	Sxz			
1	-0.1	-3	-0.5	0.2	0.1	0	2.9	38.4	12.08
2	0.6	-6.7	-1.3	0.3	0.1	0.1	7.3	38.4	4.27
3	0.1	-7.4	-1.5	0	0.1	0.1	7.5	38.4	4.09
4	0	-7	0	0	0	0	7	38.4	4.48
5	0	-6.4	0	0	0	0	6.4	38.4	4.97
6	0	-5.9	0	0	0	0	5.9	38.4	5.55
7	0	-5.3	0	0	0	0	5.3	38.4	6.24
8	0.1	-3.6	0.1	0.1	-0.1	-0.1	3.7	38.4	9.28
9	-2	-2.1	-0.9	-0.2	0.5	-0.4	1.8	38.4	20.52
10	2	-1.4	-1.2	-0.3	0	0.2	3.5	38.4	9.85
11	-2.3	0.6	-1.1	0	0	0.1	3	38.4	11.97
12	0.8	2	-0.5	0.3	0.1	-0.1	2.5	38.4	14.15
13	0	-2.3	-1.3	0	0	0.1	2.3	30.72*	12.36
14	0.1	-1.1	0.1	0	0	0	1.2	38.4	32.35
15	0.2	0	0.2	0	0	0	0.2	38.4	174.28
16	-0.2	0	-0.2	0	0	0	0.2	38.4	191.24

* Allowable stress includes a stress reduction factor for the weld: 0.8 x allowable stress.

Table 11.2.4-7 BWR Canister P_m Stresses During a 60g Bottom Impact (No Internal Pressure)

Section Location	P_m Stress (ksi)						SI (ksi)	Allowable Stress (ksi)	Margin of Safety
	Sx	Sy	Sz	Sxy	Syz	Sxz			
1*	-0.1	-3.1	-0.6	0.2	0.1	0	3.2	38.4	11.13
2	0.5	-6.9	-1.4	0.3	0.1	0.1	7.4	38.4	4.16
3	0.4	-7.1	-1.3	0.2	0.1	0.1	7.5	38.4	4.08
4	0	-7.2	0	0	0	0	7.2	38.4	4.29
5	0	-6.6	0	0	0	0	6.6	38.4	4.8
6	0	-6	0	0	0	0	6	38.4	5.41
7	0	-5.4	0	0	0	0	5.4	38.4	6.15
8	0.1	-3.6	0.1	0.1	-0.1	-0.1	3.7	38.4	9.28
9	-2	-2.1	-0.9	-0.2	0.5	-0.4	1.8	38.4	20.52
10	-0.9	-1.5	1.7	0.1	-0.3	-0.9	3.5	38.4	9.85
11	-2.3	0.6	-1.1	0	0	0.1	3	38.4	11.97
12	0.8	2	-0.5	0.3	0.1	-0.1	2.5	38.4	14.15
13	0	-2.3	-1.3	0	0	0.1	2.3	30.72**	12.36
14*	0.1	-1.1	0.1	0	0	0	1.2	38.4	31.18
15	0.2	0	0.2	0	0	0	0.2	38.4	174.36
16	-0.2	0	-0.2	0	0	0	0.2	38.4	190.95

*Stresses at these locations are increased by 5% to account for the heavier BWR fuel basket/fuel assemblies.

**Allowable stress includes stress reduction factor for weld: 0.8 x stress allowable.

Table 11.2.4-8 Canister Buckling Evaluation Results for 60g Bottom End Impact

	PWR Canister	BWR Canister
Longitudinal (Axial) Stress* Sy (psi)	7,400	7,200
Circumferential (Hoop) Stress* Sz (psi)	1,500	1,300
In-Plane Shear Stress Syz (psi)	100	300
Elastic Buckling Interaction Equations		
Q1	0.142	0.122
Q2	0.159	0.152
Q3	0.219	0.188
Q4	0.142	0.122
Plastic Buckling Interaction Equations		
Q5	0.159	0.152
Q6	0.219	0.188
Q7	0.159	0.152
Q8	0.219	0.188

Component stresses include thermal stresses.

* Compressive stresses

Table 11.2.4-9 $P_m + P_b$ Stresses for PWR Support Disk - 60g Concrete Cask Bottom End Impact (ksi)

Section[1]	S_x	S_y	S_{xy}	Stress Intensity	Allowable Stress	Margin of Safety
66	37.6	18.1	15.1	45.8	130.9	1.86
120	17.7	37.3	-15.2	45.6	130.9	1.87
82	37.5	18.1	-14.6	45.3	130.9	1.89
72	17.9	37.2	14.8	45.2	130.9	1.89
42	8.4	-24.2	-2.3	32.9	130.1	2.95
40	8.4	-24.2	2.3	32.9	130.1	2.95
56	8.4	-24.2	2.3	32.9	130.1	2.96
12	-24.2	8.4	2.3	32.9	130.1	2.96
28	-24.1	8.4	2.3	32.9	130.1	2.96
54	8.4	-24.2	-2.3	32.9	130.1	2.96
14	-24.2	8.4	-2.3	32.9	130.1	2.96
26	-24.1	8.4	-2.3	32.8	130.1	2.96
90	24.3	3.5	-10.3	29.3	130.9	3.46
122	24.4	3.8	-10.4	29.3	130.9	3.46
106	24.3	3.7	10.3	29.2	130.9	3.48
74	24.3	3.9	10.3	29.1	130.9	3.5
99	3	23.7	10.2	29	130.9	3.51
115	3.5	23.7	-10.1	28.6	130.9	3.58
114	9.1	11.2	-14.2	28.5	130.9	3.59
83	3.4	23.8	-10	28.5	130.9	3.59
67	3.4	23.6	10.1	28.5	130.9	3.59
88	11.1	9.5	-14.1	28.2	130.9	3.64
104	11.2	9.4	13.3	26.7	130.9	3.91
98	10.5	11	13.3	26.6	130.9	3.92
3	-19.8	-11.1	-7.7	24.4	124.3	4.1
4	-11.2	-19.8	-7.7	24.4	124.3	4.1
1	-19.8	-11.1	-7.7	24.4	124.3	4.1
2	-11.2	-19.8	-7.7	24.4	124.3	4.1
51	-5.5	-22.4	-4.2	23.4	128.1	4.47
49	-5.5	-22.4	4.3	23.4	128.1	4.47
9	-22.4	-5.5	4.2	23.4	128.1	4.47
23	-22.4	-5.5	-4.2	23.4	128.1	4.47
7	-22.4	-5.5	-4.2	23.4	128.1	4.48
21	-22.4	-5.5	4.2	23.4	128.1	4.48
35	-5.5	-22.4	-4.2	23.4	128.1	4.48
37	-5.4	-22.4	4.2	23.4	128.1	4.48
39	9.3	-12.4	4.3	23.3	130.1	4.58
11	-12.4	9.3	-4.3	23.3	130.1	4.59
53	9.3	-12.4	-4.3	23.3	130.1	4.59
25	-12.4	9.3	-4.3	23.3	130.1	4.59

1. Section locations are shown in Figures 3.4.4.1-7 and 3.4.4.1-8.

Table 11.2.4-10 $P_m + P_b$ Stresses for BWR Support Disk - 60g Concrete Cask Bottom End Impact (ksi)

Section[1]	Sx	Sy	Sxy	Stress Intensity	Allowable Stress	Margin of Safety
257	54.5	19.9	11	57.7	90	0.56
171	10.3	52.8	8	54.3	90	0.66
108	9	52.9	-7.7	54.2	90	0.66
234	10.9	52.8	-6.9	53.9	90	0.67
129	50.5	16.5	10.9	53.7	90	0.68
65	49.8	15.7	-10.9	53	90	0.7
182	49.8	9.1	10.6	52.4	90	0.72
192	49.2	13.9	-10.3	52	90	0.73
300	7.7	50.4	7	51.6	90	0.75
119	48	8.4	-9.4	50.1	90	0.8
54	48	8.3	9.4	50.1	90	0.8
246	47.7	9.1	-9	49.7	90	0.81
103	14.1	16.5	11.4	26.8	90	2.36
235	-4.8	21.1	1.6	26	90	2.46
229	13.5	16.1	11.1	25.9	90	2.47
140	10.5	-14.2	-3.9	25.9	90	2.48
77	10.5	-14.2	3.9	25.9	90	2.48
269	10.5	-14.2	-3.8	25.9	90	2.48
203	10.5	-14.2	3.8	25.9	90	2.48
295	13.3	15.6	-11	25.6	90	2.52
301	-4.7	20.4	-2.5	25.5	90	2.52
134	1.6	11.8	-11.6	25.4	90	2.55
197	1.6	11.8	11.6	25.4	90	2.55
71	1.6	11.8	11.6	25.4	90	2.55
263	1.6	11.7	-11.6	25.3	90	2.56
172	-3.5	21.5	-1.6	25.1	90	2.58
166	13	15.4	-10.8	25	90	2.59
40	15.3	-9	2.9	25	90	2.6
27	15.3	-9	-2.9	25	90	2.6
228	-12.3	-4.5	11.8	24.9	90	2.61
165	-12.3	-4.6	-11.8	24.9	90	2.61
102	-12.3	-4.5	11.8	24.9	90	2.61
294	-12.3	-4.6	-11.8	24.9	90	2.61
252	-20.5	-6.5	-8.6	24.6	90	2.66
124	-20.6	-6.5	-8.6	24.6	90	2.66
60	-20.5	-6.5	8.6	24.6	90	2.66
187	-20.5	-6.5	8.6	24.6	90	2.66
109	-2.6	21.4	2.6	24.6	90	2.67
73	5	13.9	11.4	24.5	90	2.68
199	4.5	14.3	11.1	24.2	90	2.72

1. Section locations are shown in Figures 3.4.4.1-13 through 3.4.4.1-16

11.2.5 Explosion

The analysis of a design basis flood presented in Section 11.2.9 shows that the flood exerts a pressure of 22 psig on the canister, and that the Universal Storage System experiences no adverse effects due to this pressure. The pressure of 22 psig is considered to bound any pressure due to an explosion occurring in the vicinity of the ISFSI.

11.2.5.1 Cause of Explosion

An explosion affecting the Universal Storage System may be caused by industrial accidents or the presence of explosive substances in the vicinity of the ISFSI. However, no flammable or explosive substances are stored or used at the storage facility. In addition, site administrative controls exclude explosive substances in the vicinity of the ISFSI. Therefore, an explosion affecting the site is extremely unlikely. This accident is evaluated in order to provide a bounding pressure that could be used in the event that the potential of an explosion must be considered at a given site.

11.2.5.2 Analysis of Explosion

Pressure due to an explosion event is bounded by the pressure effects of a flood having a depth of 50 feet. The Transportable Storage Canister shell is evaluated in Section 11.2.9 for the effects of the flood having a depth of 50 feet, and the results are summarized in Tables 11.2.9-1 and 11.2.9-2.

There is no adverse consequence to the canister as a result of the 22 psig pressure exerted by a design basis flood. This pressure conservatively bounds an explosion event.

11.2.5.3 Corrective Actions

In the unlikely event of a nearby explosion, inspection of the concrete casks is required to ensure that the air inlets and outlets are free of debris, and to ensure that the monitoring system and screens are intact. No further recovery or corrective actions are required for this accident.

11.2.5.4 Radiological Impact

There are no radiological consequences for this accident.

THIS PAGE INTENTIONALLY LEFT BLANK

11.2.6 Fire Accident

This section evaluates the effects of a bounding condition hypothetical fire accident, although a fire accident is a very unlikely occurrence in the lifetime of the Universal Storage System. The evaluation demonstrates that for the hypothetical thermal accident (fire) condition the cask meets its storage performance requirements.

11.2.6.1 Cause of Fire

A fire may be caused by flammable material or by a transport vehicle. However, there are no flammable materials present in the ISFSI area. While it is possible that a transport vehicle could cause a fire while transferring a loaded storage cask at the ISFSI, this fire will be confined to the vehicle and will be rapidly extinguished by the persons performing the transfer operations or by the site fire crew. The maximum permissible flammable fluid (diesel fuel) in the transport vehicle is 50 gallons.

11.2.6.2 Detection of Fire

A fire in the vicinity of the Universal Storage System will be detected by observation of the fire or smoke.

11.2.6.3 Analysis of Fire

The vertical concrete cask with its internal contents, initially at the steady state normal storage condition, is subject to a hypothetical fire accident. The fire is due to the ignition of a flammable fluid, and operationally, the volume of flammable fluid that is permitted to be on the ISFSI is limited to 50 gallons. The lowest burning rate (change of depth per unit time of flammable fluid for a pool of fluid) reported in the Edition of the Fire Protection Handbook [37] is 5 inches/hour for kerosene. The flammable liquid is assumed to cover a 15 foot square area, corresponding to the center to center distance of the concrete casks less the foot print of the concrete cask, which is a 128 inch diameter circle. The depth (D) of the 50 gallons of flammable liquid is calculated as:

$$D = \frac{50\,(\text{gallons}) \times 231\,(\text{in}^3/(\text{gallon})}{15 \times 15 \times 144\,(\text{in}^2) - 3.14 \times 128^2 / 4\,(\text{in}^2)}$$

$$D = 0.6 \text{ inches}$$

With a burning rate of 5 inches/hour, the fire would continue for 7.2 minutes. The fire accident evaluation in this section conservatively considers an 8-minute fire. The temperature of the fire is taken to be 1475°F, which is specified for the fire accident condition in 10 CFR 71.73c(3).

The fire condition is an accident condition and is initiated with the concrete cask in a normal operating steady state condition. To determine the maximum temperatures of the concrete cask components, the two-dimensional axisymmetric finite element model for the BWR configuration described in Section 4.4.1.1 is used to perform a transient analysis. However, the effective properties for the canister content for specific heat, density and thermal conductivity for the PWR are used, to conservatively maximize the thermal diffusivity, which results in higher temperatures for the canister contents during the fire accident condition.

The initial condition of the fire accident transient analysis is based on the steady state analysis results for the normal condition of storage, which corresponds to an ambient temperature of 76°F in conjunction with solar insolation (as specified in Section 4.4.1.1). The fire condition is implemented by constraining the nodes at the inlet to be 1475°F for 8 minutes (see Figure 11.2.6-1). One of the nodes at the edge of the inlet is attached to an element in the concrete region. This temperature boundary condition is applied as a stepped boundary condition. During the 8-minute fire, solar insolation is also applied to the outer surface of the concrete cask. At the end of the 8 minutes, the temperature of the nodes at the inlet is reset to the ambient temperature of 76°F. The cool down phase is continued for an additional 10.7 hours to observe the maximum canister shell temperature and the average temperature of the canister contents.

The maximum temperatures of the fuel cladding and basket are obtained by adding the maximum temperature change due to the fire transient to the maximum component temperature for the normal operational condition. The maximum component temperature are presented in Table 11.2.6-1, which shows that the component temperatures are below the allowable temperatures. The limited duration of the fire and the large thermal capacitance of the concrete cask restricted the temperatures above 244°F to a region less than 3 inches above the top surface of the air inlets. The maximum bulk concrete temperature is 138°F during and after the fire accident. This corresponds to an increase of less than 3°F compared to the bulk concrete temperature for normal condition of storage. These results confirm that the operation of the concrete cask is not adversely affected during and after the fire accident condition.

11.2.6.4 Corrective Actions

Immediately upon detection of the fire, appropriate actions should be taken by site personnel to extinguish the fire. The concrete cask should then be inspected for general deterioration of the concrete, loss of shielding (spalling of concrete), exposed reinforcing bar, and surface discoloration that could affect heat rejection. This inspection will be the basis for the determination of any repair activities necessary to return the concrete cask to its design basis configuration.

11.2.6.5 Radiological Impact

There are no significant radiological consequences for this accident. There may be local spalling of concrete during the fire event, which could lead to some minor reduction in shielding effectiveness. The principal effect would be local increases in radiation dose rate on the cask surface.

Figure 11.2.6-1 Temperature Boundary Condition Applied to the Nodes of the Inlet for the Fire Accident Condition

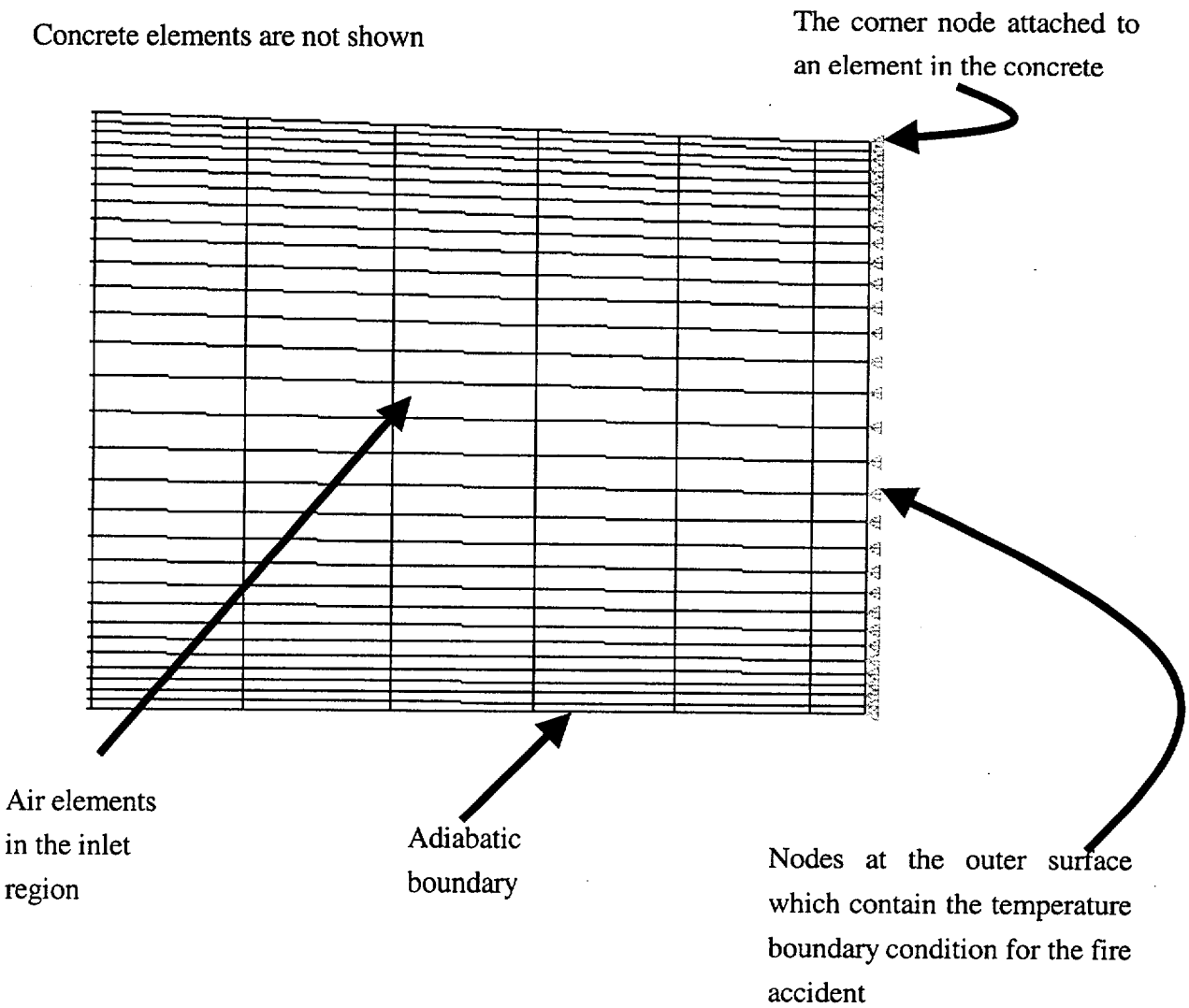

Table 11.2.6-1 Maximum Component Temperatures (°F) During and After the Fire Accident

Component	PWR Maximum temperature (°F)	PWR Allowable temperature (°F)	BWR Maximum temperature (°F)	BWR Allowable temperature (°F)
Fuel clad	710	1058	691	1058
Support disk	655	800	664	700
Heat transfer disk	652	700	662	700
Canister shell	459	800	416	800
Concrete*	244	350	244	350

* Temperatures of 244°F and greater are within 3 inches of the inlet, which does not affect the operation of the concrete cask.

THIS PAGE INTENTIONALLY LEFT BLANK

11.2.7 Maximum Anticipated Heat Load (133°F Ambient Temperature)

This section evaluates the Universal Storage System response to storage operation at an ambient temperature of 133°F. The condition is analyzed in accordance with the requirements of ANSI/ANS 57.9 to evaluate a credible worst-case thermal loading. A steady state condition is considered in the thermal evaluation of the system for this accident condition.

11.2.7.1 Cause of Maximum Anticipated Heat Load

This condition results from a weather event that causes the concrete cask to be subject to a 133°F ambient temperature with full insolation.

11.2.7.2 Detection of Maximum Anticipated Heat Load

Detection of the high ambient temperature condition will be by the daily measurement of ambient temperature and concrete cask outlet air temperature.

11.2.7.3 Analysis of Maximum Anticipated Heat Load

Using the same methods and thermal models described in Section 11.1.1 for the off-normal conditions of severe ambient temperatures (106°F and -40°F), thermal evaluations are performed for the concrete cask and the canister with its contents for this accident condition. The principal PWR and BWR cask component temperatures for this ambient condition are:

Component	133°F Ambient Max Temp. (°F)		Allowable Max Temp. (°F)	
	PWR	BWR	PWR	BWR
Fuel Cladding	715	702	1058	1058
Support Disks	664	677	800	700
Heat Transfer Disks	661	675	700	700
Canister Shell	408	432	800	800
Concrete	262	266	350	350

This evaluation shows that the component temperatures are within the allowable temperatures for the extreme ambient temperature conditions.

Thermal stress evaluations for the concrete cask are performed using the method and model presented in Section 3.4.4. The concrete temperature results obtained from the thermal analysis for this accident condition are applied to the structural model for stress calculation. The maximum stress, 7,160 psi in the reinforcing steel, occurs in the circumferential direction. The margin of safety is 54,000 psi/7,160 psi -1 = +6.5. The maximum compressive stress, 655 psi, in the concrete occurs in the vertical direction. The maximum circumferential compressive stress in the concrete is 94 psi. The margin of safety is [0.7(4,000 psi)/655 psi] -1 = +3.3. These stresses are used in the loading combination for the concrete cask shown in Section 3.4.4.2.

11.2.7.4 Corrective Actions

The high ambient temperature condition is a natural phenomenon, and no recovery or corrective actions are required.

11.2.7.5 Radiological Impact

There are no dose implications due to this event.

11.2.8 Earthquake Event

This section provides an evaluation of the response of the vertical concrete cask to an earthquake imparting a horizontal acceleration of 0.26 g at the top surface of the concrete pad. This evaluation shows that the loaded or empty vertical concrete cask does not tip over or slide in the earthquake event. The vertical acceleration is defined as 2/3 of the horizontal acceleration in accordance with ASCE 4-86 [36].

11.2.8.1 Cause of the Earthquake Event

Earthquakes are natural phenomena to which the storage system might be subjected at any U.S. site. Earthquakes are detected by the ground motion and by seismic instrumentation on and off site.

11.2.8.2 Earthquake Event Analysis

In the event of earthquake, there exists a base shear force or overturning force due to the horizontal acceleration ground motion and a restoring force due to the vertical acceleration ground motion. This ground motion tends to rotate the concrete cask about the bottom corner at the point of rotation (at the chamfer). The horizontal moment arm extends from the center of gravity (C.G.) toward the outer radius of the concrete cask. The vertical moment arm reaches from the C.G. to the bottom of the cask. When the overturning moment is greater than or equal to the restoring moment, the cask will tip over. To maximize this overturning moment, the dimensions for the Class 3 PWR configuration, which has the highest C.G., are used in this evaluation. Based on the requirements presented in NUREG-0800 [22], the static analysis method is considered applicable if the natural frequency of the structure is greater than 33 cycles per second (Hz).

The combined effect of shear and flexure is computed as:

$$\frac{1}{f^2} = \frac{1}{f_f^{\,2}} + \frac{1}{f_s^{\,2}} = \frac{1}{348.6} + \frac{1}{150.7} \quad [19]$$

or

$$f = 105.2 \text{ Hz} > 33 \text{ Hz}$$

where:

f_f = frequency for the first free-free mode based on flexure deformation only (Hz),

f_s = frequency for the first free-free mode based on shear deformation only (Hz).

The frequency f_f is computed as:

$$F_f = \frac{\lambda^2}{2\pi L^2}\sqrt{\frac{EI}{M}} = \frac{4.730^2}{2\pi(226)^2}\sqrt{\frac{(3.38\times10^6)\times(1.4832\times10^7)}{2.005}} \quad [19]$$

$f_f = 348.6$ Hz

where:

$\lambda = 4.730$,

$L = 226$ in, length of concrete cask,

$E = 3.38 \times 10^6$ psi, modulus of elasticity for concrete at 200°F,

$$I = \text{moment of inertia} = \frac{\pi(D_o^4 - D_i^4)}{64} = \frac{\pi\left[(136\text{ in})^4 - (79.5\text{ in})^4\right]}{64} = 1.4832\times10^7\text{ in}^4,$$

$$\rho = \frac{140}{1728\times386.4} = 2.096\times10^{-4}\text{ lbm/in}^3\text{, mass density,}$$

$M = \pi(68^2 - 39.75^2) \times (2.096 \times 10^{-4}) = 2.005$ lbm/in

The frequency accounting for the shear deformation is:

$$f_s = \frac{\lambda_s}{2\pi L}\sqrt{\frac{KG}{\mu}} = \frac{3.141593}{2(3.141595)(226)}\sqrt{\left(\frac{(0.6947)(1.40\times10^6)}{2.096\times10^{-4}}\right)} \quad [19]$$

$f_s = 150.7$ Hz

where:

$\lambda_s = \pi$,

$L = 226$ in, length of concrete cask,

$$K = \frac{6(1+\nu)(1+m^2)^2}{(7+6\nu)(1+m^2)+(20+12\nu)m^2}\text{, shear coefficient,}$$

$= 0.6947,$

$$\mu = \frac{140}{1728 \times 386.4} = 2.096 \times 10^{-4} \text{ lbm/in}^3, \text{ mass density of the material,}$$

$$G = \frac{0.5E}{(1+\nu)} = \frac{0.5(3.38 \times 10^6)}{(1+0.2)} = 1.408 \times 10^6 \text{ psi}, \text{ modulus of rigidity,}$$

and,

$m = R_i/R_o = 39.75/68 = 0.5846,$

$\nu = 0.2$, Poisson's ratio for concrete.

Since the fundamental mode frequency is greater than 33 Hz, static analysis is appropriate.

11.2.8.2.1 Tip-Over Evaluation of the Vertical Concrete Cask

To maintain the concrete cask in equilibrium, the restoring moment, M_R must be greater than, or equal to, the overturning moment, M_o (i.e. $M_R \geq M_o$). Based on this premise, the following derivation shows that 0.26g acceleration of the design basis earthquake at the surface of the concrete pad is well below the acceleration required to tip-over the cask.

The combination of horizontal and vertical acceleration components is based on the 100-40-40 approach of ASCE 4-86 [36], which considers that when the maximum response from one component occurs, the response from the other two components are 40% of the maximum. The vertical component of acceleration is obtained by scaling the corresponding ordinates of the horizontal components by two-thirds.

Let:

$a_x = a_z = a$ = horizontal acceleration components
$a_y = (2/3)\ a$ = vertical acceleration component
G_h = Vector sum of two horizontal acceleration components
G_v = Vertical acceleration component

There are two cases that have to be analyzed:

Case 1) The vertical acceleration, a_y, is at its peak: ($a_y = 2/3a$, $a_x = .4a$, $a_z = .4a$)

$$G_h = \sqrt{a_x^2 + a_z^2}$$

$$G_h = \sqrt{(0.4 \times a)^2 + (0.4 \times a)^2} = 0.566 \times a$$

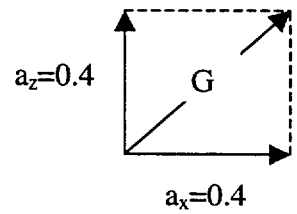

$$G_v = 1.0 \times a_y = 1.0 \times \left(a \times \frac{2}{3}\right) = 0.667 \times a$$

Case 2) One horizonal acceleration, a_x, is at its peak: (a_y=.4 x 2/3a, $a_x = a$, $a_z = .4a$)

$$G_h = \sqrt{a_x^2 + a_z^2}$$

$$G_h = \sqrt{(1.0 \times a)^2 + (0.4 \times a)^2} = 1.077 \times a$$

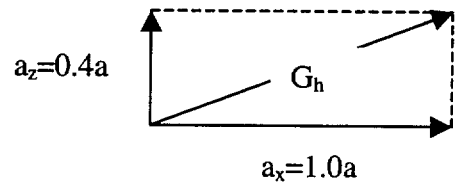

$$G_v = 0.4 \times a_y = 0.4 \times \left(a \times \frac{2}{3}\right) = 0.267 \times a$$

In order for the cask to resist overturning, the restoring moment, M_R, about the point of rotation, must be greater than the overturning moment, M_o, that:

$$M_R \geq M_o \text{, or}$$

$$F_r \times b \geq F_o \times d \Rightarrow (W \times 1 - W \times G_v) \times b \geq (W \times G_h) \times d$$

where:

- d = vertical distance measured from the base of the VCC to the center of gravity
- b = horizontal distance measured from the point of rotation to the C.G.
- W = the weight of the VCC
- F_o = overturning force
- F_r = restoring force

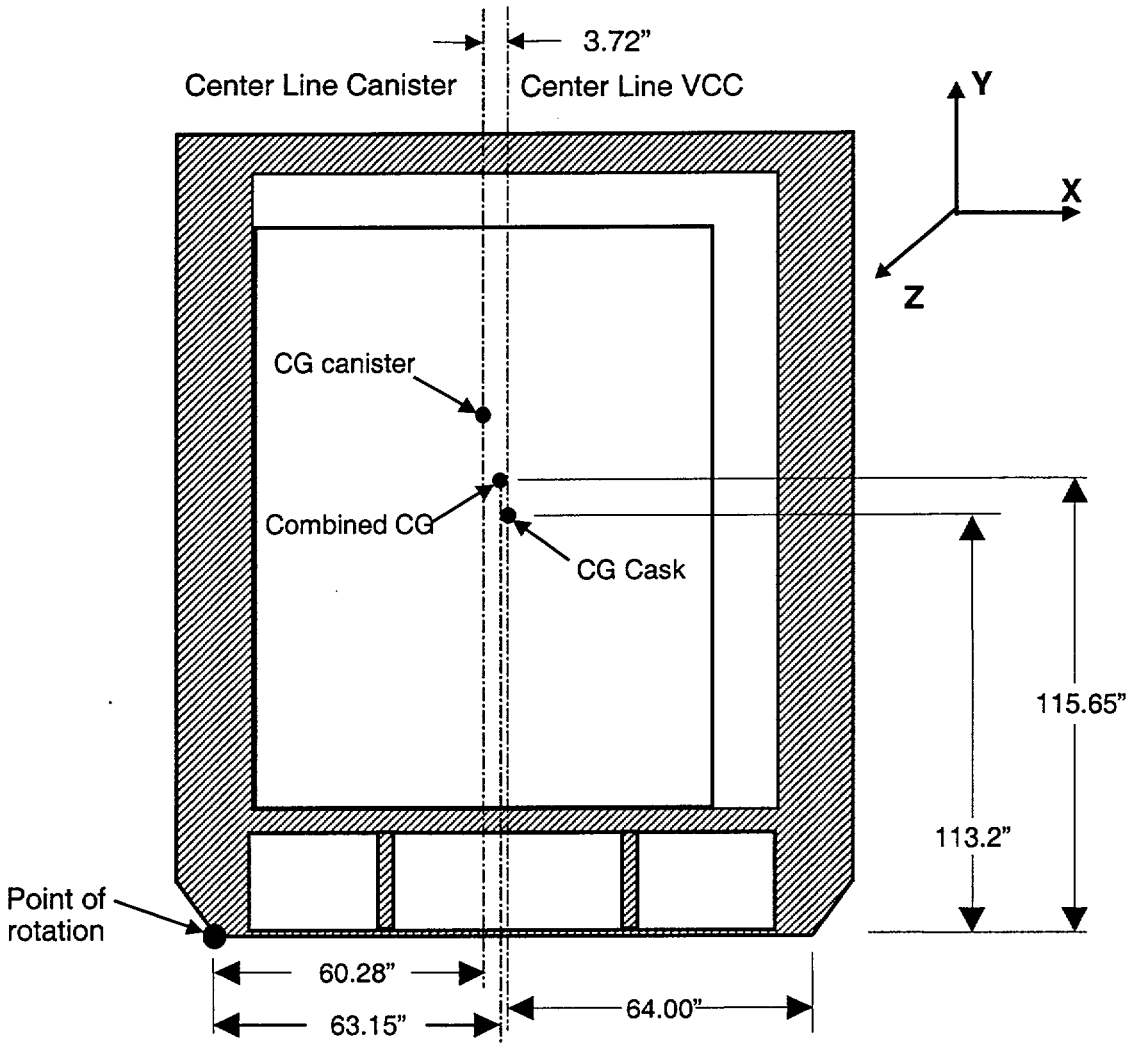

substituting for G_h and G_v gives:

Case 1

$$(1-0.667a)\frac{b}{d} \geq 0.566 \times a$$

$$a \leq \frac{b/d}{0.566 + 0.667\, b/d}$$

Case 2

$$(1-0.267a)\frac{b}{d} \geq 1.077a$$

$$a \leq \frac{b/d}{1.077 + 0.267(b/d)}$$

Because the canister is not attached to the concrete cask, the combined center of gravity for the concrete cask, with the canister in its maximum off-center position, must be calculated. The point of rotation is established at the outside lower edge of the concrete cask.

The inside diameter of the concrete cask is 74.5 inches and the outside diameter of the canister is 67.06 inches; therefore, the maximum eccentricity between the two is:

$$e = \frac{74.50\,\text{in} - 67.06\,\text{in}}{2} = 3.72\ \text{in.}$$

The horizontal displacement, x, of the combined C.G. due to eccentric placement of the canister is

$$x = \frac{70{,}783(3.72)}{308{,}432} = 0.85\,\text{in}$$

Therefore,

$$b = 64 - 0.85 = 63.15\ \text{in.}$$

The C.G. of the loaded Class #3 VCC is

$$d = 115.65\ \text{in.}$$

1) $a \le \dfrac{63.15/115.65}{0.566 + 0.667 \times 63.15/115.65}$

$a \le 0.59g$

2) $a \le \dfrac{63.15/115.65}{1.077 + 0.267 \times 63.15/115.65}$

$a \le 0.45g$

Therefore, the minimum ground acceleration that may cause a tip-over of a loaded concrete cask is 0.45g. Since the 0.26g design basis earthquake ground acceleration for the UMS system is less than 0.45g, the storage cask will not tip-over.

The factor of safety is 0.45 / 0.26 = 1.73, which is greater than the required factor of safety of 1.1 in accordance with ANSI/ANS-57.9.

Since an empty vertical concrete cask has a lower C.G. as compared to a loaded concrete cask, the tip-over evaluation for the empty concrete cask is bounded by that for the loaded concrete cask.

11.2.8.2.2 Sliding Evaluation of the Vertical Concrete Cask

To keep the cask from sliding on the concrete pad, the force holding the cask (F_s) has to be greater than or equal to the force trying to move the cask.

Based on the equation for static friction:

$$F_s = \mu N \geq G_h W$$
$$\mu\left(1 - G_v\right)W \geq G_h W$$

where:

μ = coefficient of friction
N = the normal force
W = the weight of the concrete cask
G_v = vertical acceleration component
G_h = resultant of horizontal acceleration component

Substituting G_h and G_v for the two cases:

Case 1) $\mu(1 - 0.667a) \geq 0.566\,a$

$$\mu \geq \frac{0.566a}{1 - 0.667a}$$

Case 2) $\mu(1 - 0.267a) \geq 1.077\,a$

$$\mu \geq \frac{1.077a}{1 - 0.267a}$$

For a = 0.26g

Case 1) $\mu \geq 0.18$

Case 2) $\mu \geq 0.30$

The analysis shows that the minimum coefficient of friction, μ, required to prevent sliding of the concrete cask is 0.30. The coefficient of friction between the steel bottom plate of the concrete cask and the concrete surface of the storage pad, 0.35 [21], is greater than the coefficient of friction required to prevent sliding of the concrete cask. Therefore, the concrete cask will not slide under design-basis earthquake conditions. The factor of safety is 0.35 / 0.30 =1.17 which is greater than the required factor of safety of 1.1 in accordance with ANSI/ANS-57.9.

11.2.8.2.3 Stress Generated in the Vertical Concrete Cask During an Earthquake Event

To demonstrate the ability of the concrete cask to withstand earthquake loading conditions, the fully loaded cask is conservatively evaluated for seismic loads of 0.5g in the horizontal direction and 0.5g in the vertical direction. These accelerations reflect a more rigorous seismic loading, and

therefore, bound the design basis earthquake event. No credit is taken for the steel inner liner of the concrete cask. The maximum compressive stress at the outer and inner surfaces of the concrete shell are conservatively calculated by assuming the vertical concrete cask to be a cantilever beam with its bottom end fixed. The maximum compressive stresses are:

$$\sigma_{v\ outer} = (M / S_{outer}) + ((1+a_y)(W_{vcc}) / A) = -72 - 44 = -116 \text{ psi},$$
$$\sigma_{v\ inner} = (M / S_{inner}) + ((1+a_y)(W_{vcc}) / A) = -42 - 44 = -86 \text{ psi},$$

where:

$a =$ 0.50 g, horizontal direction,
$a_y =$ 0.50 g, vertical direction,
H = 115.4 in., fully loaded C.G.,
W_{vcc}= 279,000 lbf, concrete cask weight (includes canister and basket weight used in seismic evaluation),
OD = 136 in., concrete exterior diameter,
ID = 79.50 in., concrete interior diameter,
$A = \pi (OD^2 - ID^2) / 4 = 9{,}562.8 \text{ in.}^2$,
$I = \pi (OD^4 - ID^4) / 64 = 14.83 \times 10^6 \text{ in.}^4$,
$S_{outer} = 2I / OD = 218{,}088.2 \text{ in.}^3$,
$S_{inner} = 2I / ID = 373{,}035.0 \text{ in.}^3$,
$w = a_x W_{vcc} / 225.88 = 618$ lbf / in.
$M = w (225.88)^2 / 2 = 1.58 \times 10^7$ in.-lbf , the maximum bending moment at the support.

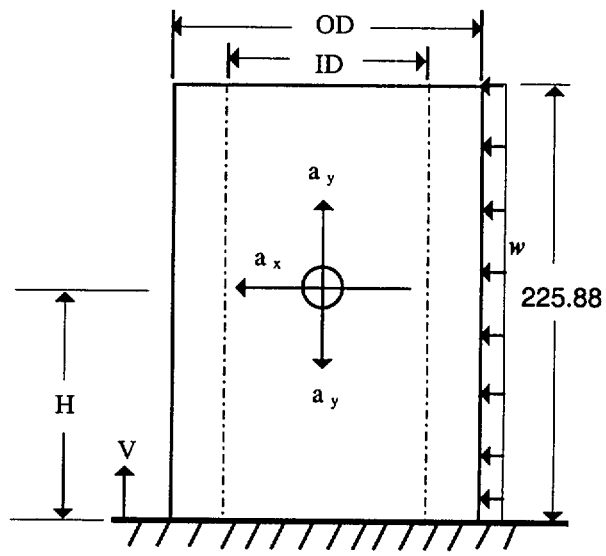

The calculated compressive stresses are used in the load combinations for the vertical concrete cask as shown in Table 3.4.4.2-1.

11.2.8.3 Corrective Actions

Inspection of the vertical concrete casks is required following an earthquake event. The positions of the concrete casks should be verified to ensure they maintain the 15-foot center-to-center spacing established in Section 8.1.3. The temperature monitoring system should be checked for operation.

11.2.8.4 Radiological Impact

There are no radiological consequences for this accident.

11.2.9 Flood

This evaluation considers design basis flood conditions of a 50-foot depth of water having a velocity of 15 feet per second. This flood depth would fully submerge the Universal Storage System. Analysis demonstrates that the Vertical Concrete Cask does not slide or overturn during the design-basis flood. The hydrostatic pressure exerted by the 50-foot depth of water does not produce significant stress in the canister. The Universal Storage System is therefore not adversely impacted by the design basis flood.

Small floods may lead to a blockage of concrete cask air inlets. Full blockage of air inlets is evaluated in Section 11.2.13.

11.2.9.1 Cause of Flood

The probability of a flood event at a given ISFSI site is unlikely because geographical features, and environmental factors specific to that site are considered in the site approval and acceptance process. Some possible sources of a flood are: (1) overflow from a river or stream due to unusually heavy rain, snow-melt runoff, a dam or major water supply line break caused by a seismic event (earthquake); (2) high tides produced by a hurricane; and (3) a tsunami (tidal wave) caused by an underwater earthquake or volcanic eruption.

11.2.9.2 Analysis of Flood

The concrete cask is considered to be resting on a flat level concrete pad when subjected to a flood velocity pressure distributed uniformly over the projected area of the concrete cask. Because of the concrete cask geometry and rigidity, it is analyzed as a rigid body. Assuming full submersion of the concrete cask and steady-state flow conditions, the drag force, F_D, is calculated using classical fluid mechanics for turbulent flow conditions. A safety factor of 1.1 for stability against overturning and sliding is applied to ensure that the analyses bound design basis conditions. The coefficient of friction between carbon steel and concrete used in this analysis is 0.35 [23].

Analysis shows that the concrete cask configured for storing the Class 3 PWR spent fuel, because of its center of gravity, weight, and geometry has the least resistance of the five configurations to

flood velocity pressure. Conservatively, the analysis is performed for a canister containing no fuel. The Class 3 PWR cask configuration analysis is as follows.

The buoyancy force, F_b, is calculated from the weight of water (62.4 lbs/ft^3) displaced by the fully submerged concrete cask. The displacement volume of the concrete cask containing the canister is 1,724 ft^3. The displacement volume is the volume occupied by the cask and the transport canister less the free space in the central annular cavity of the concrete cask.

$$F_b = \text{Vol} \times 62.4 \text{ lbs/ft}^3$$
$$= 107{,}557 \text{ lbs.}$$

Assuming the steady-state flow conditions for a rigid cylinder, the total drag force of the water on the concrete cask is given by the formula:

$$F_D = (C_D)(\rho)(V^2)\left(\frac{A}{2}\right) \qquad [24]$$
$$= 32{,}810 \text{ lbs.}$$

where:

C_D = Drag coefficient, which is dependent upon the Reynolds Number (Re). For flow velocities greater than 6 ft/sec, the value of C_D approaches 0.7 [24].

ρ = mass density of water = 1.94 slugs/ft^3

D = Concrete cask outside diameter (136.0 in. / 12 = 11.33 ft)

V = velocity of water flow (15 ft/sec)

A = projected area of the cask normal to water flow (diameter 11.33 ft × overall height 18.95 ft = 214.7 ft^2)

The drag force required to overturn the concrete cask is determined by summing the moments of the drag force and the submerged weight (weight of the cask less the buoyant force) about a point on the bottom edge of the cask. This method assumes a pinned connection, i.e., the cask will rotate about the point on the edge rather than slide. When these moments are in equilibrium, the cask is at the point of overturning.

$$F_D \times \left(\frac{h}{2}\right) = \left(W_{cask} - F_b\right) \times r$$

$$F_D = 98{,}960 \text{ lbs}$$

where:

h	=	concrete cask overall height (18.95 ft)
W_{CASK}	=	concrete cask weight = 272,912 lbs
		(Loaded concrete cask - fuel = 308,432 lbs- 35,520 lbs)
F_b	=	buoyant force = 107,557 lbs
r	=	concrete cask radius (5.67 ft)

Solving the drag force equation for the velocity, V, that is required to overturn the concrete cask:

$$V = \sqrt{\frac{2F_D}{C_D \rho A}}$$

= 24.8 ft/sec. (including safety factor of 1.1)

To prevent sliding, the minimum coefficient of friction (with a safety factor of 1.1) between the carbon steel bottom plate of the concrete cask and the concrete surface upon which it rests is,

$$\mu_{min} = \frac{(1.1)F_{D15}}{F_y} = \frac{(1.1)32{,}810 \text{ lb}}{(272{,}912 - 107{,}557) \text{ lb}} = 0.22$$

where:

F_y	=	the submerged weight of the concrete cask.

The analysis shows that the minimum coefficient of friction, μ, required to prevent sliding of the concrete cask is 0.22. The coefficient of friction between the steel bottom plate of the concrete cask and the concrete surface of the storage pad (0.35) is greater than the minimum coefficient of friction required to prevent sliding of the concrete cask. Therefore, the concrete cask does not slide under design-basis flood conditions.

The water velocity required to overturn the concrete cask is greater than the design-basis velocity of 15 ft/sec. Therefore, the concrete cask is not overturned under design basis flood conditions.

The flood depth of 50 feet exerts a hydrostatic pressure on the canister and the concrete cask. The water exerts a pressure of 22 psi (50 x 62.4/144) on the canister, which results in stresses in the canister shell. Canister internal pressure is conservatively taken as 0 psi. The canister structural analysis for the increased external pressure due to flood conditions is performed using an ANSYS finite element model as described in Section 3.4.4.1.

The resulting maximum canister stresses for flood loads are summarized in Tables 11.2.9-1 and 11.2.9-2 for primary membrane and primary membrane plus bending stresses, respectively.

The sectional stresses shown in Tables 11.2.9-1 and 11.2.9-2 at 16 axial locations are obtained for each angular division of the model (a total of 19 angular locations for each axial location). The locations of the stress sections are shown in Figure 3.4.4.1-4. Consequently, there is no adverse consequence to the canister as a result of the hydrostatic pressure due to the flood condition.

The concrete cask is a thick monolithic structure and is not affected by the hydrostatic pressure due to design basis flood. Nonetheless, the stresses in the concrete due to the drag force (F_D) are conservatively calculated as shown below. The concrete cask is considered to be fixed at its base.

F_D = 32,810 lbs
D = 136.0 in. (concrete exterior diameter)
ID = 79.5 in. (concrete interior diameter)
h = 225.88 in. (cask overall height)
$A = \pi (D^2 - ID^2) / 4 = 9{,}563 \text{ in.}^2$
(Cross-sectional area)
$I = \pi (D^4 - ID^4) / 64 = 14.83\times10^6 \text{ in.}^4$
(Moment of Inertia)
$S = 2I/D = 218{,}088 \text{ in.}^3$
(Section Modulus for outer surface)
$w = F_D/h = 145.3$ lbf / in.
$M = w(h)^2 / 2 = 3.7\times10^6$ in.-lbs
(Bending Moment at the base)

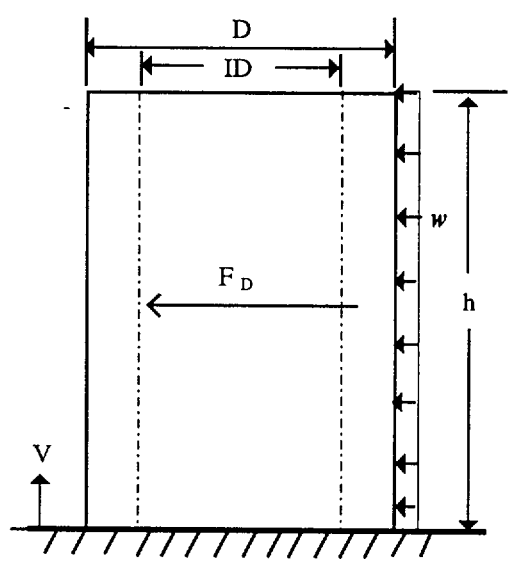

Maximum stresses at the base surface:

$\sigma_v = M / S_{outer} = 16.9$ psi (tension or compression)

The compressive stresses are included in load combination No. 7 in Table 3.4.4.2–1. As shown in Table 3.4.4.2–1, the maximum combined stresses for the load combination due to dead, live, thermal and flood loading, are less than the allowable stress.

11.2.9.3 Corrective Actions

Inspection of the concrete casks is required following a flood. While the cask does not tip over or slide, a potential exists for collection of debris or accumulation of silt at the base of the cask, which could clog or obstruct the air inlets. Operation of the temperature monitoring system should be verified, as flood conditions may have impaired its operation.

11.2.9.4 Radiological Impact

There are no dose consequences associated with the design basis flood event.

Table 11.2.9-1 Canister Increased External Pressure (22 psi) with No Internal Pressure (0 psi) Primary Membrane (P_m) Stresses (ksi)

Section No.[1]	Angle (degrees)	SX	SY	SZ	SXY	SYZ	SXZ	Stress Intensity	Allowable Stress [2]	Margin of Safety
1	0	-0.2	-2.2	-0.9	0.3	0	-0.1	2.09	40.08	18.16
2	0	-1.5	1.4	1.8	0.3	0	0.2	3.28	40.08	11.21
3	0	0.2	-0.6	2.7	-0.6	0.1	0.2	3.69	40.08	9.87
4	0	0	-0.6	-1.2	0	0	-0.1	1.18	39.76	32.70
5	0	0	-0.6	-1.2	0	0	-0.1	1.17	36.98	30.63
6	0	0	-0.6	-1.2	0	0	-0.1	1.17	36.52	30.24
7	0	0	-0.6	-1.2	0	0	-0.1	1.17	38.55	31.98
8	0	0	-0.5	-1.1	0	0	-0.1	1.09	40.08	35.67
9	0	-0.3	-0.2	-0.3	-0.1	0	0	0.27	40.08	149.28
10	0	0.3	-0.1	-0.1	-0.1	0	0	0.47	40.08	85.08
11	180	-0.3	0.1	-0.1	0	0	0	0.41	40.08	96.61
12	180	0.1	-0.2	-0.2	0	0	0	0.31	40.08	129.85
13	180	0	-0.3	-0.2	0.1	0	0	0.38	40.08	103.92
14	80	-0.3	0	-0.3	-0.3	0.2	0	0.73	40.08	53.64
15	70	0	0	0	0	0	0	0.02	40.08	Large
16	70	0	0	0	0	0	0	0.02	40.08	Large

[1] See Figure 3.4.4.1-4 for definition of locations and angles of stress sections.

[2] ASME Service Level D is used for material allowable stress.

Table 11.2.9-2 Canister Increased External Pressure (22 psi) with No Internal Pressure (0 psi) Primary Membrane plus Bending ($P_m + P_b$) Stresses (ksi)

Section No.[1]	Angle (degrees)	SX	SY	SZ	SXY	SYZ	SXZ	Stress Intensity	Allowable Stress[2]	Margin of Safety
1	0	-1.7	-5.2	-0.2	0.0	0.0	0.1	5.00	60.12	11.02
2	0	-0.7	9.9	4.5	0.7	0.0	0.4	10.79	60.12	4.57
3	0	1.0	-14.0	-1.0	-0.8	0.1	-0.1	15.07	60.12	2.99
4	0	0.0	-0.6	-1.2	0.0	0	-0.1	1.19	59.64	48.99
5	0	0.0	-0.6	-1.2	0	0	-0.1	1.19	55.47	45.69
6	0	0.0	-0.6	-1.2	0	0	-0.1	1.19	54.79	45.12
7	0	0.0	-0.6	-1.2	0	0	-0.1	1.19	57.83	47.68
8	0	0	-0.8	-1.2	0	0.0	-0.1	1.16	60.12	50.87
9	180	-0.2	0.2	-0.2	0.2	0.0	0.0	0.52	60.12	114.79
10	20	0.1	-0.3	-0.2	-0.2	0.1	-0.1	0.57	60.12	103.78
11	180	-0.2	0.8	0.1	0.1	0.0	0	1.00	60.12	59.31
12	0	0.6	0.1	0.0	0.1	0.0	0.0	0.56	60.12	105.50
13	180	0.4	-0.2	0.0	0.1	0	0.0	0.57	60.12	104.73
14	180	-7.1	-0.1	-7.2	-0.2	0.2	0	7.12	60.12	7.45
15	0	0.6	0	0.5	0	0	0	0.55	60.12	108.23
16	0	-0.3	0	-0.3	0	0	0	0.26	60.12	231.93

[1] See Figure 3.4.4.1-4 for definition of locations and angles of stress sections.

[2] ASME Service Level D is used for material allowable stress.

THIS PAGE INTENTIONALLY LEFT BLANK

11.2.10 Lightning Strike

This section evaluates the impact of a lightning strike on the Vertical Concrete Cask. The evaluation shows that the cask does not experience adverse effects due to a lightning strike.

11.2.10.1 Cause of Lightning Strike

A lightning strike is a random weather-related event. Because the Vertical Concrete Cask is located on an unsheltered pad, the cask may be subject to a lightning strike. The probability of a lightning strike is primarily dependent on the geographical location of the ISFSI site, as some geographical regions experience a higher frequency of storms containing lightning than others.

11.2.10.2 Detection of Lightning Strike

A lightning strike on a concrete cask may be visually detected at the time of the strike, or by visible surface discoloration at the point of entry or exit of the current flow. Most reactor sites in locations experiencing a frequency of lightning bearing storms have lightning detection systems as an aid to ensuring stability of site electric power.

11.2.10.3 Analysis of the Lightning Strike Event

The analysis of the lightning strike event assumes that the lightning strikes the upper-most metal surface and proceeds through the concrete cask liner to the ground. Therefore, the current path is from the lightning strike point on the outer radius of the top flange of the storage cask, down through the carbon steel inner shell and the bottom plate to the ground. The electrical current flow path results in current-induced Joulean heating along that path.

The integrated maximum current for a lightning strike is a peak current of 250 kiloamps over a period of 260 microseconds, and a continuing current of up to 2 kiloamps for 2 seconds in the case of severe lightning discharges [25].

From Joule's Law, the amount of thermal energy developed by the combined currents is given by the following expression [26]:

$$Q = 0.0009478R\left[I_1^2(dt_1) + I_2^2(dt_2)\right]$$
$$= (22.98 \times 10^3)\ R\ \text{Btu} \qquad \text{[Equation 11.2.10.1]}$$

where:

Q = thermal energy (BTU)
I_1 = peak current (amps)
I_2 = continuing current (amps)
dt_1 = duration of peak current (seconds)
dt_2 = duration of continuing current (seconds)
R = resistance (ohms)

The maximum lightning discharge is assumed to attach to the smallest current-carrying component, that is, the top flange connected to the cask lid.

The propagation of the lightning through the carbon steel cask liner, which is both permeable and conductive, is considered to be a transient. For static conditions, the current is distributed throughout the shell. In a transient condition the current will be near the surface of the conductor. Similar to a concentrated surface heat flux incident upon a small surface area, a concentrated current in a confined area of the steel shell will result in higher temperatures than if the current were spread over the entire area, which leads to a conservative result. This conservative assumption is used by constraining the current flow area to a 90 degree sector of the circular cross section of the steel liner as opposed to the entire cross section. The depth of the current penetration (δ in meters) is estimated [27] as:

$$\delta = \frac{1}{\sqrt{\pi \mu f \sigma}}$$

where:

μ = permeability of the conductor = $100\mu_0$ ($\mu_0 = 4\pi \times 10^{-7}$ Henries/m)
σ = electrical conductivity (seimens/meter) = $1/\rho$
= 1/resistivity = $1/9.78 \times 10^{-8}$ (ohm-m)
f = frequency of the field (Hz)

The pulse is represented conservatively as a half sine form, so that the equivalent $f = 1/2\tau$, where τ is the referenced pulse duration. Two skin depths, corresponding to different pulse duration, are computed. The larger effective frequency will result in a smaller effective area to conduct the current. The effective resistance is computed as:

$$R = \frac{\rho\, l}{a}$$

where:

R	= resistance (ohms)
ρ	= resistivity = 9.78×10^{-8} (ohm-m)
l	= length of conductor path
a	= area of conductor (m^2)

Using the current level of the pulse and the duration in conjunction with the carbon steel liner, the resulting energy into the shell is computed using Equation 11.2.10.1.

This thermal energy dissipation is conservatively assumed to occur in the localized volume of the carbon steel involved in the current flow path through the flange to the inner liner. Assuming no heat loss or thermal diffusion beyond the current flow boundary, the maximum temperature increase in the flange due to this thermal energy dissipation is calculated [28] as:

$$\Delta T = \frac{Q}{mc}$$

where:

ΔT	= temperature change (°F)
Q	= thermal energy (BTU)
C	= 0.113 Btu/lbs °F
m	= mass (lbm)

The ΔT_1 for the peak current (250KA, 260 μsec) is found to be 4.7°F.

The ΔT_2 for the continuous current (2 kA, 2 sec) is found to be negligible (0.0006°F).

The ΔT_1 corresponds to the increase in the maximum temperature of the steel within the current path. For the concrete to experience an increase in temperature, the heat must disperse from the steel surface throughout the steel. Using the total thickness of the steel, over the 90 degree section, the increase in temperature would be proportional to the volume of steel in this sector resulting in a temperature rise of less than 1°F.

Therefore the increase in concrete temperature attributed to Joulean heating is not significant.

11.2.10.4 Corrective Actions

The casks should be visually inspected for any damage following the lightning event and actions taken as appropriate.

11.2.10.5 Radiological Impact

There are no dose implications due to the lightning event.

11.2.11 Tornado and Tornado Driven Missiles

This section evaluates the strength and stability of the Vertical Concrete Cask for a maximum tornado wind loading and for the impacts of tornado generated missiles. The design basis tornado characteristics are selected in accordance with Regulatory Guide 1.76 [29].

The evaluation demonstrates that the concrete cask remains stable in tornado wind loading in conjunction with impact from a high energy tornado missile. The performance of the cask is not significantly affected by the tornado event.

11.2.11.1 Cause of Tornado and Tornado Driven Missiles

A tornado is a random weather event. Probability of its occurrence is dependent upon the time of the year and geographical areas. Wind loading and tornado driven missiles have the potential for causing damage from pressure differential loading and from impact loading.

11.2.11.2 Detection of Tornado and Tornado Driven Missiles

A tornado event is expected to be visually observed. Advance warning of a tornado and of tornado sightings may be received from the National Weather Service, local radio and television stations, local law enforcement personnel, and site personnel.

11.2.11.3 Analysis of Tornado and Tornado Driven Missiles

Classical techniques are used to evaluate the loading conditions. Cask stability analysis for the maximum tornado wind loading is based on NUREG-0800 [30], Section 3.3.1, "Wind Loadings," and Section 3.3.2, "Tornado Loadings." Loads due to tornado-generated missiles are based on NUREG-0800, Section 3.5.1.4, "Missiles Generated by Natural Phenomena."

The concrete cask stability in a maximum tornado wind is evaluated based on the design wind pressure calculated in accordance with ANSI/ASCE 7-93 [31] and using classical free body stability analysis methods.

Local damage to the concrete shell is assessed using a formula developed for the National Defense Research Committee (NDRC) [32]. This formula is selected as the basis for predicting depth of missile penetration and minimum concrete thickness requirements to prevent scabbing of the

concrete. Penetration depths calculated using this formula have been shown to provide reasonable correlation with test results (EPRI Report NP-440) [33].

The local shear strength of the concrete shell is evaluated on the basis of ACI 349-85 [34], Section 11.11.2.1, discounting the reinforcing and the steel internal shell. The concrete shell shear capacity is also evaluated for missile loading using ACI 349-85, Section 11.7.

The cask configuration used in this analysis combines the height of the tallest (Class 3 PWR) cask with the weight and center of gravity of the lightest (Class 1 PWR) cask. This configuration bounds all other configurations for cask stability. The cask properties considered in this evaluation are:

H = Cask Height = 225.88 in (Class 3 PWR)
D_o = Cask Outside Diameter = 136.0 in
D_i = Inside Diameter of concrete shell = 79.5 in
W_{VCC} = Weight of the cask with canister, basket and full fuel load = 292,401 lbs
A_c = Cross section area of concrete shell = 9,563 in^2
I_c = Moment of inertia of concrete shell = 14.83×10^6 in^4
f_c' = Compressive strength of concrete shell = 4,000 psi

Tornado Wind Loading (Concrete Cask)

The tornado wind velocity is transformed into an effective pressure applied to the cask using procedures delineated in ANSI/ASCE 7-93 Building Code Requirements for Minimum Design Loads in Buildings and Other Structures. The maximum pressure, q, is determined from the maximum tornado wind velocity as follows:

$$q = (0.00256)\ V^2 \text{ psf}$$

where:

V = Maximum tornado wind speed = 360 mph

The velocity pressure exposure coefficient for local terrain effects K, Importance Factor I, and the Gust Factor G, may be taken as unity (1) for evaluating the effects of tornado wind velocity pressure. Then:

$$q = (0.00256)(360)^2 = 331.8 \text{ psf}$$

Considering that the cask is small with respect to the tornado radius, the velocity pressure is assumed uniform over the projected area of the cask. Because the cask is vented, the tornado-induced pressure drop is equalized from inside to outside and has no effect on the cask structure.

The total wind loading on the projected area of the cask, F_w is then computed as:

$$F_w = q \times G \times C_f \times A_p$$
$$= 36{,}100 \text{ lbs}$$

where:

q = Effective velocity pressure (psf) = 331.8 psf.

C_f = Force Coefficient = 0.51 (ASCE 7-93, Table 12 with $D\ q^{1/2} = 206.4$ for a moderately smooth surface, h/D = 18.8 ft /11.3 ft = 1.7)

A_f = Projected area of cask = (225.88 in × 136.0 in)/144 = 213.3 ft^2

G = Constant = 1.0

The wind overturning moment, M_w, is computed as:

$$M_w = F_w \times H/2 = 36{,}100 \text{ lbs} \times 225.88 \text{ in}/12 \times 1/2 \cong 340{,}000 \text{ ft-lbs}$$

where H is the cask height.

The stability moment, M_s, of the cask (with the canister, basket and no fuel load) about an edge of the base, is:

$$M_s = W_{cask} \times D_o/2$$

where:

D_o = Cask base plate diameter = 128.0 in

W_{cask} = Weight of the cask with canister

≅ 292,401 lbs (Class 1 PWR)

M_s = 292,401 lbs × 128.0 in /12 × 1/2 = 1.56×10^6 ft-lbs

ASCE 7-93 requires that the overturning moment due to wind load shall not exceed two-thirds of the dead load stabilizing moment unless the structure is anchored. Therefore, the margin of safety, MS, against overturning is:

$$MS = \frac{M_S}{M_W} - 1 = \frac{(0.67)1.56 \times 10^6}{3.40 \times 10^5} - 1 = +2.07 .$$

A coefficient of friction of 0.12 (36,100/ 292,000) between the cask base and the concrete pad on which it rests will inhibit sliding.

Against a coefficient of friction of steel on concrete of approximately 0.35 [23], the margin of safety, MS, against sliding is:

$$MS = \frac{0.35}{0.12} - 1 = +1.92 .$$

The stresses in the concrete due to the tornado wind load are conservatively calculated below. The concrete cask is considered to be fixed at its base.

F_W = 36,100 lbs

D = 136.0 in. (concrete outside diameter)

ID = 79.5 in. (concrete inside diameter)

H = 225.8 in. /12 = 18.82 ft

A = $\pi (D^2 - ID^2) / 4 = 9{,}563 \text{ in}^2$

I = $\pi (D^4 - ID^4) / 64 = 14.83 \times 10^6 \text{ in}^4$ (Moment of Inertia)

M = $\frac{F_w \times H}{2} \cong 340{,}000$ lbs-ft

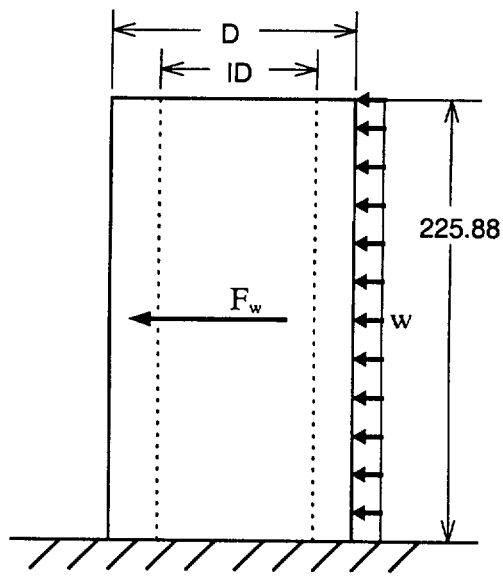

Maximum stresses:

$$\sigma = \frac{Mc}{I} = 18.7 \text{ psi} \qquad \text{(tension or compression)}$$

where:

c = D/2 = 68.0 in.

The compressive stresses are included in the load combination No. 3 in Table 3.4.4.2-1, since they are governing stresses for the load combination. As shown in Tables 3.4.4.2-1 and 3.4.4.2-2, the maximum combined stresses for the load combination of dead, live, thermal and tornado wind are less than the allowable stress.

Tornado Missile Loading (Concrete Cask)

The Vertical Concrete Cask is designed to withstand the effects of impacts associated with postulated tornado generated missiles identified in NUREG-0800, Section 3.5.1.4.III.4, Spectrum I missiles. These missiles consist of: 1) a massive high kinetic energy missile (4,000 lbs automobile, with a frontal area of 20 square feet that deforms on impact); 2) a 280 lbs, 8-inch-diameter armor piercing artillery shell; and 3) a small 1-inch diameter solid steel sphere. All of these missiles are assumed to impact in a manner that produces the maximum damage at a velocity of 126 mph (35% of the maximum tornado wind speed of 360 mph). The cask is evaluated for impact effects associated with each of the above missiles.

The principal dimensions and moment arms used in this evaluation are shown in Figure 11.2.11-1.

The concrete cask has no openings except for the four outlets at the top and four inlets at the bottom. The upper openings are configured such that a 1-inch diameter solid steel missile cannot directly enter the concrete cask interior. Additionally, the canister is protected by the canister structural and shield lids. The canister is protected from small missiles entering the lower inlets by a steel pedestal (bottom plate). Therefore, a detailed analysis of the impact of a 1-inch diameter steel missile is not required.

Concrete Shell Local Damage Prediction (Penetration Missile)

Local damage to the cask body is assessed by using the National Defense Research Committee (NDRC) formula [32]. This formula is selected as the basis for predicting depth of penetration and minimum concrete thickness requirements to prevent scabbing. Penetration depths calculated by using this formula have been shown to provide reasonable correlation with test results [33].

Concrete shell penetration depths are calculated as follows:

$$x/2d \leq 2.0$$

where:

d = Missile diameter = 8 in
x = Missile penetration depth = $[4KNWd^{-0.8}(V/1000)^{1.8}]^{0.5}$

where:

K= Coefficient depending on concrete strength
= $180/(f_c')^{1/2} = 180/(4000)^{1/2} = 2.846$
N= 1.14 Shape factor for sharp nosed missiles
W= Missile weight = 280 lbs
V= Missile velocity = 126 mph = 185 ft/sec
$x = [(4)(2.846)(1.14)(280)(8^{-0.8})(185/1000)^{1.8}]^{0.5}$
= 5.75 inches
$x/2d = 5.75/(2)(8) = 0.359 < 2.0$

The minimum concrete shell thickness required to prevent scabbing is three times the predicted penetration depth of 5.75 inches based on the NDRC formula, or 17.25 inches. The concrete cask wall thickness includes 28.25 inches of concrete, which is more than the thickness required to prevent damage due to the penetration missile. This analysis conservatively neglects the 2.5-inch steel shell at the inside face of the concrete shell.

Closure Plate Local Damage Prediction (Penetration Missile)

The concrete cask is closed with a 1.5-inch thick steel plate bolted in place. The following missile penetration analysis shows that the 1.5-inch steel closure plate is adequate to withstand the impact of the 280-lbs armor piercing missile, impacting at 126 mph.

The perforation thickness of the closure steel plate is calculated by the Ballistic Research Laboratories Formula with K = 1, formula number 2-7, in Section 2.2 of Topical Report BC-TOP-9A, Revision 2 [35].

$$T = [0.5m_mV^2]^{2/3}/672d = 0.523 \text{ inch}$$

where:

T = Perforation thickness
m_m = Missile mass = W/g = 280 lbs/32.174 ft/sec^2 = 8.70 slugs
g = Acceleration of gravity = 32.174 ft/sec^2

BC-TOP-9A recommends that the plate thickness be 25% greater than the calculated perforation thickness, T, to prevent perforation. Therefore, the recommended plate thickness is:

$$T = 1.25 \times 0.523 \text{ in.} = 0.654 \text{ in.}$$

The closure plate is 1.5 inches thick; therefore the plate is adequate to withstand the local impingement damage due to the specified armor piercing missile.

Overall Damage Prediction for a Tornado Missile Impact (High Energy Missile)

The concrete cask is a free-standing structure. Therefore, the principal consideration in overall damage response is the potential of upsetting or overturning the cask as a result of the impact of a high energy missile. Based on the following analysis, it is concluded that the cask can sustain an impact from the defined massive high kinetic energy missile and does not overturn.

From the principle of conservation of momentum, the impulse of the force from the missile impact on the cask must equal the change in angular momentum of the cask. Also, the impulse force due to the impact of the missile must equal the change in linear momentum of the missile. These relationships may be expressed as follows:

Change in momentum of the missile, during the deformation phase

$$\int_{t_1}^{t_2} (F)(dt) = m_m(v_2 - v_1)$$

where:

F	=	Impact impulse force on missile
m_m	=	Mass of missile = 4000 lbs/g = 124 slugs/12 = 10.4 (lbs sec^2 /in)
t_1	=	Time at missile impact
t_2	=	Time at conclusion of deformation phase
v_1	=	Velocity of missile at impact = 126 mph = 185 ft/sec
v_2	=	Velocity of missile at time t_2

The change in angular momentum of the cask, about the bottom outside edge/rim, opposite the side of impact is:

$$\int_{t_1}^{t_2} M_c(dt) = \int_{t_1}^{t_2} (H)(F)(dt) = I_m(\omega_1 - \omega_2)$$

Substituting,

$$\int (F)(dt) = m_m(v_2 - v_1) = \frac{I_m(\omega_1 - \omega_2)}{H}$$

where:

M_c = Moment of the impact force on the cask

I_m = Concrete cask mass moment of inertia, about point of rotation on the bottom rim

ω_1 = Angular velocity at time t_1

ω_2 = Angular velocity at time t_2

m_c = Mass of concrete cask = $W_c/g = 292{,}401/32.174$

= 9,076 slugs/12 = 756.3 lbs sec^2 /in)

I_{mx} = Mass moment of inertia of concrete cask about x axis through its center of gravity

$\cong 1/12(m_c)(3r^2 + H^2)$ (Conservatively assuming a solid cylinder.)

$\cong (1/12)(756.3)\,[(3)(68.0)^2 + (225.88)^2] = 4.09\times10^6$ lbs-sec^2-in

$I_m = I_{mx} + (m_c)(d_{CG})^2 = 4.09\times10^6 + (756.3)(121.05)^2 = 15.9\times10^6$ lbs-sec^2-in.

d_{CG} = The distance between the cask CG and a rotation point on base rim = 121.05 in. (See Figure 11.2.11-1.)

Based on conservation of momentum, the impulse of the impact force on the missile is equated to the impulse of the force on the cask.

$$m_m(v_2 - v_1) = I_m(\omega_1 - \omega_2)/H$$

at time t_1, v_1 = 185 ft/sec and ω_1 = 0 rad/sec

at time t_2, v_2 = 0 ft/sec

During the restitution phase, the final velocity of the missile depends upon the coefficient of restitution of the missile, the geometry of the missile and target, the angle of incidence, and on the amount of energy dissipated in deforming the missile and target. On the basis of tests conducted by EPRI, the final velocity of the missile, v_f, following the impact is assumed to be zero. Assuming

conservatively that all of the missile energy is transferred to the cask, and equating the impulse of the impact force on the missile to the impulse of the force on the cask,

$$(10.4)(v_2 - 185 \text{ ft/sec} \times 12 \text{ in/ ft}) = 15.9\times10^6 \text{ lbs-sec}^2\text{-in } (0 - \omega_2)/225.88$$

$$\omega_2 = 0.328 \text{ rad/sec} \quad (\text{when } v_2 = 0)$$

Back solving for v_2

$$v_2 = 261.6 \times \omega_2 = (261.6)(0.328) = 85.8 \text{ in/sec}$$

where the distance from the point of missile impact to the point of cask rotation is $\sqrt{132.0^2 + 225.88^2} = 261.6$ in. (See Figure 11.2.11-1). The line of missile impact is conservatively assumed normal to this line.

Equating the impulse of the force on the missile during restitution to the impulse of the force on the cask yields:

$$-[m_m(v_f - v_2] = I_m (\omega_f - \omega_2)/H$$

$$-[10.4(0 - 85.8)] = 15.9\times10^6 \text{ lbs-sec}^2\text{-in } (\omega_f - 0.328)/225.88$$

$$\omega_f = 0.341 \text{ rad/sec}$$

where:

v_f = 0
v_2 = 85.8 in/sec
ω_2 = 0.328 rad/sec

Thus, the final energy of the cask following the impact , E_k , is:

$$E_k = (I_m)(\omega_f)^2/(2) = (15.9\times10^6)(0.341)^2/(2) = 9.24\times10^5 \text{ in-lb}_f$$

The change in potential energy, E_p, of the cask due to rotating it until its center of gravity is above the point of rotation (the condition where the cask will begin to tip-over and the height of the center of gravity has increased by the distance, h_{PE}, see Figure 11.2.11-1) is:

$$E_p = (W_{cask})(h_{PE})$$
$$E_p = 292{,}401 \text{ lbs} \times 17.6 \text{ in}$$
$$E_p = 5.15\times10^6 \text{ in-lb}_f$$

The massive high kinetic energy tornado generated missile imparts less kinetic energy than the change in potential energy of the cask at the tip-over point. Therefore, cask overturning from missile impact is not postulated to occur. The margin of safety, MS, against overturning is:

$$MS = \frac{5.15\times10^6}{9.24\times10^5} - 1 = +4.6$$

<u>Combined Tornado Wind and Missile Loading (High Energy Missile)</u>

The cask rotation due to the heavy missile impact is calculated as (See Figure 11.2.11-1 for dimensions):

$$h_{KE} = E_k / W_c = 9.24\times10^5 \text{ in-lb}_f / 292{,}000 \text{ lbs} = 3.16 \text{ in}$$

Then

$$\cos\beta = (h_{CG} + h_{KE}) / d_{CG}$$
$$\cos\beta = (107.39 + 3.16) / 121.05 = 0.8843$$
$$\beta = 27.8 \text{ deg}$$
$$\cos\alpha = 107.39 / 121.05 = 0.8591$$
$$\alpha = 30.8 \text{ deg}$$
$$e = d_{CG} \sin\beta$$
$$e = 121.05 \sin 27.8 = 58.3 \text{ in}$$

Therefore, cask rotation after impact = α - β = 30.8 - 27.8 = 3.0 deg

The available gravity restoration moment after missile impact:

$$= (W_c)(e)$$
$$= 292{,}000 \text{ lbs} \times 58.3 \text{ in}/12$$
$$= 1.42\times10^6 \text{ ft-lbs} >> \text{Tornado Wind Moment} = 3.40\times10^5 \text{ ft-lbs}$$

Therefore, the combined effects of tornado wind loading and the high energy missile impact loading will not overturn the cask. Considering that the overturning moment should not exceed two-thirds of the restoring stability moment, the margin of safety, MS, is:

$$MS = \frac{0.67(1.42\times10^6)}{340\times10^5} - 1 = +1.80$$

Local Shear Strength Capacity of Concrete Shell (High Energy Missile)

This section evaluates the shear strength of the concrete at the top edge of the concrete shell due to a high energy missile impact based on ACI 349-85, Chapter 11, Section 11.11.2.1, on concrete punching shear strength.

The force developed by the massive high kinetic energy missile having a frontal area of 20 square feet, is evaluated using the methodology presented in Topical Report, BC-TOP-9A.

$$F = 0.625(v)(W_M)$$
$$F = 0.625(185 \text{ ft/sec})(4{,}000 \text{ lbs}) = 462.5 \text{ kips}$$
$$F_u = LF \times F = 1.1 \times 462.5 = 508.8 \text{ kips}$$

Based on a rectangular missile contact area, having proportions of 2 (horizontal) to 1 (vertical) and the top of the area flush with the top of the concrete cask, the required missile contact area based on the concrete punching shear strength (neglecting reinforcing) is calculated as follows.

$V_c = (2+4/\beta_c)\,(f_c')^{1/2} b_o\, d$, where $\beta_c = 2/1 = 2$

$V_c = 4\,(f_c')^{1/2} b_o\, d$

$d = 28.25 \text{ in} - 3.25 \text{ in} = 25 \text{ in}$

$(f_c')^{1/2} = 63.24$ psi, where $f_c' = 4{,}000$ psi

b_o = perimeter of punching shear area at d/2 from missile contact area

$b_o = (2b + 25) + 2(b + 12.5) = 4b + 50$

$V_u = \Phi(V_c + V_s)$, where $V_s = 0$, assuming no steel shear

$V_u = \Phi V_c = \Phi\, 4\,(f_c')^{1/2} b_o\, d = (0.85)(4)(63.24)(4b + 50)(25) = 21{,}501\, b + 268{,}770.$

Setting, V_u equal to F_u and solving for b

$508.8\times10^3 = 21{,}501\, b + 268{,}770$

$b = 11.12$ inches (say 1.0 ft)

The implied missile impact area required $= 2b \times b = 2 \times 1 \times 1 = 2.0$ sq ft $<$ 20.0 sq ft

Thus, the concrete shell alone, based on the concrete conical punching strength and discounting the steel reinforcement and shell, has sufficient capacity to react to the high energy missile impact force.

The effects of tornado winds and missiles are considered both separately and combined in accordance with NUREG-800, Section 3.3.2 II.3.d. For the case of tornado wind plus missile loading, the stability of the cask is assessed and found to be acceptable. Equating the kinetic energy of the cask following missile impact to the potential energy yields a maximum postulated rotation of the cask, as a result of the impact, of 3.0 degrees. Applying the total tornado wind load to the cask in this configuration results in an available restoring moment considerably greater than the tornado wind overturning moment. Therefore, overturning of the cask under the combined effects of tornado winds, plus tornado-generated missiles, does not occur.

Tornado Effects on the Canister

The postulated tornado wind loading and missile impacts are not capable of overturning the cask, or penetrating the boundary established by the concrete cask. Consequently, there is no effect on the canister. Stresses resulting from the tornado-induced decreased external pressure are bounded by the stresses due to the accident internal pressure discussed in Section 11.2.1.

11.2.11.4 Corrective Actions

A tornado is not expected to result in the need to take any corrective action other than an inspection of the ISFSI. This inspection would be directed at ensuring that inlets and outlets had not become blocked by wind-blown debris and at checking for obvious (concrete) surface damage.

11.2.11.5 Radiological Impact

Damage to the vertical concrete cask after a design basis accident does not result in a radiation exposure at the controlled area boundary in excess of 5 rem to the whole body or any organ. The penetrating missile impact is estimated to reduce the concrete shielding thickness, locally at the point of impact, by approximately 6 inches. Localized cask surface dose rates for the removal of 6 inches of concrete are estimated to be less than 250 mrem/hr for the PWR and BWR configurations.

Figure 11.2.11-1 Principal Dimensions and Moment Arms Used in Tornado Evaluation

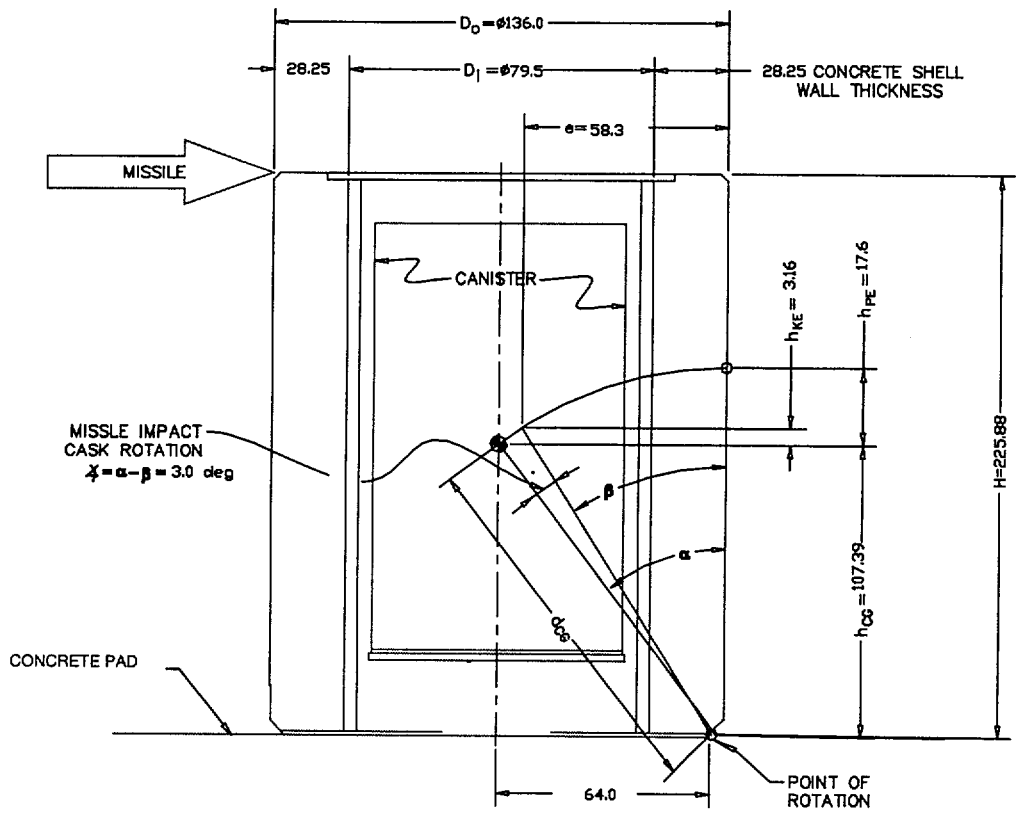

11.2.12 Tip-Over of Vertical Concrete Cask

Tip-over of the Vertical Concrete Cask (cask) is a non-mechanistic, hypothetical accident condition that presents a bounding case for evaluation. There are no design basis accidents that result in the tip-over of the cask.

Functionally, the cask does not suffer significant adverse consequences due to this event. The concrete cask, canister, and basket maintain design basis shielding, geometry control of contents, and contents confinement performance requirements.

Results of the evaluation show that supplemental shielding will be necessary, following the tip-over and until the cask can be righted, because the bottom ends of the concrete cask and the canister have significantly less shielding than the sides and tops of these components.

11.2.12.1 Cause of Cask Tip-Over

A tip-over of the cask is possible in an earthquake that significantly exceeds the design basis described in Section 11.2.8. No other events related to design bases are expected to result in a tip-over of the cask.

11.2.12.2 Detection of Cask Tip-Over

The tipped-over configuration of the concrete cask will be obvious during site inspection following the initiating event.

11.2.12.3 Analysis of Cask Tip-Over

For a tip-over event to occur, the center of gravity of the concrete cask and loaded canister must be displaced beyond its outer radius, i.e., the point of rotation. When the center of gravity passes beyond the point of rotation, the potential energy of the cask and canister is converted to kinetic energy as the cask and canister rotate toward a horizontal orientation on the ISFSI pad. The subsequent motion of the cask is governed by the structural characteristics of the cask, the ISFSI pad and the underlying soil.

\he objective of the evaluation of the response of the concrete cask in the tip-over event is to determine the maximum acceleration to be used in the structural evaluation of the loaded canister and basket (Section 11.2.12.4). The methodology to determine the concrete cask response follows the methodology contained in NUREG/CR-6608, "Summary and Evaluation of Low-Velocity Impact Tests of Solid Steel Billet Onto Concrete Pads" [38]. The LS-DYNA program is used in the evaluation. The validation of the analysis methodology is shown in Section 11.2.12.3.3.

The parameters of the ISFSI pad and foundation are:

Concrete thickness	36 inches maximum
Pad subsoil thickness	10 feet minimum
Specified concrete compressive strength	$\leq$ 4,000 psi at 28 days
Concrete dry density (ρ)	$125 \leq \rho \leq 140$ lbs/ft^3
Soil in place density (ρ)	$100 \leq \rho \leq 120$ lbs/ft^3
Soil Modulus of Elasticity	$\leq$ 60,000 psi (PWR) or $\leq$ 30,000 psi (BWR)

11.2.12.3.1 Analysis of Cask Tip-Over for PWR Configurations

The finite element model includes a half section of the concrete cask, the concrete ISFSI pad and soil subgrade, as shown:

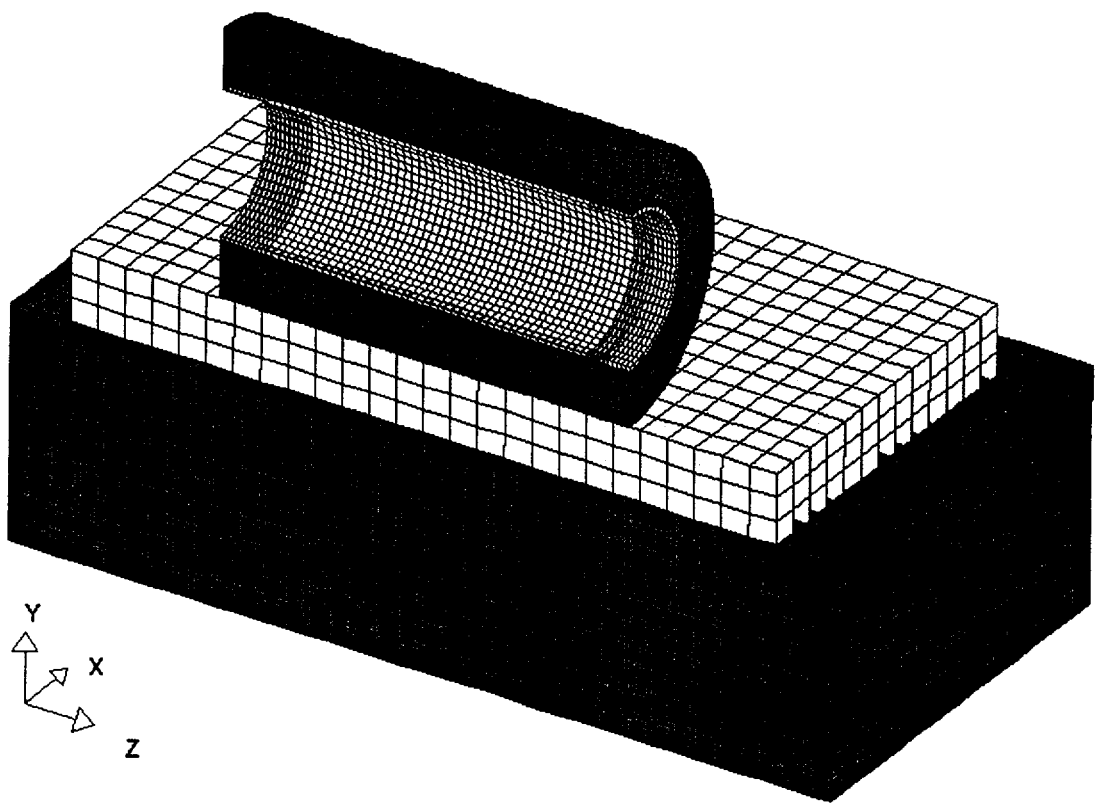

The concrete pad in the model corresponds to a pad 30-feet by 30-feet square and 3-feet thick, supporting one concrete cask in the center of the pad. The soil under the concrete pad is considered to be 35-feet by 35-feet square and 10-feet thick. Only one-half of the concrete cask, pad and soil configuration is modeled due to symmetry.

The concrete is represented as a homogeneous isotropic material. The concrete cask (outer shell) and the pad are modeled as material Type Number 16 in LS-DYNA. The values for concrete pad and soil properties provided below are typical values for the input to the LS-DYNA model:

Compressive Strength ($f_c^{'}$)	= 4,000 psi	
Density (ρ_c)	= 125 pcf	
Poisson's Ratio (ν_c)	= 0.22	(NUREG/CR-6608 [38])
Modulus of Elasticity (E_c)	$= 33\ \rho_c^{1.5}\sqrt{f_c^{'}}$ = 2.917E6 psi	(ACI 318-95)
Bulk Modulus (K_c)	$= \dfrac{E_c}{3(1-2\nu_c)}$ = 1.736E6 psi	(Blevins [19])

The material properties used in the model for the soil below the ISFSI pad are:

Density	= 120 pcf	
Poisson's Ratio (ν_s)	= 0.45	(NUREG/CR-6608)
Modulus of Elasticity	= 60,000 psi	

The concrete cask steel liner has the properties:

Density	= 0.284 lbs/in^3
Poisson's ratio	= 0.31
Modulus of elasticity	= 2.9E7 psi

To account for the weight of the shield plug, the loaded canister, and the concrete cask pedestal, effective densities are used for the elements in the first row of the steel liner in the model adjacent to the impact plane of symmetry. These densities represent the regions (6° in the circumferential direction) of the steel liner subjected to the weight of the shield plug, the loaded canister and the

pedestal, during the side impact (tip-over) condition. The contact angle (6°) is determined based on the canister/basket analysis for the tip-over condition (Section 11.2.12.4).

Boundary Conditions and Initial Conditions

A friction coefficient of 0.25 is used at the interface between the steel liner and the concrete shell, between the concrete cask and the pad, and between the pad and the soil. For all the embedded faces (three side surfaces and the bottom surface) of the soil in the model, the displacements in the direction normal to the surface are restrained. The symmetry boundary conditions are applied for all nodes at the plane of symmetry.

The initial condition corresponds to the concrete cask in a horizontal position with an initial vertical velocity into the concrete pad. The pad and soil are initially at rest.

The distribution of initial velocity of the concrete cask is simulated by applying an angular velocity (ω) to the entire cask. The point of rotation is taken to be the lower edge of the base of the concrete cask. The angular velocity value is computed by considering energy conservation at the cask "center of gravity over corner" tip condition versus the side impact condition.

From energy conservation:

$$mgh = \frac{I\omega^2}{2}$$

where:

mg = total weight of the loaded concrete cask
= 292,401 lbs (PWR Class 1*)
= 303,317 lbs (PWR Class 2*)
= 308,432 lbs (PWR Class 3*)
* See Table 1.2-1 for the description of Class.

h = height change of the concrete cask center of gravity (L_{CG}) = $\sqrt{R^2 + \left(\frac{L_{CG}}{2}\right)^2} - R$

= 59.11 inches (PWR Class 1)
= 62.80 inches (PWR Class 2)
= 66.16 inches (PWR Class 3)

where:

L_{CG} = location of the center of gravity above the pad for the concrete cask
= 107.39 inches (PWR Class 1)
= 111.73 inches (PWR Class 2)
= 115.65 inches (PWR Class 3)

R = radius of the concrete cask = 68 inches

I = total mass moment of inertia of the concrete cask about the point of rotation
= 7,779,111 lbs-sec^2-inch (PWR Class 1)
= 8,610,059 lbs-sec^2-inch (PWR Class 2)
= 9,264,863 lbs-sec^2-inch (PWR Class 3)

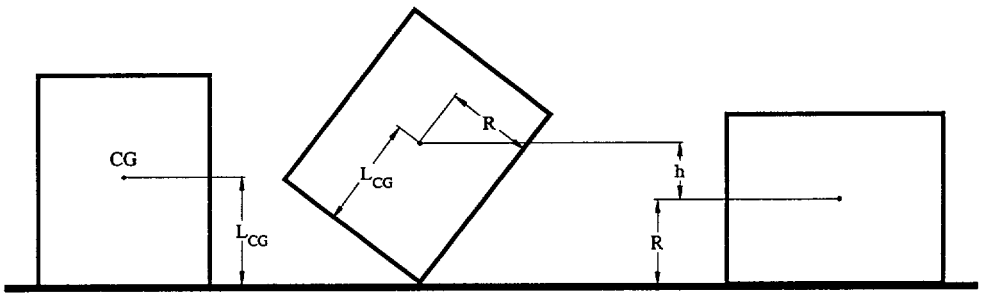

The mass moment of inertia for the concrete shell and the steel liner is calculated using the formula for a hollow right circular cylinder (Blevins).

$$I = \frac{m}{12}(3R_1^2 + 3R_2^2 + 4L^2) + md^2$$

where:

m = mass (lbs-sec^2/in)

R_1 and R_2 = the outer and inner radius of the cylinder (inch)

L = height of the cylinder (inch)

d = distance between the center of gravity and the point of rotation (inch)

For the mass of the shield plug, loaded canister and the pedestal, the formula for the moment of inertia for a solid cylinder is used:

$$I = \frac{m}{12}(3R^2 + 4L^2) + md^2$$

where:

m = mass of the cylinder (lbs-sec^2/in)
R = radius of the cylinder (inch)
L = height of the cylinder (inch)
d = distance between the two pivot axes (inch)

The angular velocity is given by $\omega = \sqrt{\frac{2mgh}{I}}$

= 1.493 radians/sec (PWR Class 1)
= 1.488 radians/sec (PWR Class 2)
= 1.484 radians/sec (PWR Class 3)

Filter Frequency

The accelerations are evaluated at the inner surface of the cask liner, which physically corresponds to the interface of the liner and the loaded canister nearest the plane of impact. Following the methodology contained in NUREG/CR-6608, the Butterworth filter is applied to the nodal accelerations. The filter frequency is based on the fundamental mode of the cask.

The fundamental natural frequency of a beam in transverse vibration due to flexure only is given by Blevins as:

$$f = \frac{\lambda^2}{2\pi}\sqrt{\frac{EI}{\rho AL^4}}$$

where:

$\lambda = 3.92660231$ for a pin-free beam

The frequencies of the concrete (f_c) and the steel liner (f_s) are computed as:

Area of concrete cask = $\pi\ \{(68)^2 - (39.75)^2\} = 9562.8\ \text{in}^2$

Moment of inertia of concrete cask = $\frac{\pi}{4}\{(68)^4 - (39.75)^4\} = 14{,}832{,}070\ \text{in}^4$

$$f_c = 805819 \frac{\lambda^2}{L^2}$$

= 284 Hz (PWR Class 1)
= 261 Hz (PWR Class 2)
= 244 Hz (PWR Class 3)

Area of steel liner = $\pi \{(39.75)^2 - (37.25)^2\} = 604.8 \text{ in}^2$

Moment of inertia of steel liner = $\frac{\pi}{4}\{(39.75)^4 - (37.25)^4\} = 448{,}673 \text{ in}^4$

$$f_s = 861068 \frac{\lambda^2}{L^2}$$

= 303 Hz (PWR Class 1)
= 279 Hz (PWR Class 2)
= 260 Hz (PWR Class 3)

Since the concrete cask is short compared to its diameter, the contribution of the flexibility due to shear is also incorporated. This is accomplished by using Dunkerley's formula (Blevins). The system frequency is:

$$\frac{1}{f^2} = \frac{1}{f_c^2} + \frac{1}{f_s^2}$$

Thus, the system frequencies are 207 Hz (PWR Class 1), 191 Hz (PWR Class 2), and 178 Hz (PWR Class 3). A cut-off frequency of 210 Hz (PWR Class 1), 190 Hz (PWR Class 2), and 180 Hz (PWR Class 3) is conservatively applied to filter the analysis results and measure the peak accelerations.

Results of the Transient Analysis

The accelerations at key locations of the concrete cask liner, which are required in the evaluation of the loaded canister/basket model (Section 11.2.12.4) are:

Location on Component	Position Measured from the Bottom of the Concrete Cask (inches)			Acceleration (g)		
	PWR Class 1	PWR Class 2	PWR Class 3	PWR Class 1	PWR Class 2	PWR Class 3
Top support disk	176.7	185.2	196.3	29.1	32.1	34.3
Top of the canister structural lid	197.9	207.0	214.6	31.8	35.1	36.9

11.2.12.3.2 Analysis of Cask Tip-Over for BWR Configurations

The BWR finite element model is similar to that for the PWR configuration. The concrete pad in this model corresponds to a pad 30-feet by 30-feet and 3-feet thick, supporting one concrete cask in the center of the pad. The soil under the concrete pad is considered to be 35-feet by 35-feet in area and 10-feet thick.

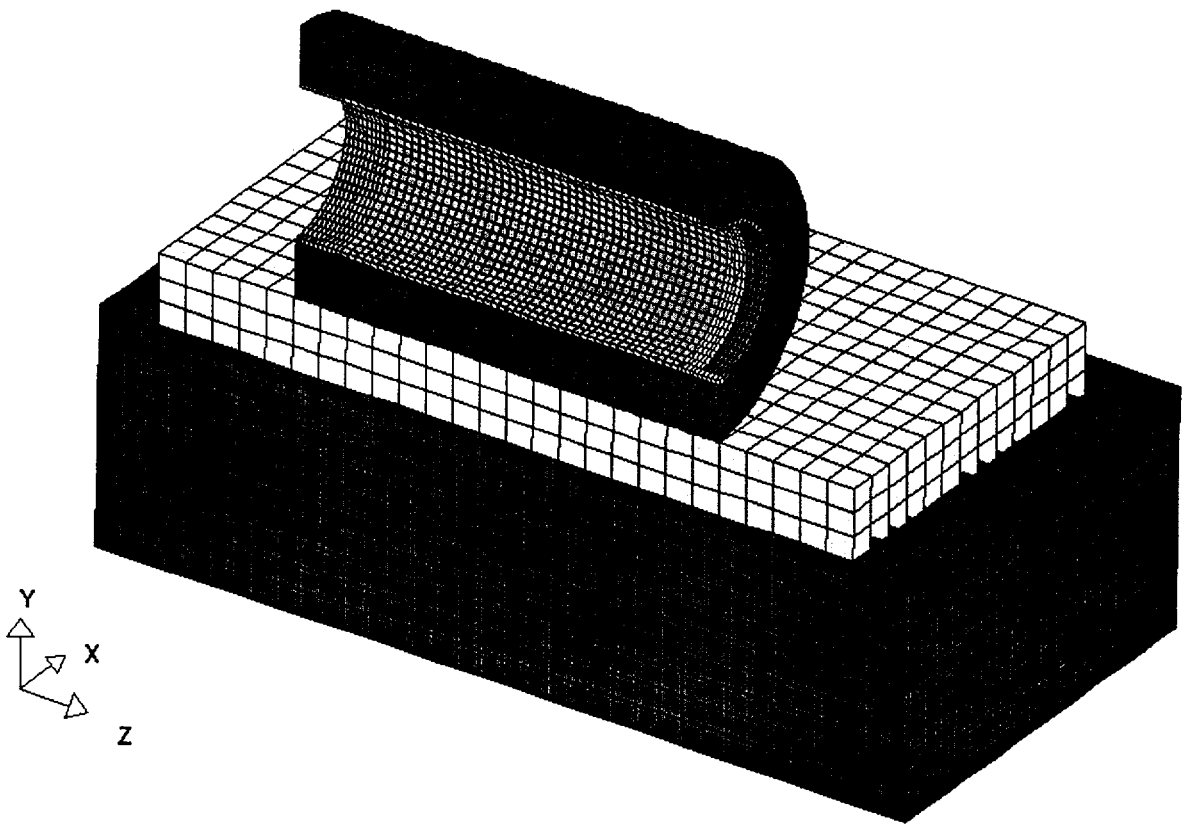

The material properties used in this model for the soil below the ISFSI pad are the same as those for the PWR model, except the modulus of elasticity of the soil is 30,000 psi.

Initial Conditions

The initial velocity for the BWRs was calculated in the same fashion as for the PWRs, but using the following data:

mg = total weight of the loaded concrete cask
= 307,087 lbs (BWR Class 4*)
= 312,210 lbs (BWR Class 5*)
* See Table 1.2-1 for the description of Class.

h = height change of the concrete cask center of gravity (L_{CG}) = $\sqrt{R^2 + \left(\frac{L_{CG}}{2}\right)^2} - R$

= 63.26 inches (BWR Class 4)
= 65.54 inches (BWR Class 5)

where:

L_{CG} = location of the center of gravity above the pad for the concrete cask
= 112.27 inches (BWR Class 4)
= 114.93 inches (BWR Class 5)

I = total mass moment of inertia of the concrete cask about the point of rotation
= 8,785,335 lbs-sec^2-inch (BWR Class 4)
= 9,243,624 lbs-sec^2-inch (BWR Class 5)

The angular velocity is given by $\omega = \sqrt{\frac{2mgh}{I}}$

= 1.487 radians/sec (BWR Class 4)
= 1.488 radians/sec (BWR Class 5)

Filter Frequency

The filter frequency for the BWRs was calculated in the same fashion as for the PWRs but using the following data:

$f_c = 805819 \frac{\lambda^2}{L^2}$

= 257 Hz (BWR Class 4)
= 247 Hz (BWR Class 5)

$$f_s = 861{,}068 \frac{\lambda^2}{L^2}$$
$$= 275 \text{ Hz (BWR Class 4)}$$
$$= 263 \text{ Hz (BWR Class 5)}$$

Thus, the system frequencies are 188 Hz (BWR Class 4), and 180 Hz (BWR Class 5). A cut-off frequency of 190 Hz (BWR Class 4), and 180 Hz (BWR Class 5) is conservatively applied to filter the analysis results and measure the peak accelerations.

Results of the Transient Analysis

The accelerations at key locations of the concrete cask liner, which are required in the evaluation of the loaded canister/basket model (Section 11.2.12.4) are:

Location on Component	Position Measured from the bottom of the Concrete Cask (inches)		Acceleration (g)	
	BWR-4	BWR-5	BWR-4	BWR-5
Top support disk	178.7	182.9	24.4	25.3
Top of the canister structural lid	208.4	213.2	27.9	29.1

11.2.12.3.3 Validation of the Analysis Methodology

Tip-over tests of a steel billet onto a concrete pad were conducted and reported in NUREG/CR-6608. The purpose of the tests was to provide data, against which, analysis methodology could be validated. Using the geometry described in the benchmark along with the modeling methodology, these analyses were re-performed using the LS-DYNA program.

Using the filter frequency reported in the NUREG/CR-6608 benchmark, the following results are obtained:

Nodes / Gauge Location	Maximum Experiment (g)	NAC Analysis (g)
16115 / A1	237.5	237.1
17265 / A5	231.5	229.4

11.2.12.4 Analysis of Canister and Basket for Cask Tip-Over Event

Structural evaluations are performed for the transportable storage canister and fuel basket support disks for tip-over accident conditions for both PWR and BWR fuel configurations. ANSYS finite element models are used to evaluate this side impact loading condition.

Comparison of maximum stress results to the allowable stress intensities shows that the canister and support disks are structurally adequate for the concrete cask tip-over condition and satisfies the stress criteria in accordance with the ASME Code, Section III, Division I, Subsection NB and NG, respectively.

The structural response of the PWR and BWR canisters and fuel baskets to the tip-over condition is evaluated using ANSYS three-dimensional finite element models consisting of the top portion of the canister, the top five fuel basket support disks, and the fuel basket top weldment disk. The PWR with Fuel Class 1 configuration is used to evaluate the PWR canister and fuel basket, and the BWR with Fuel Class 4 configuration is used to evaluate the BWR canister and fuel basket. These two representative configurations are chosen because they bound the maximum load-per-support disk for the respective fuel configurations. For each fuel configuration analyzed, the structural analyses are performed for various fuel basket drop orientations in order to ensure that the maximum primary membrane (P_m) and primary membrane plus primary bending ($P_m + P_b$) stresses are evaluated. For the PWR fuel configuration, fuel basket drop orientations of 0°, 18.22°, 26.28°, and 45° are evaluated (see Figure 11.2.12.4.1-1). For the BWR fuel configuration, fuel basket drop orientations of 0°, 31.82°, 49.46°, 77.92°, and 90° are evaluated (see Figure 11.2.12.4.2-1).

11.2.12.4.1 Analysis of Canister and Basket for PWR Configurations

Four three-dimensional models of the PWR canister and fuel basket are evaluated for side loading conditions that conservatively simulate a tip-over event while inside the concrete cask. In each model, a different fuel basket drop orientation is used. Three-dimensional half-symmetry models are used for the basket orientation of 0° and 45°, since half-symmetry is applicable based on the support disk geometry and the drop orientation. Three-dimensional full-models are used for the basket drop orientations of 18.22° and 26.28°. Representative figures for the models are presented in this section (three-dimensional full-model with a basket orientation of 18.22°).

Model Description

The finite element model used to evaluate the PWR canister and fuel basket for the tip-over event is presented in Figure 11.2.12.4.1-2 through Figure 11.2.12.4.1-5. The figures presented are for the PWR canister and fuel basket model with a fuel basket drop orientation of 18.22° and are representative of the models for all drop orientations analyzed. Only half of the canister is shown in the figures to present the view of the fuel basket.

The canister shell, shield lid, and structural lids are constructed of SOLID45 elements, which have three degrees-of-freedom (UX, UY, and UZ) per node (see Figure 11.2.12.4.1-3). The interaction of the shield lid and structural lid with the canister shell (below the lid welds) is modeled using CONTAC52 elements with a gap size based on nominal dimensions. The interaction of the bottom edge of the shield lid with the support ring is modeled using COMBIN40 gap elements with a gap size of 1×10^{-8} inch. The interaction of the shield and structural lids is modeled using COMBIN40 gap elements with a conservative gap size of 0.08 inch, based on the flatness tolerance of the two lids. The interaction of the canister shell with the inner surface of the concrete cask is modeled using CONTAC52 elements with an initial gap size equal to the difference in the nominal radial dimensions of the outer surface of the canister and the inner surface of the concrete cask. A gap stiffness of 1×10^{6} lbs/inch is assigned to all CONTAC52 and COMBIN40 elements.

The top five fuel basket support disks and top weldment disk are modeled using SHELL63 elements, which have six degrees-of-freedom per node (UX, UY, UZ, ROTX, ROTY, and ROTZ). For the top (first) and fifth support disk, a refined mesh density is used (see Figure 11.2.12.4.1-4). The remaining support disks and the top weldment disk incorporate a course mesh density to account for the load applied to the canister shell. For the fine-meshed support disks, the tie-rod holes are modeled. CONTAC52 elements are included in the slits at the tie-rod holes. The interaction between the fuel basket support disks and top weldment disk and the canister shell is modeled using CONTAC52 elements with an initial gap size based on the nominal radial difference between the disks and canister shell. A gap stiffness of 1×10^{6} lbs/inch is assigned to all CONTAC52 elements.

The lower boundary of the canister shell (near the 5th support disk) is restrained in the axial (Y) direction. For the half-symmetry models (0° and 45° basket drop orientations), symmetry boundary conditions are applied at the plane of symmetry of the model. Since gap elements are used to represent the contact between the canister shell and the inner surface of the concrete cask, the nodes corresponding to the concrete cask are fixed in all degrees of freedom (UX, UY and UZ). In

addition, the axial (UY) and in-plane rotational degrees of freedom (ROTX and ROTZ) of the basket nodes are fixed since there is no out-of-plane loading for the support disk for a side impact condition.

Loading of the model includes an internal pressure of 15 psig (design pressure for normal condition of storage) applied to the inner surfaces of the canister, pressure loads applied to the support disk slots, and the inertial loads. The pressure load applied to the support disk slots represents the weight of the fuel assemblies, fuel tubes, and aluminum heat transfer disks multiplied by the appropriate acceleration (see Figure 11.2.12.4.1-5). For the inertial loads, a maximum acceleration of 40g is conservatively applied to the entire model in the X-direction (see Figure 11.2.12.4.1-2) to simulate the side impact during the cask tip-over event.

As shown in Section 11.2.12.3.1, the maximum acceleration of the concrete cask steel liner at the locations of the top support disk and the top of the canister structural lid during the tip-over event is determined to be 34.3g and 36.9g, respectively. To determine the effect of the rapid application of the inertia loading for the support disk, a dynamic load factor (DLF) is computed using the mode shapes of a loaded support disk. The mode shapes corresponding to the in-plane motions of the disk are extracted using ANSYS. However, only the dominant modes with respect to modal mass participation factors are used in computing the DLF. The dominant resonance frequencies and corresponding modal mass participation factors from the finite element modal analyses of the PWR support disk are:

Frequency (Hz)	% Modal Mass Participation Factor
109.7	85.8
370.1	2.7
371.1	7.2

The mode shapes for these frequencies are shown in Figures 11.2.12.4.1-8 through 11.2.12.4.1-10. The displacement depicted in these figures is highly exaggerated by the ANSYS program in order to illustrate the modal shape. The stresses associated with the actual displacement are shown in Tables 11.2.12.4.1-4 through 11.2.12.4.1-8.

Using the acceleration time history of the concrete cask steel liner at the top support disk location developed from Section 11.2.12.3.1, the DLF is computed to be 1.10. Applying the DLF to the 34.3g results in a peak acceleration of 37.7g for the top support disk. The DLFs for the canister lids are considered to be unity since the lids have significant in-plane stiffness and are considered to be

rigid (the structural lid is 3 inch thick and shield lid is 7 inch thick). Therefore, applying 40g to the entire canister/basket model is conservative.

A uniform temperature of 75°F is applied to the model to determine material properties during solution. During post processing for the support disk, temperature distribution with a maximum temperature of 700°F (at the center) and a minimum temperature of 400°F (at the outer edge) are conservatively used to determine the allowable stresses. A constant temperature of 500°F is used for the canister to determine the allowable stresses. These temperatures are the bounding temperatures for the normal, off-normal and accident conditions of storage.

Analysis Results for the Canister

The sectional stresses at 13 axial locations of the canister are obtained for each angular division of the model (a total of 80 angular locations for the full-models and 41 angular locations for the half-symmetry models). The locations for the stress sections are shown in Figure 11.2.12.4.1-6.

The stress evaluation for the canister is performed in accordance with the ASME Code, Section III, Subsection NB, by comparing the linearized sectional stresses against the allowable stresses. Allowable stresses are conservatively taken at a temperature of 500°F, except that 300°F and 250°F are used for the shield lid weld (Section 10) and the structural lid weld (Section 11). The calculated maximum temperatures for the shield lid and structural lid are 212°F and 202°F, respectively (Table 4.4.3-1). The allowable stresses for accident conditions are taken from Subsection NB as shown below. S_m and S_u are 14.8 ksi and 57.8 ksi, respectively, for Type 304L stainless steel (canister shell and structural lid). S_m and S_u are 17.5 ksi and 63.5 ksi, respectively, for Type 304 stainless steel (shield lid).

Stress Category	Accident (Level D) Allowable Stress
P_m	Lesser of 0.7 S_u or 2.4 S_m
P_m+P_b	Lesser of 1.0 S_u or 3.6 S_m

The primary membrane and primary membrane plus bending stresses for the PWR configuration for a 45° basket drop orientation are summarized in Table 11.2.12.4.1-1 and Table 11.2.12.4.1-2, respectively. The stress results for the canister are similar for all four basket drop orientation evaluations. The 45° basket orientation results are presented because this drop orientation results in the minimum margins of safety in the canister.

During the tip-over accident, the canister shell at the structural and shield lids is subjected to the inertial loads of the lids, which results in highly localized bearing stresses (Sections 7 through 9 at angular locations of approximately ± 4.5 degrees from the impact location). This stress is predominant because the weights of the structural and shield lids are transferred to the canister shell near these section locations. According to ASME Code Section III, Appendix F, bearing stresses need not be evaluated for Level D service (accident) conditions. Therefore, the stresses are not presented for the lid-bearing regions of the canister shell (Sections 7 through 9) in Tables 11.2.12.4.1-1 and 11.2.12.4.1-2. The stresses at the structural lid/canister shell weld region (Section 11) are determined by averaging the stresses over the impact region where the weld is in compression in the radial direction ($\sigma_x \leq 0.0$ psi). In accordance with ISG 4, Revision 1, a 0.8 weld reduction factor is applied to the allowable stresses for the structural lid / canister shell weld. Use of the 0.8 factor is valid because the ultimate tensile strength of the weld material exceeds the base metal strength.

The stress evaluation results for the tip-over accident condition show that the minimum margin of safety in the canister for the PWR configuration is +0.13 for P_m stresses (Section 10). For P_m+P_b stresses, the margin of safety at is +0.23 (Section 10).

Analysis Results for the Support Disks

To evaluate the most critical regions of the support disk, a series of cross sections are considered. To aid in the identification of these sections, Figure 11.2.12.4.1-7 shows the locations on a support disk for the full-models. Table 11.2.12.4.1-3 lists the cross sections versus Point 1 and Point 2, which spans the cross section of the ligament in the plane of the support disk. Note that a local coordinate system (x and y parallel to the support disk ligaments) is used for the stress evaluation.

The stress evaluation for the support disk is performed according to ASME Code, Section III, Subsection NG. According to this subsection, linearized sectional stresses are to be compared against the allowable stresses. The allowable stresses for tip-over accident conditions are taken from Subsection NG as shown below, at the temperature of the Section. The temperature distribution of the disk is determined by a thermal conduction solution for a single disk with the maximum temperature of 700°F specified at the center and the minimum temperature of 400°F specified at the outer edge as boundary conditions.

Stress Category	Accident (Level D) Allowable Stresses
P_m	Lesser of 0.7 S_u or 2.4 S_m
P_m+P_b	Lesser of 1.0 S_u or 3.6 S_m

The shield lid and structural lid provide additional stiffness to the upper portion of the canister shell, which limits the shell and support disk deformations. Therefore, the maximum $P_m + P_b$ stress, and the minimum margin of safety, occur in the 5th support disk (from the top of the basket), where the stiffness effect of the shield and structural lids is not present.

The stress evaluation results for the 5th support disk for the tip-over condition are summarized in Table 11.2.12.4.1-4 for the four basket drop orientations evaluated. As shown in Table 11.2.12.4.1-4, the 26.28° drop orientation case generates the minimum margin of safety in the support disk; therefore, the P_m and $P_m + P_b$ stress intensities for the 26.28° basket drop orientation case are presented in Tables 11.2.12.4.1-6 and 11.2.12.4.1-7, respectively. These tables list stress results with the 30 lowest margins of safety for the 5th support disk. The highest P_m stress occurs at Section 18, with a margin of safety of +0.97 (See Table 11.2.12.4.1-6 for stresses and Figure 11.2.12.4.1-7 for section locations). The highest P_m+P_b stress occurs at Section 61, with a margin of safety of +0.05 (see Table 11.2.12.4.1-7 for stresses and Figure 11.2.12.4.1-7 for section locations).

Support Disk Buckling Evaluation

For the tip-over accident, the support disks experience in-plane loads. The in-plane loads apply compressive forces and in-plane bending moments on the support disk. Buckling of the support disk is evaluated in accordance with the methods and acceptance criteria of NUREG/CR-6322 [39]. Because the ASME Code identifies 17-4PH disk material as ferritic steel, the formulas for non-austenitic steel are used.

The buckling evaluation of the support disk ligaments is based on the Interaction Equations 31 and 32 in NUREG/CR-6322. These two equations adopt the "Limit Analysis Design" approach. Other equations applicable to the calculations are noted as they are applied. The maximum forces and moments for the tip-over accident are based on the finite element analysis stress results.

Symbols and Units

P = applied axial compressive load, kip
M = applied bending moment, kip-inch
P_a = allowable axial compressive load, kip
P_{cr} = critical axial compression load, kip
P_e = Euler buckling loads, kip

P_y = average yield load, equal to profile area times specified minimum yield stress, kips (for normal operating condition)

C_c = column slenderness ratio separating elastic and inelastic buckling

C_m = coefficient applied to bending term in interaction equation

M_m = critical moment that can be resisted by a plastically designed member in the absence of axial load, kip-in.

M_p = plastic moment, kip-in.

F_a = axial compressive stress permitted in the absence of bending moment, ksi

F_e = Euler stress for a prismatic member divided by factor of safety, ksi

k = ratio of effective column length to actual unsupported length

l = unsupported length of member, in.

r = radius of gyration, in.

S_y = yield stress, ksi

A = cross sectional area of member, in^2

Z_x = plastic section modulus, in^3

λ = allowable reduction factor, dimensionless

From NUREG/CR-6322, the following equations are used to evaluate the support disk:

$$\frac{P}{P_{cr}} + \frac{C_m M}{M_m\left[1 - \frac{P}{P_e}\right]} \leq 1.0 \qquad \text{(Equation 31)}$$

$$\frac{P}{P_y} + \frac{M}{1.18\,M_p} \leq 1.0 \qquad \text{(Equation 32)}$$

where:

$$P_{cr} = 1.7 \times A \times F_a$$

$$F_a = \frac{P_a}{A} \quad \text{for } P_a = P_y\left[\frac{1 - \frac{\lambda^2}{4}}{1.11 + 0.5\lambda + 0.17\lambda^2 - 0.28\lambda^3}\right]$$

and $\lambda = \frac{1}{\pi}\left(\frac{kl}{r}\right)\sqrt{\frac{S_y}{E}}$ (accident conditions)

$$Pe = 1.92 \times A \times Fe$$

$$F_e = \frac{\pi^2 \cdot E}{1.3\left(\frac{k \cdot l}{r}\right)^2}$$ (Level D–Accident)

$$P_y = S_y \times A$$

$C_m =$ 0.85 for members with joint translation (sideways)

$$M_p = S_y \times Z_x$$

$$M_m = M_p \cdot \left(1.07 - \frac{\left(\frac{1}{r}\right) \cdot \sqrt{S_y}}{3160}\right) \leq M_p$$

Buckling evaluation is performed in all sections in the disk ligaments defined in Figure 11.2.12.4.1-7. Using the cross-sectional stresses calculated at each section located in the ligament for each loading condition, the maximum corresponding compressive force (P) and bending moment (M) are determined as:

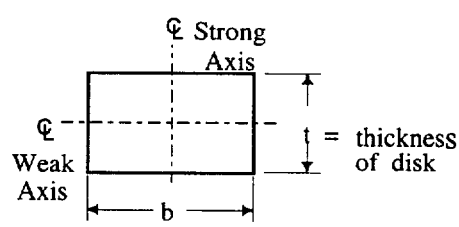

$$P = \sigma_m A$$

$$M = \sigma_b S$$

where, σ_m is the membrane stress, σ_b is the bending stress, A is the area ($b \times t$), and S is the section modulus ($tb^2/6$). Note that the strong axis bending is considered in the buckling evaluation since the disk is only subjected to in-plane load during the tip-over event.

To determine the margin of safety:

$$P_1 = P/P_{cr} \qquad M_1 = \frac{C_m M}{(1 - P/P_e)M_m} \qquad (P_1 + M_1 \leq 1)$$

and

$$P_2 = P/P_y \qquad M_2 = \frac{M}{1.18\,M_p} \qquad (P_1 + M_1 \leq 1)$$

The margins of safety are:

$$MS1 = \frac{1}{P_1 + M_1} - 1$$

and

$$MS2 = \frac{1}{P_2 + M_2} - 1$$

The support disk buckling evaluation results for the 5th support disk (the 5th support disk experiences the highest stresses) for the tip-over impact condition are summarized in Table 11.2.12.4.1-5 for the four basket drop orientations evaluated. As shown in Table 11.2.12.4.1-5, the 26.28° case generates the minimum margin of safety for buckling; therefore, the results of the buckling analysis for the 26.28° basket drop orientation case are presented in Table 11.2.12.4.1-8. This table presents the 30 minimum margins of safety for this drop orientation. As the tables demonstrate, the support disks meet the requirements of NUREG/CR-6322.

Fuel Tube Analysis

The fuel tube provides structural support and a mounting location for BORAL neutron poison plates. The fuel tube does not provide structural support for the fuel assembly. To ensure that the fuel tube remains functional during a tip-over accident, a structural evaluation of the tube is

performed for a side impact assuming a deceleration of 60g. This g-load bounds the maximum g-load (40g) calculated to occur for the PWR basket in a vertical concrete cask tipover event.

In the tipover event, the stainless steel support disks in the fuel basket support the fuel tube. The fuel basket support disks, which support the full length of the fuel tube, are spaced 4.42-inches apart (which is less than one half of the fuel tube width of 8.8 inch). Considering the fuel tube subjected to a maximum PWR fuel assembly weight of 1,602 pounds with a 60g load factor and the 30 support locations provided by the basket support disks, the fuel tube shear stress is calculated as:

Shear load = (60g)(1,602)/30 = 3,204 lbs
Area = (0.048)(8.8)(2) = 0.845 in^2
Shear Stress = 3,204/0.845 = 3,792 psi

The yield strength of the tube material, Type 304 stainless steel, is 17,300 psi at 750°F. Conservatively, using the allowable shear stress as one-half the yield strength of the tube material (8,650 psi) results in a large positive margin of safety. Conservative evaluation of the tube loading resulting from its own mass during a side-impact shows that the tube structure maintains position and function.

The load transfer of the weight of the fuel assembly to the fuel basket support disk in the side impact is through direct bearing and compression of the distributed load of the fuel assembly through the fuel tube to the support disk web. Two load conditions are considered in the fuel tube evaluation. The first considers the fuel assembly load as a distributed pressure on the inside surface of the fuel tube. The second postulates that the fuel assembly grid is located at the center of the span between the support disks and produces a localized distributed load over the effective area of the grid.

Two different ANSYS finite element models of the tube are developed for these two load conditions since the fuel tube structural performance for either load is nonlinear. As shown below, the first model represents a fuel tube section with a length of three spans, i.e., the model is supported at four locations by support disks. The model conservatively considers the fuel tube wall thickness of 0.048 inch as the only material subjected to a distributed pressure load representative of the fuel assembly deceleration of 60g. Fuel assembly stiffness is not considered in the development of the imposed pressure load on the fuel tube.

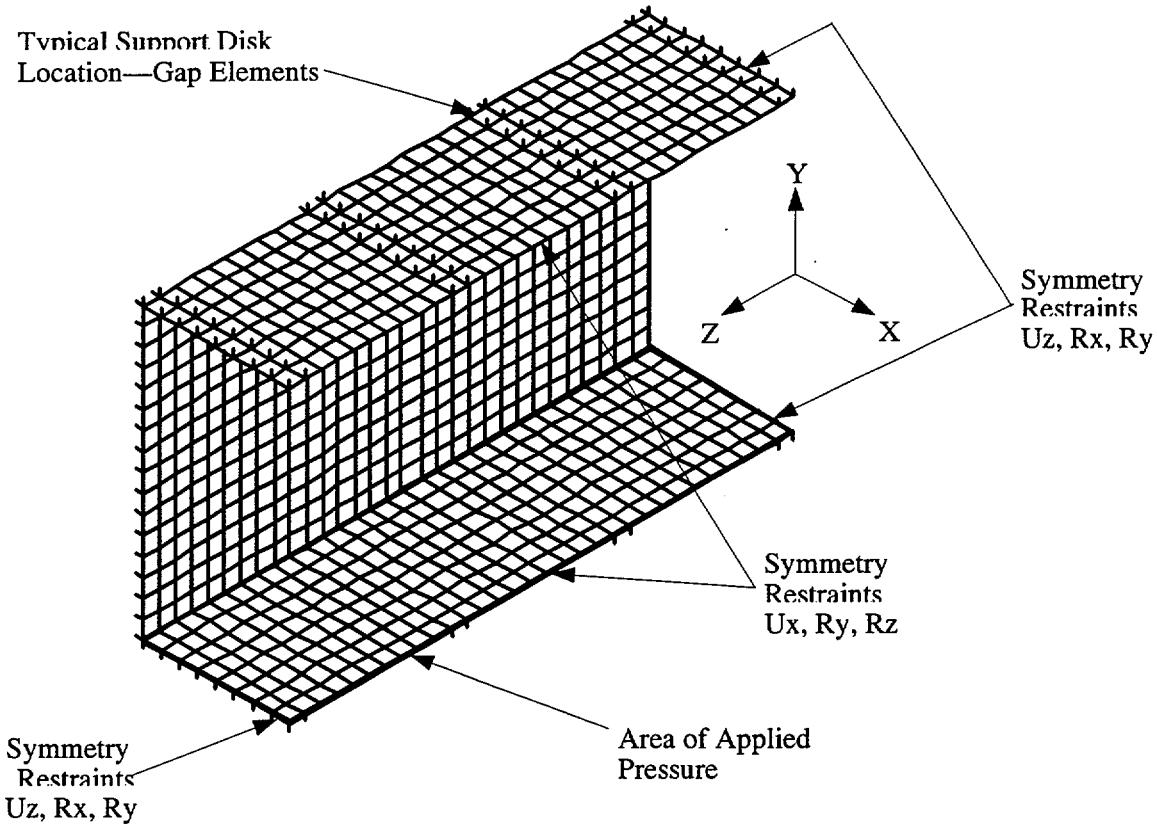

The tube is modeled with the ANSYS plastic, quadrilateral shell element (SHELL43). The support disks are represented by gap elements (CONTAC52). The outer nodes of the gap elements are fully restrained in all three translational directions. Edge restraints were applied to the model to represent symmetry boundary conditions. The effective load on the fuel tube due to the 60g deceleration of the fuel assembly is applied as a pressure to the inside area of the fuel tube.

The finite element analysis results show that the maximum stress in the tube is 23.8 ksi, which is local to the sections of the tube resting on the support disks. At 750°F the ultimate strength for Type 304 stainless steel is 63.1 ksi. The margin of safety is

$$MS = \frac{63.1}{23.8} - 1 = +1.65$$

The analysis shows that the maximum total strain is 0.026 inch/inch. Defining the acceptable elastic-plastic response of the stainless steel as one half of the material failure strain of 0.40 in./in. at 750°F [42], the resulting margin of safety is:

$$MS = \frac{0.40/2}{0.026} - 1 = +\text{large}$$

Similarly, the margin of safety for elastic-plastic stress becomes

$$MS = \frac{63.1 - 17.3}{23.8 - 17.3} - 1 = 6.05$$

where the yield strength of Type 304 stainless steel is 17.3 ksi at 750°F.

The second finite element model is used to evaluate the load condition with the fuel assembly grid located at the center of the span between two support disks. The fuel tube is subjected to a localized distributed load over the effective area of the grid. As shown below, the model is a quarter-symmetry periodic section of the fuel tube. As in the finite element model used for the distributed pressure case, this model conservatively considers a fuel tube wall thickness of 0.048 inch. The BORAL plate (0.075 inch) and stainless steel cover plate (0.018 inch) are conservatively not included in the model. The tube wall is modeled with ANSYS SHELL43 elements. The support disks are modeled with CONTAC52 elements.

Based on the Lawrence Livermore evaluation of the fuel rods for a side impact (UCID-21246), the fuel rods and fuel assemblies maintain their structural integrity during the side impact resulting from a cask tip-over accident and the displacement of the fuel tube is limited. The maximum displacement of the fuel tube section between the support disks will not exceed the "thickness" of the grid spacer, which is the distance between the outer surface of the grid and the outer surface of the fuel rod array. When the displacement of the fuel tube reaches the "thickness" of the grid spacer, the fuel rods will be in contact with the inner surface of the fuel tube and the weight of the fuel rods will be transferred through the tube wall to the support disks. Therefore, a bounding load condition for this model is simulated by applying a constant displacement of 0.08 inch in the negative Y direction to the nodes corresponding to the grid location in the model. Note that 0.08 inch displacement bounds all PWR fuel assemblies. It is assumed that the fuel assembly grid spacer is rigid and therefore a constant displacement is conservatively applied.

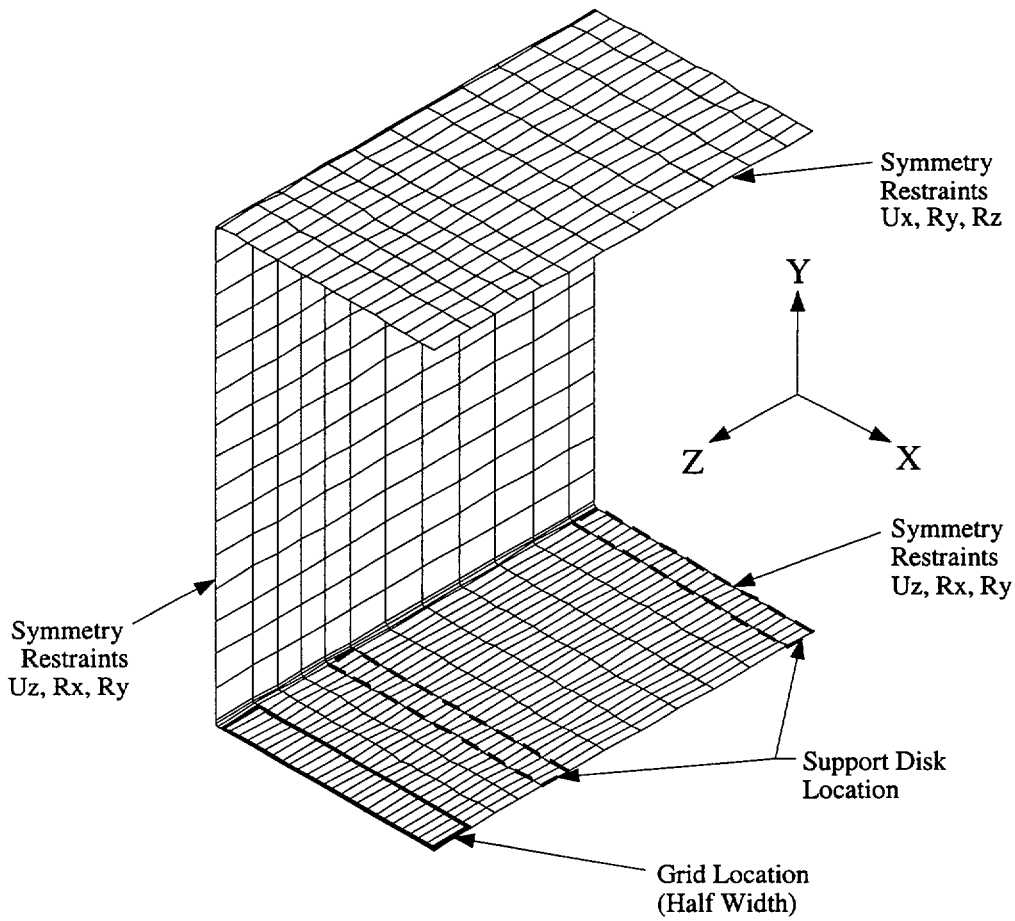

The finite element analysis results show that the maximum stress in the tube is 38.4 ksi, which is local to the corner of the tube at the grid spacer location of the model close to the side wall of the tube. At 750°F the ultimate strength for Type 304 stainless steel is 63.1 ksi. The margin of safety is

$$MS = \frac{63.1}{38.4} - 1 = +0.64$$

The analysis shows that the maximum total strain is 0.11 inch/inch. Defining the acceptable elastic-plastic response of the stainless steel as one half of the material failure strain of 0.40 in./in. at 750°F [42], the resulting margin of safety is:

$$MS = \frac{0.40/2}{0.11} - 1 = 0.82$$

Similarly, the margin of safety for elastic-plastic stress becomes

$$MS = \frac{63.1 - 17.3}{38.4 - 17.3} - 1 = 1.17$$

where the yield strength of Type 304 stainless steel is 17.3 ksi at 750°F.

Both the maximum total strain and the elastic-plastic stress analyses indicate that the tube position within the support basket is maintained.

Assurance that the BORAL remains attached to the fuel tube is evaluated by considering that loads produced by the BORAL plate and stainless steel attachment plate, assuming a 60g load, are carried by the attachment plate weld. Total load and resultant stress on the weld are calculated as:

$F_{b/ss} = (g)(\rho)(t)(w)(l)$ Load exerted by BORAL/Stainless Steel Attachment Plate

where:

- g = acceleration (g)
- ρ = density of material (lb/in^3) (The density of aluminum (0.098 lb/in^3) is conservatively used for the BORAL.
- t = thickness of material (in.)
- w = width of material (in.)
- l = length of material section (in.)

The forces on the weld due to a 12-inch section of BORAL (F_b) and a 12-inch section of stainless steel plate (F_{ss}) are:

$$F_b = (60g)(0.098\ lb/in^3)(0.075\ in.)(8.2\ in.)(12\ in.) = 43.4\ lbs$$

$$F_{ss} = (60g)(0.291\ lb/in^3)(0.018\ in.)(8.7\ in.)(12\ in.) = 32.8\ lbs$$

The total load (F_t) on a 1-inch attachment weld for a 12-inch section is:

$$F_t = 43.4 \text{ lbs} + 32.8 \text{ lbs} = 76.2 \text{ lbs}$$

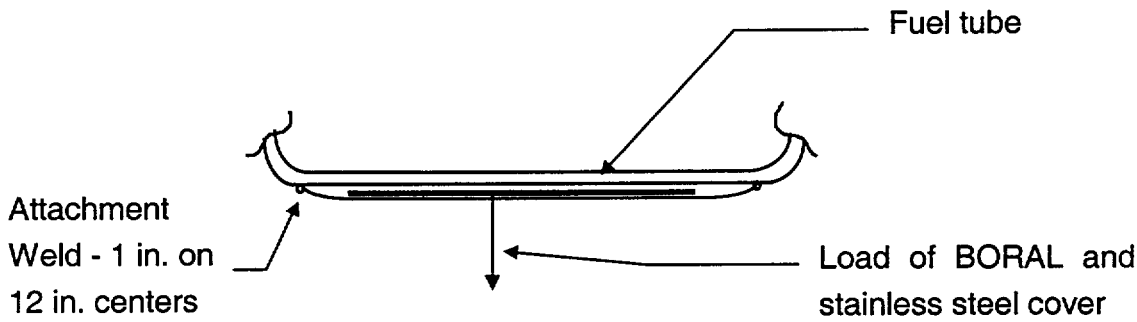

The resulting weld stress is: $\sigma = P/A = (76.2 \text{ lb}/2) / (1 \text{ in.})(0.018 \text{ in.}) = 2{,}117$ psi

Since the weld material is Type 304 stainless steel, the margin of safety (at 750°F) is:

$$MS = \frac{17{,}300}{2{,}117} - 1 = +7.2$$

Therefore, the BORAL remains enclosed on each outer surface of the fuel tube wall.

Figure 11.2.12.4.1-1 Basket Drop Orientations Analyzed for Tip-Over Conditions - PWR

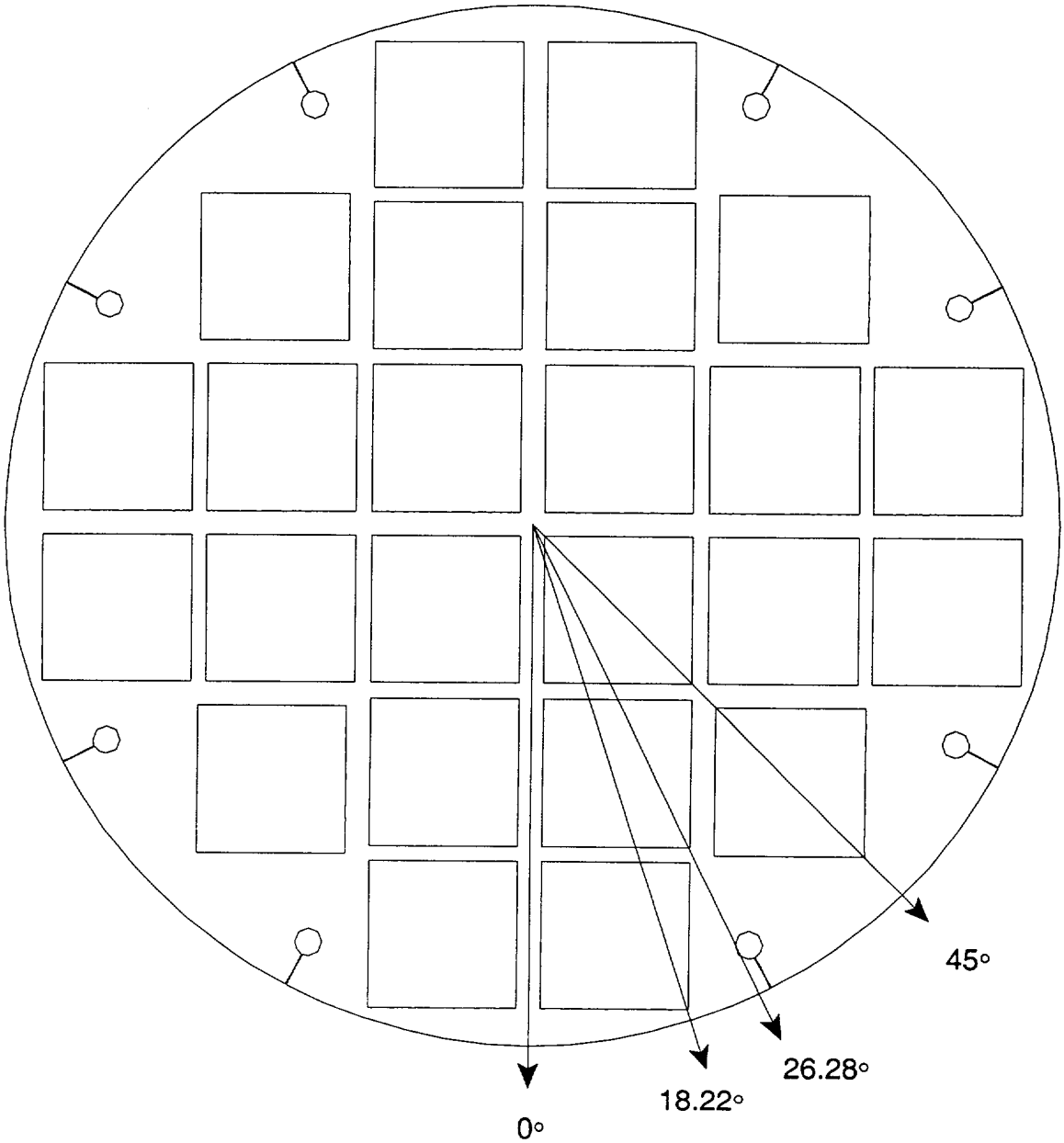

Figure 11.2.12.4.1-2 Fuel Basket/Canister Finite Element Model - PWR

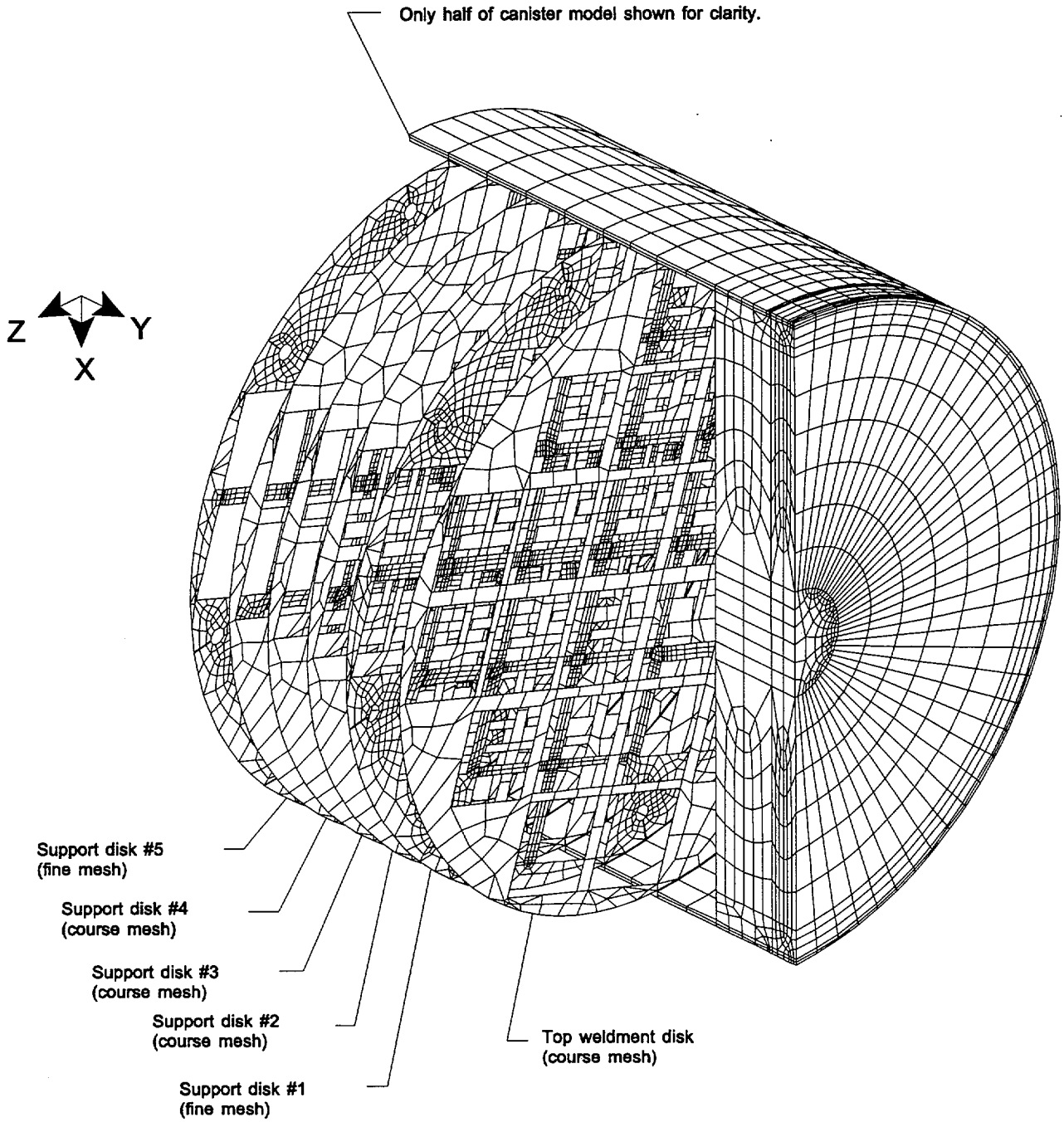

18.22° Basket Drop Orientation

Figure 11.2.12.4.1-3 Fuel Basket/Canister Finite Element Model - Canister

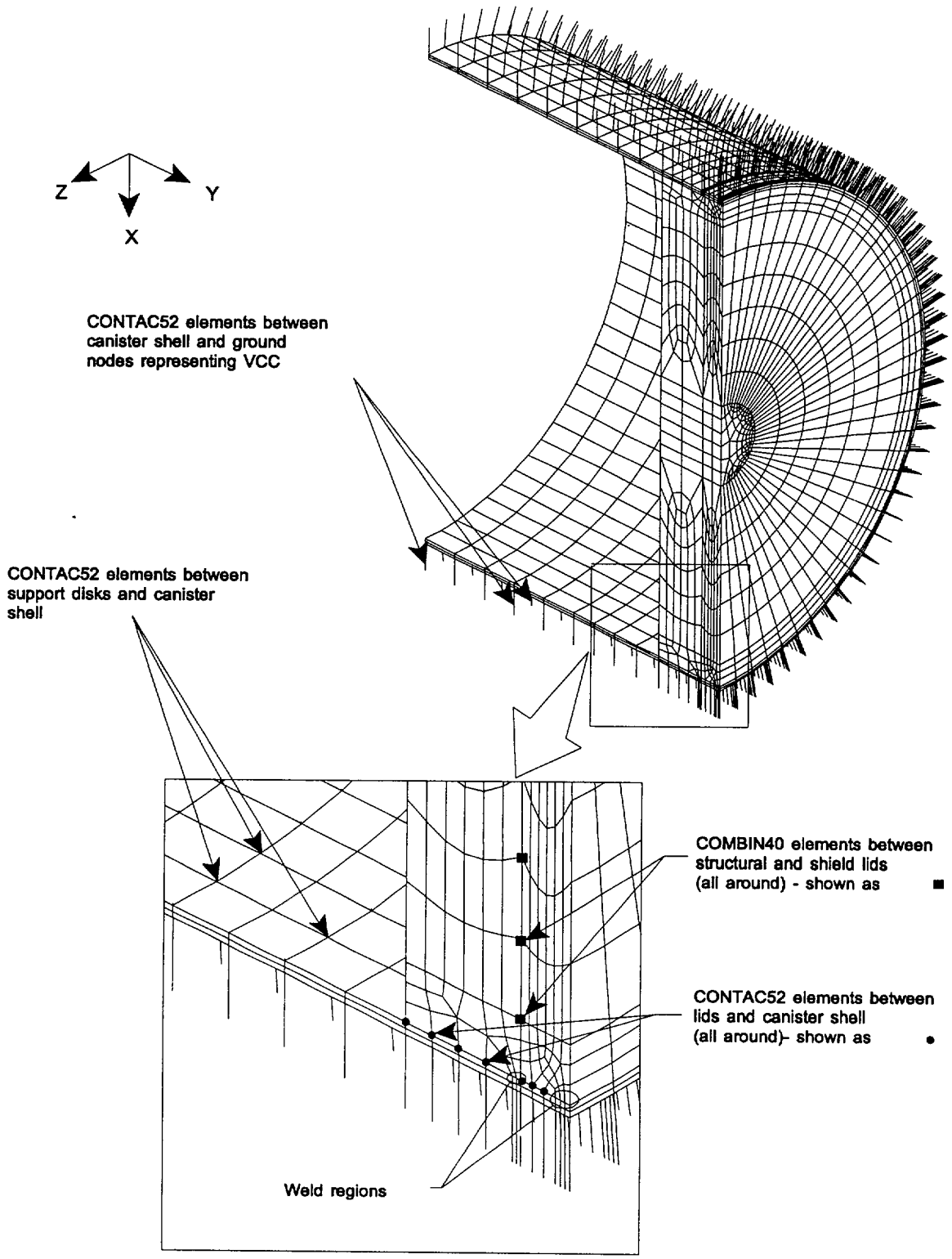

Only Half of Canister Shown for Clarity

Figure 11.2.12.4.1-4 Fuel Basket/Canister Finite Element Model - Support Disk - PWR

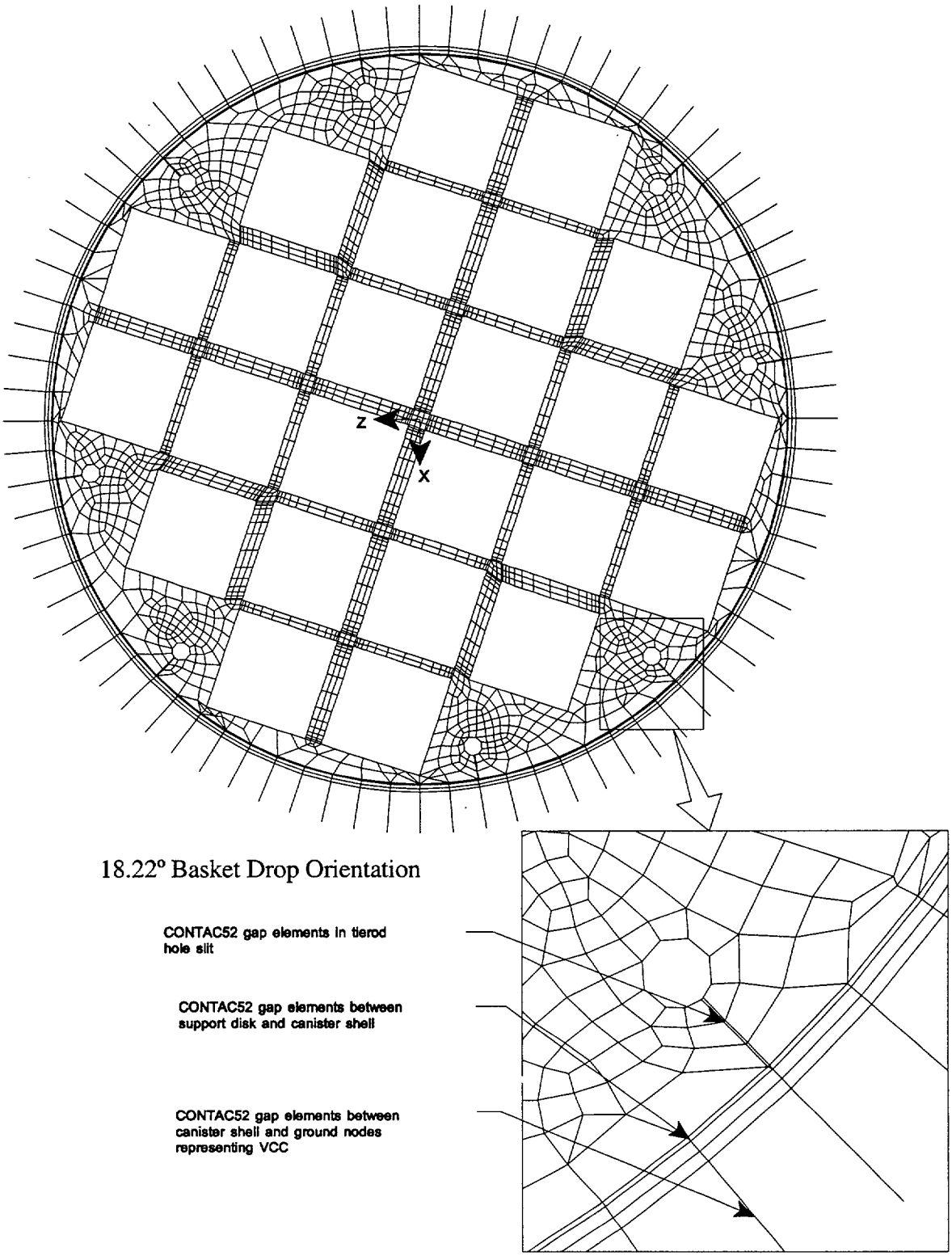

Figure 11.2.12.4.1-5 Fuel Basket/Canister Finite Element Model - Support Disk Loading - PWR

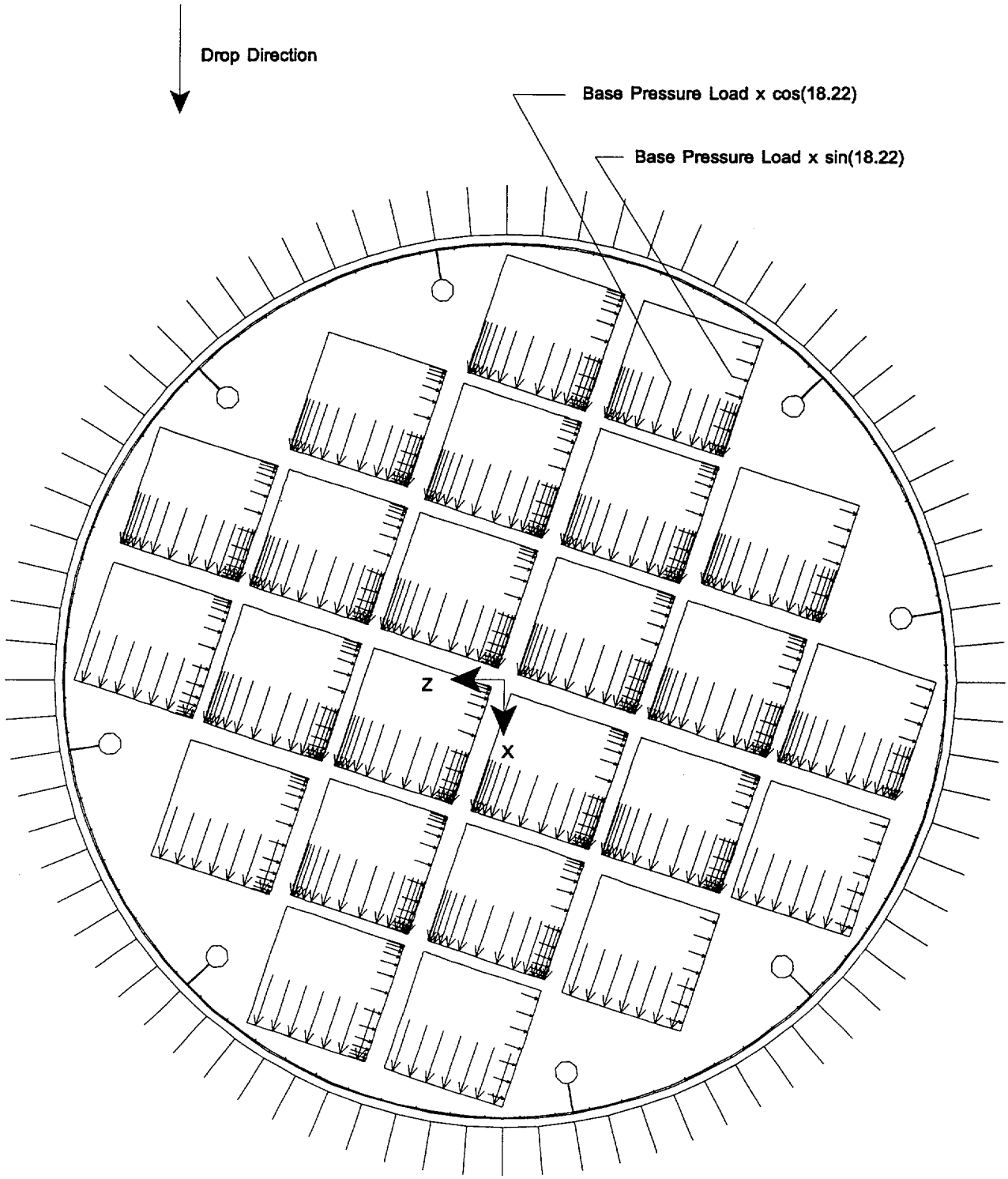

18.22° Basket Drop Orientation
Note: Finite Element Mesh Not Shown

Figure 11.2.12.4.1-6 Canister Section Stress Locations

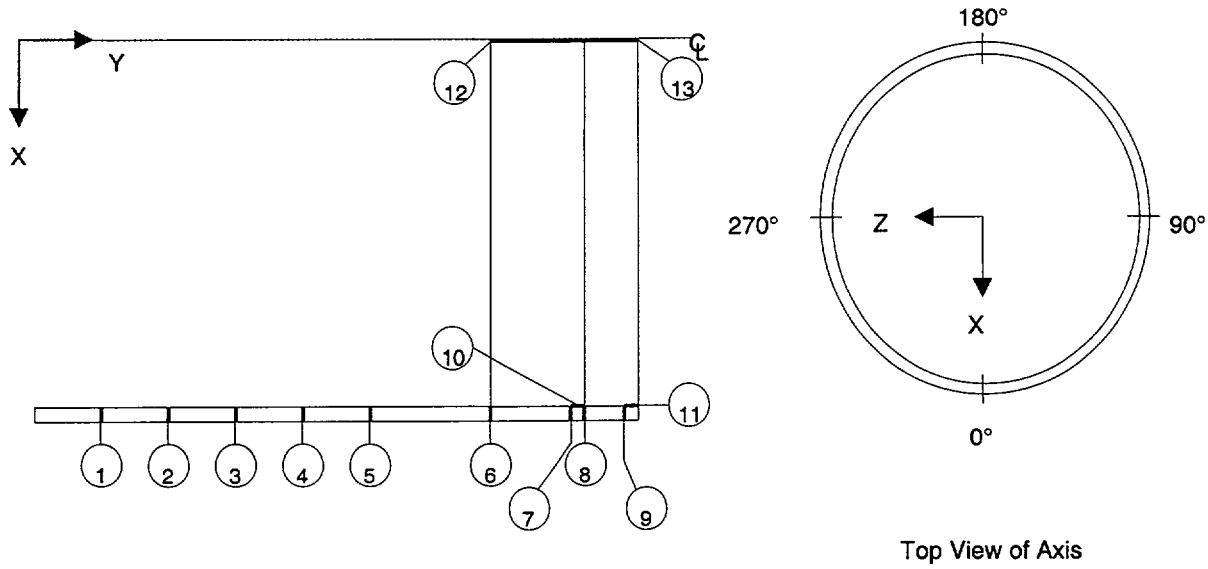

PWR 1 Section Coordinates at Z = 0 and X > 0				
	Point 1		Point 2	
Location	X	Y	X	Y
1	32.905	131.42	33.53	131.42
2	32.905	136.34	33.53	136.34
3	32.905	141.26	33.53	141.26
4	32.905	146.18	33.53	146.18
5	32.905	151.10	33.53	151.10
6	32.905	165.25	33.53	165.25
7	32.905	171.75	33.53	171.75
8	32.905	172.25	33.53	172.25
9	32.905	174.37	33.53	174.37
10	32.905	171.75	32.905	172.25
11	32.905	174.37	32.905	175.25
12	0.1	165.25	0.1	172.23
13	0.1	172.27	0.1	175.25

BWR 4 Section Coordinates at Z = 0 and X > 0				
	Point 1		Point 2	
Location	X	Y	X	Y
1	32.905	144.32	33.53	144.32
2	32.905	148.15	33.53	148.15
3	32.905	151.98	33.53	151.98
4	32.905	155.81	33.53	155.81
5	32.905	159.64	33.53	159.64
6	32.905	175.25	33.53	175.25
7	32.905	182.25	33.53	182.25
8	32.905	182.75	33.53	182.75
9	32.905	184.87	33.53	184.87
10	32.905	182.25	32.905	182.75
11	32.905	184.87	32.905	185.75
12	0.1	175.75	0.1	182.73
13	0.1	182.77	0.1	185.75

General Notes:

1) Impact from the tipover condition is at 0° (in the circumferential direction).

2) For the full 360° models, there are 80 sections at each location for a total of 1040 sections. For the half 180° models, there are 41 sections at each location for a total of 533 sections.

3) Location 10 is through the length of the shield lid weld. Locations 8 and 7 are through the canister shell at top and bottom of the shield lid weld, respectively.

4) Location 13 is through the length of the structural lid weld. Location 9 is through the canister shell at the bottom of the structural lid weld.

Figure 11.2.12.4.1-7 Support Disk Section Stress Locations - PWR – Full Model

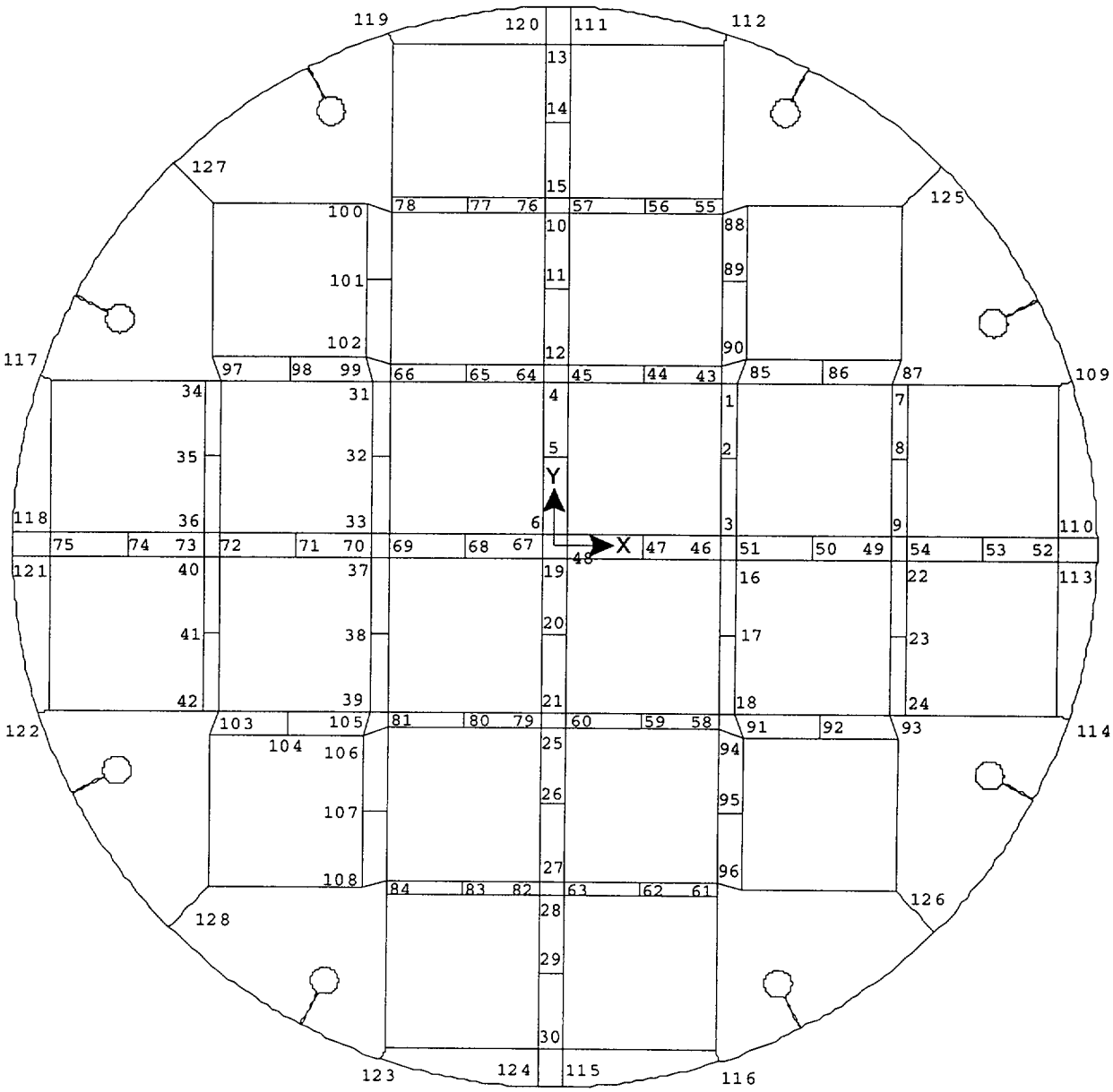

Figure 11.2.12.4.1-8 PWR - 109.7 Hz Mode Shape

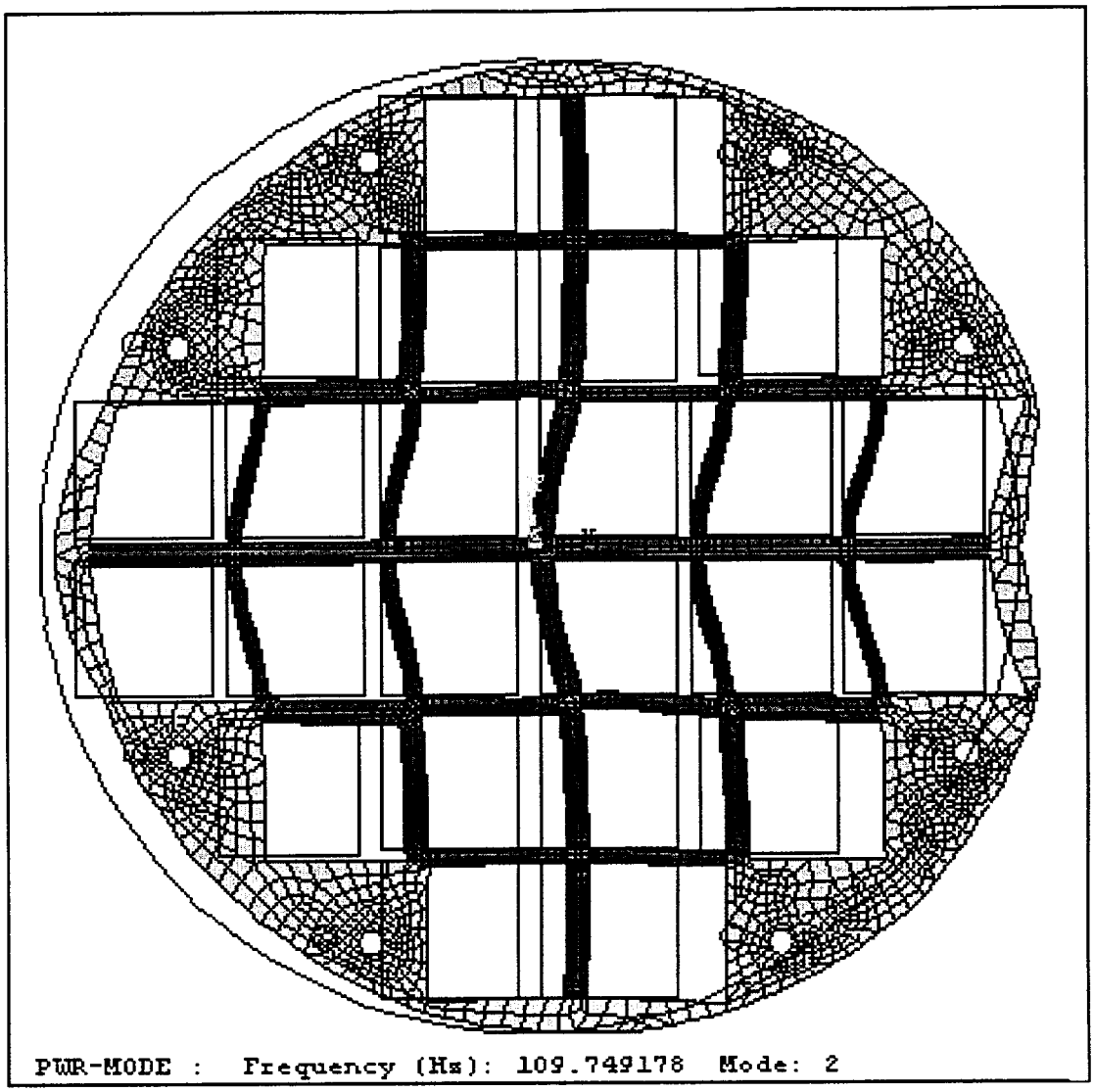

Note: Displacements are greatly exaggerated by the ANSYS program to illustrate the mode shapes.

Figure 11.2.12.4.1-9 PWR – 370.1 Hz Mode Shape

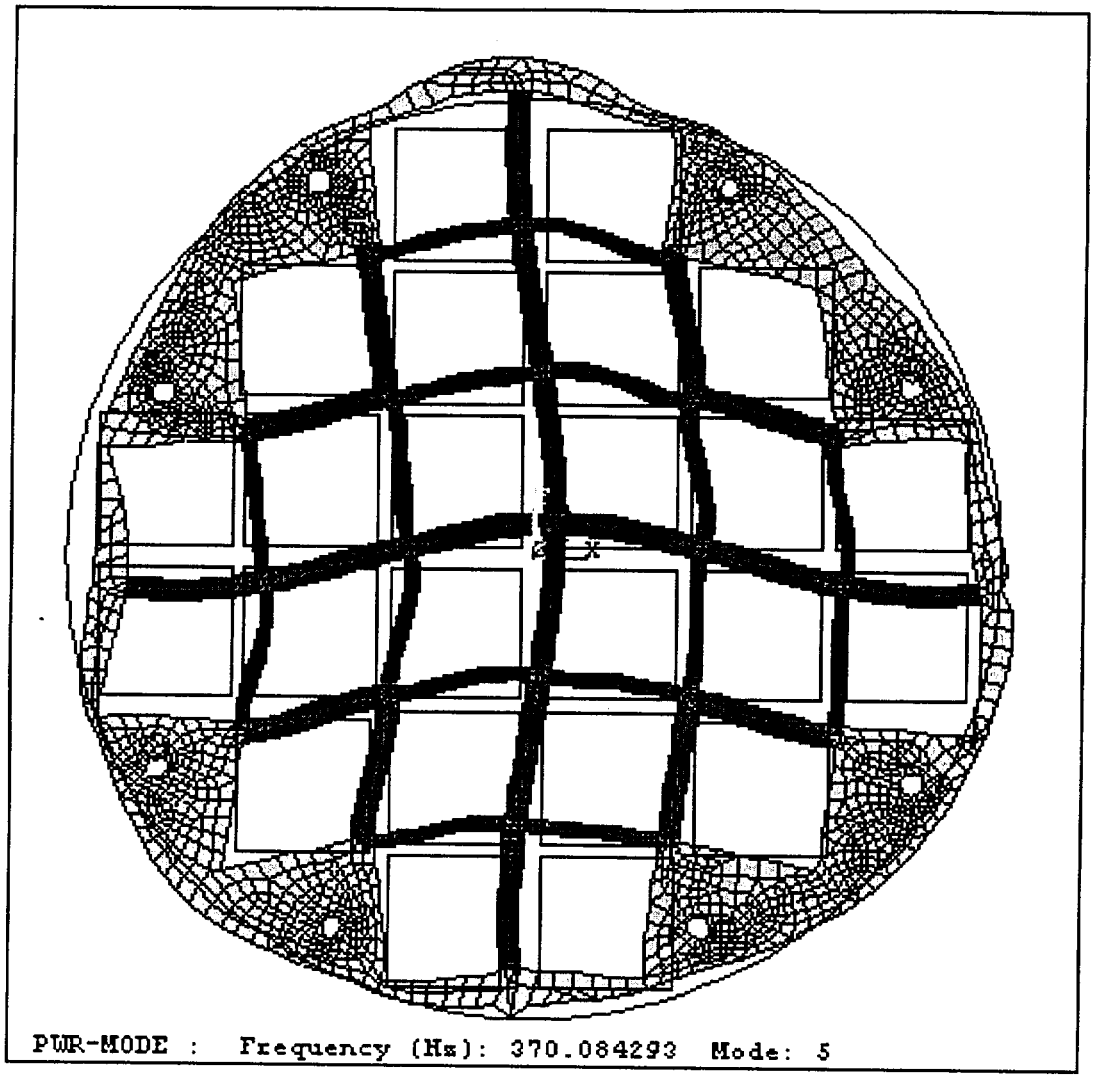

Note: Displacements are greatly exaggerated by the ANSYS program to illustrate the mode shapes.

Figure 11.2.12.4.1-10 PWR – 371.1 Hz Mode Shape

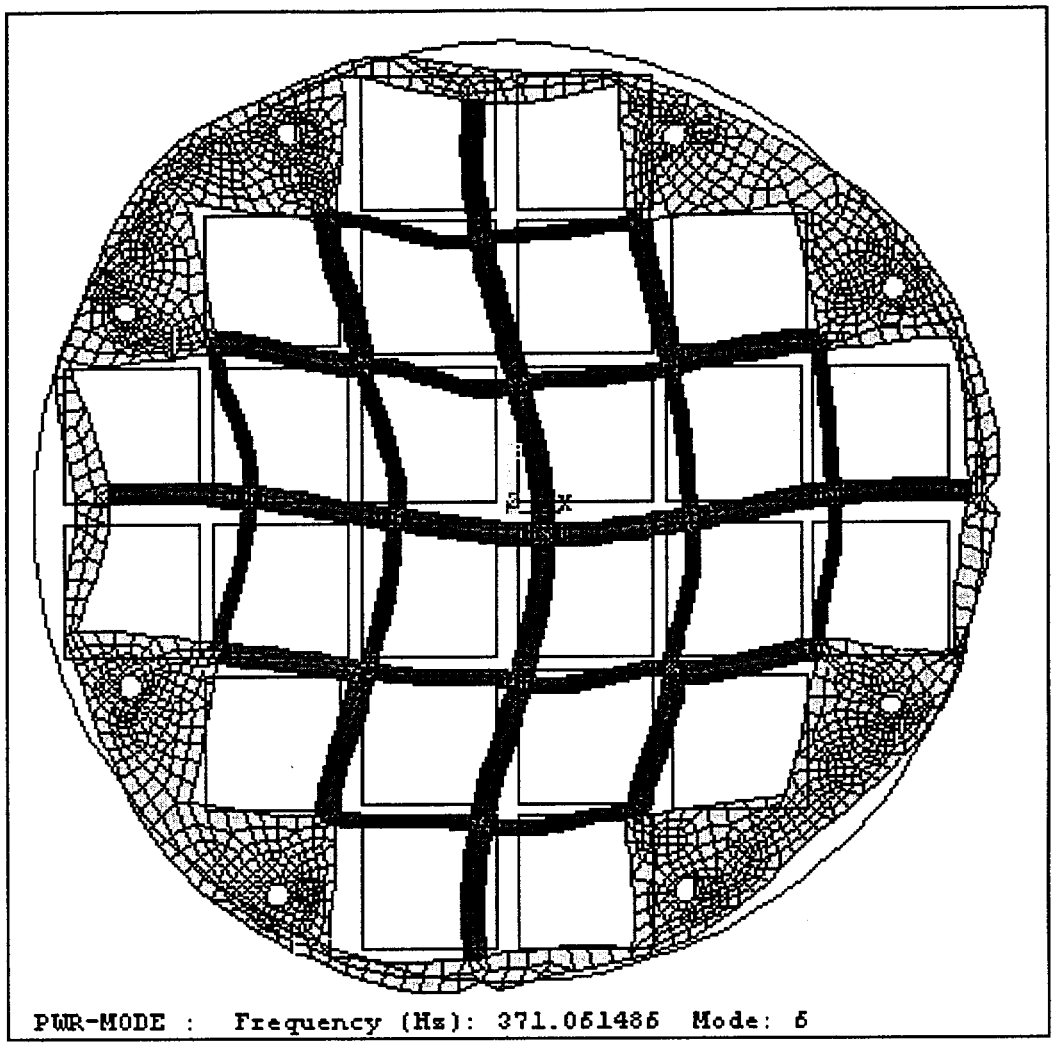

Note: Displacements are greatly exaggerated by the ANSYS program to illustrate the mode shapes.

Table 11.2.12.4.1-1 Canister Primary Membrane (P_m) Stresses for Tip-Over Conditions – PWR - 45° Basket Drop Orientation (ksi)

Section Location(1)	Section Angle (deg)	Sx	Sy	Sz	Sxy	Syz	Sxz	Stress Intensity	Allowable Stress	Margin of Safety
1	0	-1.5	6.5	1.4	-0.1	0.0	-0.2	8.06	35.52	3.41
2	0	-1.7	9.2	1.5	0.1	0.0	0.3	10.92	35.52	2.25
3	49.6	-0.2	9.4	6.3	-0.1	1.1	0.0	9.89	35.52	2.59
4	63.3	-0.3	8.9	5.1	0.1	3.4	0.5	11.24	35.52	2.16
5	90	0.1	2.8	-1.0	-0.3	6.0	0.1	12.67	35.52	1.80
6	85.6	0.0	0.3	0.1	-0.1	7.8	0.0	15.67	35.52	1.27
7(2)	8.7	1.1	0.9	7.4	2.5	-5.0	0.4	13.41	35.52	1.65
8(2)	8.7	5.3	-0.1	6.8	0.5	-3.1	-1.2	9.71	35.52	2.66
9(2)	8.7	6.6	-3.0	1.6	2.3	-3.8	-0.1	12.77	35.52	1.78
10	0	-45.3	-22.9	-40.0	0.6	-1.5	-15.0	35.45	40.08(3)	0.13
11(4)	0.0 – 8.0	-29.4	-14.4	-9.1	-4.6	-2.4	0.9	22.81	32.06(4)	0.41
12	0	-0.7	0.2	0.0	0.0	0.0	-0.1	0.93	35.52	37.09
13	0	-1.6	0.5	0.0	0.0	0.0	0.0	2.02	35.52	16.61

Stresses are presented in the cylindrical coordinate system, x = radial, y = circumferential and z = axial directions.

1. Section locations are shown in Figure 11.2.12.4.1-6.
2. Stresses are not presented for the sections with localized bearing stress. In accordance with ASME Section III, Appendix F, bearing stresses need not be evaluated for Level D service (accident) conditions.
3. Allowable stress at 300°F.
4. Stresses are determined by averaging the stresses over the impact region. A stress reduction factor of 0.8 is applied to the allowable stress at 250°F.

Table 11.2.12.4.1-2 Canister Primary Membrane + Primary Bending ($P_m + P_b$) Stresses for Tip-Over Conditions - PWR - 45° Basket Drop Orientation (ksi)

Section Location(1)	Section Angle (deg)	Sx	Sy	Sz	Sxy	Syz	Sxz	Stress Intensity	Allowable Stress	Margin of Safety
1	0	-2.0	19.3	4.3	-0.6	-0.1	-0.1	21.37	53.28	1.49
2	0	-1.9	22.3	3.0	-0.3	0.1	0.2	24.19	53.28	1.20
3	0	-2.6	22.2	6.2	0.2	0.0	-0.1	24.84	53.28	1.14
4	0	-1.8	21.0	3.8	-0.8	-0.1	-0.3	22.82	53.28	1.33
5	72.5	-0.7	20.6	12.5	0.1	3.9	-0.9	22.97	53.28	1.32
6	0	0.6	-29.7	-8.0	2.3	-1.1	-0.9	30.85	53.28	0.73
7(2)	8.7	0.7	9.4	24.5	0.2	-3.5	1.0	24.63	53.28	1.16
8(2)	8.7	4.7	8.2	21.9	-0.8	-4.9	-2.9	20.3	53.28	1.62
9(2)	8.7	8.7	-5.1	5.4	4.3	-4.6	-0.4	18.43	53.28	1.89
10	0	-46.3	-21.9	-38.2	1.1	-0.	-24.1	49.07	60.12(3)	0.23
11(4)	0.0 – 8.0	-24.4	-10.7	-2.0	-5.0	-0.4	3.2	25.03	48.09(4)	0.92
12	0	-0.9	0.1	0.0	0.0	0.0	-0.1	0.96	53.28	54.71
13	0	-0.8	1.5	0.0	0.1	0.0	0.0	2.33	53.28	21.83

Stresses are presented in the cylindrical coordinate system, x = radial, y = circumferential and z = axial directions.

1. Section locations are shown in Figure 11.2.12.4.1-6.
2. Stresses are not presented for the sections with localized bearing stress. In accordance with ASME Code Section III, Appendix F, bearing stresses need not be evaluated for Level D service (accident) conditions.
3. Allowable stress at 300°F.
4. Stresses are determined by averaging the stresses over the impact region. A stress reduction factor of 0.8 is applied to the allowable stress at 250°F.

Table 11.2.12.4.1-3 Support Disk Section Location for Stress Evaluation - PWR - Full Model

Sec. No.	Point 1		Point 2		Sec. No.	Point 1		Point 2	
	X	Y	X	Y		X	Y	X	Y
1	10.02	10.02	11.02	10.02	45	0.75	10.02	0.75	11.02
2	10.02	5.39	11.02	5.39	46	10.02	0.75	10.02	-0.75
3	10.02	0.75	11.02	0.75	47	5.39	0.75	5.39	-0.75
4	0.75	10.02	-0.75	10.02	48	0.75	0.75	0.75	-0.75
5	0.75	5.39	-0.75	5.39	49	20.29	0.75	20.29	-0.75
6	0.75	0.75	-0.75	0.75	50	15.66	0.75	15.66	-0.75
7	20.29	10.02	21.17	10.02	51	11.02	0.75	11.02	-0.75
8	20.29	5.39	21.17	5.39	52	30.44	0.75	30.44	-0.75
9	20.29	0.75	21.17	0.75	53	25.81	0.75	25.81	-0.75
10	0.75	20.29	-0.75	20.29	54	21.17	0.75	21.17	-0.75
11	0.75	15.66	-0.75	15.66	55	10.02	20.29	10.02	21.17
12	0.75	11.02	-0.75	11.02	56	5.39	20.29	5.39	21.17
13	0.75	30.44	-0.75	30.44	57	0.75	20.29	0.75	21.17
14	0.75	25.81	-0.75	25.81	58	10.02	-10.02	10.02	-11.02
15	0.75	21.17	-0.75	21.17	59	5.39	-10.02	5.39	-11.02
16	10.02	-0.75	11.02	-0.75	60	0.75	-10.02	0.75	-11.02
17	10.02	-5.39	11.02	-5.39	61	10.02	-20.29	10.02	-21.17
18	10.02	-10.02	11.02	-10.02	62	5.39	-20.29	5.39	-21.17
19	0.75	-0.75	-0.75	-0.75	63	0.75	-20.29	0.75	-21.17
20	0.75	-5.39	-0.75	-5.39	64	-0.75	10.02	-0.75	11.02
21	0.75	-10.02	-0.75	-10.02	65	-5.39	10.02	-5.39	11.02
22	20.29	-0.75	21.17	-0.75	66	-10.02	10.02	-10.02	11.02
23	20.29	-5.39	21.17	-5.39	67	-0.75	0.75	-0.75	-0.75
24	20.29	-10.02	21.17	-10.02	68	-5.39	0.75	-5.39	-0.75
25	0.75	-11.02	-0.75	-11.02	69	-10.02	0.75	-10.02	-0.75
26	0.75	-15.66	-0.75	-15.66	70	-11.02	0.75	-11.02	-0.75
27	0.75	-20.29	-0.75	-20.29	71	-15.66	0.75	-15.66	-0.75
28	0.75	-21.17	-0.75	-21.17	72	-20.29	0.75	-20.29	-0.75
29	0.75	-25.81	-0.75	-25.81	73	-21.17	0.75	-21.17	-0.75
30	0.75	-30.44	-0.75	-30.44	74	-25.81	0.75	-25.81	-0.75
31	-10.02	10.02	-11.02	10.02	75	-30.44	0.75	-30.44	-0.75
32	-10.02	5.39	-11.02	5.39	76	-0.75	20.29	-0.75	21.17
33	-10.02	0.75	-11.02	0.75	77	-5.39	20.29	-5.39	21.17
34	-20.29	10.02	-21.17	10.02	78	-10.02	20.29	-10.02	21.17
35	-20.29	5.39	-21.17	5.39	79	-0.75	-10.02	-0.75	-11.02
36	-20.29	0.75	-21.17	0.75	80	-5.39	-10.02	-5.39	-11.02
37	-10.02	-0.75	-11.02	-0.75	81	-10.02	-10.02	-10.02	-11.02
38	-10.02	-5.39	-11.02	-5.39	82	-0.75	-20.29	-0.75	-21.17
39	-10.02	-10.02	-11.02	-10.02	83	-5.39	-20.29	-5.39	-21.17
40	-20.29	-0.75	-21.17	-0.75	84	-10.02	-20.29	-10.02	-21.17
41	-20.29	-5.39	-21.17	-5.39	85	11.02	10.02	11.52	11.52
42	-20.29	-10.02	-21.17	-10.02	86	16.16	11.52	16.16	10.02
43	10.02	10.02	10.02	11.02	87	20.29	10.02	20.79	11.52
44	5.39	10.02	5.39	11.02	88	10.02	20.29	11.52	20.79

Note: See Figure 11.2.12.4.1-7 for section location.

Table 11.2.12.4.1-4 Summary of Maximum Stresses for PWR Support Disk for Tip-Over Condition

Drop Orientation	P_m			$P_m + P_b$		
	Stress Intensity (ksi)	Allowable Stress (ksi)	Margin of Safety	Stress Intensity (ksi)	Allowable Stress (ksi)	Margin of Safety
0°	58.2	90.8	+0.56	81.9	129.8	+0.58
18.22°	47.5	90.4	+0.91	111.6	130.8	+0.17
26.28°	46.0	90.4	+0.97	124.6	130.8	+0.05
45°	34.4	91.5	+1.66	101.4	129.1	+0.27

Note: See Figure 11.2.12.4.1-1 for Drop Orientation.

Table 11.2.12.4.1-5 Summary of Buckling Evaluation of PWR Support Disk for Tip-Over Condition

Drop Orientation	MS1	MS2
0°	+0.98	+0.96
18.22°	+0.31	+0.36
26.28°	+0.10	+0.15
45°	+0.31	+0.34

Note: See Figure 11.2.12.4.1-1 for Drop Orientation.

Table 11.2.12.4.1-6 Support Disk Primary Membrane (P_m) Stresses for Tip-Over Condition - PWR Disk No. 5 - 26.28° Drop Orientation (ksi)

Section Number	Sx	Sy	Sxy	Stress Intensity	Allowable Stress	Margin of Safety
18	19.5	-26.1	3.1	46.0	90.4	0.97
3	27.1	-14.8	2.7	42.2	89.3	1.12
16	-38.3	-25.9	1	38.4	89.3	1.32
1	-33.5	-14.7	0.5	33.5	90.4	1.70
94	-28.3	-21.4	2.9	29.4	90.5	2.08
17	-0.1	-26	2	26.2	89.8	2.42
96	6.1	-16.4	-3.1	23.3	91.5	2.92
95	-0.1	-22.4	1.7	22.6	91.1	3.04
88	-18.4	-7	-7	21.7	91.5	3.21
84	-17.1	-20.7	-0.8	20.9	91.5	3.38
61	-17.8	-9.7	5.1	20.3	91.5	3.51
90	15	-5	0.6	20.1	90.5	3.51
60	-11.3	-18.4	1.1	18.6	89.3	3.80
30	-18	-10.1	3	19.0	91.9	3.83
82	-17.2	-7	4.1	18.7	90.8	3.87
62	-17.8	-0.2	2.6	18.4	91.2	3.97
58	-11.4	-13.8	5.4	18.2	90.4	3.97
91	-8.2	-17.5	-1.4	17.7	90.5	4.11
63	-17.8	-12.3	0.2	17.8	90.8	4.11
83	-17.2	-0.2	1.7	17.3	91.2	4.26
7	-16.5	-12.6	-0.8	16.7	91.5	4.49
24	-1.2	-15.8	2	16.1	91.5	4.69
28	-15.4	-10	1.6	15.8	90.9	4.74
23	-0.1	-15.8	0.8	15.8	91.2	4.78
22	-9.1	-15.7	-0.5	15.7	90.8	4.78
51	-3.6	-15.1	-2	15.4	89.4	4.79
37	11.1	-4.3	0.6	15.4	89.3	4.80
79	-6	6.5	4.5	15.4	89.3	4.82
2	-0.1	-14.7	1.6	15.0	89.8	5.00
85	-4.6	-11.2	-6.4	15.1	90.5	5.00

Note: See Figure 11.2.12.4.1-2 for disk location and Figure 11.2.12.4.1-7 for section locations.

Table 11.2.12.4.1-7 Support Disk Primary Membrane + Primary Bending ($P_m + P_b$) Stresses for Tip-Over Condition - PWR Disk No. 5 - 26.28° Drop Orientation (ksi)

Section Number	Sx	Sy	Sxy	Stress Intensity	Allowable Stress	Margin of Safety
61	-123.4	-34.3	10.4	124.6	130.8	0.05
58	-115.3	-47.4	9.6	116.6	129.1	0.11
43	-95.4	-34.6	6.8	96.1	129.1	0.34
82	-92.1	-27.8	7.2	92.9	129.8	0.40
79	-86.9	-19.9	2.3	87.0	127.6	0.47
16	-54.3	-76.8	15.6	84.8	127.6	0.50
60	-82.9	-41	7.8	84.3	127.6	0.51
18	-4.1	-84.9	-2.5	85.0	129.1	0.52
46	-79.1	-52.5	10.4	82.7	127.6	0.54
55	-84.2	-31.4	5	84.7	130.8	0.54
3	9.1	-71.1	-5.7	81.0	127.6	0.57
64	-79.8	-32.4	7.2	80.9	127.6	0.58
30	-40.2	-74.7	11.7	78.3	131.3	0.68
63	-75.2	-27.9	4.9	75.7	129.8	0.71
76	72.6	21.9	5.2	73.1	129.8	0.77
48	-66.5	-43.2	3.9	67.1	125.7	0.87
19	-39.5	-66.4	2.9	66.7	125.7	0.88
6	-43.6	-63.2	5.2	64.5	125.7	0.95
94	-59.5	-44.7	11.1	65.5	129.3	0.97
21	-48.3	-59.4	5.2	61.5	127.6	1.08
45	-61.2	-14.4	-0.6	61.2	127.6	1.09
67	-56.6	-43.3	5.4	58.6	125.7	1.15
1	-49.4	-43.6	13.2	60.0	129.1	1.15
51	26.3	-30.4	4.7	57.5	127.7	1.22
33	-29.3	-54.9	7.1	56.7	127.6	1.25
39	-29.2	-52.9	6.2	54.5	129.1	1.37
24	-8.5	-52.1	4.1	52.5	130.8	1.49
81	-49.2	-30.8	5.5	50.7	129.1	1.55
4	-43.3	-43.7	5.8	49.3	127.6	1.59
28	-46.3	-28.1	9.2	50.1	129.9	1.59

Note: See Figure 11.2.12.4.1-2 for disk location and Figure 11.2.12.4.1-7 for section locations.

Table 11.2.12.4.1-8 Summary of Support Disk Buckling Evaluation for Tip-Over Condition - PWR Disk No. 5 - 26.28° Drop Orientation

Section Number	P (kip)	Pcr (kip)	Py (kip)	M (in-kip)	Mp (in-kip)	Mm (in-kip)	MS1	MS2
61	7.80	44.18	38.91	6.74	8.51	8.18	0.10	0.15
58	5.69	51.79	43.78	8.66	10.94	10.67	0.23	0.25
82	7.52	43.76	38.54	4.78	8.43	8.10	0.44	0.48
18	13.04	51.79	43.78	4.90	10.94	10.67	0.51	0.48
43	1.95	51.79	43.78	7.62	10.94	10.67	0.54	0.58
16	12.97	50.82	42.93	4.24	10.73	10.47	0.62	0.57
79	3.00	50.82	42.93	6.74	10.73	10.47	0.63	0.66
60	5.66	50.82	42.93	5.96	10.73	10.47	0.65	0.66
63	7.78	43.76	38.54	3.66	8.43	8.10	0.73	0.75
55	0.92	44.18	38.91	5.24	8.51	8.18	0.76	0.83
64	2.18	50.82	42.93	6.29	10.73	10.47	0.79	0.83
3	7.40	50.82	42.93	4.69	10.73	10.47	0.86	0.84
46	1.85	83.64	64.39	14.37	24.15	24.15	0.89	0.88
30	7.60	87.05	67.05	12.10	25.14	25.14	1.00	0.92
19	3.78	81.50	62.70	11.51	23.51	23.51	1.15	1.10
48	1.80	81.50	62.70	12.01	23.51	23.51	1.19	1.17
6	2.46	81.50	62.70	11.23	23.51	23.51	1.29	1.25
45	1.91	50.82	42.93	4.78	10.73	10.47	1.34	1.37
21	3.89	83.64	64.39	10.16	24.15	24.15	1.47	1.40
24	6.92	44.18	38.91	2.31	8.51	8.18	1.46	1.45
67	1.00	81.50	62.70	10.37	23.51	23.51	1.58	1.57
33	1.95	50.82	42.93	4.25	10.73	10.47	1.59	1.63
84	7.49	44.18	38.91	1.82	8.51	8.18	1.73	1.67
39	2.19	51.79	43.78	4.04	10.94	10.67	1.72	1.75
17	13.00	51.32	43.37	0.79	10.84	10.58	2.13	1.77
1	7.33	51.79	43.78	2.41	10.94	10.67	1.95	1.82
81	2.97	51.79	43.78	3.61	10.94	10.67	1.88	1.88
37	2.13	50.82	42.93	3.24	10.73	10.47	2.26	2.27
4	2.35	83.64	64.39	7.60	24.15	24.15	2.37	2.30
66	2.15	51.79	43.78	3.25	10.94	10.67	2.31	2.33

Note: See Figure 11.2.12.4.1-2 for disk location and Figure 11.2.12.4.1-7 for section locations.

11.2.12.4.2 Analysis of Canister and Basket for BWR Configurations

Five three-dimensional models of the BWR canister and fuel basket are evaluated for the cask tip-over event. Each model corresponds to a different fuel basket drop orientation. For the BWR fuel configuration, fuel basket drop orientations of 0°, 31.82°, 49.46°, 77.92°, and 90° are evaluated, as shown in Figure 11.2.12.4.2-1. Three-dimensional half-symmetry models are used for the basket drop orientations of 0° and 90°. Three-dimensional full-models are used for the basket orientations of 31.82°, 49.46° and 77.92°.

Model Description

The models used for the evaluation of the canister and basket for BWR configuration are similar to those used for the PWR (Section 11.2.12.4.1). The three-dimensional model used for the basket drop orientation of 31.82° is presented in Figure 11.2.12.4.2-2 and Figure 11.2.12.4.2-3.

The same modeling and analysis techniques described for the PWR model (see Section 11.2.12.4.1) are used for the BWR models.

For the inertial loads, a maximum acceleration of 30g is conservatively applied to the entire model. As shown in Section 11.2.12.3.2, the maximum acceleration of the concrete cask steel liner at the locations of the top support disk and the top of the canister structural lid during the tip-over event is determined to be 25.3g and 29.1g, respectively. Using the same method described in Section 11.2.12.4.1 for the PWR models, the DLF for the acceleration at the top support disk is computed to be 1.04. Applying the DLF to the 25.3g results in a peak acceleration of 26.4g for the top support disk.

The dominant resonance frequencies and corresponding modal mass participation factors from the finite element modal analyses of the BWR support disk are:

Frequency (Hz)	% Modal Mass Participation Factor
79.3	38.4
80.2	54.9
210.9	3.4

The mode shapes for these frequencies are shown in Figures 11.2.12.4.2-5 through 11.2.12.4.2-7. The displacement depicted in these figures is highly exaggerated by the ANSYS program in order

to illustrate the modal shape. The stresses associated with the actual displacement are shown in Tables 11.2.12.4.2-4 through 11.2.12.4.2-8.

The DLFs for the canister lids are considered to be unity since the lids have significant in-plane stiffness and are considered to be rigid. Therefore, applying 30g to the entire canister/basket model is conservative.

A uniform temperature of 75°F is applied to the model to determine material properties during solution. During post processing for the support disk, temperature distribution with a maximum temperature of 700°F (at the center) and a minimum temperature of 400°F (at the outer edge) are conservatively used to determine the allowable stresses. A constant temperature of 500° is used for the canister to determine the allowable stresses. These temperatures are the bounding temperatures for the normal, off-normal and accident conditions of storage.

Analysis Results for Canister

The sectional stresses at 13 axial locations of the canister are obtained for each angular division of the model (a total of 80 angular locations for the full-models and a total of 41 angular locations for the half-symmetry models). The locations for the stress sections are shown in Figure 11.2.12.4.1-6.

The same stress allowables used in the evaluation of the PWR canister (see Section 11.2.12.4.1) are used in evaluating the BWR canister.

The primary membrane and primary membrane plus bending stresses for the BWR configuration for a 49.46° basket drop orientation are summarized in Table 11.2.12.4.2-1 and Table 11.2.12.4.2-2, respectively. The stress results of the canister are similar for all five models. Only the 49.46° basket drop orientation results are presented for the canister because this drop orientation generates the minimum margin of safety in the canister. The stress evaluation results for tip-over accident conditions show that the minimum margin of safety in the canister for BWR configurations is +0.35 for P_m (Section 10) and +0.46 for P_m+P_b (Section 10).

Analysis Results for Support Disks

To evaluate the most critical regions of the support disk, a series of cross sections are considered. To aid in the identification of these sections, Figure 11.2.12.4.2-4 shows the locations on a support disk for the full-models. Table 11.2.12.4.2-3 lists the cross-sections with their end point locations

(Point 1 and Point 2), which spans the cross section of the ligament in the plane of the support disk. Note that a local coordinate system (x and y parallel to the support disk ligaments) is used for the stress evaluation.

The stress evaluation for the support disk is performed according to ASME Code, Section III, Subsection NG. The allowable stresses for each section are determined based on the temperature of the support disk at the section location. The temperature distribution of the disk is determined by a thermal conduction solution for a single disk with a temperature of 700°F specified at the center of the disk and a temperature of 400°F specified at the outer edge of the disk as boundary conditions. These temperatures are bounding temperatures for the normal, off-normal and accident conditions of storage.

The highest stress occurs at the 5th support disk. The stress evaluation results for the 5th support disk are summarized in Table 11.2.12.4.2-4 for the five basket drop orientations evaluated. As shown in Table 11.2.12.4.2-4, the 77.92° drop orientation case generates the minimum margin of safety in the support disk; therefore, the P_m and $P_m + P_b$ stress intensities for the 77.92° basket drop orientation case are presented in Table 11.2.12.4.2-6 and Table 11.2.12.4.2-7, respectively. These tables list the stresses with the 30 lowest margins of safety for the 5th support disk. The highest P_m stress occurs at Section 202, with a margin of safety of +0.33 (See Table 11.2.12.4.2-6 for stresses and Figure 11.2.12.4.2-4 for section locations). The highest P_m+P_b stress occurs at Section 169, with a margin of safety of +0.04 (see Table 11.2.12.4.2-7 for stresses and Figure 11.2.12.4.2-4 for section locations).

Support Disk Buckling Evaluation

The support disk buckling evaluation for the BWR support disks is performed using the same method as that presented for the PWR support disks (see Section 11.2.12.4.1). The support disk buckling evaluation results for the 5th support disk (the 5th support disk experiences the highest stresses) for the tip-over impact condition are summarized in Table 11.2.12.4.2-5 for the five basket drop orientations evaluated. As shown in Table 11.2.12.4.2-5, the 77.92° drop orientation case generates the minimum margin of safety for buckling; therefore, the results of the buckling analysis for the 77.92° basket drop orientation case are presented in Table 11.2.12.4.2-8. This table presents the results for 30 minimum margins of safety for this drop orientation. As the tables demonstrate, the support disks meet the requirements of NUREG/CR-6322.

Fuel Tube Analysis

The fuel tube provides structural support and a mounting location for BORAL neutron poison plates. The fuel tube does not provide structural support for the fuel assembly. To ensure that the fuel tube remains functional during a tip-over accident, a structural evaluation of the tube is performed for a side impact assuming a deceleration of 60g. This g-load bounds the maximum g-load (30g) calculated to occur for the BWR basket in a vertical concrete cask tipover event.

In the tipover event, the stainless steel support disks in the fuel basket support the fuel tube. The fuel basket support disks, which support the full length of the fuel tube, are spaced 3.205-inches apart (which is slightly more than one half of the fuel tube width of 5.9 inch). Considering the fuel tube subjected to a maximum BWR fuel assembly weight of 700 pounds with a 60g load factor and the 40 support locations provided by the basket support disks, the fuel tube shear stress is calculated as:

Shear load = (60g)(700)/40 = 1,050 lbs
Area = (0.048)(5.9)(2) = 0.566 in^2
Shear Stress = 1,050/0.566 = 1,855 psi

The yield strength of the tube material, Type 304 stainless steel, is 17,300 psi at 750°F. Conservatively using the allowable shear stress as one- half the yield strength of the tube material (8,650 psi) results in a large positive margin of safety. Conservative evaluation of the tube loading resulting from its own mass during a side impact shows that the tube structure maintains position and function.

The load transfer of the fuel assembly to the weight of the fuel basket support disk in the side impact is through direct bearing and compression of the distributed load of the fuel assembly through the fuel tube to the support disk web. Two load conditions are considered in the fuel tube evaluation. The first considers the fuel assembly load as a distributed pressure on the inside surface of the fuel tube. The second postulates that the fuel assembly grid is located at the center of the span between the support disks and produces a localized distributed load over the effective area of the grid.

Two different ANSYS finite element models of the tube are developed for these two load conditions since the fuel assembly structural performance for either load is nonlinear. As shown below, the first model represents a fuel tube section with a length of three spans, i.e., the model is

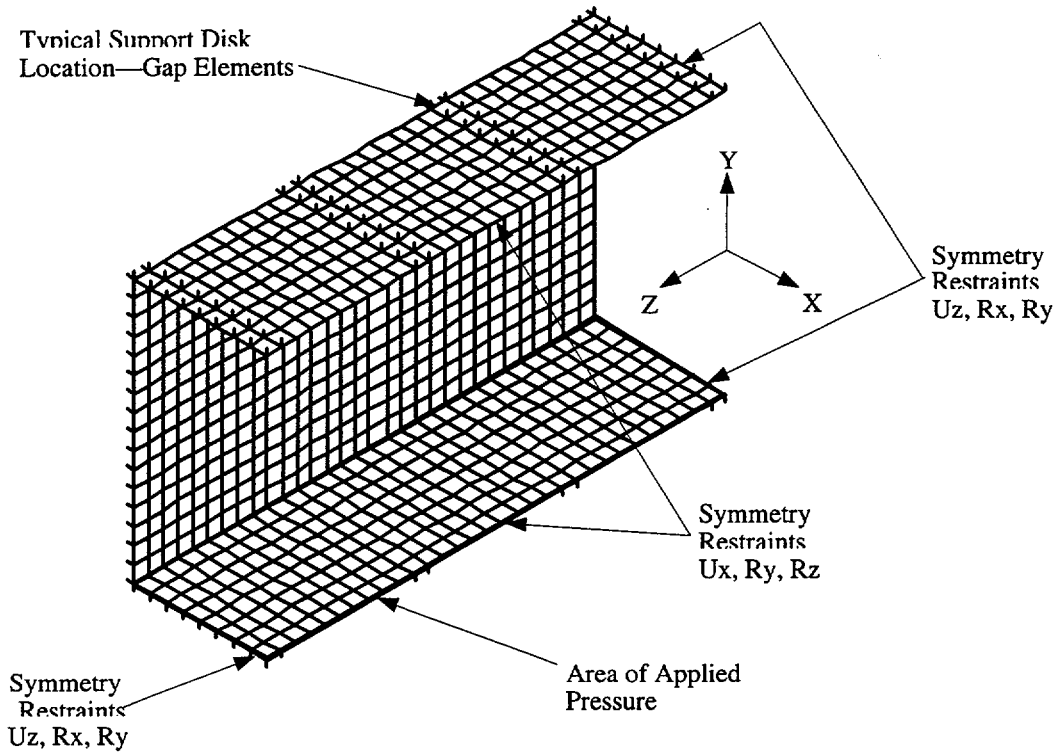

supported at four locations by support disks. The model conservatively considers the fuel tube wall thickness of 0.048 inch as the only material subjected to a distributed pressure load representative of the fuel assembly deceleration of 60g. Fuel assembly stiffness is not considered in the development of the imposed pressure load on the fuel tube.

The fuel tube is modeled with the ANSYS plastic, quadrilateral shell element (SHELL43). The support disks are represented as rigid gap elements (CONTAC52). The outer nodes of the gap elements are fully restrained in all three translational directions. Edge restraints were applied to the model to represent symmetry boundary conditions. The effective load on the fuel tube due to the 60g deceleration of the assembly is applied as a pressure to the inside area of the fuel tube.

The finite element analysis results show that the maximum stress in the tube is 19.5 ksi, which is local to the sections of the tube resting on the support disks. At 750°F the ultimate strength for Type 304 stainless steel is 63.1 ksi. The margin of safety is

$$MS = \frac{63.1}{19.5} - 1 = +2.24$$

The analysis shows that the maximum total strain is 0.0078 inch/inch. Defining the acceptable elastic-plastic response of the stainless steel as one half of the material failure strain of 0.40 in./in. at 750°F [42], the resulting margin of safety is:

$$MS = \frac{0.40/2}{0.0078} - 1 = +\text{Large}$$

Similarly, the margin of safety for elastic-plastic stress becomes

$$MS = \frac{63.1 - 17.3}{19.5 - 17.3} - 1 = +\text{Large}$$

where the yield strength of Type 304 stainless steel is 17.3 ksi at 750°F.

The second finite element model is used to evaluate the load condition with the fuel assembly grid located at the center of the span between two support disks. The fuel tube is subjected to a localized distributed load over the effective area of the grid. As shown below, the model is a quarter-symmetry periodic section of the fuel tube. As in the finite element model used for the distributed pressure case, this model conservatively considers a fuel tube wall thickness of 0.048 inch. The BORAL plate (0.135 inch) and stainless steel cover plate (0.018 inch) are conservatively not included in the model. The tube wall is modeled with ANSYS SHELL43 elements. The support disks are modeled with CONTAC52 elements. A uniform pressure corresponding to the fuel assembly weight with the 60g load is applied to the elements at the grid location of the model. The displacement in the Y direction for the nodes at the grid location of the model are coupled to represent the structural rigidity of the spacer grid.

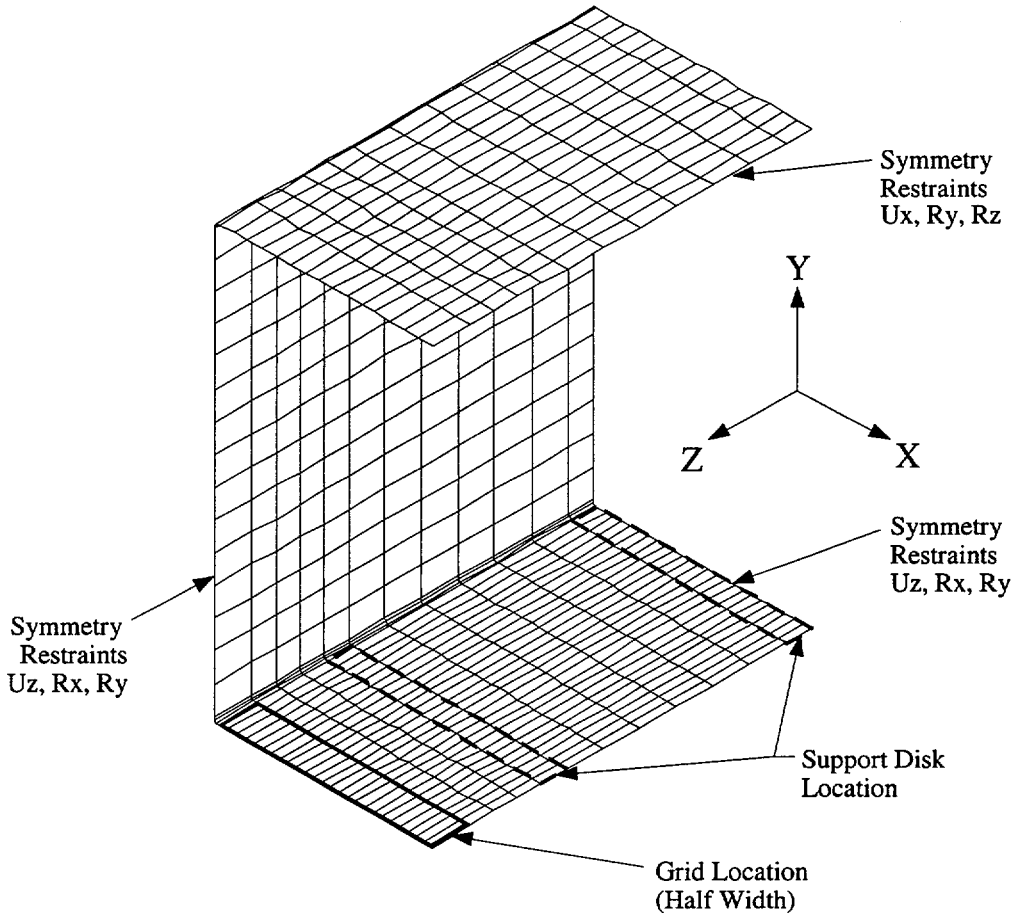

The finite element analysis results show that the maximum stress in the tube is 38.1 ksi. At 750°F the ultimate strength for Type 304 stainless steel is 63.1 ksi. The margin of safety is

$$MS = \frac{63.1}{38.1} - 1 = +0.66$$

The analysis shows that the maximum total strain is 0.10 inch/inch. Defining the acceptable elastic-plastic response of the stainless steel as one half of the material failure strain of 0.40 in./in. at 750°F [42], the resulting margin of safety is:

$$MS = \frac{0.40/2}{0.10} - 1 = +1.0$$

Similarly, the margin of safety for elastic-plastic stress becomes

$$MS = \frac{63.1 - 17.3}{38.1 - 17.3} - 1 = +1.2$$

where the yield strength of Type 304 stainless steel is 17.3 ksi at 750°F.

Both the maximum total strain and the elastic-plastic stress analyses indicate that the tube position within the support basket is maintained.

Assurance that the BORAL remains attached to the fuel tube is evaluated by considering that loads produced by the BORAL plate and stainless steel attachment plate, assuming a 60g load, are carried by the attachment plate weld. Total load and resultant stress on the weld are calculated as:

$F_{b/ss} = (g)(\rho)(t)(w)(l)$ Load exerted by BORAL/Stainless Steel Attachment Plate

where:

- g = acceleration (g)
- ρ = density of material (lb/in^3) (The density of aluminum (0.098 lb/in^3) is conservatively used for the BORAL.
- t = thickness of material (in.)
- w = width of material (in.)
- l = length of material section (in.)

The forces on the weld due to a 12-inch section of BORAL (F_b) and a 12-inch section of stainless steel plate (F_{ss}) are:

$$F_b = (60g)(0.098 \text{ lb/in}^3)(0.135 \text{ in})(5.45 \text{ in})(12 \text{ in}) = 51.9 \text{ lbs}$$

$$F_{ss} = (60g)(0.291 \text{ lb/in}^3)(0.018 \text{ in})(5.79 \text{ in})(12 \text{ in}) = 21.8 \text{ lbs}$$

The total load (F_t) on a 1-inch attachment for a 12-inch section is:

$$F_t = 57.9 \text{ lbs} + 21.8 \text{ lbs} = 73.7 \text{ lbs}$$

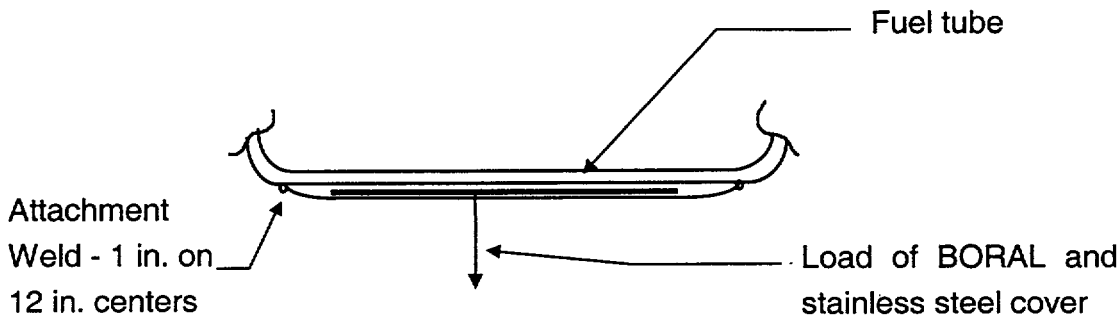

The resulting weld stress is: $\sigma = P/A = (73.7 \text{ lbs}/2) / (1 \text{ in})(0.018 \text{ in}) = 2{,}074$ psi

Since the weld material is Type 304 stainless steel, the margin of safety (at 750°F) is:

$$MS = \frac{17{,}300}{2{,}047} - 1 = +7.5$$

Therefore, the BORAL remains enclosed on each outer surface of the fuel tube wall.

Figure 11.2.12.4.2-1 Fuel Basket Drop Orientations Analyzed for Tip-Over Condition - BWR

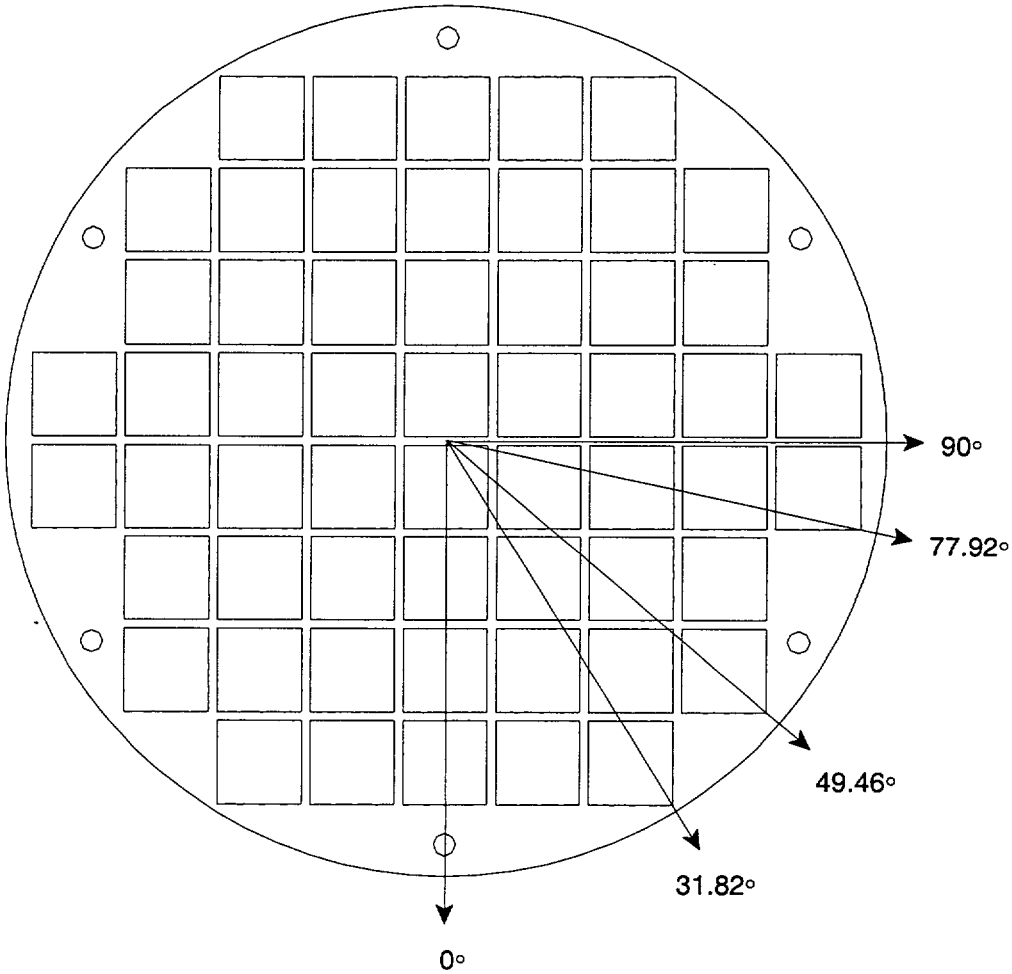

Figure 11.2.12.4.2-2 Fuel Basket/Canister Finite Element Model - BWR

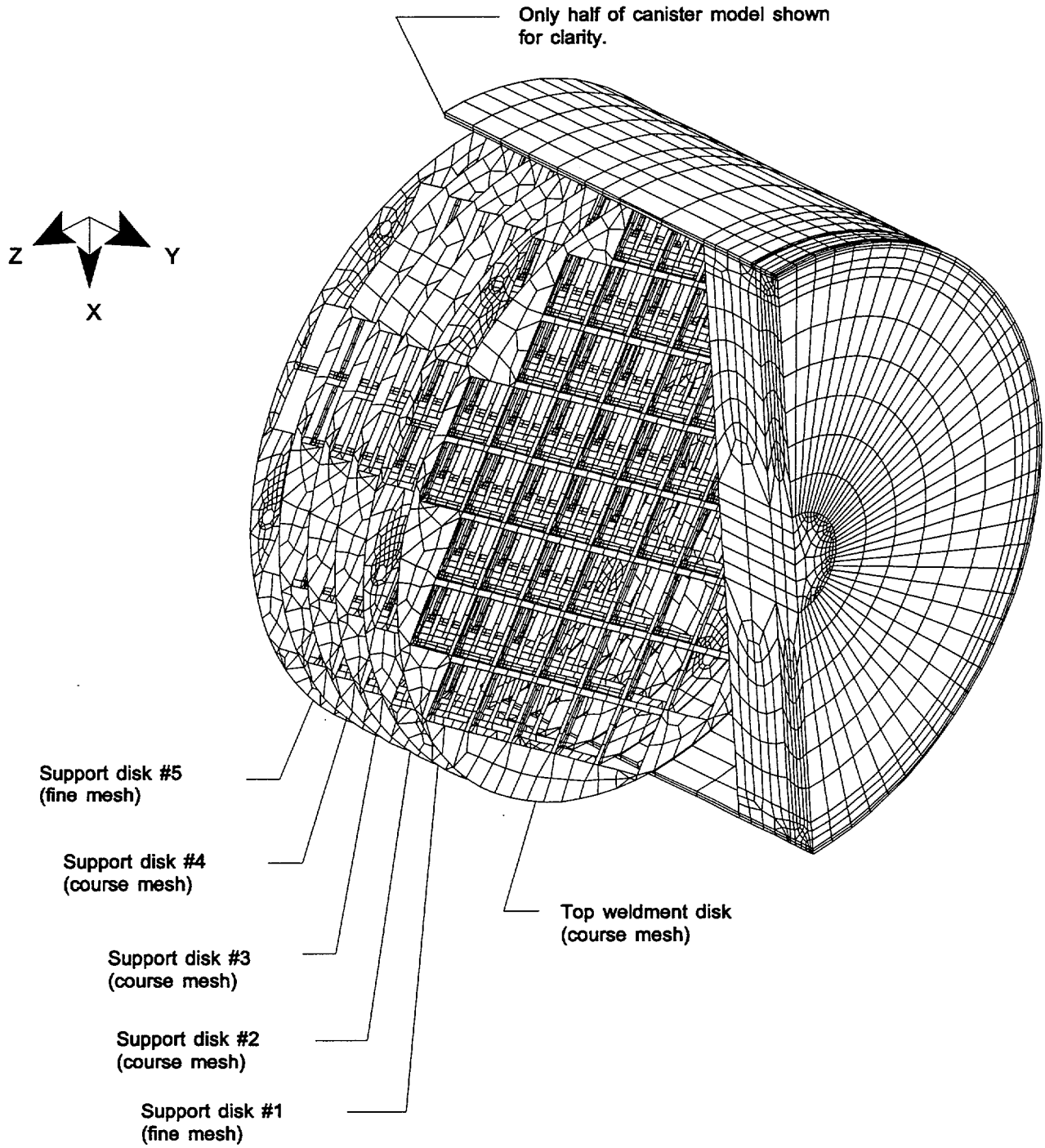

31.82° Basket Drop Orientation

Figure 11.2.12.4.2-3 Fuel Basket/Canister Finite Element Model - Support Disk - BWR

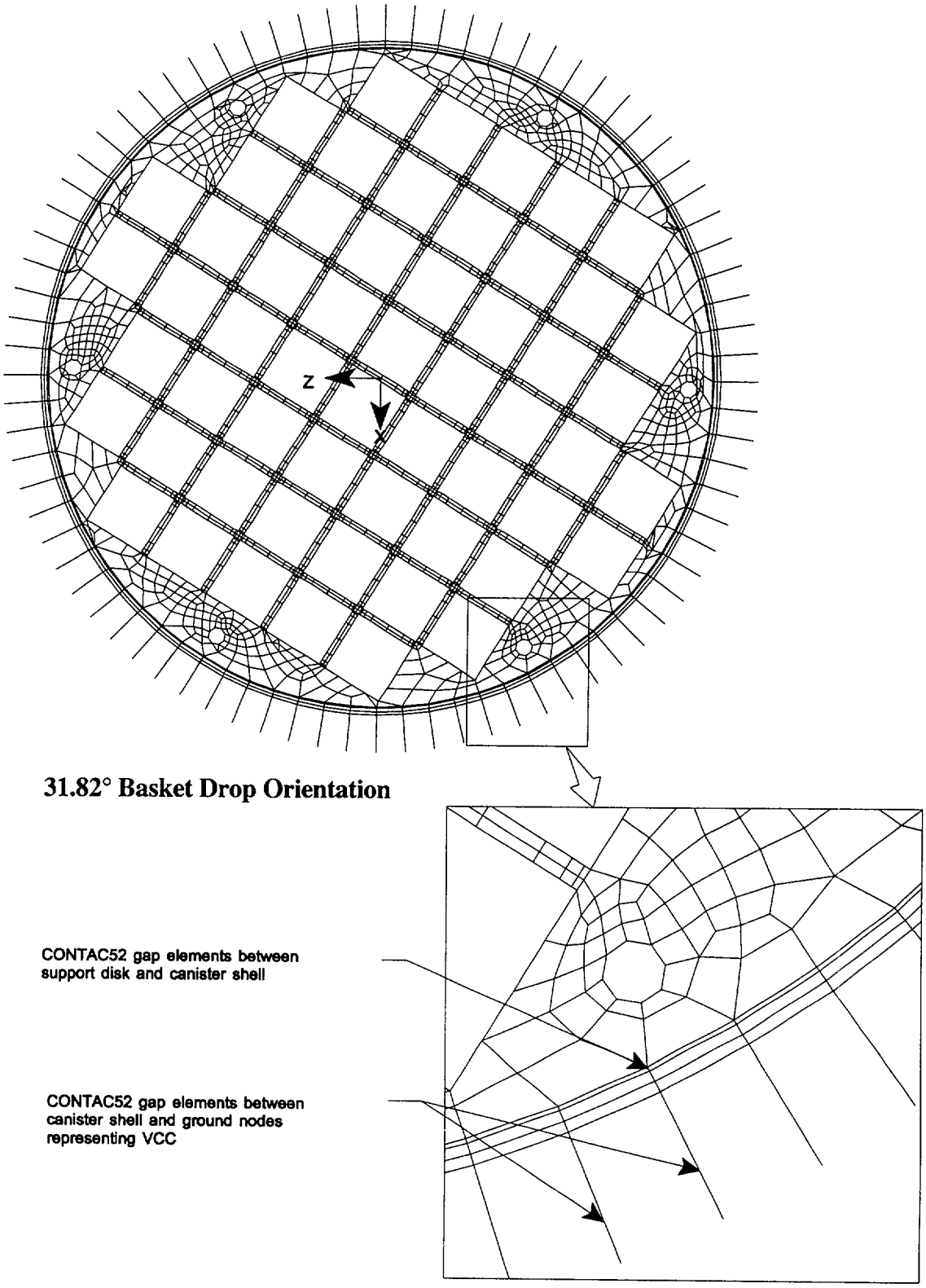

Figure 11.2.12.4.2-4 Support Disk Section Stress Locations - BWR - Full Model

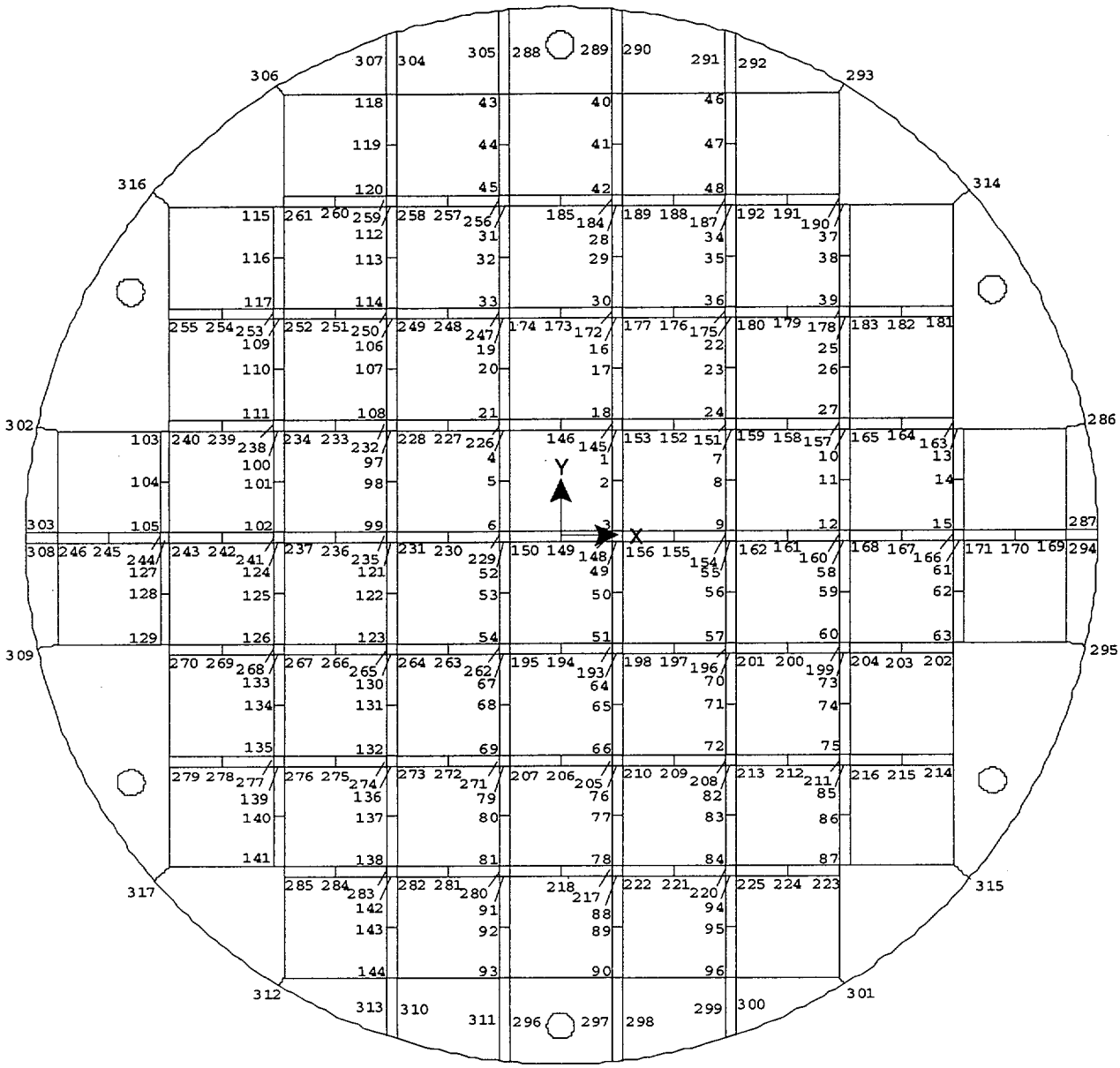

Figure 11.2.12.4.2-5 BWR – 79.3 Hz Mode Shape

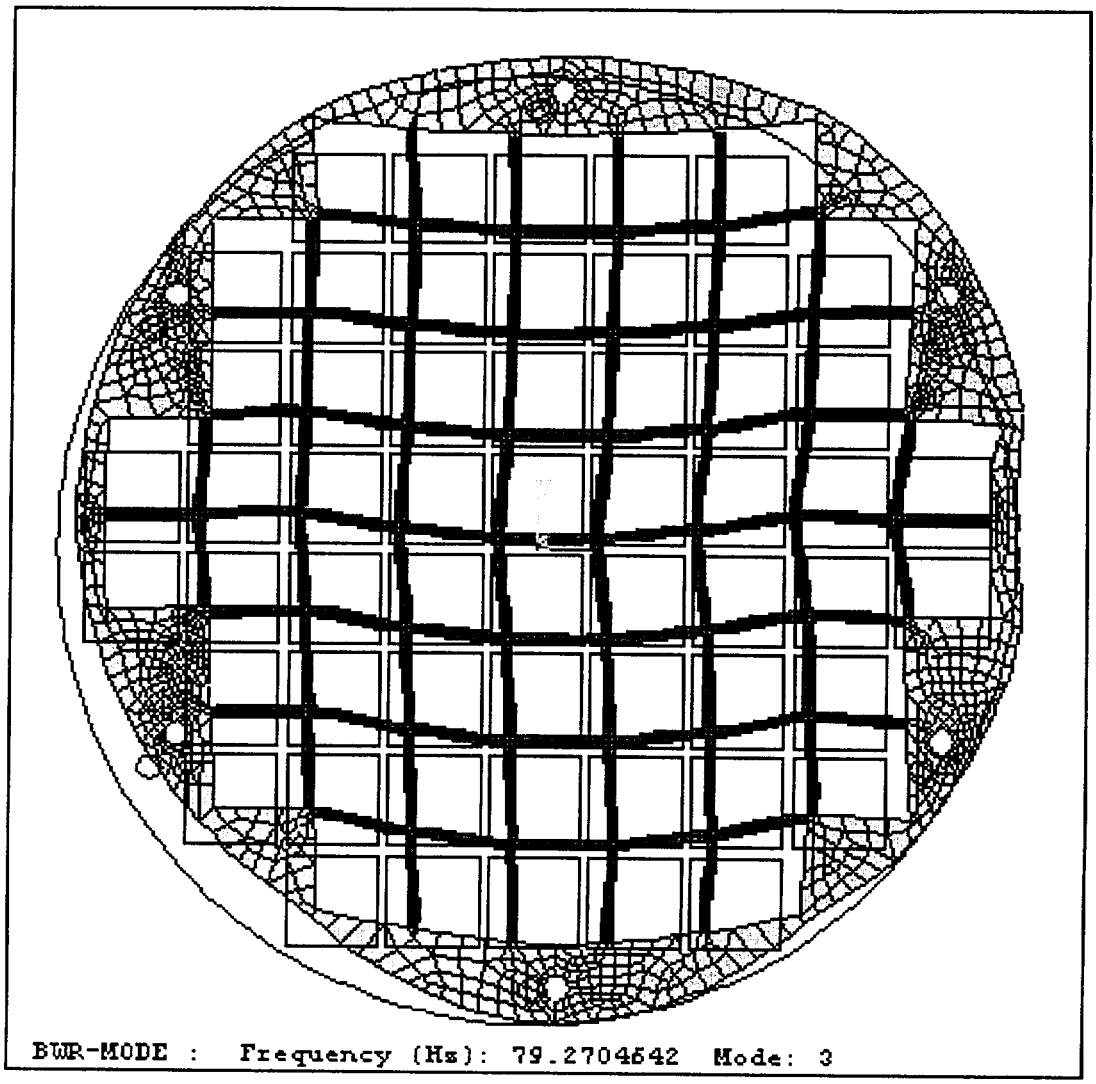

Note: Displacements are greatly exaggerated by the ANSYS program to illustrate the mode shapes.

Figure 11.2.12.4.2-6 BWR – 80.2 Hz Mode Shape

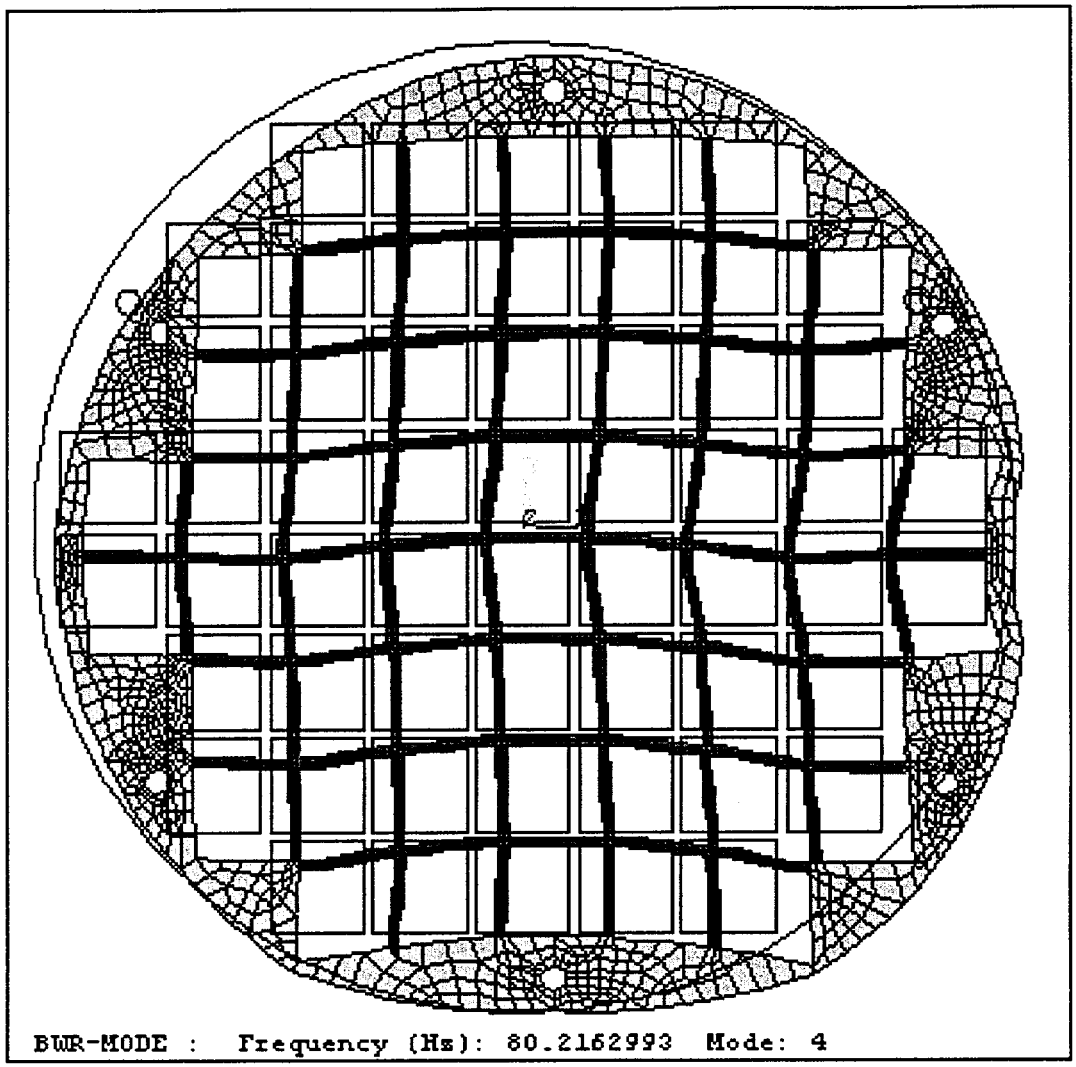

Note: Displacements are greatly exaggerated by the ANSYS program to illustrate the mode shapes.

Figure 11.2.12.4.2-7 BWR – 210.9 Hz Mode Shape

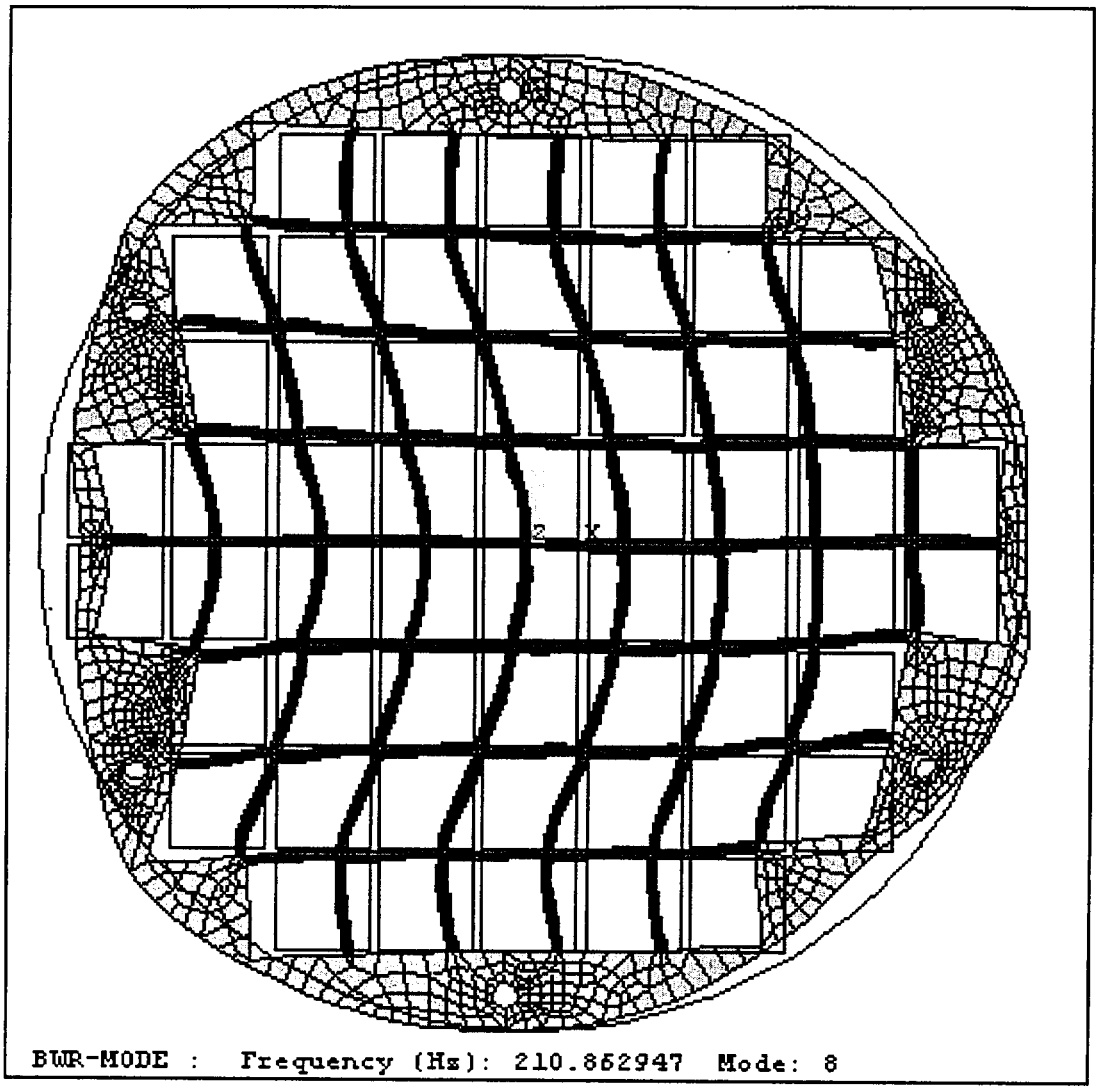

Note: Displacements are greatly exaggerated by the ANSYS program to illustrate the mode shapes.

Table 11.2.12.4.2-1 Canister Primary Membrane (P_m) Stresses for Tip-Over Conditions - BWR - 49.46° Basket Drop Orientation (ksi)

Section Location[1]	Section Angle (deg)	Sx	Sy	Sz	Sxy	Syz	Sxz	Stress Intensity	Allowable Stress	Margin of Safety
1	0	-1.2	6.2	1.4	-0.1	-0.1	0.0	7.46	35.52	3.76
2	0	-1.6	8.2	1.4	0.0	-0.2	0.1	9.77	35.52	2.63
3	0	-1.5	7.9	1.4	0.0	-0.2	-0.1	9.41	35.52	2.78
4	90	-0.1	3.0	-2.1	-0.2	3.7	0.1	8.92	35.52	2.98
5	85.5	0.0	2.8	-1.0	-0.2	4.8	-0.1	10.29	35.52	2.45
6	76.5	0.0	0.3	-0.4	0.0	6.0	0.0	12.09	35.52	1.94
7[2]	9.0	0.6	0.3	4.8	1.6	-3.8	-0.2	9.60	35.52	2.70
8[2]	351.0	4.5	0.1	5.2	-0.1	2.3	-0.6	7.06	35.52	4.03
9[2]	351.0	4.5	-1.0	1.5	-1.6	2.8	-0.2	8.17	35.52	3.35
10	0	-38.6	-16.2	-30.4	0.5	0.0	-10.7	29.74	40.08[3]	0.35
11[4]	351.9 – 8.2	-22.1	-9.9	-6.7	-0.1	0.0	1.1	15.51	32.06[4]	1.07
12	0	-0.6	0.2	0.0	0.0	0.0	-0.3	0.92	35.52	37.66
13	0	-1.0	0.3	0.0	0.0	0.0	-0.4	1.46	35.52	23.31

Stresses are presented in the cylindrical coordinate system, x = radial, y = circumferential and z = axial directions.

1. Section locations are shown in Figure 11.2.12.4.1-6.
2. Stresses are not presented for the sections with localized bearing stress. In accordance with ASME Section III, Appendix F, bearing stresses need not be evaluated for Level D service (accident) conditions.
3. Allowable stress at 300°F.
4. Stresses are determined by averaging the stresses over the impact region. A stress reduction factor of 0.8 is applied to the allowable stress at 250°F.

Table 11.2.12.4.2-2 Canister Primary Membrane + Primary Bending ($P_m + P_b$) Stresses for Tip-Over Conditions - BWR - 49.46° Basket Drop Orientation (ksi)

Section Location[1]	Section Angle (deg)	Sx	Sy	Sz	Sxy	Syz	Sxz	Stress Intensity	Allowable Stress	Margin of Safety
1	0.0	-1.6	18.5	4.6	-0.2	-0.4	0.1	20.13	53.28	1.65
2	0.0	-1.8	20.2	2.7	0.0	-0.4	0.1	22.01	53.28	1.42
3	0.0	-2.3	20.6	4.8	-0.1	-0.3	-0.1	22.92	53.28	1.32
4	0.0	-1.8	20.2	3.9	-0.2	-0.4	-0.1	22.00	53.28	1.42
5	0.0	-2.2	19.7	6.4	-0.1	-0.6	0.1	21.94	53.28	1.43
6	0.0	0.0	-21.0	-3.8	0.0	-0.7	-0.7	21.21	53.28	1.51
7[2]	351.0	0.1	6.4	17.2	0.2	2.3	0.2	17.50	53.28	2.04
8[2]	351.0	3.3	5.2	13.5	0.7	3.6	-2.1	13.02	53.28	3.09
9[2]	351.0	5.9	-3.0	3.6	-3.0	3.2	-0.6	12.44	53.28	3.28
10	0.0	-42.9	-15.8	-27.8	0.4	0.3	-19.1	41.17	60.12[3]	0.46
11[4]	351.9 – 8.1	-18.8	-7.2	-1.7	-0.1	0.0	2.6	17.86	48.09[4]	1.69
12	0.0	-0.9	0.1	-0.1	0.0	0.0	-0.5	1.37	53.28	37.81
13	0.0	-1.1	0.4	0.0	0.0	0.0	-0.1	1.56	53.28	33.07

Stresses are presented in the cylindrical coordinate system, x = radial, y = circumferential and z = axial directions.

1. Section locations are shown in Figure 11.2.12.4.1-6.
2. Stresses are not presented for the sections with localized bearing stress. In accordance with ASME Section III, Appendix F, bearing stresses need not be evaluated for Level D service (accident) conditions.
3. Allowable stress at 300°F.
4. Stresses are determined by averaging the stresses over the impact region. A stress reduction factor of 0.8 is applied to the allowable stress at 250°F.

Table 11.2.12.4.2-3 Support Disk Section Locations for Stress Evaluation - BWR - Full Model

Section[1]	Point 1		Point 2		Section[1]	Point 1		Point 2	
	X	Y	X	Y		X	Y	X	Y
1	3.14	6.6	3.79	6.6	44	-3.14	24.25	-3.79	24.25
2	3.14	3.46	3.79	3.46	45	-3.14	21.11	-3.79	21.11
3	3.14	0.33	3.79	0.33	46	10.07	27.39	10.72	27.39
4	-3.14	6.6	-3.79	6.6	47	10.07	24.25	10.72	24.25
5	-3.14	3.46	-3.79	3.46	48	10.07	21.11	10.72	21.11
6	-3.14	0.33	-3.79	0.33	49	3.14	-0.33	3.79	-0.33
7	10.07	6.6	10.72	6.6	50	3.14	-3.46	3.79	-3.46
8	10.07	3.46	10.72	3.46	51	3.14	-6.6	3.79	-6.6
9	10.07	0.33	10.72	0.33	52	-3.14	-0.33	-3.79	-0.33
10	17	6.6	17.65	6.6	53	-3.14	-3.46	-3.79	-3.46
11	17	3.46	17.65	3.46	54	-3.14	-6.6	-3.79	-6.6
12	17	0.33	17.65	0.33	55	10.07	-0.33	10.72	-0.33
13	23.92	6.6	24.57	6.6	56	10.07	-3.46	10.72	-3.46
14	23.92	3.46	24.57	3.46	57	10.07	-6.6	10.72	-6.6
15	23.92	0.33	24.57	0.33	58	17	-0.33	17.65	-0.33
16	3.14	13.53	3.79	13.53	59	17	-3.46	17.65	-3.46
17	3.14	10.39	3.79	10.39	60	17	-6.6	17.65	-6.6
18	3.14	7.25	3.79	7.25	61	23.92	-0.33	24.57	-0.33
19	-3.14	13.53	-3.79	13.53	62	23.92	-3.46	24.57	-3.46
20	-3.14	10.39	-3.79	10.39	63	23.92	-6.6	24.57	-6.6
21	-3.14	7.25	-3.79	7.25	64	3.14	-7.25	3.79	-7.25
22	10.07	13.53	10.72	13.53	65	3.14	-10.39	3.79	-10.39
23	10.07	10.39	10.72	10.39	66	3.14	-13.53	3.79	-13.53
24	10.07	7.25	10.72	7.25	67	-3.14	-7.25	-3.79	-7.25
25	17	13.53	17.65	13.53	68	-3.14	-10.39	-3.79	-10.39
26	17	10.39	17.65	10.39	69	-3.14	-13.53	-3.79	-13.53
27	17	7.25	17.65	7.25	70	10.07	-7.25	10.72	-7.25
28	3.14	20.46	3.79	20.46	71	10.07	-10.39	10.72	-10.39
29	3.14	17.32	3.79	17.32	72	10.07	-13.53	10.72	-13.53
30	3.14	14.18	3.79	14.18	73	17	-7.25	17.65	-7.25
31	-3.14	20.46	-3.79	20.46	74	17	-10.39	17.65	-10.39
32	-3.14	17.32	-3.79	17.32	75	17	-13.53	17.65	-13.53
33	-3.14	14.18	-3.79	14.18	76	3.14	-14.18	3.79	-14.18
34	10.07	20.46	10.72	20.46	77	3.14	-17.32	3.79	-17.32
35	10.07	17.32	10.72	17.32	78	3.14	-20.46	3.79	-20.46
36	10.07	14.18	10.72	14.18	79	-3.14	-14.18	-3.79	-14.18
37	17	20.46	17.65	20.46	80	-3.14	-17.32	-3.79	-17.32
38	17	17.32	17.65	17.32	81	-3.14	-20.46	-3.79	-20.46
39	17	14.18	17.65	14.18	82	10.07	-14.18	10.72	-14.18
40	3.14	27.39	3.79	27.39	83	10.07	-17.32	10.72	-17.32
41	3.14	24.25	3.79	24.25	84	10.07	-20.46	10.72	-20.46
42	3.14	21.11	3.79	21.11	85	17	-14.18	17.65	-14.18
43	-3.14	27.39	-3.79	27.39	86	17	-17.32	17.65	-17.32

1. See Figure 11.2.12.4.2-4 for section locations.

Table 11.2.12.4.2-3 Support Disk Section Locations for Stress Evaluation - BWR - Full Model (Continued)

Section[1]	Point 1		Point 2		Section[1]	Point 1		Point 2	
	X	Y	X	Y		X	Y	X	Y
87	17	-20.46	17.65	-20.46	130	-10.07	-7.25	-10.72	-7.25
88	3.14	-21.11	3.79	-21.11	131	-10.07	-10.39	-10.72	-10.39
89	3.14	-24.25	3.79	-24.25	132	-10.07	-13.53	-10.72	-13.53
90	3.14	-27.39	3.79	-27.39	133	-17	-7.25	-17.65	-7.25
91	-3.14	-21.11	-3.79	-21.11	134	-17	-10.39	-17.65	-10.39
92	-3.14	-24.25	-3.79	-24.25	135	-17	-13.53	-17.65	-13.53
93	-3.14	-27.39	-3.79	-27.39	136	-10.07	-14.18	-10.72	-14.18
94	10.07	-21.11	10.72	-21.11	137	-10.07	-17.32	-10.72	-17.32
95	10.07	-24.25	10.72	-24.25	138	-10.07	-20.46	-10.72	-20.46
96	10.07	-27.39	10.72	-27.39	139	-17	-14.18	-17.65	-14.18
97	-10.07	6.6	-10.72	6.6	140	-17	-17.32	-17.65	-17.32
98	-10.07	3.46	-10.72	3.46	141	-17	-20.46	-17.65	-20.46
99	-10.07	0.33	-10.72	0.33	142	-10.07	-21.11	-10.72	-21.11
100	-17	6.6	-17.65	6.6	143	-10.07	-24.25	-10.72	-24.25
101	-17	3.46	-17.65	3.46	144	-10.07	-27.39	-10.72	-27.39
102	-17	0.33	-17.65	0.33	145	3.14	6.6	3.14	7.25
103	-23.92	6.6	-24.57	6.6	146	0	6.6	0	7.25
104	-23.92	3.46	-24.57	3.46	147	-3.14	6.6	-3.14	7.25
105	-23.92	0.33	-24.57	0.33	148	3.14	0.33	3.14	-0.33
106	-10.07	13.53	-10.72	13.53	149	0	0.33	0	-0.33
107	-10.07	10.39	-10.72	10.39	150	-3.14	0.33	-3.14	-0.33
108	-10.07	7.25	-10.72	7.25	151	10.07	6.6	10.07	7.25
109	-17	13.53	-17.65	13.53	152	6.93	6.6	6.93	7.25
110	-17	10.39	-17.65	10.39	153	3.79	6.6	3.79	7.25
111	-17	7.25	-17.65	7.25	154	10.07	0.33	10.07	-0.33
112	-10.07	20.46	-10.72	20.46	155	6.93	0.33	6.93	-0.33
113	-10.07	17.32	-10.72	17.32	156	3.79	0.33	3.79	-0.33
114	-10.07	14.18	-10.72	14.18	157	17	6.6	17	7.25
115	-17	20.46	-17.65	20.46	158	13.86	6.6	13.86	7.25
116	-17	17.32	-17.65	17.32	159	10.72	6.6	10.72	7.25
117	-17	14.18	-17.65	14.18	160	17	0.33	17	-0.33
118	-10.07	27.39	-10.72	27.39	161	13.86	0.33	13.86	-0.33
119	-10.07	24.25	-10.72	24.25	162	10.72	0.33	10.72	-0.33
120	-10.07	21.11	-10.72	21.11	163	23.92	6.6	23.92	7.25
121	-10.07	-0.33	-10.72	-0.33	164	20.78	6.6	20.78	7.25
122	-10.07	-3.46	-10.72	-3.46	165	17.65	6.6	17.65	7.25
123	-10.07	-6.6	-10.72	-6.6	166	23.92	0.33	23.92	-0.33
124	-17	-0.33	-17.65	-0.33	167	20.78	0.33	20.78	-0.33
125	-17	-3.46	-17.65	-3.46	168	17.65	0.33	17.65	-0.33
126	-17	-6.6	-17.65	-6.6	169	30.85	0.33	30.85	-0.33
127	-23.92	-0.33	-24.57	-0.33	170	27.71	0.33	27.71	-0.33
128	-23.92	-3.46	-24.57	-3.46	171	24.57	0.33	24.57	-0.33
129	-23.92	-6.6	-24.57	-6.6	172	3.14	13.53	3.14	14.18

1. See Figure 11.2.12.4.2-4 for section locations.

Table 11.2.12.4.2-3 Support Disk Section Locations for Stress Evaluation - BWR - Full Model (Continued)

Section[1]	Point 1		Point 2		Section[1]	Point 1		Point 2	
	X	Y	X	Y		X	Y	X	Y
173	0	13.53	0	14.18	216	17.65	-13.53	17.65	-14.18
174	-3.14	13.53	-3.14	14.18	217	3.14	-20.46	3.14	-21.11
175	10.07	13.53	10.07	14.18	218	0	-20.46	0	-21.11
176	6.93	13.53	6.93	14.18	219	-3.14	-20.46	-3.14	-21.11
177	3.79	13.53	3.79	14.18	220	10.07	-20.46	10.07	-21.11
178	17	13.53	17	14.18	221	6.93	-20.46	6.93	-21.11
179	13.86	13.53	13.86	14.18	222	3.79	-20.46	3.79	-21.11
180	10.72	13.53	10.72	14.18	223	17	-20.46	17	-21.11
181	23.92	13.53	23.92	14.18	224	13.86	-20.46	13.86	-21.11
182	20.78	13.53	20.78	14.18	225	10.72	-20.46	10.72	-21.11
183	17.65	13.53	17.65	14.18	226	-3.79	6.6	-3.79	7.25
184	3.14	20.46	3.14	21.11	227	-6.93	6.6	-6.93	7.25
185	0	20.46	0	21.11	228	-10.07	6.6	-10.07	7.25
186	-3.14	20.46	-3.14	21.11	229	-3.79	0.33	-3.79	-0.33
187	10.07	20.46	10.07	21.11	230	-6.93	0.33	-6.93	-0.33
188	6.93	20.46	6.93	21.11	231	-10.07	0.33	-10.07	-0.33
189	3.79	20.46	3.79	21.11	232	-10.72	6.6	-10.72	7.25
190	17	20.46	17	21.11	233	-13.86	6.6	-13.86	7.25
191	13.86	20.46	13.86	21.11	234	-17	6.6	-17	7.25
192	10.72	20.46	10.72	21.11	235	-10.72	0.33	-10.72	-0.33
193	3.14	-6.6	3.14	-7.25	236	-13.86	0.33	-13.86	-0.33
194	0	-6.6	0	-7.25	237	-17	0.33	-17	-0.33
195	-3.14	-6.6	-3.14	-7.25	238	-17.65	6.6	-17.65	7.25
196	10.07	-6.6	10.07	-7.25	239	-20.78	6.6	-20.78	7.25
197	6.93	-6.6	6.93	-7.25	240	-23.92	6.6	-23.92	7.25
198	3.79	-6.6	3.79	-7.25	241	-17.65	0.33	-17.65	-0.33
199	17	-6.6	17	-7.25	242	-20.78	0.33	-20.78	-0.33
200	13.86	-6.6	13.86	-7.25	243	-23.92	0.33	-23.92	-0.33
201	10.72	-6.6	10.72	-7.25	244	-24.57	0.33	-24.57	-0.33
202	23.92	-6.6	23.92	-7.25	245	-27.71	0.33	-27.71	-0.33
203	20.78	-6.6	20.78	-7.25	246	-30.85	0.33	-30.85	-0.33
204	17.65	-6.6	17.65	-7.25	247	-3.79	13.53	-3.79	14.18
205	3.14	-13.53	3.14	-14.18	248	-6.93	13.53	-6.93	14.18
206	0	-13.53	0	-14.18	249	-10.07	13.53	-10.07	14.18
207	-3.14	-13.53	-3.14	-14.18	250	-10.72	13.53	-10.72	14.18
208	10.07	-13.53	10.07	-14.18	251	-13.86	13.53	-13.86	14.18
209	6.93	-13.53	6.93	-14.18	252	-17	13.53	-17	14.18
210	3.79	-13.53	3.79	-14.18	253	-17.65	13.53	-17.65	14.18
211	17	-13.53	17	-14.18	254	-20.78	13.53	-20.78	14.18
212	13.86	-13.53	13.86	-14.18	255	-23.92	13.53	-23.92	14.18
213	10.72	-13.53	10.72	-14.18	256	-3.79	20.46	-3.79	21.11
214	23.92	-13.53	23.92	-14.18	257	-6.93	20.46	-6.93	21.11
215	20.78	-13.53	20.78	-14.18	258	-10.07	20.46	-10.07	21.11

1. See Figure 11.2.12.4.2-4 for section locations.

Table 11.12.12.4.2-3 Support Disk Section Locations for Stress Evaluation - BWR - Full Model (Continued)

Section[1]	Point 1		Point 2		Section[1]	Point 1		Point 2	
	X	Y	X	Y		X	Y	X	Y
259	-10.72	20.46	-10.72	21.11	289	3.14	27.39	3.14	32.63
260	-13.86	20.46	-13.86	21.11	290	3.79	27.39	3.79	32.56
261	-17	20.46	-17	21.11	291	10.07	27.39	10.07	31.2
262	-3.79	-6.6	-3.79	-7.25	292	10.72	27.39	10.72	30.98
263	-6.93	-6.6	-6.93	-7.25	293	17	27.39	17.29	27.86
264	-10.07	-6.6	-10.07	-7.25	294	30.85	-0.33	32.78	-0.33
265	-10.72	-6.6	-10.72	-7.25	295	30.85	-6.6	32.06	-6.86
266	-13.86	-6.6	-13.86	-7.25	296	-3.14	-27.39	-3.14	-32.63
267	-17	-6.6	-17	-7.25	297	3.14	-27.39	3.14	-32.63
268	-17.65	-6.6	-17.65	-7.25	298	3.79	-27.39	3.79	-32.56
269	-20.78	-6.6	-20.78	-7.25	299	10.07	-27.39	10.07	-31.2
270	-23.92	-6.6	-23.92	-7.25	300	10.72	-27.39	10.72	-30.98
271	-3.79	-13.53	-3.79	-14.18	301	17	-27.39	17.29	-27.86
272	-6.93	-13.53	-6.93	-14.18	302	-30.85	6.6	-32.06	6.86
273	-10.07	-13.53	-10.07	-14.18	303	-30.85	0.33	-32.78	0.33
274	-10.72	-13.53	-10.72	-14.18	304	-10.07	27.39	-10.07	31.2
275	-13.86	-13.53	-13.86	-14.18	305	-3.79	27.39	-3.79	32.56
276	-17	-13.53	-17	-14.18	306	-17	27.39	-17.29	27.86
277	-17.65	-13.53	-17.65	-14.18	307	-10.72	27.39	-10.72	30.98
278	-20.78	-13.53	-20.78	-14.18	308	-30.85	-0.33	-32.78	-0.33
279	-23.92	-13.53	-23.92	-14.18	309	-30.85	-6.6	-32.06	-6.86
280	-3.79	-20.46	-3.79	-21.11	310	-10.07	-27.39	-10.07	-31.2
281	-6.93	-20.46	-6.93	-21.11	311	-3.79	-27.39	-3.79	-32.56
282	-10.07	-20.46	-10.07	-21.11	312	-17	-27.39	-17.29	-27.86
283	-10.72	-20.46	-10.72	-21.11	313	-10.72	-27.39	-10.72	-30.98
284	-13.86	-20.46	-13.86	-21.11	314	23.92	20.46	24.92	21.31
285	-17	-20.46	-17	-21.11	315	23.92	-20.46	24.92	-21.31
286	30.85	6.6	32.06	6.86	316	-23.92	20.46	-24.92	21.31
287	30.85	0.33	32.78	0.33	317	-23.92	-20.46	-24.92	-21.31
288	-3.14	27.39	-3.14	32.63					

1. See Figure 11.2.12.4.2-4 for section locations.

Table 11.2.12.4.2-4 Summary of Maximum Stresses for BWR Support Disk for Tip-Over Condition

Drop Orientation	P_m			$P_m + P_b$		
	Stress Intensity (ksi)	Allowable Stress (ksi)	Margin of Safety	Stress Intensity (ksi)	Allowable Stress (ksi)	Margin of Safety
0°	35.1	63.0	+0.80	46.1	90.0	+0.95
31.82°	25.8	63.0	+1.44	65.7	90.0	+0.37
49.46°	23.7	63.0	+1.65	55.5	90.0	+0.62
77.92°	47.5	63.0	+0.33	86.6	90.0	+0.04
90°	58.4	63.0	+0.08	69.6	90.0	+0.29

Note: See Figure 11.2.12.4.2-1 for Drop Orientation.

Table 11.2.12.4.2-5 Summary of Buckling Evaluation of BWR Support Disk for Tip-Over Condition

Drop orientation	MS1	MS2
0°	1.17	1.03
31.82°	0.56	0.53
49.46°	0.86	0.81
77.92°	0.18	0.16
90°	0.38	0.58

Table 11.2.12.4.2-6 Support Disk Primary Membrane (P_m) Stresses for Tip-Over Condition – BWR Disk No. 5 - 77.92° Drop Orientation (ksi)

Section Number	Sx	Sy	Sxy	Stress Intensity	Allowable Stress	Margin of Safety
202	-24.9	22.5	1	47.5	63.0	0.33
199	-21.8	14.8	1.3	36.6	63.0	0.72
196	-18.8	12.5	1.3	31.4	63.0	1.01
193	-16	11.2	1.3	27.2	62.8	1.30
63	-18.3	8.5	2.4	27.2	63.0	1.32
203	-24.9	-0.1	0.8	24.9	63.0	1.53
204	-24.8	-16.1	0.7	24.9	63.0	1.53
262	-13.2	10.3	1.3	23.7	62.8	1.65
201	-21.7	-16	1	21.9	63.0	1.88
200	-21.7	0	1.1	21.8	63.0	1.89
73	-18.6	2.1	-0.6	20.8	63.0	2.03
265	-10.6	9.8	1.2	20.6	63.0	2.06
166	-12.3	7.9	1.6	20.4	63.0	2.09
169	-13.9	-19.2	2.3	20.0	63.0	2.15
198	-18.7	-15.1	1	19.0	62.8	2.31
197	-18.8	0	1.1	18.9	63.0	2.34
295	-6	-15.6	-6.3	18.7	63.0	2.37
15	-9.1	8.2	2.5	18.0	63.0	2.50
268	-8.1	9.7	0.9	17.8	63.0	2.53
195	-15.9	-14.2	1	16.3	62.8	2.85
194	-15.9	0	1.1	16.1	62.8	2.91
211	-12.2	3.6	0.6	15.8	63.0	2.98
60	-12.3	2.7	2.5	15.8	63.0	2.99
61	-6.8	8.5	1	15.5	63.0	3.06
160	-10.7	4.2	1.9	15.4	63.0	3.10
171	-13.8	0.8	2	15.2	63.0	3.15
70	-14.6	0.2	-0.3	14.9	63.0	3.24
170	-13.9	0	2.1	14.5	63.0	3.34
264	-13.2	-13.2	1	14.1	63.0	3.46
13	-5.7	8.2	1	14.1	63.0	3.48

See Figure 11.2.12.4.2-4 for section locations.

Table 11.2.12.4.2-7 Support Disk Primary Membrane + Primary Bending (P_m+P_b) Stresses for Tip-Over Condition - BWR Disk No. 5 - 77.92° Drop Orientation (ksi)

Section Number	Sx	Sy	Sxy	Stress Intensity	Allowable Stress	Margin of Safety
169	-85.6	-34.9	7.1	86.6	90.0	0.04
202	-50.9	15.4	-2.3	66.5	90.0	0.35
63	1.2	63.9	-1.5	63.9	90.0	0.41
160	-61.6	-14.9	1.5	61.7	90.0	0.46
171	-60	-17.6	3	60.2	90.0	0.49
60	3.8	59.5	0.4	59.5	90.0	0.51
57	4.8	59.1	0.1	59.1	90.0	0.52
15	10.2	58.9	1.1	59.0	90.0	0.53
51	-28.2	-57	4.7	57.7	89.5	0.55
154	-57.6	-16.5	1.6	57.7	89.8	0.56
199	-54.3	3	-1.4	57.3	90.0	0.57
162	-56.8	-22.8	3.4	57.1	89.9	0.57
54	-26	-55.3	4.3	55.9	89.5	0.60
156	-54.4	-22.8	3.3	54.8	87.8	0.60
148	-54.3	-16.2	1.5	54.4	87.6	0.61
9	14.6	54.1	1.5	54.1	89.8	0.66
166	-54.1	-9.7	0.5	54.1	90.0	0.66
3	-25.2	-52.1	3.5	52.6	87.6	0.67
13	3.7	53.7	1.1	53.7	90.0	0.68
12	15.2	53.5	2.1	53.6	90.0	0.68
123	-23.9	-52.9	3.9	53.4	90.0	0.69
150	-51.3	-22.4	3.2	51.7	87.6	0.69
6	-23.6	-51.1	3.3	51.5	87.6	0.70
229	-51.1	-15.6	1.3	51.2	87.8	0.71
201	-50.2	-27.9	6.7	52.0	90.0	0.73
196	-51.2	-0.2	-1	51.3	90.0	0.76
168	-50.4	-19.2	2.9	50.7	90.0	0.78
198	-48.4	-27.4	6.3	50.1	89.5	0.79
99	-22.1	-49.4	3.1	49.7	89.8	0.81
231	-48.5	-21.6	3	48.8	89.8	0.84

See Figure 11.2.12.4.2-4 for section locations.

Table 11.2.12.4.2-8 Summary of Support Disk Buckling Evaluation for Tip-Over Condition - BWR Disk No. 5 - 77.92° Drop Orientation

Section Number	P (kip)	Pcr (kip)	Py (kip)	M (in-kip)	Mp (in-kip)	Mm (in-kip)	MS1	MS2
169	5.65	31.59	25.67	3.15	4.17	4.11	0.18	0.16
199	8.84	31.4	25.52	1.43	4.15	4.09	0.69	0.57
171	5.62	31.52	25.62	2.03	4.16	4.1	0.64	0.58
160	4.34	31.35	25.48	2.24	4.14	4.08	0.63	0.59
202	10.12	31.55	25.64	1.14	4.17	4.11	0.76	0.59
201	8.82	31.23	25.38	1.25	4.12	4.07	0.80	0.65
196	7.63	31.22	25.37	1.43	4.12	4.07	0.81	0.68
162	4.32	31.1	25.28	2.03	4.11	4.05	0.74	0.70
154	3.7	31.07	25.26	2.14	4.1	4.05	0.74	0.70
204	10.09	31.41	25.53	0.88	4.15	4.09	0.95	0.74
198	7.61	30.97	25.18	1.31	4.09	4.04	0.89	0.75
156	3.67	30.35	24.73	2	4.02	3.97	0.80	0.75
166	4.98	31.51	25.61	1.84	4.16	4.1	0.82	0.76
148	3.05	30.27	24.67	2.06	4.01	3.96	0.82	0.79
193	6.48	30.96	25.18	1.41	4.09	4.04	0.94	0.82
168	4.96	31.36	25.49	1.68	4.14	4.08	0.94	0.86
150	3.02	30.27	24.67	1.93	4.01	3.96	0.92	0.88
51	0.11	30.96	25.18	2.5	4.09	4.04	0.89	0.92
195	6.46	30.96	25.18	1.3	4.09	4.04	1.04	0.90
229	2.39	30.35	24.73	1.99	4.02	3.97	0.96	0.94
54	0.26	30.96	25.18	2.4	4.09	4.04	0.94	0.97
262	5.37	30.97	25.18	1.39	4.09	4.04	1.11	0.99
123	0.25	31.22	25.37	2.3	4.12	4.07	1.04	1.07
6	0.14	30.27	24.67	2.24	4.01	3.96	1.06	1.09
231	2.36	31.07	25.26	1.88	4.1	4.05	1.11	1.08
264	5.35	31.22	25.37	1.29	4.12	4.07	1.23	1.10
99	0.15	31.07	25.26	2.16	4.1	4.05	1.18	1.22
235	1.73	31.1	25.28	1.87	4.11	4.05	1.21	1.20
265	4.31	31.23	25.38	1.32	4.12	4.07	1.38	1.27
237	1.7	31.35	25.48	1.82	4.14	4.08	1.29	1.28

See Figure 11.2.12.4.2-4 for section locations.

11.2.12.5 Corrective Actions

The most important recovery action required following a concrete cask tip-over is the uprighting of the cask to minimize the dose rate from the exposed bottom end. The uprighting operation will require a heavy lift capability and rigging expertise. The concrete cask must be returned to the vertical position by rotation around a convenient bottom edge, and by using a method and rigging that controls the rotation to the vertical position.

Surface and top and bottom edges of the concrete cask are expected to exhibit cracking and possibly loss of concrete down to the layer of reinforcing bar. If only minor damage occurs, the concrete may be repairable by using grout. Otherwise, it may be necessary to remove the canister for installation in a new concrete cask. If the canister remains in the cask, it should be returned to its centered storage position within the cask.

The storage pad must be repaired to preclude the intrusion of water that could cause further deterioration of the pad in freeze-thaw cycles.

11.2.12.6 Radiological Impact

There is an adverse radiological consequence in the hypothetical tip-over event since the bottom end of the concrete cask and the canister have significantly less shielding than the sides and tops of these same components. The dose rate at 1 meter is calculated, using a 1–D analysis, to be approximately 34 rem/hour, and the dose at 4 meters is estimated to be approximately 4 rem/hour. Consequently, following a tip-over event, supplemental shielding should be used until the concrete cask can be uprighted. Stringent access controls must be applied to ensure that personnel do not enter the area of radiation shine from the exposed bottom of the tipped-over concrete cask.

Damage to the edges or surface of the concrete cask may occur following a tip-over, which could result in marginally higher dose rates at the bottom edge or at surface cracks in the concrete. This increased dose rate is not expected to be significant, and would be dependent on the specific damage incurred.

THIS PAGE INTENTIONALLY LEFT BLANK

11.2.13 Full Blockage of Vertical Concrete Cask Air Inlets and Outlets

This section evaluates the Vertical Concrete Cask for the steady state effects of full blockage of the air inlets and outlets at the normal ambient temperature (76°F). It estimates the duration of the event that results in the fuel cladding, the fuel basket and the concrete reaching their design basis limiting temperatures (See Table 4.1-3 for the allowable temperatures for short term conditions).

The evaluation demonstrates that there are no adverse consequences due to this accident, provided that debris is cleared within 24 hours.

11.2.13.1 Cause of Full Blockage

The likely cause of complete cask air inlet and outlet blockage is the covering of the cask with earth in a catastrophic event that is significantly greater than the design basis earthquake or a land slide. This event is a bounding condition accident and is not credible.

11.2.13.2 Detection of Full Blockage

Blockage of the cask air inlets and outlets will be visually detected during the general site inspection following an earthquake, land slide, or other events with a potential for such blockage.

11.2.13.3 Analysis of Full Blockage

The accident temperature conditions are evaluated using the thermal models described in Section 4.4.1. The analysis assumes initial normal storage conditions, with the sudden loss of convective cooling of the canister. Heat is then rejected from the canister to the Vertical Concrete Cask liner by radiation and conduction. The loss of convective cooling results in the fairly rapid and sustained heat-up of the canister and the concrete cask. To account for the loss of convective cooling in the ANSYS air flow model (Section 4.4.1.1), the elements in the model are replaced with thermal conduction elements. This model is used to evaluate the thermal transient resulting from the postulated boundary conditions. The analysis indicates that the maximum basket temperature (support disk and heat transfer disk) remain less than the allowable temperature for 24 hours after the initiation of the event. The maximum fuel cladding temperature and the maximum concrete bulk temperature remain less than the allowable temperatures for about 6 days (150 hours) after the

initiation of the event. The heat up of the fuel cladding, canister shell and concrete (bulk temperature) are shown in Figures 11.2.13-1 and 11.2.13-2, for the PWR and BWR configurations, respectively.

11.2.13.4 Corrective Actions

The obstruction blocking the are inlets must be manually removed. The nature of the obstruction may indicate that other actions are required to prevent recurrence of the blockage.

11.2.13.5 Radiological Impact

There are no significant radiological consequences for this event, as the Vertical Concrete Cask retains its shielding performance. Dose is incurred as a consequence of uncovering the concrete cask and vent system. Since the dose rates at the air inlets and outlets are higher than the nominal rate (35 mrem/hr) at the cask wall, personnel will be subject to an estimated maximum dose rate of 100 mrem/hr when clearing the inlets and outlets. If it is assumed that a worker kneeling with his hands on the inlets or outlets requires 15 minutes to clear each inlet or outlet, the estimated extremity dose is 200 mrem for the 8 openings. The whole body dose will be slightly less. In addition, some dose is incurred clearing debris away from the cask body. This dose is estimated at 50 mrem, assuming 2 hours is spent near the cask exterior surface.

Figure 11.2.13-1 PWR Configuration Temperature History—All Vents Blocked

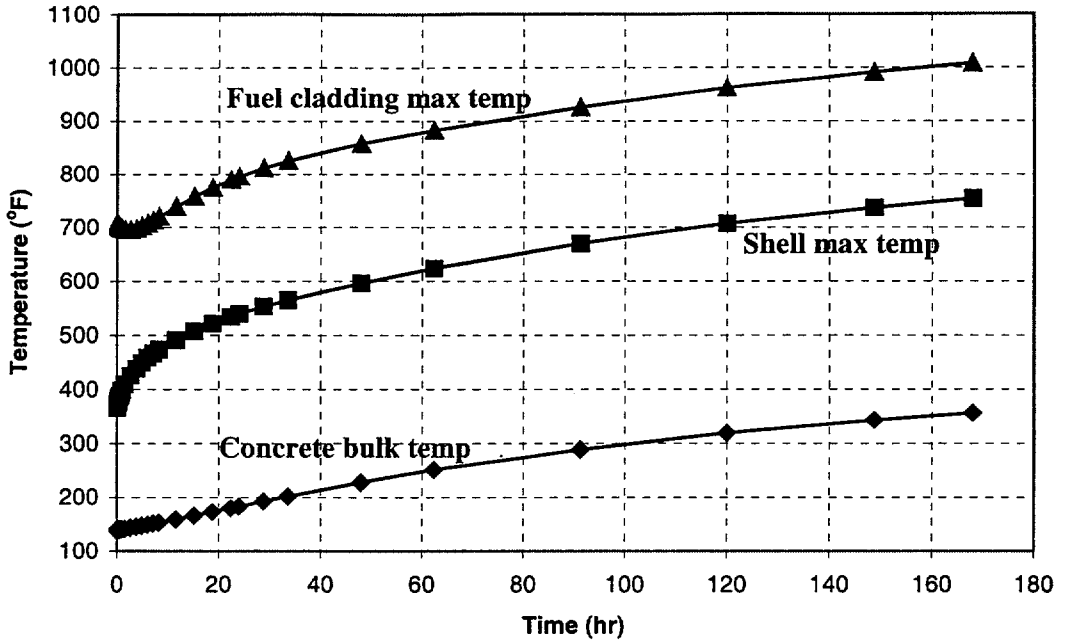

Figure 11.2.13-2 BWR Configuration Temperature History—All Vents Blocked

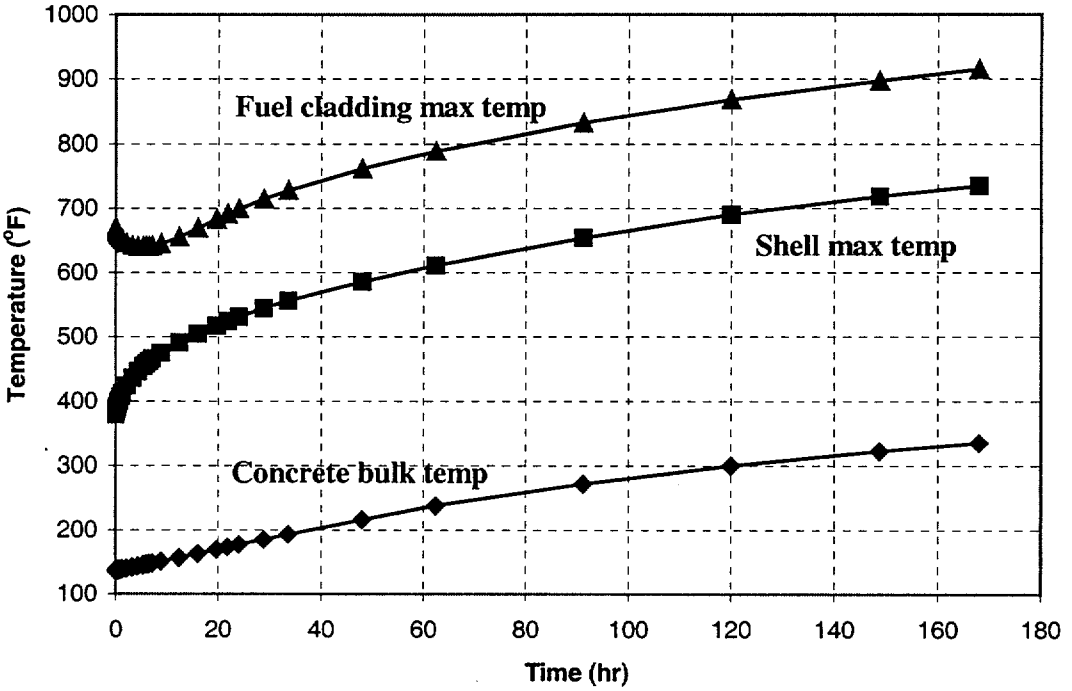

THIS PAGE INTENTIONALLY LEFT BLANK

11.2.14 Canister Closure Weld Evaluation

The closure weld for the canister is a groove weld with a thickness of 0.9 inches. The evaluation of this weld, in accordance with NRC guidance, is to incorporate a 0.8 stress reduction factor. Applying a factor of 0.8 to the weld stress allowable incorporates the stress reduction factor.

The stresses for the canister are evaluated using sectional stresses as permitted by Subsection NB of the ASME Code. Canister stresses resulting from the concrete cask tip-over accident (Section 11.2.12.4) are used for evaluation. The location of the section for the canister weld evaluation is shown in Figure 11.2.12.4.1-6 and corresponds to Section 11. The governing P_m and $P_m + P_b$ stress intensities for Section 11 and the associated allowables are listed in Tables 11.2.12.4.1-1 and Table 11.2.12.4.1-2, respectively. The factored allowables, incorporating a 0.8 stress reduction factor, and the resulting controlling Margins of Safety are:

Stress Category	Analysis Stress (ksi)	0.8 x Allowable Stress (ksi)	Margin of Safety
P_m	22.81	32.06	0.41
$P_m + P_b$	25.03	48.09	0.92

This confirms that the canister closure weld is acceptable for accident conditions.

Critical Flaw Size for the Canister Closure Weld

The closure weld for the canister is comprised of multiple weld beads using a compatible weld material for Type 304L stainless steel. An allowable (critical) flaw evaluation has been performed to determine the critical flaw size in the weld region. The result of the flaw evaluation is used to define the minimum flaw size, which must be identifiable in the nondestructive examination of the weld. Due to the inherent toughness associated with Type 304L stainless steel, a limit load analysis is used in conjunction with a J-integral/tearing modulus approach. The safety margins used in this evaluation correspond to the stress limits contained in Section XI of the ASME Code.

One of the stress components used in the evaluation for the critical flaw size is the radial stress component in the weld region of the structural lid. For an accident (Level D) event, in accordance with ASME Code Section XI, a safety factor of $\sqrt{2}$ is required. For the purpose of identifying the

stress for the flaw evaluation, the weld region corresponds to Section 11 in Figure 11.2.12.4.1-6 is considered.

The maximum tensile radial stress at Section 11 is 6.9 ksi, based on the analysis results of the tip-over accident (Section 11.2.12.4). To perform the flaw evaluation, a 10 ksi stress is conservatively used, resulting in a significantly larger safety factor than the required safety factor of $\sqrt{2}$. Using 10 ksi as the basis for the evaluation, the minimum detectable flaw size is 0.52 inch for a flaw that extends 360 degrees around the circumference of the canister. Stress components for the circumferential and axial directions are also reported in the concrete cask tip-over analysis, which would be associated with flaws oriented in the radial or horizontal directions respectively. The maximum stress for these components is 2.5 ksi, which is also enveloped by the value of 10 ksi used in the critical flaw evaluation for stresses in the radial direction. The 360-degree flaw employed for the circumferential direction is considered to be bounding with respect to any partial flaw in the weld, which could occur in the radial and horizontal directions. Therefore, using a minimum detectable flaw size of 0.375 inch is acceptable, since it is less than the very conservatively determined 0.52-inch critical flaw size.

11.2.15 Accident and Natural Phenomena Events Evaluation for Site Specific Spent Fuel

This section presents the accident and natural phenomena events evaluation of spent fuel assemblies or configurations, which are unique to specific reactor sites. These site specific fuel configurations result from conditions that occurred during reactor operations, participation in research and development programs, and from testing programs intended to improve reactor operations. Site specific fuel includes fuel assemblies that are uniquely designed to accommodate reactor physics, such as axial fuel blankets and variable enrichment assemblies, fuel with burnup that exceeds the design basis, and fuel that is classified as damaged. Damaged fuel includes fuel rods with cladding that exhibits defects greater than pinhole leaks or hairline cracks.

Site specific fuel assembly configurations are either shown to be bounded by the analysis of the standard design basis fuel assembly of the same type (PWR or BWR), or are shown to be acceptable contents, by specific evaluation of the configuration.

11.2.15.1 Accident and Natural Phenomena Events Evaluation for Maine Yankee Site Specific Fuel

Maine Yankee site specific fuels are described in Section 1.3.2.1. A thermal evaluation has been performed for Maine Yankee site specific fuels that exceed the design basis burnup, as shown in Section 4.5.1.2. As shown in that section, loading of fuel with a burnup between 45,000 and 50,000 MWD/MTU is subject to preferential loading in designated basket positions in the Transportable Storage Canister, and certain high burnup fuel may require loading in the Maine Yankee fuel can.

With preferential loading, the design basis total heat load of the canister is not changed. Consequently, the thermal performance for the Maine Yankee site specific fuels is bounded by the design basis PWR fuels. Therefore, no further evaluation is required for the thermal accident events, as presented in Sections 11.2.6, 11.2.7, and 11.2.13.

As shown in Section 3.6.1.1, the total weight of the contents of the Transportable Storage Canister for Maine Yankee fuels is bounded by the total weight for the PWR design basis fuels. However, some design parameters for the Maine Yankee site ISFSI pad are different from those for the design basis ISFSI pad. Therefore, the hypothetical accident (non-mechanistic) tip-over event is evaluated to ensure that the maximum tip-over g-load remains below the bounding g-load (40g) used in the evaluation of the PWR canister and basket in Section 11.2.12.4. The evaluation of the UMS®

Vertical Concrete Cask tip-over event on the Maine Yankee site ISFSI pad is presented in Section 11.2.15.1.1. The methodology used is similar to that used in Section 11.2.12.3.1.

Although the total weight, and the maximum g-load, for the Maine Yankee fuel is bounded by the PWR design basis fuels, the maximum weight of the consolidated fuel lattices (2,100 lbs) is larger than that of a single PWR Class 1 design basis fuel assembly (1,567 lbs). This additional weight need only be considered in the support disk evaluation for a side impact condition, similar to the analysis presented in Section 11.2.12.4.1. A parametric study is presented in Section 11.2.15.1.2 to demonstrate that the maximum stress in the support disk due to the consolidated fuel lattice remains bounded by the maximum stress for the support disk for the PWR design basis fuels for a side impact condition.

Section 11.2.15.1.3 provides the structural evaluation for the Maine Yankee fuel can for the 24-inch drop (Section 11.2.4) and the tip-over (Section 11.2.12) accident events.

A Maine Yankee site earthquake evaluation is presented in Section 11.2.15.1.4 to demonstrate the stability of the Vertical Concrete Cask on the Maine Yankee site ISFSI pad.

11.2.15.1.1 Maine Yankee Vertical Concrete Cask Tip-Over Analysis

This section evaluates the maximum acceleration of the Transportable Storage Canister and basket during the Vertical Concrete Cask tip-over event on the Maine Yankee site ISFSI pad. This evaluation applies the methodology of Section 11.2.12 for the design basis cask tip-over evaluation.

A finite element model is generated using the LS-DYNA program to determine the acceleration of the vertical concrete cask during the tip-over event.

The concrete pad in the model corresponds to a pad 31-feet by 31-feet square and 3-feet thick, supporting one concrete cask in the center of the pad. The soil under the concrete pad is considered to be 40-feet by 40-feet square and made up of two layers: a 4.5-foot thick upper layer and a 10-foot thick lower layer. Only one-half of the concrete cask, pad and soil configuration is modeled due to symmetry. Both the Class 1 and Class 2 UMS® configurations are evaluated.

The model includes a half section of the concrete cask, the concrete ISFSI pad and soil subgrade, as shown:

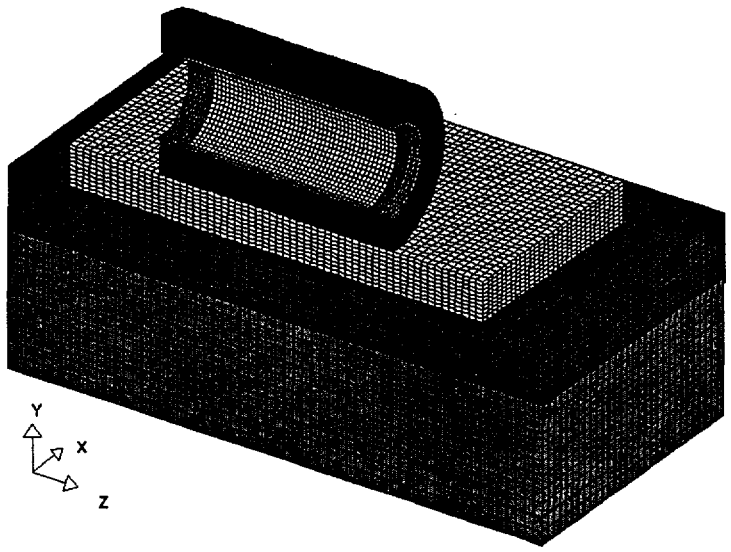

Concrete Pad Properties

Vertical concrete cask tip-over analyses are performed for ISFSI pad concrete compressive strengths of 3,000 and 4,000 psi. The Poisson's Ratio (ν_c) is 0.22. The concrete dry density is considered to be between 135 pcf and 145 pcf. To account for the weight of reinforcing bar in the pad, three values of Density (ρ) are used in the model:

ρ (lbs/ft^3)	E_c (psi)	K_c (psi)
140	2.994×10^6	1.782×10^6
145	3.156×10^6	1.879×10^6
152	3.387×10^6	2.016×10^6

The corresponding values of Modulus of Elasticity (E_c) and Bulk Modulus (K_c) are also provided, where:

Modulus of Elasticity (E_c) $= 33\rho_c^{1.5}\sqrt{f_c^{'}}$ (ACI 318-95)

Bulk Modulus (K_c) $= \dfrac{E_c}{3(1-2\nu_c)}$ (Blevins [19])

Soil Properties

The soil properties used in the model are based on two soil layers. The vertical concrete cask tip-over analyses are performed for two different combinations of soil densities: (1) 4.5-foot thick upper layer density of 135 pcf (Modulus of Elasticity, E = 162,070 psi), with a 10-foot thick lower layer density of 127 pcf (E = 31,900 psi); and (2) 4.5-foot thick upper layer density of 130 pcf, with a 10-foot thick lower layer density of 127 pcf. The Poisson's Ratio (ν_s) of the soil is 0.45.

Summary of Design Basis ISFSI Pad Parameters

The ISFSI pads and foundation shall include the following characteristics as applicable to the end drop and tip-over analyses:

Concrete thickness	36 inches maximum
Pad subsoil thickness	4.5 feet maximum (upper layer)
	10 feet minimum (lower layer)
Specified concrete compressive strength	$\leq$ 4,000 psi at 28 days
Soil in place density (ρ)	$\rho \leq 135$ lbs/ft^3 (upper layer)
	$\rho \leq 127$ lbs/ft^3 (lower layer)
Concrete dry density (ρ)	$135 \leq \rho \leq 145$ lbs/ft^3
Soil Modulus of Elasticity	$\leq$ 150,000 psi (upper layer)
	$\leq$ 30,000 psi (lower layer)

The concrete pad maximum thickness excludes the ISFSI pad footer. The compressive strength of the concrete is determined in accordance with Section 5.6 of ACI-318 with concrete acceptance in accordance with the same section. Steel reinforcement is used in the pad and footer. The soil modulus of elasticity is determined according to the test method described in ASTM D4719.

Vertical Concrete Cask Properties

The material properties used in the model for the Vertical Concrete Cask are the same as the properties used in the PWR models in Section 11.2.12.3. The tip-over impact is simulated by applying an initial angular velocity of 1.485 rad/sec (PWR Class 1) and 1.483 rad/sec (PWR Class 2), respectively, to the entire cask. The angular velocity values are determined by the method used in Section 11.2.12 based on the weight of the loaded concrete cask with Maine Yankee fuel (285,513 pounds and 297,509 pounds for PWR Class 1 and PWR Class 2, respectively).

A cut-off frequency of 210 Hz (PWR Class 1) and 190 Hz (PWR Class 2) is applied to filter the analysis results from the LS-DYNA models and determine the peak accelerations. The resulting calculated accelerations on the canister at the location of the top support disk and of the top of the structural lid are tabulated for all of the analysis cases that were run. The maximum accelerations at the two key locations on the canister for the PWR Class 1 and Class 2 configurations are:

Component Location	Position Measured from the Bottom of the Concrete Cask (inches)		Acceleration (g)	
	Class 1	Class 2	Class 1	Class 2
Top Support Disk	176.7	185.2	32.3	34.2
Top of the Canister Structural Lid	197.9	207.0	35.3	37.6

The impact accelerations for the vertical concrete cask tip-over on the Maine Yankee ISFSI pad site are observed to be slightly higher than those reported in Section 11.2.12.3.1 for the design-basis ISFSI pad. Therefore, peak accelerations are calculated for the top support disk and are evaluated with respect to the analysis presented in Section 11.2.12.4.1.

To determine the effect of the rapid application of the inertia loading for the support disk, a dynamic load factor (DLF) is computed using the method presented in Section 11.2.12.4. The DLF is computed to be 1.07 and 1.02 for PWR Class 1 and Class 2, respectively. Applying the DLFs to the 32.3g and 34.2g results in peak accelerations of 34.6g and 34.9g for the top support disk PWR Class 1 and Class 2, respectively. The DLFs for the canister lids are considered to be unity since the lids have significant in-plane stiffness and are considered to be rigid. Additional sensitivity evaluations considering varying values of the ISFSI concrete pad density have been performed. The results of those evaluations demonstrate that the maximum acceleration for the canister and basket are below 40g. Therefore, the maximum acceleration for the canister and basket for the cask tipover accident on the Maine Yankee site ISFSI pad is bounded by the 40g used in Section 11.2.12.4.1 (analysis of canister and basket for PWR configurations for tip-over event).

11.2.15.1.2 Parametric Study of Support Disk Evaluation for Maine Yankee Consolidated Fuel

A parametric study is performed to show that the PWR basket loaded with a Maine Yankee consolidated fuel lattice is bounded by the PWR basket design basis loading for a side impact condition. Only one consolidated fuel lattice, in a Maine Yankee Fuel Can, will be loaded in any single Transportable Storage Canister. However, Maine Yankee Fuel Cans holding other intact or damaged fuel can be loaded in the other three corner positions of the basket. (Maine Yankee Fuel

Cans may be loaded only in the four corner positions of the basket. See Figure 11.2.15.1.2-2 for corner positions. Therefore, the bounding case for Maine Yankee is the basket configuration with twenty (20) Maine Yankee fuel assemblies, three (3) fuel cans containing spent fuel, and one (1) fuel can containing consolidated fuel.

A two-dimensional ANSYS model is employed for the parametric study as shown in Figure 11.2.15.1.2-1. The load from a PWR fuel assembly is modeled as a pressure load at the inner surface of each support disk slot opening. The design basis fuel pressure loading (1g) is 12.26 psi. Based on the same design parameters (slot size = 9.272 in., disk thickness = 0.5 inch, and the number of disks = 30), the pressure load corresponding to a Maine Yankee standard CE 14 x 14 fuel assembly is 10.3 psi. The pressure load is 11.3 psi for a Maine Yankee fuel can holding an intact or damaged fuel assembly. For a Maine Yankee fuel can holding consolidated fuel the pressure load is 17.0 psi.

This study considers a 60g side impact condition for four different basket orientations: 0°, 18.22°, 26.28° and 45°, as shown in Figure 11.2.15.1.2-2. The 60g bounds the g-load for the PWR support disks (40g) due to the Vertical Concrete Cask tip-over accident as shown in Section 11.2.12.

A total of five cases are considered in the study. Inertial loads are applied to the support disk in all cases. The base case considers that all 24 fuel positions hold design basis PWR fuel assemblies. The other four cases (Cases 1 through 4) represent four possible load combinations for the placement of four Maine Yankee fuel cans in the corner positions, one of which holds consolidated fuel. The remaining twenty basket positions hold Maine Yankee standard 14 × 14 fuel assemblies. The basket loading positions are shown in Figure 11.2.15.1.2-2. The load combinations evaluated in the four Maine Yankee fuel can loading cases are:

Case	Basket Position 1	Basket Position 2	Basket Position 3	Basket Position 4
1	Consolidated	Damaged	Damaged	Damaged
2	Damaged	Consolidated	Damaged	Damaged
3	Damaged	Damaged	Damaged	Consolidated
4	Damaged	Damaged	Consolidated	Damaged

Table 11.2.15.1.2-1 provides a parametric comparison between the Base Case and the four cases evaluated, based on the maximum sectional stress in the support disk. As shown in the table, the maximum stress in the PWR basket support disk loaded with 20 standard fuel assemblies and four Maine Yankee fuel cans, including one holding consolidated fuel, is bounded by that for the support disk loaded with the design basis PWR fuel.

Additionally, a three-dimensional analysis was performed for Case 4 with a 26.28° drop orientation using the three-dimensional canister/basket model presented in Section 11.2.12.4.1. Results of the analysis for the top support disk, where maximum stress occurs, are presented in Tables 11.2.15.1.2-2 and 11.2.15.1.2-3. The minimum margin of safety is +1.12 and +0.11 for P_m stresses and $P_m + P_b$ stresses, respectively. The minimum margin of safety for the corresponding analysis for the design basis PWR configuration is +0.97 and +0.05 for P_m and $P_m + P_b$ stresses, respectively (see Table 11.2.12.4.1-4). Therefore, it is further demonstrated that the maximum stress in the PWR support disk loaded with Maine Yankee fuel with consolidated fuel is bounded by the stress for the PWR support disk loaded with the design basis PWR fuel.

Since no credit is taken for the structural integrity of the consolidated fuel or damaged fuel inside the fuel can, it is assumed that 100% of the fuel rods fail during an accident. For a Maine Yankee standard 14×14 fuel assembly, the volume of 176 fuel rods (100%) and 5 guide tubes will fill up the lower 103.6 inches (about at the elevation of the 21st support disk) assuming a 50% volume compaction factor. For the consolidated fuel, the volume of 283 rods (100%) and 4 connector rods will fill up the lower 109.6 inches (about at the elevation of the 22nd support disk) assuming a 75% compaction factor. The compaction factor of 75% for the consolidated fuel considers that the number of rods in the consolidated fuel is approximately 1.5 times of the number of rods in the standard Maine Yankee fuel and these rods are initially more closely spaced.

During a tip-over accident of the vertical concrete cask, the maximum total load on the support disk (top/30th disk) for the design basis PWR basket is 54.6 kips (12.26 psi × 9.272-inch × 0.5-inch × 24 × 40g), considering the design deceleration of 40g (Section 11.2.12.4). With the assumption of 100% rod failure for the damaged fuel and consolidated fuel in the Maine Yankee fuel can, the 21st disk is subjected to the maximum total load (including weight from 20 standard fuel assemblies, 3 damaged fuel assemblies and the consolidated fuel). The pressure load (1g) on the support disk corner slot corresponding to 100% failed damaged fuel is 15.3 psi (load distributed to 21 support disks) and the pressure load corresponding to the 100% failed consolidated fuel is 22.6 psi (load distributed on 22 support disks). In the tip-over accident, the g-load at the 21st disk is 30g, based on the design deceleration of 40g at the top (30th) disk. The total load (W_{21}) on the 21st support disk is:

$$W_{21} = (10.3\times20+15.3\times3+22.6\times1) \times 9.272 \times 0.5 \times 30 = 38{,}200 \text{ pounds} = 38.2 \text{ kips}$$

The support disk load is only 70% (38.2/54.6 = 0.7) of the maximum total load on the support disk due to the design basis PWR fuel load. Consequently, the maximum stress in the support disk, assuming 100% rod failure of the damaged and consolidated fuel in Maine Yankee fuel cans, is bounded by the maximum stress in the support disk calculated for the design basis fuel.

Figure 11.2.15.1.2-1 Two-Dimensional Support Disk Model

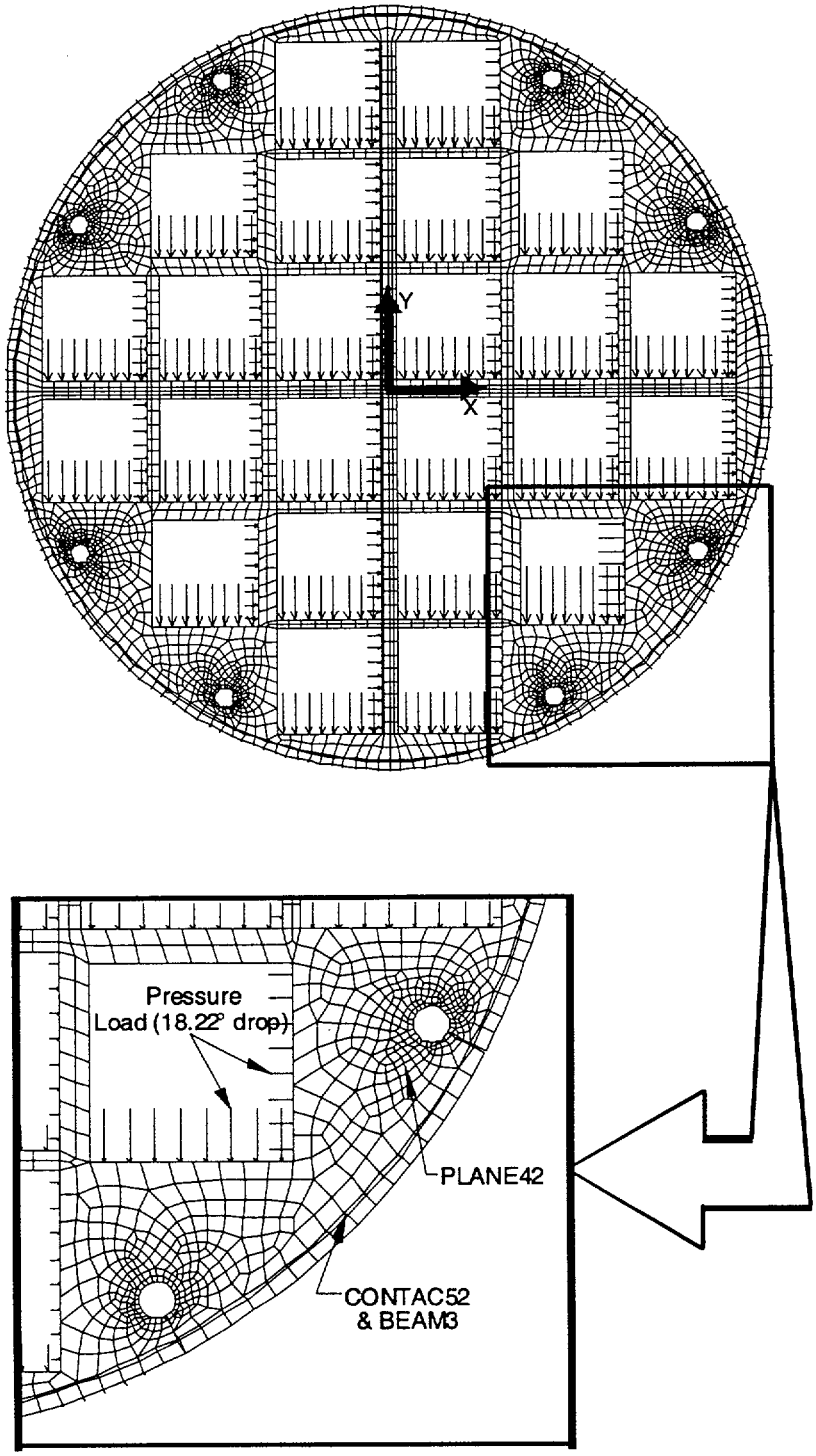

Figure 11.2.15.1.2-2 PWR Basket Impact Orientations and Case Study Loading Positions for Maine Yankee Consolidated Fuel

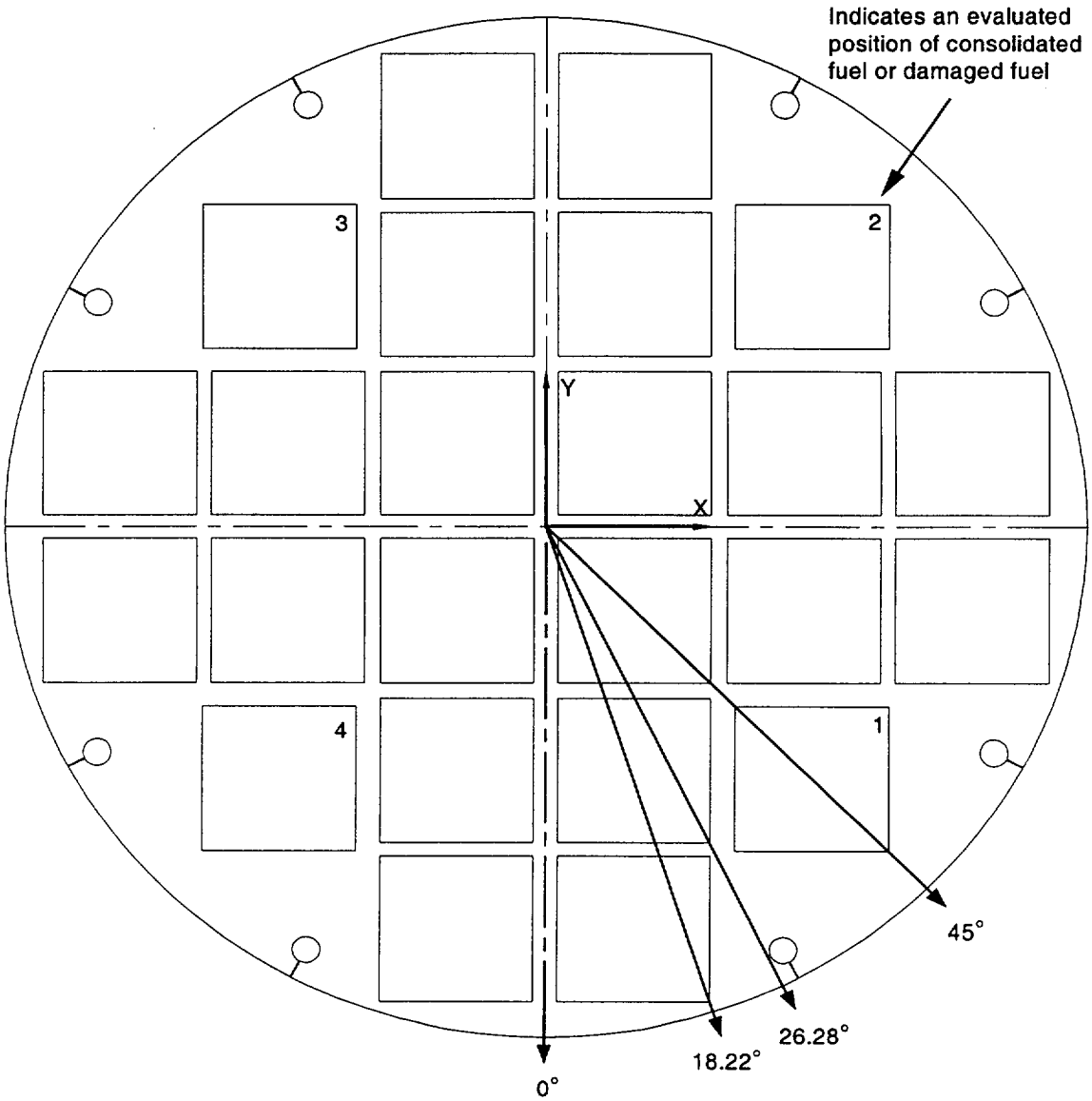

Table 11.2.15.1.2-1 Normalized Stress Ratios – PWR Basket Support Disk Maximum Stresses

Orientation[1]	Membrane Stress Ratio[2]				Membrane + Bending Stress Ratio[2]			
	0°	18.22°	26.28°	45°	0°	18.22°	26.28°	45°
Base Case	1.00	1.00	1.00	1.00	1.00	1.00	1.00	1.00
Case 1	0.91	0.94	0.94	0.94	0.96	0.94	0.94	0.94
Case 2	0.91	0.94	0.94	0.95	0.95	0.95	0.95	0.95
Case 3	0.91	0.95	0.95	0.95	0.96	0.95	0.95	0.95
Case 4	0.91	0.95	0.95	0.96	0.96	0.98	0.98	0.97

1. Orientations correspond to those shown in Figure 11.2.15.1.2-2.
2. Stress ratios are based on the maximum sectional stresses of the support disk.

Table 11.2.15.1.2-2 Support Disk Primary Membrane (P_m) Stresses for Case 4, 26.28° Drop Orientation (ksi)

Section Number	Sx	Sy	Sxy	Stress Intensity	Allowable Stress	Margin of Safety
18	19.3	-22.9	2.8	42.6	90.4	1.12
3	27.1	-12.2	2.4	39.6	89.3	1.26
16	37.1	-22.8	1	37.2	89.3	1.4
1	32.3	-12.1	0.6	32.3	90.4	1.8
94	26.8	-19	2.7	27.6	90.5	2.28
17	-0.1	-22.8	1.9	23.1	89.8	2.9
88	18.3	-5.6	-7.3	21.6	91.5	3.23
96	6.7	-13.8	-3.2	21.4	91.5	3.27
95	-0.1	-19.9	1.5	20	91.1	3.55
90	15.3	-3.5	0.8	18.9	90.5	3.8
84	15.6	-18.5	-0.4	18.6	91.5	3.93
61	15.7	-10.5	4.7	18.5	91.5	3.96
60	10.2	-17.5	1.3	17.7	89.3	4.03
82	15.7	-7.8	3.8	17.2	90.8	4.27
37	11.9	-4.3	0.6	16.3	89.3	4.49
58	10.3	-12.1	5	16.3	90.4	4.54
62	15.7	-0.2	2.6	16.3	91.2	4.59
83	15.7	-0.2	1.7	15.8	91.2	4.75
91	-7.4	-15.4	-1.5	15.7	90.5	4.78
63	15.6	-9.9	0.5	15.7	90.8	4.8
30	14.1	-9.3	3.1	15.6	91.9	4.89
33	14.6	-4.7	2.3	15.1	89.3	4.93
108	13.5	-5.6	-3.9	15.1	91.5	5.07
24	-2	-14.3	1.7	14.5	91.5	5.31
79	-5.3	6.3	4.1	14.2	89.3	5.31
23	-0.1	-14.2	0.7	14.2	91.2	5.41
22	-7.3	-14.1	-0.4	14.2	90.8	5.42
28	13.2	-9.1	1.8	13.9	90.9	5.56
7	13.6	-11.9	-0.7	13.8	91.5	5.62
46	-2.4	-10.8	5.1	13.2	89.3	5.74

Note: See Figure 11.2.12.4.1-7 for Section locations.

Table 11.2.15.1.2-3 Support Disk Primary Membrane + Primary Bending ($P_m + P_b$) Stresses for Case 4, 26.28° Drop Orientation (ksi)

Section Number	Sx	Sy	Sxy	Stress Intensity	Allowable Stress	Margin of Safety
61	-116.4	-39.3	10.1	117.7	130.8	0.11
58	-109.5	-43.9	8.7	110.6	129.1	0.17
43	-92.6	-32.4	6.2	93.2	129.1	0.39
82	-87.8	-27.9	7	88.6	129.8	0.46
60	-81.6	-39.9	7.7	83	127.6	0.54
79	-82	-18.9	2	82	127.6	0.56
55	-83.5	-29.3	4.6	83.9	130.8	0.56
16	-52.5	-71.9	15	80.1	127.6	0.59
46	-77.1	-49.3	9.5	80	127.6	0.59
64	-76.2	-31.8	7	77.2	127.6	0.65
30	-34.4	-75.2	13.1	79.1	131.3	0.66
18	-2.8	-77.6	-2.9	77.8	129.1	0.66
3	10.1	-65.4	-6	76.5	127.6	0.67
63	-75.4	-26	4.3	75.8	129.8	0.71
76	69	21	4.7	69.5	129.8	0.87
48	-66	-42.7	4	66.7	125.7	0.89
19	-38.2	-65.3	2.6	65.5	125.7	0.92
6	-43.2	-62	5.4	63.4	125.7	0.98
45	-63.2	-15.3	-0.2	63.2	127.6	1.02
94	-56.3	-40.8	10.4	61.5	129.3	1.1
21	-47.1	-57.5	5.3	59.7	127.6	1.14
67	-54.5	-42.3	5.3	56.5	125.7	1.22
1	-47.7	-40.7	12.7	57.3	129.1	1.25
33	-29.7	-52.9	7.4	55	127.6	1.32
51	26.7	-27.3	3.9	54.5	127.7	1.34
39	-29	-49.8	6.3	51.6	129.1	1.5
81	-49.9	-29.5	5.3	51.2	129.1	1.52
84	-48	-26.1	6.2	49.7	130.8	1.63
4	-41.7	-43.6	5.3	48	127.6	1.66
28	-44.6	-29.6	8.3	48.2	129.9	1.69

Note: See Figure 11.2.12.4.1-7 for Section locations.

11.2.15.1.3 Structural Evaluation for the Maine Yankee Fuel Can

Twenty-Four Inch Drop of the Vertical Concrete Cask

The 24-inch drop of the Vertical Concrete Cask onto an unyielding surface (Section 11.2.4) results in accelerations that are bounded by the 60g acceleration used in this structural evaluation for the Maine Yankee fuel can. The compressive load (P) on the tube is the combined weight of the lid, side plates and tube body.

The compressive load (P) is:

$$P = (17.89 + 6.57 + 78.77) \times 60 = 6{,}193.8 \text{ lbs, use } 8{,}500 \text{ lbs.}$$

The compressive stress (S_c) in the tube body is:

$$S_c = \frac{P}{A} = \frac{8{,}500}{1.714} = 4{,}959 \text{psi}$$

The margin of safety (MS) is determined based on the accident condition allowable primary membrane stress (0.7 S_u) at a bounding temperature of 600°F for Type 304 stainless steel:

$$MS = \frac{0.7S_u}{S_c} - 1 = \frac{0.7(63{,}300)}{4{,}959} - 1 = +7.9$$

The potential buckling of the tube is evaluated, using the Euler formula, to determine the critical buckling load (P_{cr}):

$$P_{cr} = \frac{\pi^2 EI}{L_e^2} = \frac{\pi^2 (25.2 \times 10^6)(20.98)}{2(157.8)} = 16.5 \text{ x } 10^6 \text{ lbs}$$

where:

$$E = 25.2 \times 10^6 \text{ psi}$$

$$I = \frac{8.62^4 - 8.52^4}{12} = 20.98 \text{ in.}^4$$

L_e = 2L (worst case condition)

L = tube body length (157.8 in.)

Because the maximum compressive load (8,500 lbs under the accident condition) is much less than the critical buckling load (16.5×10^6 psi) the tube has adequate resistance to buckling.

Tip–Over of the Vertical Concrete Cask

The majority of the fuel can tube body is contained within the fuel tube in the basket assembly. Because both the tube body of the fuel can and the fuel tube have square cross sections, they are effectively in full contact (for 153.0 in. longitudinally) during a side impact and no significant bending stress is introduced into the tube body. The last 4.8 inches of the tube body and the 5.0 inches length of the side plates are unsupported past the fuel tube flange in the side impact orientation.

The tube body is evaluated as a cantilevered beam with the combined weight (P) of the overhanging tube body and side plates and conservatively, concentrated at the top end of the side plates multiplied by a deceleration factor of 60g. Note that the maximum g-load for the PWR basket is 40g for the tip-over accident (Section 11.2.12).

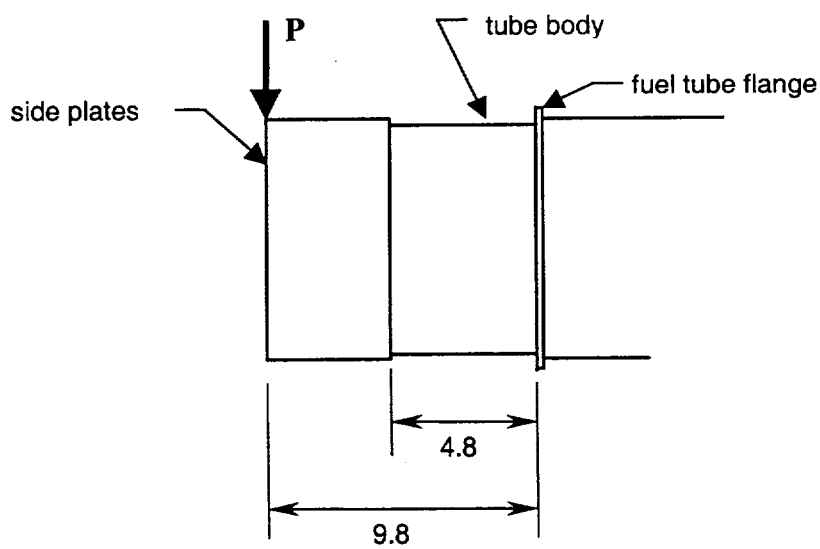

The maximum bending moment (M) is:

$$M = Pg \times L = 25(60)(9.8) = 14{,}700 \text{ lbs·in.}$$

where:

P = 25 lbs (weight of the overhung tube and side plates)

g = 60 (conservative g-load that bounds the tip over condition)

L = 9.8 in. (the total overhung length of the tube body and side plates)

The maximum bending stress, f_b, is:

$$f_b = \frac{Mc}{I} = \frac{14{,}700(4.31)}{20.98} = 3{,}020 \text{ psi}$$

where:

c = half of the outer dimension of the tube

I = the moment of inertia

The shear stress (τ) is:

$$\tau = \frac{Pg}{A} = \frac{25(60)}{1.714} = 875 \text{ psi}$$

where:

A = the cross-sectional area of the tube = 1.714 in^2

The principle stresses are calculated to be 3,255 psi and - 470 psi, and the corresponding stress intensity is determined to be 3,725 psi.

The margin of safety (MS) is calculated based on the allowable primary membrane plus bending stress (1.0 S_u) at a bounding temperature of 600°F for Type 304 stainless steel:

$$MS = \frac{1.0S_u}{\sigma_{max}} - 1 = \frac{63{,}300 \text{ psi}}{3{,}725 \text{ psi}} - 1 = +16$$

As discussed in Section 11.2.15.1.2, the Maine Yankee fuel can may hold a 100% failed damaged fuel lattice or consolidated fuel lattice. An evaluation is performed to demonstrate that the fuel can maintains its integrity during a tip-over accident for this condition. The fuel can is evaluated using the methodology presented in Section 11.2.12.4.1 for the PWR Fuel Tube Analysis for a 60-g side impact condition. This g-load bounds the maximum g-load (40g) for the PWR basket in the concrete cask tip-over event. Similar to the finite element model used for the PWR fuel tube analysis for the uniform pressure case (see Section 11.2.12.4.1), an ANSYS finite element model is generated to represent a section of the damage fuel can with a length of three spans, i.e. the model is supported at four locations by the support disks. The fuel tube, the BORAL plate, and its stainless steel cover plate are conservatively ignored in the model. A bounding uniform pressure is applied to the lower inside surface of the fuel can wall. The pressure is determined based on the weight of the 100% failed consolidated fuel (2,100 lbs × 60g) occupying a length of 109.6 inches (see Section 11.2.15.1.2) as shown below. The inside dimension of the fuel can is 8.52-inches.

$$P = \frac{2{,}100}{109.6(8.52)} \times 60 = 135 \text{ psi}$$

The finite element analysis results show that the maximum stress in the fuel can is 25.4 ksi, which is local to the sections of the tube resting on the support disks. At 750°F the ultimate strength for Type 304 stainless steel is 63.1 ksi. The Margin of Safety is:

$$MS = \frac{63.1}{25.4} - 1 = +1.48$$

The analysis shows that the maximum total strain is 0.05 inch/inch. Defining the acceptable elastic-plastic response of the stainless steel as one half of the material failure strain of 0.40 in./in. at 750°F, the resulting Margin of Safety is:

$$MS = \frac{0.40/2}{0.05} - 1 = +3.0$$

Similarly, the Margin of Safety for elastic-plastic stress is:

$$MS = \frac{63.1 - 17.3}{25.4 - 17.3} - 1 = +4.65$$

where the yield strength of Type 304 stainless steel is 17.3 ksi at 750°F.

Therefore the Maine Yankee fuel can maintains its integrity for the accident conditions.

11.2.15.1.4 Maine Yankee Site Specific Earthquake Evaluation of the Vertical Concrete Cask

This section provides an evaluation of the response of the vertical concrete cask to an earthquake imparting a horizontal acceleration of 0.38g at the top surface of the concrete pad. The evaluation shows that the loaded or empty vertical concrete cask does not tip over or slide in the earthquake event. The methodology used in this evaluation is identical to that presented in Section 11.2.8.

Tip-Over Evaluation of the Vertical Concrete Cask

To maintain the concrete cask in equilibrium, the restoring moment, M_R must be greater than, or equal to, the overturning moment, M_o (i.e. $M_R \geq M_o$). Based on this premise, the following derivation shows that a 0.38g acceleration of the design basis earthquake at the surface of the concrete pad is well below the acceleration required to tip-over the cask.

The combination of horizontal and vertical acceleration components is based on the 100-40-40 approach of ASCE 4-86 [36], which considers that when the maximum response from one component occurs, the response from the other two components are 40% of the maximum. The vertical component of acceleration is obtained by scaling the corresponding ordinates of the horizontal components by two-thirds.

Using this method, two cases are evaluated where:

$a_x = a_z = a$ = horizontal acceleration components
$a_y = (2/3)\ a$ = vertical acceleration component
G_h = Vector sum of two horizontal acceleration components
G_v = Vertical acceleration component

In the first case, the horizontal acceleration is at its maximum. In the second, one horizontal acceleration is at its maximum.

Case 1) The vertical acceleration, a_y, is at its peak: ($a_y = 2/3a$, $a_x = 0.4a$, $a_z = 0.4a$)

$$G_h = \sqrt{a_x^2 + a_z^2}$$

$$G_h = \sqrt{(0.4 \times a)^2 + (0.4 \times a)^2} = 0.566 \times a$$

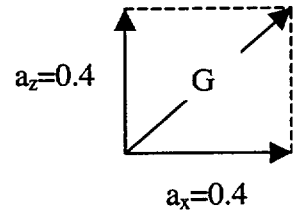

$$G_v = 1.0 \times a_y = 1.0 \times \left(a \times \frac{2}{3} \right) = 0.667 \times a$$

Case 2) One horizonal acceleration, a_x, is at its peak: ($a_y = 0.4 \times 2/3a$, $a_x = a$, $a_z = 0.4a$)

$$G_h = \sqrt{a_x^2 + a_z^2}$$

$$G_h = \sqrt{(1.0 \times a)^2 + (0.4 \times a)^2} = 1.077 \times a$$

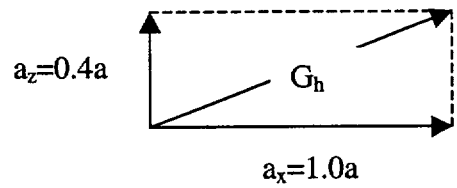

$$G_v = 0.4 \times a_y = 0.4 \times \left(a \times \frac{2}{3} \right) = 0.267 \times a$$

In order for the cask to resist overturning, the restoring moment, M_R, about the point of rotation, must be greater than the overturning moment, M_o, that:

$$M_R \geq M_o \text{, or}$$

$$F_r \times b \geq F_o \times d \Rightarrow (W \times 1 - W \times G_v) \times b \geq (W \times G_h) \times d$$

where:

- d = vertical distance measured from the base of the Vertical Concrete Cask to the center of gravity
- b = horizontal distance measured from the point of rotation to the C.G.
- W = the weight of the Vertical Concrete Cask
- F_o = overturning force
- F_r = restoring force

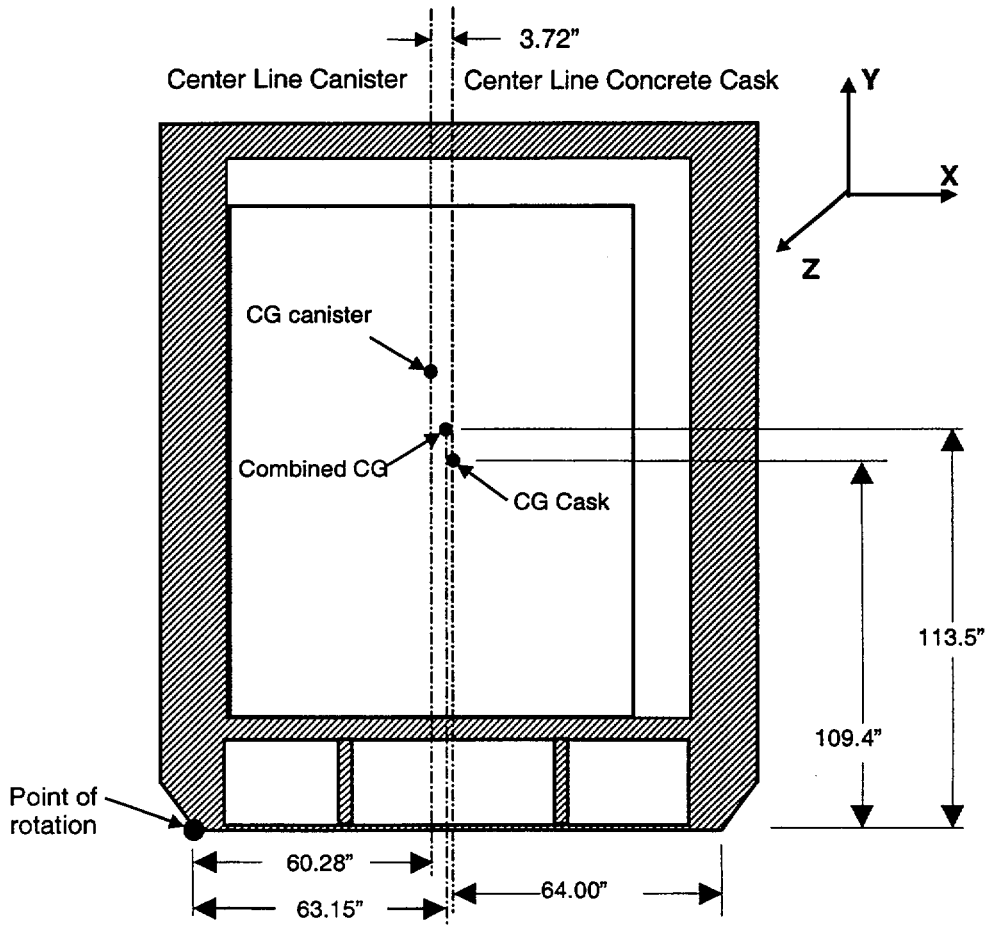

Substituting for G_h and G_v gives:

Case 1

$$(1 - 0.667a)\ \frac{b}{d} \geq 0.566 \times a$$

$$a \leq \frac{b/d}{0.566 + 0.667\left(b/d\right)}$$

Case 2

$$(1 - 0.267a)\frac{b}{d} \geq 1.077a$$

$$a \leq \frac{b/d}{1.077 + 0.267\left(b/d\right)}$$

Because the canister is not attached to the concrete cask, the combined center of gravity for the concrete cask, with the canister in its maximum off-center position, must be calculated. The point of rotation is established at the outside lower edge of the concrete cask.

The inside diameter of the concrete cask is 74.5 inches and the outside diameter of the canister is 67.06 inches; therefore, the maximum eccentricity between the two is:

$$e = \frac{74.50\,\text{in} - 67.06\,\text{in}}{2} = 3.72\,\text{in.}$$

The horizontal displacement, x, of the combined C.G. due to eccentric placement of the canister is

$$x = \frac{70{,}783(3.72)}{308{,}432} = 0.85\,\text{in}$$

Therefore,

$$b = 64 - 0.85 = 63.15\,\text{in.}$$

and

$$d = 113.5\,\text{in.}$$

The C.G. of the loaded Maine Yankee Vertical Concrete Cask is conservatively assumed to be 113.5 inches, which bounds all of the Maine Yankee UMS® Storage System configurations.

1) $a \le \dfrac{63.15/113.5}{0.566 + 0.667 \times \left(63.15/113.5\right)}$

$a \le 0.59g$

2) $a \le \dfrac{63.15/113.5}{1.077 + 0.267 \times \left(63.15/113.5\right)}$

$a \le 0.45g$

Therefore, the minimum ground acceleration that may cause a tip-over of a loaded concrete cask is 0.45g. Since the 0.38g design basis earthquake ground acceleration for the UMS® System at the Maine Yankee site is less than 0.45g, the storage cask will not tip-over.

The factor of safety is 0.45 / 0.38 = 1.18, which is greater than the required factor of safety of 1.1 in accordance with ANSI/ANS-57.9.

Since an empty vertical concrete cask has a lower C.G. as compared to a loaded concrete cask, the tip-over evaluation for the empty concrete cask is bounded by that for the loaded concrete cask.

Sliding Evaluation of the Vertical Concrete Cask

To keep the cask from sliding on the concrete pad, the force holding the cask (F_s) has to be greater than or equal to the force trying to move the cask.

Based on the equation for static friction:

$$F_s = \mu N \geq G_h W$$
$$\mu\left(1 - G_v\right)W \geq G_h W$$

Where:

μ = coefficient of friction
N = the normal force
W = the weight of the concrete cask
G_v = vertical acceleration component
G_h = resultant of horizontal acceleration component

Substituting G_h and G_v for the two cases:

Case 1) $\mu(1 - 0.667a) \geq 0.566\,a$

$$\mu \geq \frac{0.566a}{1 - 0.667a}$$

Case 2) $\mu(1 - 0.267a) \geq 1.077\,a$

$$\mu \geq \frac{1.077a}{1 - 0.267a}$$

For a = 0.38g

Case 1) $\mu \geq 0.29$

Case 2) $\mu \geq 0.45$

The analysis shows that the minimum coefficient of friction, μ, required to prevent sliding of the concrete cask is 0.45. The coefficient of friction between the steel bottom plate of the concrete cask and the concrete surface (broom finish) of the storage pad, 0.50, is greater than the coefficient of friction required to prevent sliding of the concrete cask [45,46]. Therefore, the concrete cask will not slide under design-basis earthquake conditions. The factor of safety is 0.50 / 0.45 =1.11 which is greater than the required factor of safety of 1.1 in accordance with ANSI/ANS-57.9 [1].

11.2.15.1.5 Buckling Evaluation for High Burnup Fuel Rods

This section addresses the potential buckling of intact Combustion Engineering 14 x 14 fuel rods with a burnup between 45,000 and 50,000 MWD/MTU and having a cladding oxide layer up to 80 microns (0.003 inch) thick. An end drop orientation is considered with an acceleration of 60g, which subjects the fuel rod to axial loading. A reduced clad thickness is assumed, due to the 80 micron thick cladding oxide layer.

For the buckling evaluation for the end drop orientation, the fuel rods are laterally restrained by the grids and may come into contact with the fuel assembly base. The only vertical constraint for the fuel rod is the base of the assembly. The weight of the fuel pellets is included in this evaluation, as the pellets are considered to be vertically supported by the cladding. A two-dimensional model comprised of ANSYS BEAM3 elements, shown in Figure 11.2.15.1.5-1, is used for the evaluation. This evaluation is considered to be the bounding condition (as opposed to an evaluation, which considers the cladding only).

During the end drop, the fuel rod impacts the fuel assembly base. The fuel rod itself will respond as an elastic bar under a sudden compression load at its bottom end. The duration of this impact is bounded by the first extentional mode shape of the fuel rod. Contribution of higher frequency extentional modes of the rod would tend to shorten the duration of impact of the fuel rod with the fuel assembly base. The fuel rod, upon initiation of impact, corresponds to an undeformed state. In the process of the impact, the compression of the fuel rod will increase to a maximum and then return to a near uncompressed state, at which point the time of impact has been completed. This actually represents half of a cycle of the lowest frequency mode shape of the fuel rod. The shape of the time dependence of the deformation is sinusoidal. The single extentional mode shape can also be considered to be a single degree of freedom with a corresponding mass and stiffness. In viewing such an event as a spring mass system, the time variation of the deformation during the impact is expected to be sinusoidal.

The buckling mode for the fuel rod is governed by the boundary conditions. For this configuration, the grids provide a lateral support, but no vertical support. The only vertical restraint is considered to be at the point of contact of the fuel rod and the base of the assembly. The weight of the fuel rod pellets and cladding is assumed to be uniformly distributed along the length of the fuel rod. In the end drop, this results in the maximum compressive load occurring at the base of the fuel rod. The first buckling mode shape corresponding to these conditions is computed as shown in Figure 11.2.15.1.5-2.

Typically eigenvalue buckling is applied for static environments. For dynamic loading, it is assumed that the duration of the loading is sufficiently long to allow the system to experience the complete load, even as the deformation associated with the buckling is commenced. For dynamic loading, the lateral motion, which would correspond to the buckled shape, will correspond to the lowest mode shape. This lowest frequency mode shape is shown in Figure 11.2.15.1.5-2 and corresponds to a frequency of 26.3 Hz. The similarity of the two shapes shown in Figure 11.2.15.1.5-2 is expected, since both have the same displacement boundary conditions, the same stiffness matrix, and the same governing finite element equations, i.e.,

$$[K]\{\phi_i\} = \lambda_i\ [A]\{\phi_i\}$$

where:

[K] = structure stiffness matrix
$\{\phi_i\}$ = eigenvector
λ_i = eigenvalue
[A] = mass matrix for the mode shape calculation or stress stiffening matrix for the buckling evaluation

Based on the time duration of the impact and the inherent inability of the fuel rod to rapidly displace in the lateral direction, the effect of the actual lateral motion of buckling can be computed with a dynamic load factor (DLF) [47]. The expression for the DLF for a half-sine loading for a single degree of freedom is given by

$$\text{DLF} = \frac{2\beta \cos(\pi/2\beta)}{1 - \beta^2}$$

where:

β = ratio of the first extentional mode frequency to the first lateral mode frequency

These values, computed in this section, are $\beta = 8.32$ and DLF = 0.244.

This DLF is applied to the end drop acceleration of 60g, which is the bounding load to potentially result in the buckling of the fuel rod. The product of 60g × DLF (= 14.6g) is well below the vertical

acceleration corresponding to the first buckling mode shape, 39.0g as computed in this section. This indicates that the time duration of the impact of the fuel onto the fuel assembly base is of sufficiently short nature that buckling of the fuel rod cannot occur.

An effective cross-sectional property is used in the model to consider the properties of the fuel pellet and the fuel cladding. The modulus of elasticity (EX) for the fuel pellet has a nominal value of 26.0 x 10^6 psi [48]. To be conservative, only 50 percent of this value is used in the evaluation. The EX for the fuel pellet was, therefore, taken to be 13.0 x 10^6 psi. The value of EX (10.47 x 10^6 psi) was used for the irradiated Zircaloy cladding (ISG-12). Reference information shows that there is no additional reduction of the ductility of the cladding due to extended burnup into the 45,000 – 50,000 MWD/MTU range [49].

The bounding dimensions and physical data (minimum clad thickness, maximum rod length and minimum number of support grids) for the Maine Yankee fuel rod used in the model are:

Outer diameter of cladding (inches)	0.44
Cladding thickness (inches)	0.023*
Cladding density (lb/in^3)	0.237
Fuel pellet density (lb/in^3)	0.396

*Note that the cladding thickness has been reduced by 80 microns (0.003 inch).

The elevation of the grids, measured from the bottom of the fuel assembly are: 2.3, 33.0, 51.85, 70.7, 89.6, 108.4, 127.3 and 144.9 (inches).

The effective cross-sectional properties (EI_{eff}) for the beam are computed by adding the value of EI for the cladding and the pellet, where:

E = modulus of elasticity (lb/in^2)
I = cross-sectional moment of inertia (in^4)

The lowest frequency for the extentional mode shape was computed to be 218.9 Hz. The first mode shape corresponds to a frequency of 26.3 Hz. Using the expression for the DLF previously discussed, the DLF is computed to be 0.244 (β = 8.32).

The buckling calculation used the same model employed for the mode shape calculation. The load that would potentially buckle the fuel rod in the end drop is due to the deceleration of the rod. This loading was implemented by applying a 1g acceleration in the direction that would result in compressive loading of the fuel rod. The acceleration required to buckle the fuel rod is computed to be 39.0g. This acceleration is much higher than the effective g-load of 14.6g corresponding to the end drop. Therefore, the fuel rods do not buckle during a 60g end drop.

Figure 11.2.15.1.5-1 Two-Dimensional Beam Finite Element Model for Maine Yankee Fuel Rod

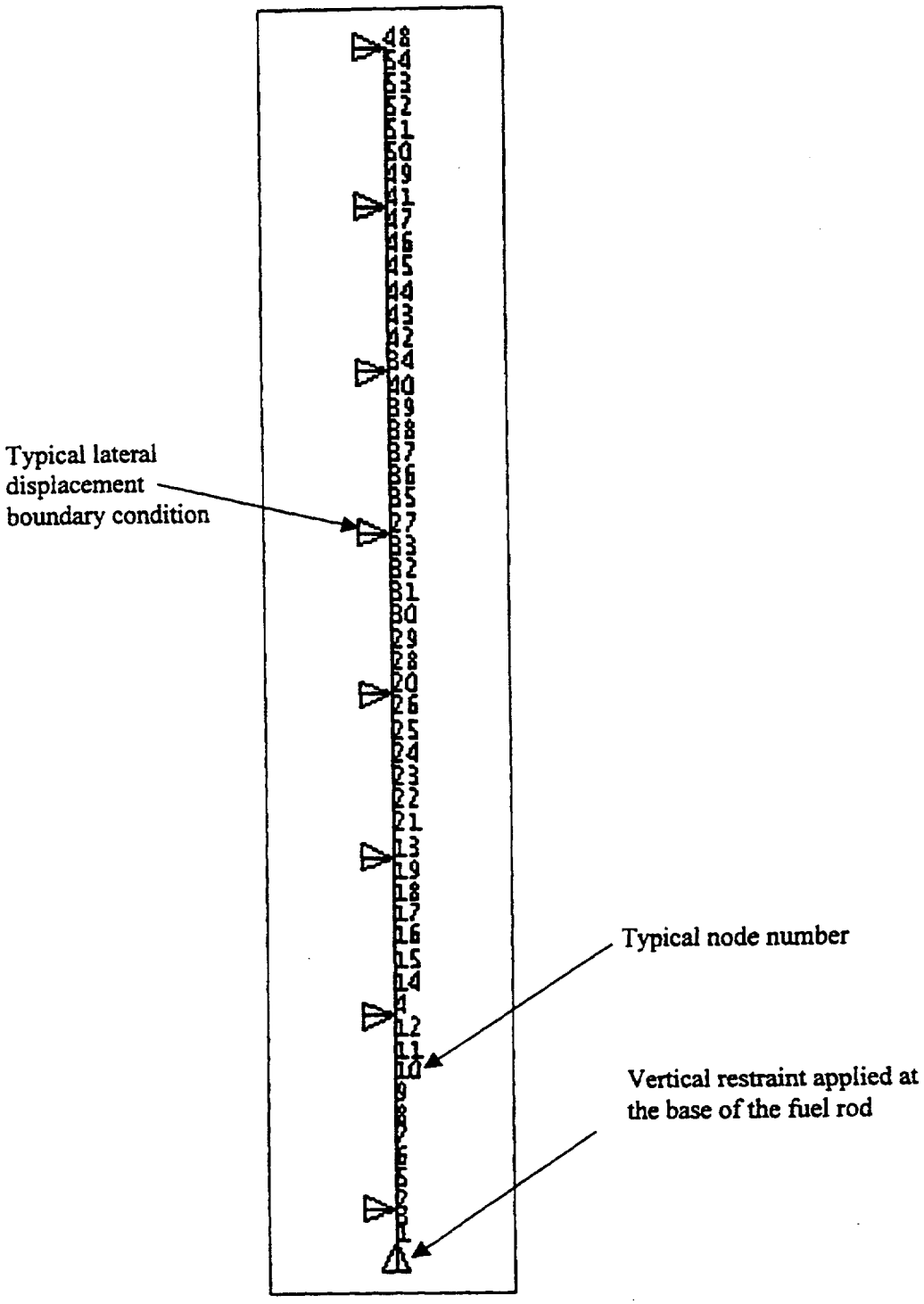

Figure 11.2.15.1.5-2 Mode Shape and First Buckling Shape for the Maine Yankee Fuel Rod

First Lateral Dynamic
Mode Shape at 26.3 Hertz

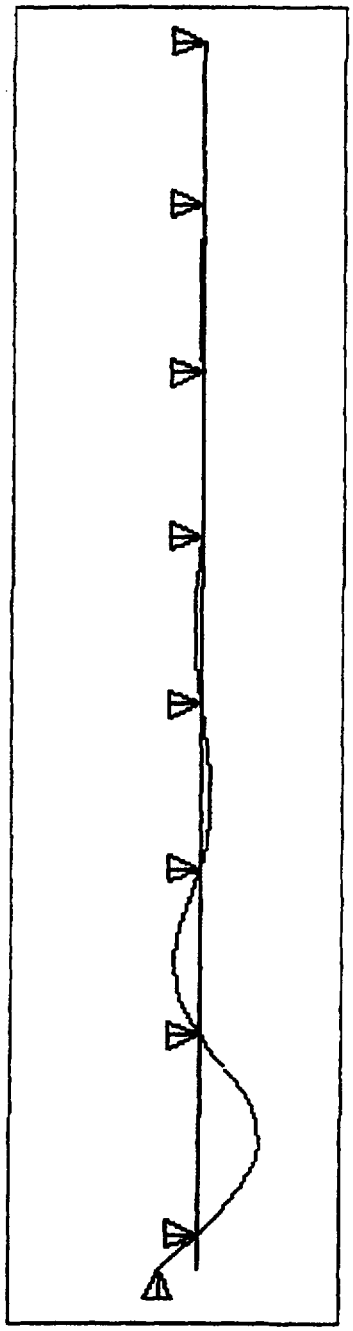

First Buckling
Shape at 39.0g

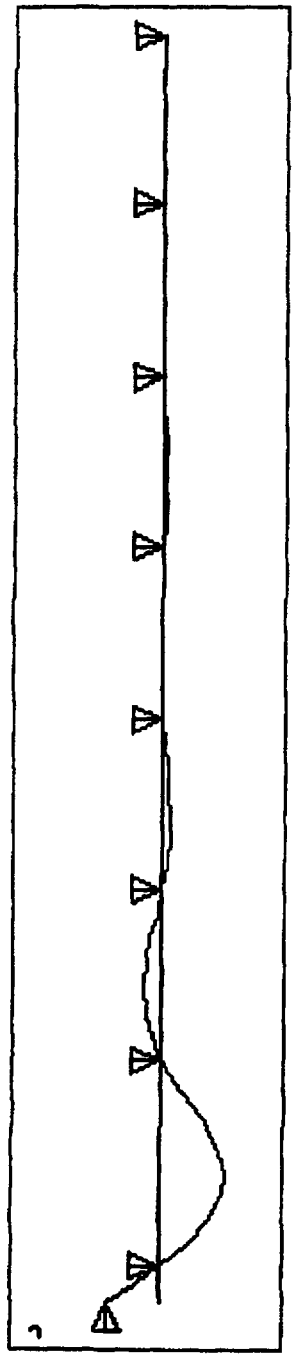

11.2.16 Damaged Fuel Assembly Hardware Evaluation

This section addresses the potential buckling and structural failure of a fuel rod in an assembly with one or more missing support grids up to an unsupported length of fuel rod of 60 inches.

Buckling Evaluation for a Fuel Rod in a Fuel Assembly with Missing Grid Strap(s)

In the following buckling evaluation of an intact fuel assembly, a grid strap is considered to be missing. The buckling load is maximized at the bottom of the fuel assembly. The bounding evaluation is the removal of the grid strap, which maximizes the spacing at the lowest possible vertical elevation. This occurs when the grid at the 33.0-inch elevation is removed, resulting in a grid spacing of approximately 50.0 inches (60.0 inches conservatively used).

The case of the missing grid is evaluated using the same methodology as for the fuel assembly with all the grids being present (See Section 11.2.15.1.5). The bounding dimensions and physical data (minimum clad thickness, maximum rod length and minimum number of support grids) for the Maine Yankee fuel rod used in the model are:

Outer diameter of cladding (inches)	0.44
Cladding thickness (inches)	0.023
Cladding density (lb/in^3)	0.237
Fuel pellet density (lb/in^3)	0.396
Fuel pellet Modulus of Elasticity (psi)	13.0×10^6
Zircaloy cladding Modulus of Elasticity (psi)	10.47×10^6

The cladding thickness has been reduced by an oxidation layer of 80 microns (0.003 inch). The fuel pellet modulus of elasticity is conservatively reduced 50%, The modulus of elasticity of the Zircaloy cladding is taken from ISG-12 [50].

The elevations of the grids in the model, measured from the bottom of the fuel assembly are: 2.3, 51.85, 70.7, 89.6, 108.4, 127.3 and 144.9 (inches). The grid at 51.85 inches is assumed located at 62.3 inches.

With the grid missing, the frequency of the fundamental lateral mode shape is 7.9 Hz. The natural frequency of the fundamental extensional mode was determined to be 218.9 Hz. The DLF is computed to be 0.072, resulting in an effective acceleration of 0.072 x 60 = 4.3 g. Using the same method to compute the acceleration at which buckling occurs, the lowest buckling acceleration is 14.8 g, which is significantly greater than 4.3 g. Therefore, the fuel rod, with the bounding case of a single missing grid, does not buckle during an end drop. Figures 11.2.16-1 and 11.2.16-2 show the finite element model and buckling results and mode shape.

Figure 11.2.16-1 Two-Dimensional Beam FEM for Fuel Rod with Missing Grid

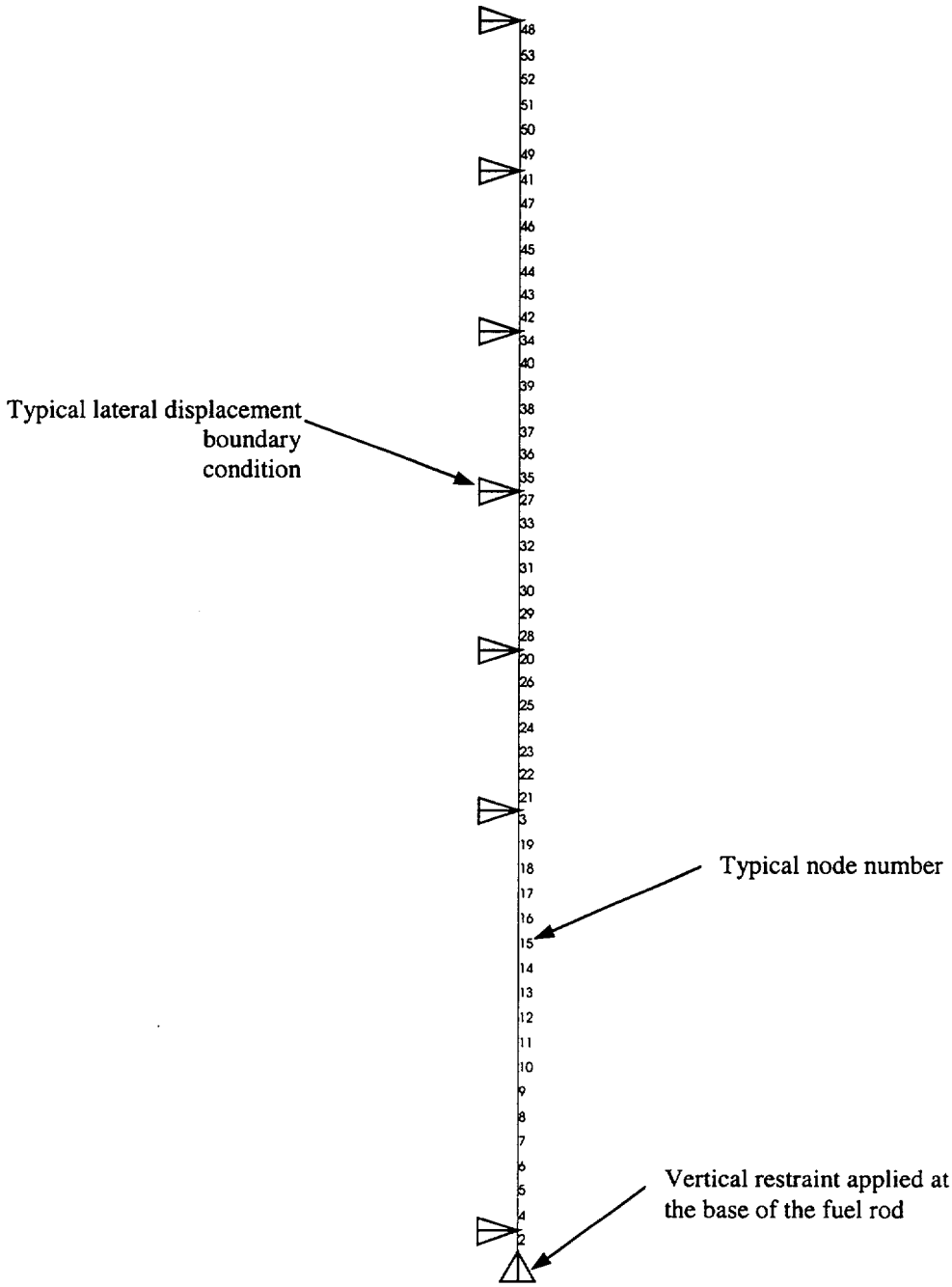

Figure 11.2.16-2 Modal Shape and First Buckling Mode Shape for a Fuel Rod with a Missing Grid

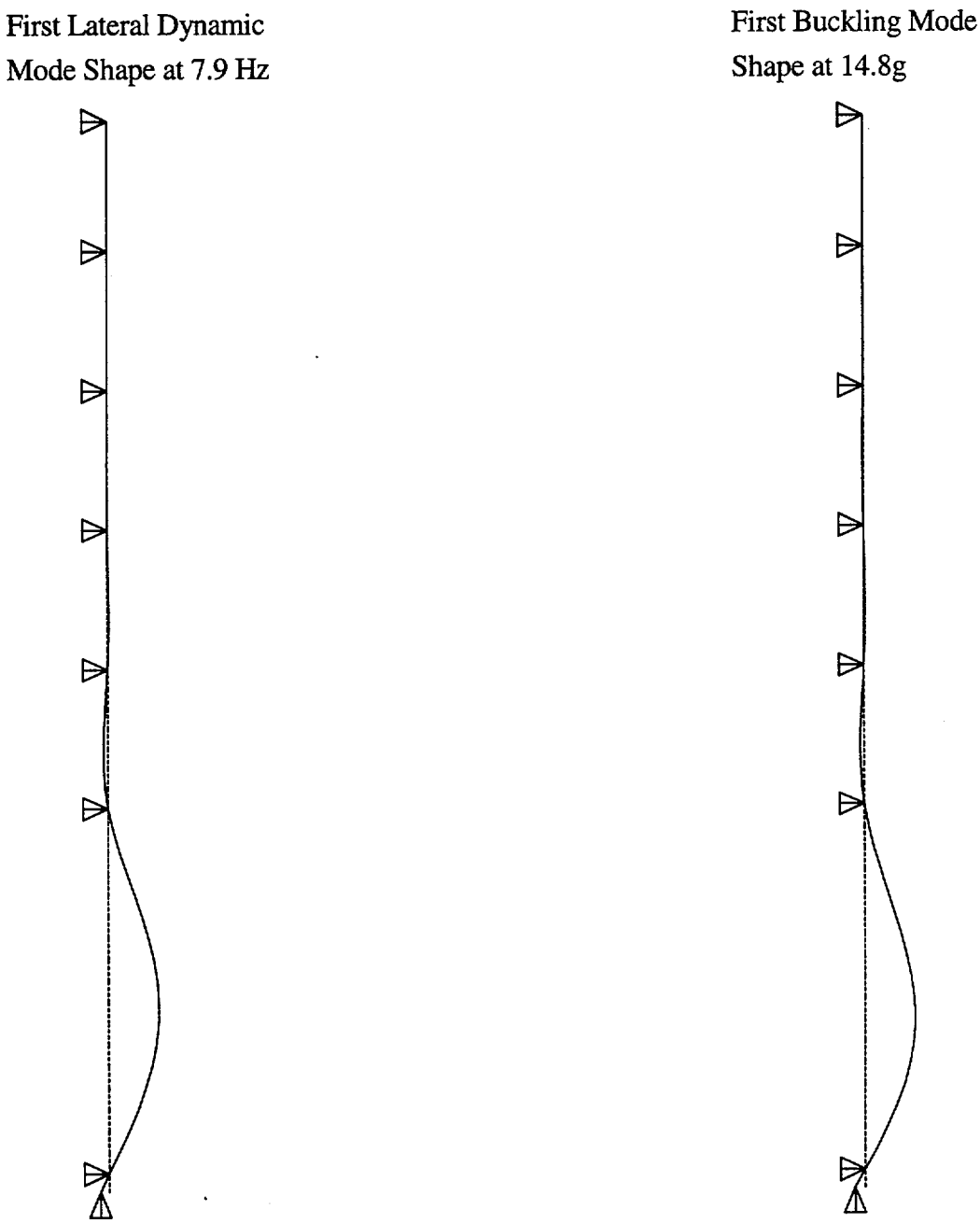

Structural Evaluation of Maine Yankee Fuel Rod in a Fuel Assembly with a Missing Grid

The Maine Yankee fuel rod is evaluated for a 60 g side drop with a missing support grid in the fuel assembly. The span between support grids is assumed to be 60.0 inches (actual span is 49.5 inches).

Analysis Input:

Fuel Rod OD	0.44 in.
Clad ID	0.394 in.
E_{clad}	10.47E6 psi
E_{fuel}	13.0E6 psi
Clad density	0.237 lb/in^3
Fuel density	0.396 lb/in^3
Cross-Sectional area:	
A_{clad}	0.030 in^2
A_{fuel}	0.122 in^2

The mass of the fuel rod per unit length is:

$$m = \frac{0.396(0.122) + 0.237(0.030)}{386.4} = 0.000143 \text{ lb-s}^2/\text{in}^2$$

EI for the fuel rod is:

$$EI_{clad} = 10.47E6 \frac{\pi\left(0.22^4 - 0.197^4\right)}{4} = 6878 \text{ lb-in}^2$$

$$EI_{fuel} = 13.0E6 \frac{\pi\left(0.197^4\right)}{4} = 15378 \text{ lb-in}^2$$

$$EI = 6878 + 15378 = 22{,}256 \text{ lb-in}^2$$

During a side drop, the maximum deflection of a fuel rod is based on the fuel rod spacing of the fuel assembly. The pitch (center to center spacing) of fuel rods is 0.58 inches [51]. The maximum pitch is across the diagonal of the fuel assembly. The maximum pitch is:

$$dp = \frac{0.58}{\sin 45} = 0.82 \text{ in.}$$

The maximum deflection of a fuel rod is at the top of the fuel assembly and the minimum deflection is at the bottom of the fuel assembly.

Assuming a 17 x 17 array (which envelopes the Maine Yankee 14 x 14 array), the maximum fuel rod deflection is:

(17-1) x (0.82-0.44) = 6.08 inches.

The deflection of a simply supported beam with a distributed load is given by the equation:

$$\Delta = \frac{5\omega l^4}{384EI} = \frac{5(g\omega)l^4}{384\left(EI_{total}\right)} \qquad [52]$$

$$g = \frac{384\Delta\left(EI_{total}\right)}{5\omega l^4}$$

The cladding bending stress is given by the equation:

$$S = \frac{Mc}{I} = \frac{\left(\left(g\omega l^2\right)/8\right)c}{I_{clad}}\left(\frac{EI_{clad}}{EI_{total}}\right)$$

Inserting the equation for 'g':

$$S = \frac{384\Delta c E_{clad}}{40 \times l^2}$$

The bending stress in the fuel rod is:

$$S = \frac{384 \times 6.08 \times 0.22 \times 10.47E6}{40(60)^2} = 37.4 \text{ ksi}$$

where:

c = 0.22 inch distance from center of fuel rod to extreme outer fiber

$$I = \frac{EI_{total}}{E_{clad}} = \frac{22256}{10.47E6} = 0.0021\,in^4$$

The maximum hoop stress due to the fuel rod internal pressure is determined to be 19.1 ksi (131.4 MPa per Tables 4.4.7-3 and 4.5.1.2-1). Therefore, the maximum axial stress is 9.6 ksi (one half of the hoop stress [53]).

The bearing stress between two fuel rods under a 60g load is:

$$S_{brg} = 0.591\sqrt{\frac{\omega E}{K_D}} = 0.591\sqrt{\frac{(0.000143 \times 386.4) \times 60 \times 10.47E6}{0.22}} = 7.4\,ksi \quad [53]$$

where:

$$K_D = \frac{D_1 D_2}{D_1 + D_2} = \frac{0.44 \times 0.44}{0.44 + 0.44} = 0.22$$

The total stress is:

$$S = 37.4 + 9.6 + 7.4 = 54.4\,ksi$$

The margin of safety for ultimate strength is:

$$MS = \frac{83.4}{54.4} - 1 = 0.53$$

where:

S_u = 83.4 ksi (575 Mpa) Irradiated Zircaloy-4 Ultimate Strength Allowable (Fig 3-2 [54])

The margin of safety for yield strength is:

$$MS = \frac{78.3}{54.4} - 1 = 0.44$$

where:

$S_y = 78.3$ ksi (540 Mpa) Irradiated Zircaloy-4 Yield Strength Allowable (Fig 3-2 [54])

The maximum bearing stress occurs between the bottom fuel rod and the fuel tube. The bearing stress is:

$$S_{brg} = 0.591\sqrt{\frac{17 \times 0.000143 \times 386.4 \times 60 \times 10.47E6}{0.44}} = 21.6 \text{ ksi}$$

The bending stress is negligible because the maximum deflection is equal to the spacing of the fuel rods established by the grid. Therefore the top fuel rod is bounding.

THIS PAGE INTENTIONALLY LEFT BLANK

11.3 References

1. ANSI/ANS-57.9-1992, "Design Criteria for an Independent Spent Fuel Storage Installation (Dry Type)," American Nuclear Society, May 1992.
2. Code of Federal Regulations, "Packaging and Transportation of Radioactive Materials," Part 71, Title 10, April 1996.
3. NAC Document No. EA790-SAR-001, "Safety Analysis Report for the UMS™ Universal Transport Cask,'' Docket No. 71-9270.
4. Code of Federal Regulations, "Licensing Requirements for the Independent Storage of Spent Nuclear Fuel and High-Level Radioactive Waste," Part 72, Title 10, January 1996.
5. Olander, D.R., "Fundamental Aspects of Nuclear Reactor Fuel Elements," U.S. Department of Energy Technical Information Center, 1985.
6. NRC, "Standard Review Plan for Dry Cask Storage Systems," NUREG–1536, Final Report, January 1997.
7. EPA Federal Guidance Report No.11, Limiting Values of Radionuclide Intake and Air Concentration and Dose Conversion Factors for Inhalation, Submersion and Ingestion, 1988.
8. EPA Federal Guidance Report No.12, External Exposure to Radionuclides in Air, Water and Soil, 1993.
9. NRC Regulatory Guide 1.109, Calculation of Annual Doses to Man from Routine Releases of Reactor Effluents for the Purpose of Evaluating Compliance with 10CFR50 Appendix I, 1977.
10. Code of Federal Regulations, Part 20, "Standards for Protection Against Radiation," 1993.
11. NRC Regulatory Guide 8.34, "Monitoring Criteria and Methods to Calculate Occupational Radiation Doses," 1992.
12. NRC Regulatory Guide 1.25, Assumptions Used for the Potential Radiological consequences of a Fuel Handling Accident and Storage Facility for Boiling and Pressurized Water Reactors, 1972.

13. Nuclear Regulatory Commission, "Atmospheric Dispersion Models for Potential Accident Consequence Assessments at Nuclear Power Plants," Regulatory Guide 1.145, September 1980.

14. SAND80-2124, "Transportation Accident Scenarios for Commercial Spent Fuel," Sandia National Laboratories, February 1981.

15. NRC, "Standard Review Plan for Dry Cask Storage Systems," Draft NUREG–1536, February 1996.

16. Kreith & Bohn, *Principles of Heat Transfer,* 5th Edition, West Publishing Company, St. Paul, Minnesota, 1993.

17. Regulatory Guide 1.60, "Design Response Spectra for Seismic Design of Nuclear Power Plants," Revision 1, December 1973.

18. ANSYS Revision 5.2, Computer Program, ANSYS, Inc., Houston, Pennsylvania.

19. Blevins, R.D., *Formulas for Natural Frequency and Mode Shape,* Krieger Publishing Co., Malabar, Florida, 1995.

20. "Topical Safety Analysis Report for the NAC Storable Transport Cask for use at an Independent Spent-Fuel Storage Installation," NAC-T-90002, Revision 3, NAC Services, Inc., Norcross, Georgia, July 1994.

21. Funk, R. "Shear Friction Transfer Mechanisms for Supports Attached to Concrete," American Concrete International Journal, Volume 11, No. 7, pp 53-58, July, 1989.

22. NRC, "Three Components of Earthquake Motion," NUREG-0800, Revision 1, Section 3.7.2, Subsection II.6.

23. "Steel to Concrete Coefficient of Friction, Preliminary Tests," Report No. CEB 77-46, Tennessee Valley Authority, Knoxville, Tennessee, December 1977.

24. Roberson, J.A. and C.T. Crowe, "Engineering Fluid Mechanics," Houghton Mifflin Co., Boston, Massachusetts, 1975.

25. Cianos, N., and E.T. Pierce, "A Ground Lightning Environment for Engineering Usage," Technical Report No. 1, Stanford Research Institute, Menlo Park, California, Contract No. LS-2817-A3, SRI Project No. 1834, August 1972.

26. Summer, W.I., "American Electrician's Handbook," 10th Edition, McGraw-Hill, Inc., New York, 1981.

27. Fink, D.G., and Beaty, W. H., "Standard Handbook for Electrical Engineers," 13th Edition, McGraw-Hill, Inc., New York, 1993.

28. Black, W.Z. and J.G. Hartley, *Thermodynamics,* 2nd Edition, Harper Collins Publishers, 1991.

29. U.S. NRC Regulatory Guide 1.76, "Design Basis Tornado for Nuclear Power Plants," April 1974.

30. NUREG-0800, "Standard Review Plan," US NRC, June 1987. (Missile masses taken from Draft Revision 3, April 1996.)

31. "Minimum Design Loads for Building and Other Structures," ASCE 7-93, American Society of Civil Engineers, New York, May 12, 1994.

32. "A Review of Procedures for the Analysis and Design of Concrete Structures to Resist Missile Impact Effects," NSS 5-940.1, Nuclear and Systems Sciences Group, Holmes & Narver, Inc., Anaheim, California, September 1975.

33. Full-Scale Tornado-Missile Impact Tests," EPRI NP-440, Sandia Laboratories for the Electric Power Research Institute, Palo Alto, California, July 1977.

34. "Code Requirements for Nuclear Safety Related Concrete Structures (ACI-349-85) and Commentary-ACI 349R-85," American Concrete Institute, Detroit, Michigan, March 1986.

35. Topical Report, "Design of Structures for Missile Impact," BC-TOP-9A, Revision 2, Bechtel Power Corporation, San Francisco, California, September 1974.

36. "Seismic Analysis of Safety-related Nuclear Structures and Commentary on Standard for Seismic Analysis of Safety-related Nuclear Structures," ASCE 4-86, American Society of Civil Engineers, September 1986.

37. Cote, Arthur E., Fire Protection Handbook, 18th Edition, National Fire Protection Association, Quincy, Massachusetts.

38. NUREG/CR-6608, "Summary and Evaluation of Low-Velocity Impact Tests of Solid Steel Billet onto Concrete Pads," Lawrence Livermore National Laboratory, February 1998.

39. NUREG/CR-6322, "Buckling Analysis of Spent Fuel Basket," Lee, A.S., and Bumpas, S.E., Office of Nuclear Material and Safeguards, U.S. Nuclear Regulatory Commission, Washington, DC, May 1995.

40. EPRI TR-108760, "Validation of EPRI Methodology of Analysis of Spent-Fuel Cask Drop and Tipover Events," ANATECH Corp., San Diego, CA, August 1997.

41. Green, Robert E, "Machinery's Handbook 25th Edition," Industrial Press Inc., New York, 1996.

42. NUREG/CR-0481, SAND77-1872, "An assessment of Stress-Strain Data Suitable for Finite-Element Elastic-Plastic Analysis of Shipping Containers," Henry J. Rack & Gerald A. Knorosky, September 1978.

43. Biggs, J.M., Introduction to Structural Dynamics, McGraw-Hill, Inc., New York, 1964.

44. Boyer, H. E., Atlas of Stress-Strain Curves, ASM International, Metals Park, Ohio, 1987.

45. ACI 116R-90, "Cement and Concrete Technology," American Concrete Institute, 1990.

46. ACI 302.1R-89, "Guide for Concrete Floor and Slab Construction," American Concrete Institute, 1989.

47. Clough, R.W., and Joseph Penzien, "Dynamics of Structures," 2nd Edition, McGraw-Hill, Inc., New York, NY, 1993.

48. Rust, J. H., Nuclear Power Plant Engineering, Georgia Institute of Technology, 1979.

49. NUREG/CR-5009, "Assessment of the Use of Extended Burnup Fuel in Light Water Power Reactors," Battelle Pacific Northwest Labs, Richland, Washington, February 1988.

50. ISG-12, "Buckling of Irradiated Fuel Under Bottom End Drop Conditions," Interim Staff Guidance –12, Nuclear Regulatory Commission, June 1999.

51. "Maine Yankee Atomic Power Company Specification for Independent Spent Fuel Storage Installation and Transport Facility," NAC Document 12412-DI-01, NAC International, Atlanta, Georgia.

52. Blake, Alexander, "Practical Stress Analysis in Engineering Design," 2nd Edition, Marcell Dekker, Inc., New York, 1990.

53. Young, Warren C., "Roark's Formulas for Stress & Strain," 6th Edition, McGraw-Hill, 1989.

54. "Fuel-Assembly Behavior Under Dynamic Impact Loads Due to Dry-Storage Cask Mishandling," EPRI NP-7419, ABB Combustion Engineering, Inc., Windsor, Connecticut, July 1991.